Mitochondrial function in atherosclerosis and vascular smooth muscle cells

Johannes Reinhold

University of Cambridge – Gonville and Caius College

Cardiovascular Division, Department of Medicine

July 2018

This dissertation is submitted for the degree of Doctor of Philosophy

Abstract

Mitochondrial function in atherosclerosis and vascular smooth muscle cells

Johannes Reinhold

Atherosclerosis is the leading cause of death in the Western world. Although mitochondrial DNA (mtDNA) damage has been implicated in atherosclerosis, it is unclear whether the damage is sufficient to impair mitochondrial respiration, and mitochondrial dysfunction has not been demonstrated. Treatment of vascular smooth muscle cells (VSMCs) with an atherogenic lipid, oxidised low-density lipoprotein (OxLDL), dose dependently decreased basal and maximal respiration and fat-feeding of apolipoprotein E deficient (ApoE-/-) mice reduced mitochondrial DNA copy number relative to nuclear DNA in aortas. Mitochondrial respiration of ApoE-/- mouse aortas, assessed through a 24-well Seahorse extracellular flux analyser, was not affected prior to the development of atherosclerotic plaques. Developed human carotid atherosclerotic plaques were dissected into defined regions including healthy media, shoulder region, fibrous cap and core and their respiration was investigated. The respiratory reserve capacity (RRC) of the shoulder region was similar to the media. However, the cap RRC was significantly reduced compared to healthy media. In contrast, the extracellular acidification rates (ECAR) of the media, shoulder, cap and core regions were

similar. In addition, mtDNA copy number was significantly reduced in tissues derived from human plaques compared to healthy arteries and expression of complexes I and II of the electron transfer chain (ETC) were significantly reduced in plaque VSMCs. OxLDL induced mitophagy in human VSMCs and plaque VSMCs demonstrated increased levels of mitophagy without compensatory upregulation of proteins involved in mitochondrial biogenesis. Understanding the role of mitochondrial metabolism and signalling is important for our understanding of disease progression and may lead to future therapeutic targets.

Declaration

I hereby declare that my thesis entitled:

“Mitochondrial function in atherosclerosis and vascular smooth muscle cells”

• Is the result of my own work and includes nothing which is the outcome of work done in collaboration except as declared in the Preface and specified in the text

• Is not substantially the same as any that I have submitted, or, is being concurrently submitted for a degree or diploma or other qualification at the University of Cambridge or any other University or similar institution except as declared in the Preface and specified in the text. I further state that no substantial part of my dissertation has already been submitted, or, is being concurrently submitted for any such degree, diploma or other qualification at the University of Cambridge or any other University of similar institution except as declared in the Preface and specified in the text

• Does not exceed the prescribed word limit

Acknowledgements

I would like to thank my supervisors, Professor Martin Bennett and Dr Mike Murphy, for their support, helpful discussions and their encouragement to pursue my research interests.

I am also grateful for the help and advice I received from members of both laboratories. From Martin Bennett's laboratory I would particularly like to thank Dr Anna Uryga who gave helpful advice and supported me in laboratory techniques and experiments including Western blot and generation of lentiviral particles, Nichola Figg for preparation of immunohistochemistry slides, Alison Finigan for helping with animal maintenance and procedures, and Dr Aarti Shah for helping with cDNA generation.

From Mike Murphy's laboratory I would like to thank Tracy Prime, for helping me set up and providing me with tissues for control experiments as well as Dr Angela Logan and Dr Sabine Arndt for performing mass spectrometry on my tissue samples. Thomas Bright and Dr Liz Hinchy introduced me to a technique used for measurement of ATP and ADP in tissues and I would also like to thank Dr Andrew James for many helpful discussions and advice.

Dr Hannah Bridges and Dr Joe Carroll gave useful advice in relation to the Seahorse extracellular flux analysers. Simon McCallum introduced me to the departmental confocal microscope. I would like to thank Dr Richard Butler for providing me with an adjustment to his ImageJ plug-in that I used for image analysis in this thesis.

I am grateful for the time and enthusiasm Professor Krishna Chatterjee dedicated to the success of the Wellcome Trust PhD programme for clinicians and, of course, the Wellcome Trust for providing the funding for the programme and this project.

Abbreviations

ADP	Adenosine diphosphate
Ant	Antimycin
ApoE-/-	Apolipoprotein E null
ATM	Ataxia telangiectasia mutated
a.u.	Arbitrary unit
BCA	Bicinchoninic acid
B2M	β_2 microglobulin
DAMPs	Damage-associated molecular patterns
DMEM	Dulbecco's modified Eagle's medium
DMSO	Dimethyl sulfoxide
ECAR	Extracellular acidification rate
EDTA	Ethylenediaminetetraacetic acid
ETC	Electron transport chain
EV	RVSMCs expressing empty vector
FCCP	Carbonyl cyanide-4-(trifluoromethoxy)phenylhydrazone
FCS	Foetal calf serum
Gpx1	Glutathione peroxidase 1
GSH	Glutathione
HSPs	Heat shock proteins
HIF-1α	Hypoxia-inducible factor 1α
IL	Interleukin
LDL	Low-density lipoprotein
LDLR	Low-density lipoprotein receptor
LOX-1	Lectin-like OxLDL receptor-1, also known as SR-E1
LPS	Lipopolysaccharide
MDA	Malondialdehyde
MI	Myocardial infarction
MitoB	Mass spectrometric probe targeted to mitochondria via TPP that reacts with H_2O_2 to form MitoP
MitoP	Mass spectrometric probe resulting from conversion of MitoB by H_2O_2 forming a phenol product
MitoQ	Ubiquinone based antioxidant targeted to mitochondria
MMP	Matrix metalloproteinase
MOPS	3-(*N*-morpholino)propanesulfonic acid
mtDNA	Mitochondrial DNA
MTT	3-(4,5-dimethylthiazol-2-yl)-2,5-diphenyltetrazolium bromide
NAD(P)	Nicotinamide adenine dinucleotide (phosphate) [NAD(P)H– reduced form]
NFκB	Nuclear factor kappa B
NLRP3	NLR family, pyrin domain containing 3
OCR	Oxygen consumption rate
ONOO−	Peroxynitrite
OxLDL	Oxidised low-density lipoprotein
O_2•−	Superoxide

PAMPs	Pathogen-associated molecular patterns
PBS	Phosphate-buffered saline
PGC-1	Peroxisome proliferator-activated receptor gamma coactivator 1
PHD	Prolyl hydroxylase
Pi	Phosphate
Prx	Peroxiredoxin
PolG	DNA polymerase γ
qPCR	Quantitative polymerase chain reaction
ROS	Reactive oxygen species
Rot	Rotenone
rpm	Revolutions per minute
RRC	Respiratory reserve capacity
RT	Room temperature
RVSMCs	Rat vascular smooth muscle cells
SD	Standard deviation
SEM	Standard error of the mean
SIRT+	RVSMCs overexpressing sirtuin-1
SIRT-	RVSMCs overexpressing deacetylase-deficient sirtuin-1^{H365Y}
SIRT1	Sirtuin (silent mating type information regulation 2 homolog)-1
SOD2	Superoxide dismutase 2
SR-	Scavenger Receptor-
TBARS	Thiobarbituric acid-reactive substances
TBST	Tris-buffered saline with 0.05% Tween 20
TLR	Toll-like receptor
TPP	Triphenylphosphonium
U	Unit
VSMC	Vascular smooth muscle cells
WT	Wild type

Table of Contents

List of Figures

List of Tables

1 Introduction

1.1 Atherosclerosis

Atherosclerosis causing myocardial infarction and stroke is the leading cause of morbidity and mortality in the developed world (Krishnamurthi et al., 2013; Murray et al., 2012). With an ageing population, the burden of atherosclerosis is set to increase unless the disease trajectory is modified (Roth et al., 2015). Although classical risk factors such as a positive family history, smoking, hypertension, obesity, hypercholesterolaemia / hyperlipidaemia, diabetes, aging and male sex are well known (Dawber, Moore, & Mann, 1957), not all of these risk factors are modifiable. Nevertheless, significant improvements can be achieved through alteration of these risk factors, as exemplified by the clinical effectiveness of the Hydroxymethylglutaryl Coenzyme A (HMGCoA) reductase inhibitor drugs (statins) (M. A.-A. S. Group, 1994; S. S. S. S. Group, 1994). Understanding the mechanisms of atherosclerosis may in future open new therapeutic strategies to address this debilitating disease.

Atherosclerosis is a chronic inflammatory disease affecting the medium-sized and large arteries. It has been described as a stage-wise process consisting of 1) endothelial dysfunction, 2) fatty streak formation, 3) formation of an advanced complicated lesion and 4) unstable fibrous plaques (Ross, 1999) (Figure 1-1). Although simplifying the disease process, this framework highlights that in different stages of the disease various mechanisms drive disease progression.

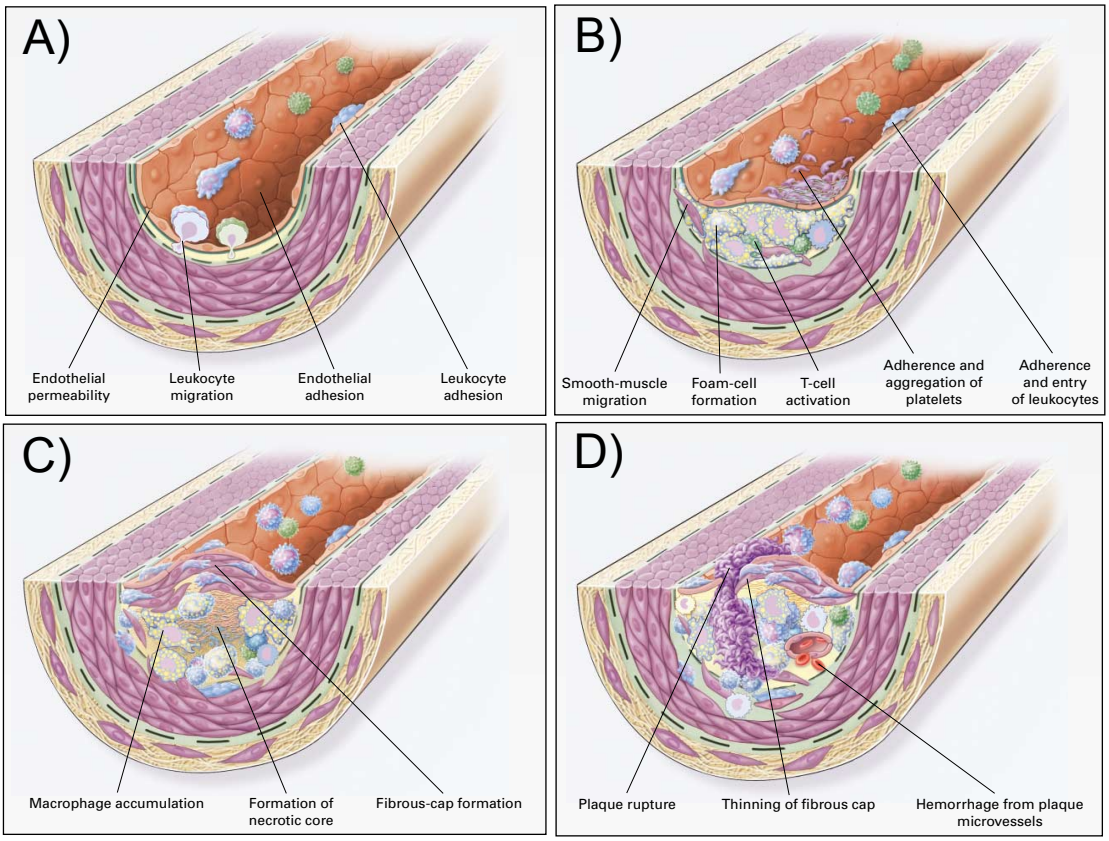

Figure 1-1 Stages of atherosclerosis

Adapted from Ross (1999). A) Endothelial Dysfunction. Permeability of endothelial layer to lipoproteins increases. Endothelial cells express adhesion molecules facilitating adhesion of leukocytes and their migration to the intima. B) Fatty streak formation. Fatty streaks are formed by lipid-laden foam cells (monocytes, macrophages and T-lymphocytes) and later in the disease process VSMCs. C) Advanced, complicated atherosclerotic lesion. A fibrous cap, made up of VSMCs covers the necrotic core. D) Unstable atherosclerotic plaque. Thinning of the fibrous cap can lead to plaque rupture or ulceration with thrombus formation.

Endothelial dysfunction is considered to be an early stage of atherosclerosis. The endothelial layer becomes permeable to lipoproteins and other plasma constituents and expresses endothelial adhesion molecules such as intercellular adhesion molecule 1 (ICAM1), vascular-cell adhesion molecule 1 (VCAM1), and selectins, facilitating the recruitment of leukocytes to the developing atherosclerotic lesion (section 1.1.1). Monocytes and

macrophages, as well as VSMCs recruited to these sites phagocytose lipids and oxidised lipids [Oxidised low-density lipoprotein (LDL) (OxLDL)] and become so-called lipid-laden foam cells and early fatty streaks are formed (Jonasson, Holm, Skalli, Bondjers, & Hansson, 1986; Ross, 1999). During the formation of the advanced, complicated lesion a fibrous cap, made up largely from VSMCs and extracellular matrix, separates the lipid-laden atherosclerotic core from the lumen. It is the thinning and rupture of this protective cap that is responsible for a large proportion of unstable coronary artery disease (Burke et al., 1997; Calvert et al., 2011).

1.1.1 Atherosclerosis – inflammation and immunity

The discovery of inflammation in atherogenesis and the involvement of both the innate and adaptive immune systems as main drivers of this process have been reviewed extensively in the past (Hansson & Libby, 2006; Libby, 2012; Ross, 1999; Witztum & Lichtman, 2014).

Endothelial cells are activated through a wide range of stimuli including injury (Ross, 1999), altered shear stress (Mondy et al., 1997) or modified lipids (see 1.1.3) causing up-regulation of cytokines and chemokines (Hansson & Libby, 2006). Adhesion molecules, cytokines and their receptors involved in the recruitment of inflammatory cells during atherogenesis include intercellular adhesion molecule 1 (ICAM-1) (Nakashima, Raines, Plump, Breslow, & Ross, 1998), C-C motif chemokine (CC) ligand 2 (CCL2) also known as monocyte chemoattractant protein 1 (MCP1) (Gu et al., 1998; Papadopoulou, Corrigall, Taylor, & Poston, 2008) and its corresponding receptor CC receptor 2 (CCR2) (Boring, Gosling, Cleary, & Charo, 1998), CC

ligand 5 (CCL5, also known as regulated on activation, normal T cell expressed and secreted [RANTES]), CCL11, C-X-C motif chemokine (CXC) ligand (CXCL) 10 (CXCL10), CXCL11, CXCL16, and C-X_3-C motif chemokine ligand 1 (CX_3CL1) (Hansson & Libby, 2006), highlighting the active process of inflammatory cell recruitment during this disease process. Monocytes, binding to endothelial VCAM-1 through very late antigen-4 (VLA-4), migrate into the intima as a response to locally formed chemokines and differentiate into macrophages after macrophage colony-stimulating factor (M-CSF) stimulation (Hansson & Libby, 2006).

We now know that innate immunity in atherosclerosis involves a huge array of soluble factors and their receptors and different cell types including monocytes or macrophages, granulocytes, mast cells, dendritic cells (DCs) natural killer (NK) cells and B1 lymphocytes (Bobryshev & Lord, 1995; Chistiakov, Orekhov, & Bobryshev, 2016; Jonasson et al., 1986; Kovanen, Kaartinen, & Paavonen, 1995). The innate immune system is also required for activation of the adaptive immune system. Dendritic cells mediate the juncture from innate immunity to adaptive immunity in atherosclerosis through uptake of foreign antigens and their presentation to T-lymphocytes. T-lymphocytes release cytokines, thus further activating leukocytes and inducing humoral immunity through activation of B-lymphocytes (Chistiakov et al., 2016). A full discussion of the role of the adaptive immunity in atherosclerosis is beyond the scope of this introduction, but has been reviewed elsewhere (Chistiakov et al., 2016; Witztum & Lichtman, 2014).

The innate immune system is normally activated through foreign materials or patterns such as exogenous pathogens. As the first line of

defence, the role of the innate immune system is to recognise such material, neutralise it through phagocytosis and also induce tissue repair (Witztum & Lichtman, 2014). An important principle of the innate immune system is the recognition of foreign and self to avoid damage to the organism's cells and tissues. Such pathogen-associated molecular patterns (PAMPs) are specific structures shared by a wide range of pathogens, including teichoic acids (gram-positive bacteria), lipopolysaccharide (LPS) (gram-negative bacteria), double-stranded RNA (certain viruses), and mannans (yeast) (Medzhitov & Janeway, 1997).

As there is evidence that infections are not the primary cause of atherogenesis (Wright et al., 2000), it has been hypothesised that the recognition of damage-associated molecular patterns (DAMPs) trigger the innate immune response in atherosclerosis. Similar to PAMPs, DAMPs are specific structures that are not recognised as endogenous but instead treated as foreign material. They are structures that are not normally accessible to the immune system, including heat shock proteins (HSPs), high-mobility group protein 1, and chemically-modified molecules such as advanced glycation end-products (Witztum & Lichtman, 2014), cholesterol crystals (Duewell et al., 2010), and mitochondrial DNA (section 1.3). For example, immunization of normocholesterolaemic rabbits with HSP such as recombinant HSP65 induced atherosclerosis (Xu et al., 1992).

DAMPs are ligands for scavenger receptors expressed on the surface of immune cells, of which ten classes have been identified so far (Prabhudas et al., 2014). Although several molecules can act as DAMPs, much of our knowledge stems from the study of OxLDL due to its major effects on

atherogenesis. For example, three of the most commonly studied scavenger receptors are scavenger receptor (SR)-A1 (SR-A1), SR-B2 [also known as cluster of differentiation 36 (CD36)], and SR-E1 [(lectin-like OxLDL receptor-1 (LOX-1)], each of which binds OxLDL (Zani et al., 2015). DAMPs are also recognised by toll-like receptors (TLRs) (Levitan, Volkov, & Subbaiah, 2010). The role of scavenger receptors and TLRs is discussed in section 1.1.3 in the context of OxLDL.

Inflammasomes are protein complexes that recognise a wide range of inflammation inducing stimuli including PAMPs and DAMPs controlling the production of cytokines such as interleukin (IL)-1β (IL1β) and IL18 (Strowig, Henao-Mejia, Elinav, & Flavell, 2012). Recognition of DAMPs by the innate immune system can lead to the activation of the NLRP3 inflammasome. The NLRP3 inflammasome then activates caspase-1, which in turn cleaves pro-IL1β to IL1β. NLRP3 expression needs to be induced by a priming signal followed by activation through a second signal. The signals priming the NLRP3 inflammasome are diverse and include ROS, proteases, monosodium urate crystals and ATP (Strowig et al., 2012; Wen, Ting, & O'Neill, 2012). For example, cholesterol crystals activate the NLRP3 inflammasome in peripheral blood mononuclear cells (PBMC) *in vitro* and also cause NLRP3-dependent inflammation *in vivo*. NLRP3 activation can regulate the inflammatory response and atherogenesis in LDL receptor-/- (LDLR-/-) mice through interleukin-1 (IL1) signalling. For example, irradiated LDLR-/- mice reconstituted with NLRP3-, apoptosis-associated speck-like protein containing a caspase activation and recruitment domain (ASC)-, or IL1α/β-deficient bone marrow have significantly reduced atherosclerotic plaque and IL18 serum

concentrations (Duewell et al., 2010). Similar results were observed after siRNA-mediated silencing of NLRP3 in ApoE-/- mice and such silencing also improved markers of plaque stability by increasing VSMC content and decreasing macrophage and lipid content (Zheng, Xing, Gong, Mu, & Xing, 2014). However, a study by a different group using ApoE-/- mice with additional knockout of the Nlrp3 inflammasome pathway, i.e, ApoE-/- Nlrp3-/-, ApoE-/- Asc-/-, or ApoE-/- caspase-1-/-, found no effects on atherogenesis after fat-feeding (Menu et al., 2011).

Nlrp3 inflammasome activation may also be relevant in human atherosclerosis. mRNA levels of Nlrp3, ASC, caspase-1, IL1β and IL18 were all increased in atherosclerotic carotid endarterectomy samples compared to healthy aortas and iliac arteries (Paramel Varghese et al., 2016). The same study found an association of single nucleotide polymorphisms (SNPs) in the downstream regulatory unit of Nlrp3 to mRNA levels in PBMCs, although there was no association between SNPs and risk of myocardial infarction.

1.1.2 Oxidative stress in atherosclerosis

It is well established that a variety of ROS, produced in vivo, have the capacity to oxidatively modify target biological molecules. Major reactive oxidants in vivo are: superoxide, hydroxyl radical, alkoxyl radical, and peroxyl radical, hydrogen peroxide, peroxynitrous acid, hypochlorous acid, and singlet oxygen (Niki, 2018). Their reaction with target molecules in turn leads to the production of hydroperoxides, hydroxyl fatty acids, isoprostane and neuroprostane, epoxides, oysterols, chlorohydrins and chlorinated compounds, nitro-compounds and importantly the oxidation of antioxidant scavengers (Niki, 2018).

There is ample evidence that oxidative damage occurs in atherosclerosis and it is thought that such modifications perpetuate the disease process. For example, the degree of lipid peroxidation correlates with the stage of the atherosclerotic lesion in human atherosclerosis (Kuhn et al., 1992). Similarly, tyrosine-nitrates (Sucu et al., 2003), and chlorinated compounds (Messner, Albert, McHowat, & Ford, 2008) are increased in human atherosclerotic plaque compared to healthy arteries. Antioxidative components such as peroxiredoxins in turn have been found to be more oxidated in murine atherosclerotic aortas compared to healthy aortas (Mayr et al., 2005).

Key players in the initiation and propagation of atherosclerosis are oxidised lipids such as OxLDL as discussed in section 1.1.3. Oxidative stress can also lead to DNA damage and may therefore facilitate atherosclerosis, which is further discussed in section 1.1.5.

Not surprisingly, the use of antioxidants in the prevention or treatment of atherosclerosis has therefore been studied extensively. However, the use of Vitamin C, Vitamin E or antioxidant cocktails, has not demonstrated any effects on cardiovascular outcomes in larger studies (Kris-Etherton et al., 2004). Sections 1.2.2 and 1.3.3 explore the role of mitochondria in the production of ROS and may offer an explanation to the lack of effect of antioxidants in the prevention of atherosclerosis.

1.1.3 Oxidised lipids and their receptors in atherosclerosis

It is widely accepted that LDL can be modified through oxidation *in vivo* resulting in increased proinflammatory and proatherogenic properties (Levitan et al., 2010). Modified LDL is often referred to as OxLDL, however, there is

great heterogeneity of *ex vivo*-derived OxLDL preparations and no clear definition of OxLDL exists. Modified LDL preparations have been arbitrarily divided into “minimally modified LDL” (mmLDL) and “extensively oxidized LDL” (OxLDL), the former being recognised by the LDL receptor but not by most of the scavenger receptors, and the latter being recognised by the scavenger receptors but not by the native LDL receptor (LDLR) (Levitan et al., 2010). To complicate matters further, the preparation of LDL forms varies between different laboratories and even with identical protocols the end-products vary considerably due to initial fatty acid composition and even antioxidant status of the original LDL (Levitan et al., 2010). The extent of oxidation of LDL is frequently reported as nmol of thiobarbituric acid-reactive substances (TBARS), determined by measurement of malondialdehyde (MDA). However, only certain lipid peroxidation products generate MDA and MDA can be generated through other mechanisms (Janero, 1990). Therefore results need to be interpreted with caution particularly when comparing TBARS levels from different laboratories.

It should be noted that despite the general acceptance of the important role of OxLDL on atherogenesis, it is not entirely clear where and to what extent LDL is oxidised *in vivo*. In addition, at least seven major compound groups in OxLDL exert biological effects on target cells and tissues, namely: phospholipid products, sphingolipid products, free fatty acid products, oxysterols, cholesteryl ester products, short-chain aldehydes (hydroxynonenal and MDA), and apo B modifications (Levitan et al., 2010). As OxLDL preparations contain many active compounds it is often unclear which of the

compounds mediate certain effects, and the effects observed can vary between groups (Levitan et al., 2010).

Macrophages express various scavenger receptors, which allow for the recognition of ligands, their uptake and subsequent degradation. Following a recent expert consensus the nomenclature of human scavenger receptors has been updated and now includes 10 classes (A-J) of scavenger receptors (Prabhudas et al., 2014). The most widely studied scavenger receptors in atherosclerosis are SR-A1, SR-B2 (formally known as CD36), and SR-E1 (LOX-1) (Zani et al., 2015). These three Scavenger receptors are all involved in the recognition and uptake of OxLDL. Binding of ligands such as modified lipids to SR-A1 can lead to either clathrin-dependent or clathrin-independent uptake and activation of p38 MAPK, JNK2 and ERK signalling, facilitating foam cell formation and apoptosis of macrophages (Ricci et al., 2004; X. D. Zhu et al., 2011). ApoE-/- mice deficient in SR-A1 have decreased atherosclerotic lesions (Suzuki et al., 1997).

Lack of SR-B2 (CD36) in human macrophages leads to reduced inflammatory signalling and nuclear factor kappa B (NFκB) activation upon OxLDL stimulation (Janabi et al., 2000). Binding to SR-B2 leads to lipid raft-mediated uptake of the ligand and also activation of p38, JNK, Fak, and Vav, affecting a wide range of responses including foam cell formation, platelet activation, apoptosis, angiogenesis, inflammation and cell adhesion and migration (Zani et al., 2015). LDLR-/- mice that are also deficient in SR-E1 (LOX-1) have reduced atherosclerosis and inflammatory NFκB signalling (Mehta et al., 2007). The effects of this scavenger receptor are mediated

through clathrin-independent uptake of Ox-LDL, which in turn activates p42/p44 MAPK, p38 MAPK and NFκB. (Zani et al., 2015).

OxLDL can also be recognised by TLRs to induce uptake. For example, mmLDL induces macropinocytosis through the TLR4 signalling complex, leading to TLR4 phosphorylation and ultimately activation of ERK1/2, Rac, Cdc42 and Rho (Choi et al., 2009). TLR2, TLR4 and TLR9 all have been implicated in the development of atherosclerosis through inflammatory signalling after binding of DAMPs such as OxLDL (Roshan, Tambo, & Pace, 2016). Interestingly, there is also interdependency of scavenger receptor and TLR signalling. For example, binding of OxLDL or beta-amyloid to SR-B2 facilitates assembly of TLR 4 and -6 heterodimers and subsequent NFκB and IL1β inflammatory signalling (Stewart et al., 2010).

Whilst the minimally modified LDL species tend to be recognised by TLR and LDL-R, the extensively oxidised LDL forms are recognised primarily by SR-A1, SR-B2 (CD36), and SR-E1 (LOX-1) (Levitan et al., 2010). There are also multiple other mechanisms of OxLDL uptake that can induce inflammatory signalling, but a review of them is beyond the scope of this report (Levitan et al., 2010).

The interaction between oxidised lipids and mitochondrial function and signalling is discussed in greater detail in section 1.3.

1.1.4 The Importance of vascular smooth muscle cell viability to determine plaque stability

VSMCs play an important role in all phases of atherosclerosis. Early hypotheses of atherogenesis suggested that in response to injury VSMCs migrate from the arterial media to the intima [reviewed in Ross (1999)]. Intimal thickening could then lead to progressive blood flow obstruction through proliferation and production of extracellular matrix. This theory is supported by observations in animal models and humans where injury through inflation of balloons or by wire leads to restenosis through neo-intimal VSMC accumulation (W. McBride, Lange, & Hillis, 1988; Steele et al., 1985). VSMCs also play a key role in inflammation and foam cell formation in atherosclerosis. For example, during early atherosclerosis VSMCs can express adhesion molecules and chemokines, which facilitate recruitment of inflammatory cells derived from the immune system to the atherosclerotic plaque (Mach et al., 1999). Furthermore, through their scavenger receptors VSMCs take up modified lipoproteins (see section 1.1.3). However, a number of studies have questioned the dogma that VSMCs are detrimental for disease progression, and instead suggest that the stability of the atherosclerotic plaque, which in turn is predominantly determined by the extracellular matrix produced by VSMCs in the fibrous cap, determines disease morbidity and mortality. This theory is supported by observations that statins, which only exert limited effects on atherosclerotic plaque size, have substantial effects on clinical outcome (M. A.-A. S. Group, 1994; S. S. S. S. Group, 1994; Weissberg, Clesham, & Bennett, 1996). Bennett's group has also shown that survival of VSMCs is crucial for fibrous cap stability (Clarke et al., 2006). In this study,

selective induction of VSMC apoptosis in ApoE-/- mice via the diphtheria toxin receptor, caused thinning of the fibrous cap, loss of extracellular matrix, accumulation of cell debris and significant intimal inflammation (Clarke et al., 2006).

We have recently shown that premature senescence of VSMCs promotes atherosclerosis (J. Wang et al., 2015). Overexpression of telomeric repeat binding factor 2 (TRF2), an important shelterin protein protecting telomere structure, decreases VSMCs senescence, reduces DNA damage, facilitates DNA repair, and is protective in ApoE-/- fat-fed mice. In contrast, a point mutation in TRF2, causing a substitution of threonine residue 188 to alanine (T188A) in the protein, results in constitutively inactive TRF2, promotes atherosclerosis and leads to multiple features typical of vulnerable lesions.

These observations support the theory that exacerbated cell death and senescence of VSMCs determines clinical disease. The mechanisms leading to VSMC senescence and apoptosis are numerous and beyond the scope of this introduction. However, one of the mechanisms that may be particular relevant is ROS-mediated accumulation of DNA damage in the progression of atherosclerosis as discussed in section 1.1.5.

The precursor lesion for plaque rupture is the ‘thin-cap fibroatheroma’ where a fibrous cap of less than 65 μm comprising VSMCs and matrix separates a relatively large necrotic core from the arterial lumen (Burke et al., 1997; Calvert et al., 2011). Such thin-cap fibroatheromata might not only be caused by excessive VSMC apoptosis but also by limited proliferation or senescence. Identifying targets to improve VSMC survival and function and

thereby improving atherosclerotic plaque stability may offer future therapeutic strategies. It is therefore important to better understand the biology of atherosclerotic plaques, particularly the cap region, to help identify pathways that determine VSMC health.

1.1.5 DNA damage in atherosclerosis

DNA damage is present in atherosclerotic plaques as well as in circulating cells from patients with coronary artery disease. For example, genetic instability correlates with coronary artery disease severity and there is also evidence of chromosome abnormalities including loss of the Y-chromosome, XXY karyotype and trisomy 7, 10 and 18 in atherosclerotic plaques (Botto et al., 2001; Casalone et al., 1991; J. Mercer, Mahmoudi, & Bennett, 2007). VSMCs derived from atherosclerotic plaques have increased levels of double-stranded DNA breaks compared to VSMCs from healthy arteries, and increased accumulation of γH2AX and ataxia telangiectasia–mutated (ATM) proteins, markers of DNA damage and repair, respectively (Mahmoudi et al., 2008), while statins increase DNA repair in VSMCs mediated through Nijmegen breakage syndrome (NBS)-1 and the human double minute protein (Hdm2) (Mahmoudi et al., 2008). In addition, ApoE-/- mice heterozygous for ATM (ApoE-/- ATM+/-) have accelerated atherosclerosis as well as metabolic changes and mitochondrial dysfunction (J. R. Mercer et al., 2010), and VSMCs derived from human atherosclerotic plaques not only have increased ATM and γH2AX, but also decreased telomeric repeat-binding factor-2 (TRF2) expression (J. Wang et al., 2015). Upon irradiation, TRF2 is rapidly phosphorylated in an ATM-dependent

manner and localises to sites of DNA damage (H. Tanaka et al., 2005). Overexpression of TRF2 in mouse VSMCs in turn reduces DNA damage and decreases senescence with beneficial effects on measures of atherosclerotic plaque stability such as the cap/core ratio (J. Wang et al., 2015). There are also reports of loss of heterozygosity and microsatellite instability in atherosclerotic plaques, prompting comparisons with neoplastic diseases (Hatzistamou, Kiaris, Ergazaki, & Spandidos, 1996). Indeed, clonal expansion of a low proportion of VSMC determines accumulation after vascular injury and in murine atherosclerosis (Chappell et al., 2016). However, although somatic mutations are present in VSMC forming plaques (Casalone et al., 1991), it is currently unclear whether this is the cause of proliferation (Chappell et al., 2016) and atherosclerotic lesions do not become cancerous.

Thus there is compelling evidence that DNA damage occurs in atherosclerosis and that this can perpetuate disease progression at least in mouse models of atherosclerosis. As DNA mutations occur more frequently in mtDNA compared to nuclear DNA (see also 1.2.1) various groups have investigated the role of mtDNA mutations in atherosclerosis. This is further discussed in section 1.3.2.

1.1.6 Animal models of atherosclerosis

The study of atherosclerosis has been greatly facilitated by the use of animal models. In humans the disease process takes many decades and one of the challenges has therefore been to accelerate the progression of atherogenesis in any animal model. As hypercholesterolaemia and

hyperlipidaemia are considered main risk factors for atherosclerosis, strategies frequently revolve around increasing plasma lipid levels in animals.

The most commonly used animal models for atherosclerosis are in decreasing order: genetically manipulated mice with or without additional fat-feeding, hypercholesterolaemic rabbits, pigs and non-human primates (Getz & Reardon, 2012). The advantages of larger animals, particularly pigs and primates, are that the lipoprotein profile has more similarities with humans, there is greater tissue availability and non-invasive measurements can be taken. Furthermore, larger animals are also more appropriate to study atherosclerosis affecting the coronary arteries. However, such animal models are expensive and are generally less suitable for genetic modification limiting their use in the study of atherosclerosis (Getz & Reardon, 2012).

Currently, mice remain the most widely studied animals in atherogenesis, particularly apolipoprotein E-/- (ApoE-/-) and LDL receptor-/- (LDLR-/-) mice.

1.1.6.1 ApoE-/- mouse model

Apolipoprotein E (ApoE), produced primarily by the liver, is a major constituent of lipoproteins, and plays an important role in their clearance. Two groups simultaneously developed ApoE-/- mice demonstrating hypercholesterolaemia and atherosclerosis (Plump et al., 1992; S. H. Zhang, Reddick, Piedrahita, & Maeda, 1992). These mice are characterised by increased hypercholesterolaemia (494 mg/dl) compared to control animals (60 mg/dl), which can be further increased through a high-fat diet (1821 mg/dl) (Plump et al., 1992). Although human atherosclerosis is largely mediated

through LDL, the hypercholesterolaemia in these mice is largely due to intermediate density lipoproteins (IDL) and very low-density lipoproteins (VLDL). ApoE-/- mice develop atherosclerosis throughout the arterial tree but there is a predilection for the aortic root and the lesser curvature of the aortic arch as well as certain areas of the more distal aorta primarily at arterial branch points (Nakashima, Plump, Raines, Breslow, & Ross, 1994). There are, however, limitations to this model. ApoE also influences macrophage biology, immune function and adipose tissue biology therefore affecting atherosclerosis through mechanisms other than hypercholesterolaemia (Getz & Reardon, 2012).

1.1.6.2 LDLR-/- mice

Knockout of the LDL receptor (LDLR) leads to significantly increased plasma cholesterol levels in mice (Ishibashi et al., 1993). LDLR-/- mice need to be aged considerably (>1 year) to develop atherosclerosis if fed a normal chow or alternatively need to be kept on a high-fat diet (Getz & Reardon, 2012). As LDLR knock-out has fewer off-target effects, this model may be more appropriate in certain situations, particularly when bone marrow transplantation models are used.

Thus, different animal models of atherosclerosis have their limitations. Caution in the interpretation of results is needed, particularly when trying to draw conclusions about disease mechanisms in humans.

1.2 Mitochondria

Mitochondria are thought to have evolved through symbiosis between prokaryotes and primitive eukaryotic cells (Sagan, 1967). Mitochondria have long been regarded as the “powerhouses” of cells, providing energy in the form of ATP for cellular function. However, a more nuanced view of mitochondrial function has developed, suggesting that mitochondria are important for a variety of cellular processes, including regulation of cellular metabolism, cell cycle regulation, cellular signalling, regulation of cell survival, and cell death (H. M. McBride, Neuspiel, & Wasiak, 2006; Murphy, 2009).

1.2.1 Mitochondrial DNA and its maintenance

The human mitochondrial genome is a circular double strand DNA molecule of 16,569 base pairs encoding for some but not all of the proteins of the electron transfer chain (ETC) and ATP synthase as well as rRNAs and tRNAs required for mitochondrial translation. The proteins for both replication and transcription of mtDNA are encoded in nuclear DNA and imported into the mitochondrial matrix via specialised transport mechanisms. Importantly, mtDNA is not packaged by histones, instead mammalian cells can contain thousands of mtDNA molecules distributed over several hundred nucleoids (Falkenberg, Larsson, & Gustafsson, 2007).

mtDNA is prone to mutations causing maternally-inherited mitochondrial myopathies (Holt, Harding, & Morgan-Hughes, 1988; Wallace et al., 1988). However, even healthy tissue from human adults contains mtDNA mutations (Cortopassi & Arnheim, 1990). The susceptibility of mtDNA to mutations has been explained by its close proximity to the inner mitochondrial

membrane and therefore potentially high exposure to ROS, due to lack of protective histones, and the lack of some DNA damage repair mechanisms (Graziewicz, Longley, & Copeland, 2006). For example, oxidative modification is not limited to nuclear DNA but also affects mtDNA forming 8-hydroxydeoxyguanosine (8-OH-dG) (Hayakawa, Torii, Sugiyama, Tanaka, & Ozawa, 1991). Such modifications are associated with ageing and induction of ROS-mediated oxidative DNA damage with doxorubicin exacerbates the age-related decline in electron transfer chain activity (Yamada, Sugiyama, Kosaka, Hayakawa, & Ozawa, 1995). Furthermore, not only oxidative damage can be detected in ageing tissue, but also deletions, as exemplified in studies on human heart and brain tissues (Cortopassi & Arnheim, 1990). It is well established that there is heteroplasmy, i.e. the coexistence of mutated and normal mtDNA, within tissues and it is thought that certain thresholds of pathogenic mtDNA are required to cause dysfunction of the electron transfer chain (Corral-Debrinski, Horton, et al., 1992; Hayashi et al., 1991; Larsson, 2010).

Several pathways have evolved that preserve the integrity of mtDNA and therefore mitochondrial function: 1) relatively faithful DNA replication, transcription and translation; 2) mtDNA damage repair mechanisms; 3) redox homeostasis limiting the damaging effects of ROS (see also section 1.2.2); 4) mitochondrial fission and fusion and mitochondrial autophagy or mitophagy of damaged mitochondria (see also section 1.2.3.1) (Scheibye-Knudsen, Fang, Croteau, Wilson, & Bohr, 2015).

Faithful replication of mtDNA requires the assembly of the minimal replisome consisting of the mtDNA polymerase γ (PolG) with both its subunits,

PolGA and PolGB (Carrodeguas, Theis, Bogenhagen, & Kisker, 2001), as well as the Twinkle helicase (Twinkle) and mitochondrial single-stranded binding protein (mtSSB) (Korhonen, Pham, Pellegrini, & Falkenberg, 2004). Mutations in the proof-reading domain of PolG (D257A) in PolG-/- or “mutator mice” lead to accumulation of mtDNA mutations, and increased hydrogen peroxide (H_2O_2) production at later time points (Logan et al., 2014). PolG-/- mice have shorter life spans and are more prone to atherosclerosis (Trifunovic et al., 2004; E. Yu et al., 2013).

Twinkle is essential for mouse embryonic development but conditional knockout of Twinkle has been achieved causing severe mtDNA loss in heart and skeletal muscle (Milenkovic et al., 2013). In contrast, transgenic overexpression of Twinkle in mice (Tw+) leads to increased mtDNA copy number in various tissues that does not affect mouse development, at least until 16 months of age (Tyynismaa et al., 2004). Twinkle overexpression can ameliorate pathological remodelling after myocardial infarction (MI) in mice (A. Tanaka et al., 2013) and protects superoxide dismutase-deficient mouse cardiomyocytes from increased levels of ROS (Pohjoismaki et al., 2013). Increased mtDNA copy number is also protective against volume overload-induced heart failure independently of the function of the electron transfer chain (ETC) (Ikeda et al., 2015). The authors of this study demonstrate that Twinkle overexpression reduces mitochondrial-derived ROS production and activation of matrix metalloproteinases 2 and 9 (MMP2, MMP9), all of which are known to facilitate heart failure. However, the mechanisms by which Twinkle overexpression protects from damaging ROS production are not completely understood.

Although initial evidence suggested that mitochondria lack mtDNA repair capacity (Clayton, Doda, & Friedberg, 1974) it is now commonly accepted that mitochondria have a functioning base-excision repair mechanism, but are deficient in nucleotide excision-repair and mismatch repair (Bogenhagen, 1999). Other repair mechanisms such as homologous recombination and non-homologous end joining have so far not been described in mitochondria (Larsson, 2010). The paucity of mtDNA repair mechanisms combined with the frequency of mtDNA mutations underscores the importance of other mechanisms to maintain mtDNA integrity. These mechanisms include tight regulation of ROS through buffering as discussed in 1.2.2 and mitochondrial homeostasis as discussed in 1.2.3.

1.2.2 The electron transport chain, reactive oxygen species and redox signalling

Reactive oxygen species have long been considered as a damaging side product of oxidative phosphorylation, however a more nuanced view of the biological significance of ROS has evolved (Collins et al., 2012). Mitochondria are an important source of cellular ROS, although other cellular oxidoreductases are also able to produce ROS (Murphy, 2009). Superoxide (O_2•−) is the proximal ROS generated within mitochondria through a one-electron reduction of O_2 (Murphy, 2009). In mammalian cells mitochondrial complexes I and III are thought to be the main sources of O_2•− but there are also others (Chouchani, Methner, et al., 2014; Murphy, 2009). Figure 1-2 summarises reactions of the electron transport chain and indicates origins of mitochondrial ROS.

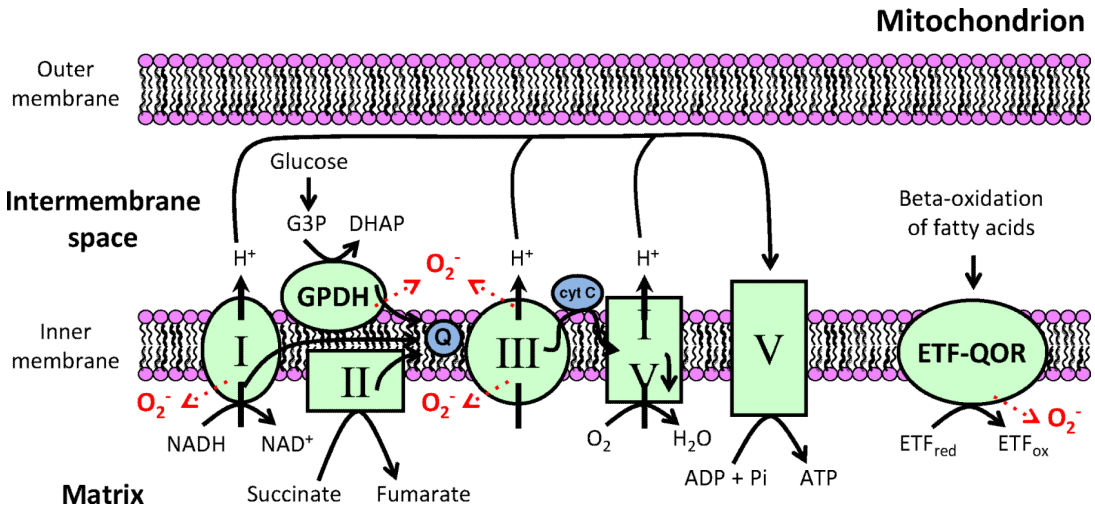

Figure 1-2 The electron transport chain and sources of mitochondrial ROS

Reproduced from Pelletier, Lepow, Billingham, Murphy, and Siegel (2012): In the electron transport chain, complex I (NADH dehydrogenase) and complex III (coenzyme Q: cytochrome c – oxidoreductase) are the main sources of superoxide. Glycerol-3-phosphate dehydrogenase (GPDH) and the electron transferring flavoprotein ubiquinone oxidoreductase (ETF-QOR) can also produce superoxide. G3P - Glycerol-3-phosphate; DHAP - dihydroxyacetone phosphate; cyt C - cytochrome C; I-IV - electron transfer complexes I-IV; V - ATPase; Q - coenzyme Q/ubiquinone.

O_2•− is rapidly converted to hydrogen peroxide (H_2O_2) by manganese superoxide dismutase (MnSOD), which is highly expressed in the mitochondrial matrix (Balaban, Nemoto, & Finkel, 2005). H_2O_2 can readily pass through mitochondrial membranes and although it is not the most reactive ROS, it is considered to be the main ROS involved in redox signalling by mitochondria. O_2•− can also form the highly reactive peroxynitrite (ONOO−) through reaction with nitric oxide (NO•) (Collins et al., 2012).

Within the mitochondrial matrix there is a high concentration of peroxiredoxins (Prxs) which effectively scavenge H_2O_2, and it has been calculated that around 90% of H_2O_2 generated in the mitochondrial matrix

targets Prx3, the most prominent mitochondrial isoform (Cox, Winterbourn, & Hampton, 2010). Other regulators of H_2O_2 include glutathione peroxidase 1 (Gpx1), which uses mitochondrial glutathione (GSH) as a means of recycling the enzyme (Collins et al., 2012).

Redox processes can cause reversible alterations of critical cysteine residues on signalling proteins, including sulphenylation, S-nitrosation/S-nitrosylation, glutathionylation and formation of disulphide bonds (Chouchani, James, Fearnley, Lilley, & Murphy, 2011; Collins et al., 2012; Hurd, James, Lilley, & Murphy, 2009; Murphy, 2012), altering their activity within mitochondria and cells. For example, redox modification of complex I of the electron transport chain through reversible nitrosation can reduce its activity *in vivo* (Chouchani et al., 2013). Redox signalling by mitochondria has been implicated in a variety of biological processes including oxygen sensing, differentiation, immunity, mitochondrial function, hormone signalling and regulation of life span [reviewed in Collins et al. (2012)].

1.2.3 Mitochondrial homeostasis

Mitochondria (and mtDNA) are prone to oxidative damage and therefore need mechanisms to maintain homeostasis to avoid dysfunction. mtDNA repair mechanisms have already been discussed in section 1.2.1. Here I will focus on mitochondrial dynamics and particularly autophagy of mitochondria (mitophagy) (section 1.2.3.1) and mitochondrial biogenesis (section 1.2.3.2).

1.2.3.1 Mitochondrial dynamics and mitophagy

Through fission and autophagy dysfunctional mitochondria can be degraded to preserve a pool of functioning mitochondria. Fusion of mitochondria is thought to facilitate communication between mitochondria and thereby access to proteins only encoded in the mitochondrion, and to buffer transient mitochondrial defects. In contrast, fission leads to fragmentation of mitochondria, which can segregate dysfunctional mitochondria, which then undergo mitochondrial autophagy or mitophagy (Friedman & Nunnari, 2014).

If mitochondrial fusion is disrupted this leads to mitochondrial segregation and dysfunction probably due to loss of functional mtDNA (H. Chen, Chomyn, & Chan, 2005). Thus mitochondrial dynamics need to be highly regulated to avoid dysfunctional mitochondria. Mitochondrial fission and fusion are controlled by the dynamin-related proteins (DRPs). Whilst fission is mediated by DRP1 and FIS1 in mammals (Smirnova, Shurland, Ryazantsev, & van der Bliek, 1998; Twig et al., 2008), fusion requires the coordinated action of the DRPs MFN1/MFN2 and OPA1 (H. Chen et al., 2005). Mitochondrial membrane potential controls the cleavage of OPA1 mediated by the zinc metalloprotease OMA1 (Head, Griparic, Amiri, Gandre-Babbe, & van der Bliek, 2009). The presence of the long and short forms of OPA1 in turn are important to determine mitochondrial shape as illustrated in Figure 1-3, adapted from (Friedman & Nunnari, 2014).

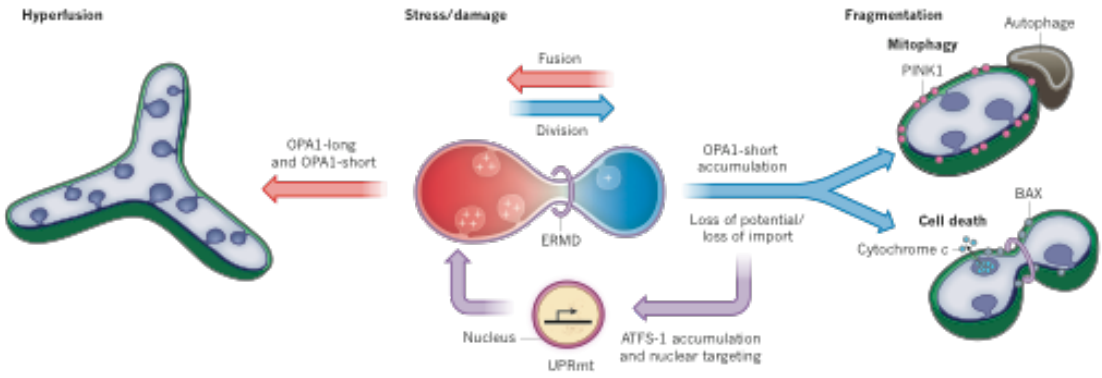

Figure 1-3 Mitochondrial stress responses [reproduced from Friedman and Nunnari (2014)]

Stress or damage to mitochondria can lead to a loss of mitochondrial membrane potential (blue) activating the unfolded protein stress response pathway (UPRmt) through accumulation of the activating transcription factor associated with stress (ATFS1). This in turn activates mitochondrial repair pathways and facilitates metabolic adaptation. Loss of mitochondrial membrane potential can also cause OPA1 –short accumulation leading to attenuated mitochondrial fusion, ER-mediated mitochondrial division (ERMD), fragmentation and mitophagy or cell death. Mitochondrial damage leading to OPA1-short and OPA1-long dependent hyperfusion is thought to transiently buffer mitochondrial dysfunction (Friedman & Nunnari, 2014).

Autophagy has been divided into non-selective autophagy, for example during energy deprivation to preserve nutrient and building blocks, and cargo-specific autophagy. The latter allows for removal of redundant or damaged organelles and depending on the organelle involved has been termed pexophagy (peroxisomes), ribophagy (ribosomes) or, when mitochondria are the target, mitophagy (Youle & Narendra, 2011). Much of our knowledge about mitophagy is derived from investigations in yeast. One of the key proteins mediating mitophagy in yeast is Atg32, located on the outer mitochondrial membrane and interacting with Atg8 and Atg11 (Okamoto, Kondo-Okamoto, & Ohsumi, 2009). Atg32 can directly bind to Atg8 or indirectly through binding to Atg11 leading to recruitment into the

autophagosome which then fuses with lysosomes to form the autophagolysosome (Youle & Narendra, 2011).

In mammalian cells, fission and fusion are key steps prior to mitophagy. Using a photolabeling strategy of individual mitochondria, Twig et al. (2008) demonstrated frequent cycles of fission and fusion in mammalian cells. However, fission produced daughter mitochondria, with differing membrane potential. One of the daughter mitochondria became hyperpolarised, whilst the other became depolarised after the fission event. Interestingly, daughter mitochondria with a normal membrane potential had a higher probability of subsequent fusion then those with a depolarised membrane potential, which also have reduced expression of OPA1. Inhibition of fission (DRP1 and FIS1) also decreases mitophagy and results in the accumulation of damaged mitochondrial proteins. In reverse, overexpression of OPA1 reduces mitophagy, suggesting that mitochondrial fission is required for mitophagy (Twig et al., 2008).

Following fission dysfunctional mitochondria need to be targeted for degradation. The mammalian orthologue of Atg8 is LC3, of which two forms exist, LC3-I, the cytosolic form, and LC3-II, the membrane-bound form. LC3 mediates transfer of cargo to the autophagosome after starvation (Kabeya et al., 2000), but although the LC3 pathway is involved in the degradation of mitochondria, this form of autophagy is not specific to this organelle (Youle & Narendra, 2011).

The most extensively studied pathway for mitophagy is mediated by PTEN-induced putative kinase protein 1 (PINK1) and the E3 ubiquitin ligase parkin. Interestingly, mutations in either of the corresponding genes lead to

early-onset Parkinson's disease (Kitada et al., 1998; Valente et al., 2004). Removal of the *Drosophila melanogaster* PINK1 homologue (CG4523) leads to male sterility, apoptosis in the muscle, dopaminergic neuronal degeneration, locomotive defects and abnormal mitochondrial morphology as well as increased sensitivity to oxidative stress (Clark et al., 2006; Park et al., 2006). Similar phenotypes are observed after parkin loss, but the phenotype of double mutants is identical to single gene mutants, suggesting that PINK1 and parkin act in the same pathway. Transgenic parkin overexpression rescues parts of the effect of PINK1 loss indicating that parkin acts downstream of PINK1.

In functional mitochondria, PINK1 is degraded by the mitochondrial protease preselin-associated rhomboid-like protein (PARL). When the mitochondrial inner membrane becomes depolarised, this degradation is inhibited and PINK1 accumulates on the mitochondrial outer membrane (MOM) where it can recruit parkin (Jin et al., 2010). Subsequently further proteases have been identified that mediate PINK1 degradation in polarised mitochondria such as mitochondrial processing peptidase (MPP), m-AAA and ClpXP (Greene et al., 2012). A cleavage product of PINK1, if not degraded by the cytosolic proteasome, binds to parkin thereby inhibiting its translocation to mitochondria (Fedorowicz et al., 2014). Depolarisation of the mitochondrial inner membrane (MIM) leads to PINK1 autophosphorylation at Ser228 and Ser402 and mutations of these sites inhibits parkin recruitment (Okatsu et al., 2012). Activated PINK1 also phosphorylates parkin at Ser65 (Kondapalli et al., 2012) and ubiquitin at Ser65 (Koyano et al., 2014) thereby activating parkin activity. Activated parkin ubiquitinates several MOM proteins leading to

the recruitment of autophagy receptors such as Nucleoporin 62/sequestosome 1 (p62/SQSTM1), the neighbour of BRCA 1 (NBR1), and optineurin (Ploumi, Daskalaki, & Tavernarakis, 2017)

Activation of the PINK1/parkin pathway also activates mitochondrial fission involving mitofusins (Poole et al., 2008; Ziviani, Tao, & Whitworth, 2010), indicating reciprocal interaction between mitochondrial morphology and mitophagy.

1.2.3.2 Mitochondrial biogenesis

Mitochondrial biogenesis is closely linked to mitochondrial clearance allowing maintenance of mitochondrial homeostasis. Since approximately 90% of mitochondrial proteins are nuclear-encoded, coordinated transcription and translation of both nuclear and mitochondrial genes are important for mitochondrial function (Picca & Lezza, 2015; Ploumi et al., 2017). For that purpose mitochondria employ protein import systems formed by the translocase of the outer mitochondrial membrane protein complex (TOM), sorting and assembly machinery (SAM) complex, and translocase of the inner mitochondrial membrane protein complex (TIM) (Ploumi et al., 2017). Imbalance in electron transport complex composition in turn leads to activation of mitochondrial degradation processes such as mitophagy, described in section 1.2.3.1.

One of the key signalling pathways in energy metabolism is cAMP response element-binding protein (CREB) activation leading to peroxisome proliferator-activated receptor-γ coactivator-1α (PGC-1α) -mediated signalling (Herzig et al., 2001). It is thus not surprising that PGC-1α affects transcription

of both nuclear and mitochondrial DNA to allow co-ordinated mitochondrial biogenesis. Some of the main factors involved in mitochondrial biogenesis and regulators of mitochondrial integrity are discussed below.

1.2.3.2.1 PGC-1α

Energy demand in cells and tissues can vary substantially and mitochondria need to be able to adapt to changing ATP requirements. A master regulator of metabolic programmes is the family of peroxisome proliferator-activated receptor γ coactivator 1 (PGC-1) and these proteins are highly expressed in tissues that are metabolically active such as brown adipose tissue (BAT), heart, skeletal muscle, kidney, and brain (Handschin & Spiegelman, 2006). Ectopic expression of PGC-1α in C2C12 myotubes increases oxygen consumption through upregulation of the expression of genes involved in oxidative phosphorylation, and mtDNA content was increased approximately two-fold (Wu et al., 1999). Mechanistically, PGC-1α expression upregulates nuclear respiratory factor 1 (NRF-1) and mitochondrial transcription factor A (TFAM), two important transcription factors for mitochondrial function (Wu et al., 1999). PGC-1α also signals through NRF-2 and oestrogen-related receptor α (ERRα). Other members of the PGC-1 family sharing a similar modular structure include PGC-1β and PGC-1-related coactivator (PRC), however currently PGC-1α remains the most thoroughly studied member (Handschin & Spiegelman, 2006). PGC-1α transcription itself is regulated by a wide array of stimuli including AMPK, activity levels, calorie restriction, NO, diabetes, and hypoxia (Handschin & Spiegelman, 2006; L. Zhu et al., 2010).

1.2.3.2.2 Sirtuin-1

Sirtuins are highly conserved NAD(+)-dependent deacetylases that regulate lifespan in lower organisms and have been connected to cellular stress resistance, genomic stability, tumourigenesis and energy metabolism in mammalian cells (Finkel, Deng, & Mostoslavsky, 2009). Sirtuin-1, the best studied of the sirtuin family members, acts as an intracellular energy sensor and is activated by an increased AMP/ATP ratio through AMPK and NAD+/NADH signalling (Canto et al., 2009). The most frequently studied targets of sirtuins are histones (Triolo & Sternglanz, 1996), p53 (Vaziri et al., 2001), forkhead proteins (Brunet et al., 2004), E2F (C. Wang et al., 2006) and PGC-1 (Nemoto, Fergusson, & Finkel, 2005) (Figure 1-4). Importantly, PGC-1α is a major deacetylation target of sirtuin-1, regulating the mitochondrial response to nutrient deprivation, and sirtuin-1 may also affect mitochondrial function through modulation of autophagy (I. H. Lee et al., 2008).

Work from our laboratory has shown that sirtuin-1 expression is reduced in human atherosclerotic plaques compared to healthy aortas or internal mammary arteries (Gorenne et al., 2013). Furthermore, inhibition of sirtuin-1 in VSMCs reduced DNA repair and induced apoptosis through reduced activation of the Nijmegen Breakage Syndrome-1 repair protein, and VSMC-specific deletion of sirtuin-1 increased atherosclerosis in ApoE-/- mice (Gorenne et al., 2013). However, the effects of sirtuin-1 on human atherosclerosis are less clear. Resveratrol, a small molecule activator or sirtuin-1, can prolong life-span in yeast (Howitz et al., 2003), but clinical studies have so far failed to show convincing beneficial effects on atherosclerosis (Zordoky, Robertson, & Dyck, 2015).

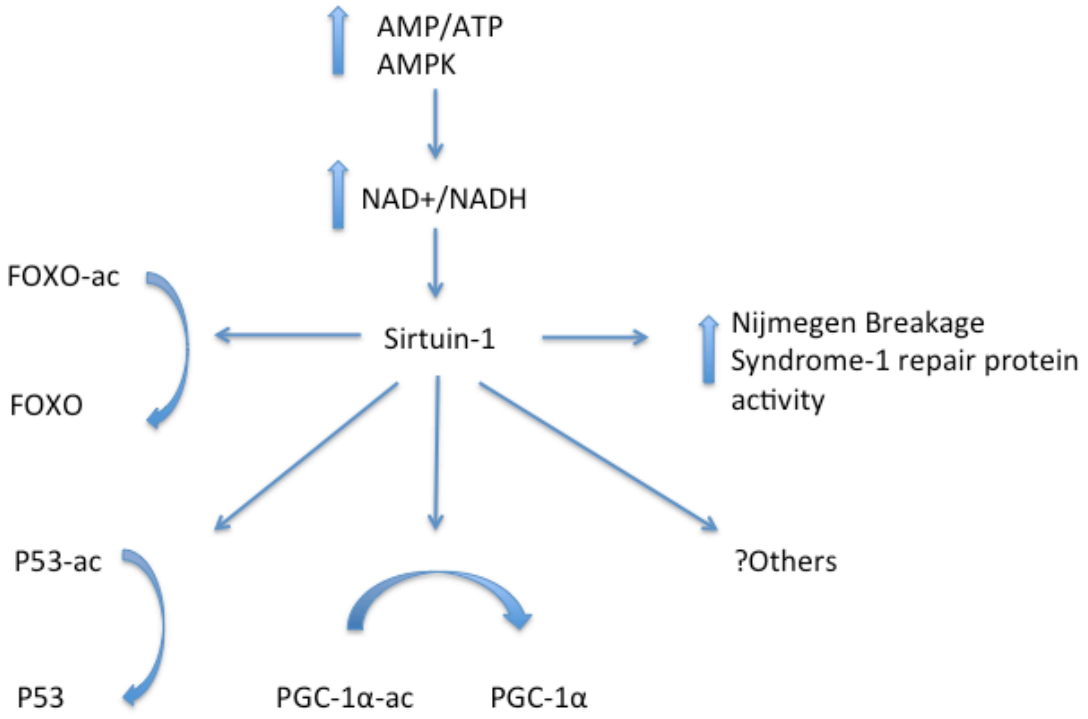

Figure 1-4 Schematic of sirtuin-1 regulation and signalling

The nicotinamide adenine dinucleotide (NAD+/NADH) dependent histone deacetylase sirtuin-1 has many targets other than histones. Adenosine triphosphate (ATP), adenosine monophosphate (AMP), Forkhead box O3 (FOXO3), tumour protein p53 (p53), acetylation (ac).

1.2.3.2.3 Mitochondrial transcription factor A

PGC-1α activation leads to the expression of mitochondrial proteins including TFAM and the mitochondrial transcription factors B1 and B2 (TFB1M and TFB2M) (Picca & Lezza, 2015). TFAM has not only been implicated in mtDNA transcription but is also an important regulator of mtDNA copy number (M. I. Ekstrand et al., 2004). Nils-Göran Larsson's group has overexpressed human TFAM in mice and demonstrated a direct proportionality between TFAM levels and mtDNA copy number without affecting respiratory enzyme activity or mitochondrial volume density (M. I.

Ekstrand et al., 2004). Overexpression of TFAM decreases mitochondrial-derived ROS and leads to upregulation of matrix metalloproteinases -2 and -9, thereby attenuating volume overload-induced concentric cardiac hypertrophy (Ikeda et al., 2015). Furthermore, TFAM has also been implicated in mitochondrial base-excision repair (Canugovi et al., 2010) highlighting the importance of this protein in mtDNA regulation.

1.2.3.2.4 Twinkle helicase

Twinkle helicase (Twinkle) and DNA polymerase γ (PolG) as well as mtSSB form the minimal replisome required for replication of mammalian mtDNA. Twinkle is essential for mouse embryonic development and is thought to be the only mammalian mtDNA helicase as conditional knockout leads to significant mtDNA depletion in the heart and skeletal muscle of mice (Milenkovic et al., 2013).

Transgenic mice overexpressing Twinkle have increased mtDNA copy number (Tyynismaa et al., 2004) and Twinkle overexpression protects Sod2+/- mice against superoxide-induced cardiomyopathy (Pohjoismaki et al., 2013). Interestingly the mtDNA mutation load is significantly reduced in transgenic Twinkle/Sod2+/- mice compared to Sod2+/- mice suggesting that increased Twinkle availability improves mtDNA integrity (Pohjoismaki et al., 2013). The exact mechanism of reduced mtDNA mutation load however is not understood. Nevertheless, since mtDNA integrity is perturbed in many diseases, manipulation of mtDNA homeostasis could provide interesting therapeutic targets for such diseases.

1.2.3.2.5 DNA polymerase γ

As described above, PolG forms part of the minimal replisome required for mammalian mtDNA replication. The 3'-5' exonuclease activity of PolG, necessary for proof-reading newly synthesised mtDNA, has been ablated by a mutation (D257A) (Trifunovic et al., 2004). "Mutator mice" or "PolG-/- mice" were generated that have increased mitochondrial point mutations and deletions and are characterised by reduced lifespan and evidence of premature aging such as osteoporosis, increased kyphosis, weight loss, anaemia, reduced subcutaneous fat and cardiomegaly. Interestingly, during aging these mice have increased levels of mitochondrial H_2O_2 as measured by the MitoP/MitoB ratio (Logan et al., 2014).

1.3 Evidence for mitochondrial involvement in atherosclerosis

Despite the increasing interest in the role of mitochondria in atherosclerosis, much of the data available to date is correlative and a causative role of mitochondrial dysfunction in atherogenesis remains elusive. Because ROS cause modifications of LDL forming OxLDL, it is frequently assumed that dysfunctional mitochondria influence this disease process. The paucity of data may in part be explained by a lack of tools to manipulate mitochondrial biology *in vivo* and specifically in certain tissues or cell types. In the following section I will review the data supporting a link between mitochondrial dysfunction and atherosclerosis.

1.3.1 Mitochondria and endothelial dysfunction

Endothelial dysfunction is considered an early event in the pathogenesis of atherosclerosis (Ross, 1999) (section 1.1). Many atherosclerotic triggers such as fatty acids (Du et al., 2006), hyperglycaemia (T. Yu, Robotham, & Yoon, 2006) and tobacco smoke (Vayssier-Taussat et al., 2001) cause altered mitochondrial physiology or production of ROS in endothelial cells (ECs) [reviewed in (Dromparis & Michelakis, 2013)].

ROS derived from mitochondria in turn lead to oxidation of LDL at least *in vitro* (Mabile et al., 1997). There is further evidence that electrophilic lipids but not non-electrophilic lipids accumulate in mitochondria and that this accumulation correlates with increased ROS production (Landar et al., 2006). This in turn could fuel a vicious circle of OxLDL formation and mitochondrial dysfunction (Dromparis & Michelakis, 2013).

OxLDL can stimulate adhesion of monocytes to endothelial cells (Berliner et al., 1990) through upregulation of adhesion molecules on both monocytes and ECs (Levitan et al., 2010; Schwartz et al., 1994). OxLDL binding to the lectin-like OxLDL receptor 1 (LOX-1, SR-E1) of endothelial cells induces dose-dependent intracellular ROS and subsequent NFκB activation (Cominacini et al., 2000). Interestingly, decreasing mitochondrial ROS through inhibition of complex II, uncoupling of mitochondria, or by scavenging through the MnSOD system, reverses hyperglycaemia-induced activation of protein kinase C, formation of advanced glycation end-products and activation of NFκB in ECs (Nishikawa et al., 2000).

Endothelial dysfunction is at least in part determined by the reduced bioavailability of NO. Interestingly, administration of MitoQ, an antioxidant

targeted to mitochondria through the lipophilic cation triphenylphosphonium (TPP), restores the *ex vivo* endothelium-dependent dilatation in aged mice through improving NO bioavailability by decreasing superoxide production (Gioscia-Ryan et al., 2014).

1.3.2 Mitochondrial DNA damage and atherosclerosis

Although they were not directly studying the vasculature, but instead heart tissues from individuals with coronary artery disease, Corral-Debrinski, Shoffner, Lott, and Wallace (1992) found that mtDNA damage correlates with age and atherosclerosis. Interestingly, increased mtDNA damage was present in the left ventricle but not the right. Energy expenditure of the left ventricle may be more susceptible to nutrient depletion from ischaemic heart disease, which as the authors suggest could lead to reactive oxygen species production during reperfusion. This theory is plausible and supported by work in the Murphy laboratory demonstrating that succinate, accumulates during ischaemia, is rapidly consumed upon reperfusion through retrograde electron transport (RET) at complex I, generating large quantities of ROS (Chouchani, Pell, et al., 2014).

However, these studies have examined cardiac tissue rather than vascular tissue. The first studies investigating the relationship between reactive oxygen- and nitrogen species and mtDNA damage and function in vascular cells were in Marschall Runge's laboratory. Cultured human aortic VSMCs and human umbilical vein endothelial cells (HUVEC) were treated with H_2O_2 or ONOO- and mtDNA and nuclear DNA damage assessed by qPCR. The assay used compares the relative efficiency of replication of a

long DNA segment compared to a short DNA segment, based on the principle that oxidative damage to DNA will stall the replication fork. Damage in the long segment normalised to the short segment, which statistically has a much smaller chance of oxidative DNA damage, allows for quantification of either mitochondrial or nuclear DNA damage. The authors show that both H_2O_2 and ONOO- induce more damage in mtDNA compared to nuclear DNA, and that damage occurs in both endothelial cells and VSMCs (Ballinger et al., 2000). Furthermore, mtDNA damage was reflected in reduced mitochondrial RNA and mitochondrial protein synthesis, as well as reduced ATP content (Ballinger et al., 2000). Subsequently this group demonstrated that mtDNA damage precedes atherosclerosis in ApoE-/- mice, that mtDNA damage at later time points correlates with the degree of atherosclerosis, and mice lacking mitochondrial MnSOD have increased levels of ROS and increased atherosclerosis (Ballinger et al., 2002). Our group has demonstrated that ApoE-/- mice heterozygous for the protein kinase ataxia telangiectasia mutated (ATM) (ApoE-/- ATM+/-) have increased nuclear DNA damage but also increased mtDNA damage, as well as reduced oxidative phosphorylation and altered metabolism similar to that occurring during the metabolic syndrome in humans. This phenotype was also associated with increased atherosclerosis (J. R. Mercer et al., 2010). Treatment with MitoQ rescued features of the metabolic syndrome and reduced the monocyte content of plaques in these mice (J. R. Mercer et al., 2012). Similarly, PolG-/- mice crossed with ApoE-/- mice (PolG-/- ApoE-/-) have increased mtDNA damage, mitochondrial dysfunction, and accelerated atherosclerosis compared to ApoE-/- mice (E. Yu et al., 2013). Similar to the study by Ballinger et al.

(2002), this work showed that mtDNA damage occurs before the development of atherosclerotic plaques, suggesting that mtDNA damage promotes atherosclerosis. To investigate whether the effect of mtDNA damage on atherosclerosis is mediated through increased mitochondrial ROS the MitoP/MitoB ratio was calculated. Mitochondrial ROS levels were not different in PolG-/- ApoE-/- vs. ApoE-/- mice, suggesting that mtDNA damage promotes atherosclerosis independently of ROS (E. Yu et al., 2013). However, the study was not powered to identify possible subtle differences in ROS between these groups (E. Yu et al., 2013). mtDNA damage has also been found in human atherosclerotic plaques (E. Yu et al., 2013) suggesting a role in human atherogenesis.

The mechanisms by which mtDNA damage promotes atherosclerosis are not completely understood. However, potential mechanisms include activation of inflammation through mtDNA released from the cell (section 1.3.3) and effects on cell survival mediated either directly or indirectly through ROS as discussed in section 1.3.4.

1.3.3 The role of mitochondria in inflammation

Section 1.2.2 has introduced the concept that mitochondria produce ROS that contribute to intracellular redox signalling via modification of thiol residues. ROS produced by the cellular NADPH oxidases have long been known to be important for creating the respiratory burst of phagocytic cells (Pelletier et al., 2012). However more recently, ROS derived from mitochondria have been implicated in the immune response, particularly in innate immunity. For example, ROS mediate the response to

lipopolysaccharide (LPS) -driven MAPK activation and cytokine production (Bulua et al., 2011). Using N-acetylcysteine (NAC) as a scavenger for ROS the authors demonstrated reduced JNK and p38 phosphorylation as well as IL-6 production by fibroblasts following stimulation with LPS. Mitochondria-derived ROS can also cause inflammation in the absence of external inflammatory stimuli. For example, Tschopp's group showed that by inhibiting mitophagy cells accumulate dysfunctional mitochondria, which produce higher levels of ROS, which in turn promote inflammation through NLRP3 inflammasome activation (R. Zhou, Yazdi, Menu, & Tschopp, 2011). There is further evidence that ROS generated through RET at complex I may be a driver of inflammation. Macrophages stimulated with LPS switch metabolism from oxidative phosphorylation to glycolysis and accumulate large quantities of succinate (Tannahill et al., 2013), which in turn stabilises HIF-1α and increases IL-1β production. Succinate may exert its effects in part through RET (Chouchani, Pell, et al., 2014). Indeed, more recently it has been shown that the effects of LPS are greatly enhanced by succinate and that inhibition of RET by various means can reduce IL-1β production (Mills et al., 2016). HIF-1α may also be stabilised by ROS generated through complex III (Chandel et al., 2000). The mechanisms by which HIF-1α is stabilised under aerobic conditions are not completely understood. HIF-1α stabilisation may be afforded through reversible redox modification of target proteins. For example, hydroxylation of HIF-1α by prolyl hydroxylase (PHD) leads to ubiquitination of HIF-1α and subsequent proteosomal degradation (Bruick & McKnight, 2001; Epstein et al., 2001). PHD is inhibited by 2-hydroxyglutarate derived from the tricarboxylic acid (TCA) cycle intermediate 2-oxoglutarate (Burr et al., 2016).

HIF-1α is an important mediator of inflammation and immunity suggesting that mitochondria could integrate various stimuli to direct cell responses including metabolism, immune function and differentiation (Palazon, Goldrath, Nizet, & Johnson, 2014).

Although it is compelling to think of ROS as mediators of inflammation in atherosclerosis, targeting ROS in clinical trials has largely been unsuccessful. Several studies have been conducted investigating Vitamin C, Vitamin E or antioxidant cocktails, but the larger studies have not demonstrated any effects on cardiovascular outcomes (Kris-Etherton et al., 2004). However, none of these strategies directly target mitochondrial ROS. Targeting antioxidants such as ascorbate (MitoC) (Finichiu et al., 2015) or ubiquinone (MitoQ) (Kelso et al., 2001) directly to mitochondria may be more promising. Indeed as already discussed in section 1.3.2 MitoQ can significantly affect atherosclerotic plaque composition in mice (J. R. Mercer et al., 2012) suggesting that altering mitochondrial redox signalling may be a treatment strategy for atherosclerosis or indeed other chronic inflammatory diseases.

Mitochondria can also mediate inflammation through mechanisms independent of ROS signalling. Mitochondria, as evolutionary endosymbionts (Sagan, 1967) contain mostly non-methylated CpG motifs (B. Liu et al., 2016). These immunogenic motifs activate innate immune cells similarly to bacterial DNA. For example, injury in trauma patients leads to release of mtDNA into the circulation (Q. Zhang et al., 2010). Such mitochondrial damage-associated molecular patterns (DAMPs) in turn activate inflammatory cascades in human peripheral blood mononuclear cells (PMNCs) through binding to TLR9

resulting in systemic inflammation and organ injury (Q. Zhang et al., 2010). During apoptosis, oxidised mtDNA can directly bind to and activate the NLRP3 inflammasome increasing the production of IL1β (Shimada et al., 2012). Endogenous danger signals arising from mitochondria and the activation of the NLRP3 inflammasome may thus be important steps in the development of atherosclerosis as discussed in section 1.1.1.

In addition, succinate can not only lead to RET as described above but also bind to the G protein-coupled receptor GPR91 and trigger an inflammatory response, at least in dendritic cells. Through binding to GPR91 succinate greatly amplifies the effects induced by polyinosinic-polycytidylic acid [poly(I:C)] such as Erk1/2 phosphorylation (Rubic et al., 2008). Interestingly, this receptor is also expressed on activated monocytes, but its role in atherosclerosis has not been studied, yet.

Previously, Otsu's group has demonstrated that autophagy is an adaptive response in the failing heart upon haemodynamic stress (Nakai et al., 2007), and that cardiac specific deletion of lysosomal deoxyribonuclease (DNase) II, an enzyme digesting mtDNA in the lysosome, increases mortality, inflammation and dilated cardiomyopathy in pressure overload treated mice (Oka et al., 2012). These effects are abolished by either ODN2088, a synthetic oligodeoxynucleotide 'GCGGG' which blocks the unmethylated CpG/TLR9 interaction, or by ablation of *Tlr9* suggesting that mtDNA, which has not been degraded, activates inflammation through activation of the TLR9 pathway (Oka et al., 2012). Synthetic CpG motifs, which activate the TLR9 pathway (ODN2006, TCGTCGTTTTGTCGTTTTGTCGT) also increase IFNα secretion in atherosclerotic plaques (Niessner et al., 2006), indicating that

such a pathway is also important in atherogenesis. The role of TLRs in atherosclerosis is further discussed in section 1.1.3.

Thus mitochondrial dysfunction may perpetuate inflammation in atherosclerosis directly and indirectly through production of ROS and through DAMPs activating two important inflammatory cascades, the NLRP3 pathway and the TLR9 pathway. Succinate, an important TCA intermediate could also act through binding to GPR91, although the latter pathway is currently not researched in atherosclerosis.

1.3.4 Mitochondria as regulators of cell survival and cell death

Cell death has traditionally been divided into apoptosis, the planned and coordinated death of cells, necrosis or accidental cell death which is frequently associated with extensive inflammation, autophagic cell death, and mitotic catastrophe resulting from deficient cell cycle checkpoints and cellular damage (Kroemer, Galluzzi, & Brenner, 2007). Mitochondria are crucial to integrate a variety of signals ultimately determining cell fate. For example, mitochondrial outer membrane permeabilisation is the terminal process leading to cell death via the release of cytochrome c and activation of caspases, as well as cessation of bioenergetics and redox function of mitochondria (Kroemer et al., 2007).

It is thus not surprising that mitochondria regulate cell fate in numerous organs and disease processes including in the cardiovascular, neurological, and renal systems. For example, ischaemia/reperfusion injury shares common pathways across different organs and tissues and mitochondria are crucial in this process. Ischaemia/reperfusion injury can be greatly diminished

through nitrosylation of cysteine residue 39 (Cys39) of complex I of the ETC using the mitochondrially targeted probe MitoSNO. This posttranslational protein modification locks complex I into a de-active state preventing excessive ROS production during reperfusion (Chouchani et al., 2013). We now have evidence that it is the accumulation of succinate during ischaemia that drives RET during reperfusion thereby generating large amounts of superoxide (Chouchani, Pell, et al., 2014). This mechanism appears not to be limited to the heart as administration of MitoQ to scavenge mitochondrial ROS also diminishes kidney reperfusion injury (Dare et al., 2015). However, the theory of succinate mediated RET and ROS production during ischaemia/reperfusion injury has been controversial not least because loss of succinate during reperfusion may also be explained by efflux rather than RET and because pre-conditioning does not prevent succinate accumulation during ischaemia despite its protective effect on reperfusion (Andrienko, Pasdois, Pereira, Ovens, & Halestrap, 2017).

There is also evidence that mitochondria not only act as mediators of signals leading to cell death, but damage or dysfunction of mitochondria can cause cell death. For example, induction of mitochondrial ROS through proteasome inhibition leads to Bax- and caspase-mediated apoptosis that can be inhibited by the antioxidant N-acetyl-l-cysteine (NAC) (Papa, Gomes, & Rockwell, 2007). Similarly, after nerve growth factor withdrawal, MitoQ is more effective than $MitoE_2$ in preventing ROS-mediated neural cell death compared to $MitoE_2$ (McManus, Murphy, & Franklin, 2014). $MitoE_2$ contains the α-tocopherol moiety of vitamin E linked to TPP and penetrates the MIM to

a lesser degree than MitoQ, suggesting that it is mitochondrial ROS rather than cytosolic ROS that determines cell fate (McManus et al., 2014).

Mitochondrial ROS has also been implicated in apoptosis of VSMCs. A product of lipid peroxidation, 4-hydroxynonenal, induces apoptosis of VSMCs in a dose-dependent manner. This effect is sensitive to rotenone, suggesting that complex I-derived superoxide mediates this effect. In contrast, reducing ROS derived from other cellular sources through inhibition of NADPH oxidase, xanthine oxidase, or cyclooxygenase does not have similar effects (J. Y. Lee et al., 2006), further highlighting the importance of the cellular localisation of ROS to elicit signalling effects.

1.4 Aims of this study

The aims of this study are to determine:

1. Which, if any, mediators of atherosclerosis induce mitochondrial dysfunction in cultured VSMCs. The main focus is on OxLDL and LPS.
2. Whether the mtDNA damage that occurs in atherosclerosis is sufficient to affect mitochondrial function in human atherosclerosis.
3. Whether mitochondrial dysfunction induced by OxLDL affects mitochondrial clearance (mitophagy) and mitochondrial biogenesis in cultured human VSMCs.
4. Whether fat-feeding alters mitochondrial function in ApoE-/- mice prior to the development of atherosclerosis.

2 Materials and Methods

2.1 Materials and general procedures

All chemicals and reagents were obtained from Sigma-Aldrich (St. Louis, USA), unless otherwise stated. Milli-Q ultrapure water (Merck Millipore, MA, USA) was used unless stated otherwise.

2.1.1 Animal husbandry and mouse strains used

All animal studies were performed under UK Home Office licenses and following ethical review by the University of Cambridge Animal Welfare and Ethical Review Body (AWERB). Trained animal technicians performed husbandry. Colonies of ApoE-/- mice on a C57BL/6 background (Jackson Laboratory) were maintained in-house, overseen by Alison Finigan from Professor Bennett's laboratory. Initial experiments on the optimisation of extracellular flux analysis in tissues were done on various mouse strains, ages and sex that were being sacrificed for other reasons and tissues that would otherwise have been discarded were used for these experiments.

2.1.2 LDL preparations

LDL (BT-903) and OxLDL (BT-910) were obtained from Bioquote limited and stored at 4^{o}C. According to the manufacturer OxLDL was prepared by using 20 μM $CuSO_4$ (oxidant) in PBS at 37^{o}C for 24 hours. Oxidation was terminated by addition of excess EDTA. Oxidised LDL was membrane filtered and aseptically packaged in a solution containing PBS at

pH 7.4 and 0.3 mM EDTA. Each lot was analysed on agarose gel electrophoresis for migration versus LDL and a TBARS assay was used (typical value of 27.4 nmoles of MDA/mg Protein) to confirm oxidation. The manufacturer also tested samples for receptor binding to peritoneal macrophages in conjuction with DiIOxLDL. The manufacturer detected no endotoxins.

2.1.3 Mitochondrial inhibitor stock solutions

The oligomycin supplied (Sigma O4876) contains ≥ 60% oligomycin A but also oligomycin B and C. A stock solution of 2 mg/ml was prepared in sterile DMSO and stored at -20^{o}C. Likewise, 2.5 mM stock solutions of carbonyl cyanide 4-(trifluoromethoxy)phenylhydrazone (FCCP) (Sigma C2920), rotenone (Sigma R8875) and antimycin A (A8674 Sigma) were prepared in DMSO and stored at -20^{o}C.

2.1.4 MitoB

MitoB was synthesised by Professor Richard Hartley's laboratory and stored in Dr. Michael Murphy's laboratory at -20^{o}C. A 0.5 mM stock solution in 0.9% sterile sodium chloride was prepared and stored in aliquots at -20^{o}C for use in *in-vivo* studies.

2.1.5 Human tissue acquisition

Human aortas were obtained from patients undergoing cardiac transplantation or valve replacement at Papworth Hospital, Papworth Everard, UK, after written informed consent has been obtained. The cardiothoracic

surgical teams performed the procedures and samples were stored in DMEM at 4^{o}C until transfer to the Cardiovascular Division at Addenbrooke's Hospital by courier after a maximum of 24 hours. Tissues were processed on the day of transfer and consisted of snap freezing a tissue sample in liquid nitrogen for storage and diverting a section to fixation in neutral-buffered formalin for later processing. The remainder of the sample was used for isolation of VSMCs.

Human atherosclerotic plaque samples were obtained from patients undergoing carotid endarterectomies under the surgical teams at Addenbrooke's Hospital after written informed consent has been obtained. Samples were transferred to the Cardiovascular Division and processed as described above for aortic samples. Alternatively, a portion of the sample was used directly in Seahorse extracellular flux analysis experiments as described in section 2.3.2.2.

2.2 Cell culture

2.2.1 Culture medium and incubation

Cells were cultured in Dulbecco's modified Eagle's medium (DMEM) containing 4.5 g/L glucose supplemented with 10% foetal calf serum (FCS), 100 U/ml penicillin, 100 µg/ml streptomycin and 2 mM L-glutamine (culture medium in the following) in a tissue culture incubator at 37^{o}C under an atmosphere of humidified air supplemented with 5% CO_2. Tissue explants were maintained in culture medium as above but supplemented with 20% FCS.

2.2.2 Cell passaging and plating

Cells were passaged and seeded after trypsinisation. In brief, cells were washed twice with pre-warmed PBS and incubated in Trypsin-EDTA (Sigma, T3924) for approximately 1-5 minutes. Detached cells were resuspended in culture medium, counted using a Neubauer chamber, and placed into new culture ware (Corning, New York, USA). Cells were passaged at ratios of approximately 1:10 (RVSMCs), 1:3 (HEK-293T and HeLa) or 1:2 (HVSMCs and plaque VSMCs).

2.2.3 Cell freezing and thawing

Cells were trypsinised and counted as above, centrifuged at 400 x g for 5 minutes, and re-suspended in DMEM supplemented with 50% FCS and 10% DMSO at a density of $1x10^6$ cells/ml. Aliquots of cells were frozen using a Mr. Frosty™ Freezing Container (Thermo Fisher Scientific) as directed by the manufacturer and transferred to liquid N_2 for long term storage. When required, cells were rapidly thawed in a water bath (37^oC), transferred to culture medium and seeded into culture ware.

2.2.4 Rat aortic vascular smooth muscle cell culture and infection

Rat aortic vascular smooth muscle cells (RVSMCs) used in this study have previously been isolated from aortas of Wistar rats by Dr Isabelle Gorenne (Professor Bennett's laboratory) and infected with a retrovirus vector containing human sirtuin-1 or a deacetylase-deficient sirtuin-1, sirtuin-1^{H365Y}

(Gorenne et al., 2013). In brief, Phoenix^{TM} packaging cells (Orbigen, San Diego, CA) were transfected with pBabe-puro vectors encoding human sirtuin-1, sirtuin-1^{H365Y} (gift from Dr Anthony Kouzarides, Gurdon Institute, Cambridge, UK) or empty vector using SuperFect (Qiagen). The transfected cells are referred to as SIRT+, SIRT- and EV in the following text, respectively. The vector contained a selection cassette for hygromycin B that allowed selection of virus-producing cells. RVSMCs were infected with the virus suspension facilitated by 8 μg/ml hexadimethrine bromide (Polybrene) and selected with 5 μg/ml puromycin. Aliquots of 1x10^6 cells were frozen in DMEM supplemented with 50% FCS and 10% dimethyl sulfoxide (DMSO) and have been used for the present study.

2.2.5 HEK-293T

HEK-293T cells were used for pseudo-lentiviral particle production as described below. Cells were obtained from Dr Anna Uryga and propagated in culture medium before use.

2.2.6 HeLa cells

HeLa cells were used in preliminary experiments of lentiviral infection. Cells were obtained from frozen lab stocks and grown under culture conditions as described for other cell types above.

2.2.7 Human vascular smooth muscle cell isolation and culture

2.2.7.1 Aortic vascular smooth muscle cells

Human aortic VSMCs were isolated from aortic specimens obtained from Papworth Hospital as described above (section 2.1.5). The specimens were kept sterile in a tissue culture flow hood, adventitial tissue was removed, and tissue pieces of approximately 2 mm x 2 mm were dissected and placed into six-well plates. Tissue specimens were then incubated (37^{o}C, humidified air with 5% CO_2) in culture medium with 20% FCS. After outgrowth of cells, the tissue pieces were removed, cells were trypsinised and cultured in medium containing 10% FCS. Although the cells cultured with this technique had the morphological appearance of VSMCs, the cell type has not been formally assessed through the expression of cell type specific markers. Subsequently cells were passaged in ratios of 1:2 or 1:3. For this study both freshly isolated HVSMCs as well as frozen lab stocks were used.

2.2.7.2 Atherosclerotic plaque vascular smooth muscle cells

Human atherosclerotic plaque VSMCs (plaque VSMCs in the following) were isolated from carotid endarterectomy samples obtained from patients undergoing carotid endarterectomy at Addenbrooke's Hospital (see section 2.1.5.) Plaque VSMCs were cultured as described above for healthy HVSMCs. For this study both freshly isolated plaque VSMCs as well as frozen lab stocks were used.

2.3 Extracellular flux analysis

The metabolism of cultured VSMCs, mouse aortas and carotid endarterectomy-derived human atherosclerotic tissues was investigated using Seahorse Bioscience extracellular flux analysers. The Seahorse extracellular flux analysis assay uses proprietary culture plates and sensor cartridges and through its multi-well culture plate design allows for the simultaneous measurement of multiple samples. This platform simultaneously measures oxygen tension and pH in both a custom 96-well format (Seahorse XF96), used for experiments with cultured cells, and a 24-well format (Seahorse XFe24), used for measurements in tissue samples. Four temperature control wells containing no cells or tissues are used to calibrate the machine to zero. From these measurements the oxygen consumption rate (OCR) as well as the extracellular acidification rate (ECAR) can be calculated. Both of these platforms allow for the consecutive injection of up to four inhibitors or inhibitor combinations during the assay to inhibit ETC complexes and uncouple mitochondria. This assay has been increasingly used to infer mitochondrial function or dysfunction in cells and more recently intact tissues (Dunham-Snary, Sandel, Westbrook, & Ballinger, 2014; Feeley, Westbrook, Bray, & Ballinger, 2014; J. Liu et al., 2009).

2.3.1 VSMC extracellular flux analysis

VSMCs were cultured as described above, trypsinised, counted using a Neubauer chamber and seeded in 80 µl aliquots per well into Seahorse 96-well plates (Seahorse XF96 FluxPak). Cells were allowed to adhere and grow for 24 hours prior to treatment with varying doses of LDL (BT-903, Bioquote

limited), copper-oxidised LDL (OxLDL, BT-910 Bioquote limited) and lipopolysaccharide (LPS from *Escherichia coli* 0111:B4, Sigma L3012). After 24 hours treatment, cells were washed once with sterile assay medium [DMEM 4.5 g/L glucose (Sigma D5648), supplemented with 1 mM sodium pyruvate (Sigma, S8636), 31.66 mM sodium chloride (Sigma), pH adjusted to 7.4] and allowed to equilibrate to assay medium at 37^{o}C and atmospheric pCO_2 for 1 hour. Importantly, no sodium bicarbonate is added to the assay medium resulting in poor pH buffering capacity allowing simultaneous measurement of the oxygen consumption rate (OCR) and the extracellular acidification rate (ECAR). The glucose concentration in the medium has not been optimised for this assay and high concentrations of glucose may affect the metabolism of the cells. However, DMEM with identical glucose content has previously been used as the standard assay medium in the MRC mitochondrial biology unit (Bridges, Jones, Pollak, & Hirst, 2014). The medium contained phenol red, which is thought to be a significant contributor to antioxidant capacity of cell culture medium (Lewinska, Wnuk, Slota, & Bartosz, 2007). Although phenol red has previously been used in assay medium [manufacture's catalogue, Bridges et al. (2014)] any anti-oxidant activity could potentially alleviate the effects of treatments with compounds such as OxLDL, and has not been controlled for in the present study. Oligomycin, FCCP and a combination of rotenone and antimycin A, diluted in sterile assay medium, were loaded into the assay ports (25 µl per port for XF96) to allow simultaneous injection into all wells as described for each experiment. The final DMSO concentration after injection of all inhibitors (excluding FCCP dose titration experiments) was 0.2 % v/v. Although effects

of DMSO on cell viability were not directly assessed in the present study, DMSO concentrations of < 1% v/v had no apparent effect on proliferation of HeLa cells in a previous study (Ben Trivedi, Kitabatake, & Doi, 1990).

However, more subtle effects of DMSO on cellular metabolism may be possible and in future experiments an alternative vehicle such as ethanol should be considered. OCR and ECAR were calculated before and after injection of the inhibitors. Measurement cycles comprised 3 minutes of mixing followed by 3 minutes of O_2 and pH measurement. Three measurements were obtained at baseline and then following injection of the inhibitors. Results were normalised to average protein concentrations per treatment group obtained using a bicinchoninic acid (BCA) protein assay (Pierce) on a second 96-well culture plate treated in parallel (RVSMCs) or protein concentration per well determined after completion of the assay (HVSMCs and plaque VSMCs).

2.3.2 Tissue extracellular flux analysis

2.3.2.1 Mouse aortic tissue

Mice were sacrificed by rising CO_2 concentrations and cervical dislocation, exsanguinated through cardiac puncture and their aortas were harvested and placed into either pre-warmed DMEM assay medium or ice-cold PBS depending on the experimental setup. This step was performed with Ms Alison Finigan from Professor Bennett's laboratory, a fully trained animal technician, to comply with regulations, increase consistency and decrease experimental time therefore increasing tissue viability. Using a stereo-microscope (Leica M80, 7.5-60x magnification) surrounding fat tissue and

branching arteries were removed from the aorta. The aortas were then either opened longitudinally as previously described (Feeley et al., 2014) or left as intact aortic rings. Sections (2-4 mm length) yielding comparable masses were prepared and placed into separate wells of an islet capture well culture plate (Seahorse Bioscience) pre-filled with 250 µl warmed DMEM assay medium (37^{o}C). Wells A1, B4, C3 and D6 were left blank as negative control wells and tissues were immobilized using the capture screens provided. The assay medium was replaced immediately before loading the plate into the XFe24 analyser. Dilutions of the inhibitors oligomycin, FCCP, rotenone and antimycin A in 75 µl DMEM assay medium were loaded into the injection ports to achieve final assay concentrations as described in each experiment. Measurement cycles were 3 minutes of mixing followed by 2 minutes waiting time and then 3 minutes of O_2 and pH measurement. Four measurements were obtained, both as baseline and following injection of the inhibitors.

2.3.2.2 Human atherosclerotic plaque tissue

Human carotid atherosclerotic plaques were obtained from patients undergoing carotid endarterectomy at Addenbrooke's Hospital, Cambridge, UK, after informed written consent had been obtained. To avoid delay in sample processing and tissue degradation the samples were collected from the operating theatre as soon as they became available, transferred to the laboratory and dissected under a stereo-microscope (Leica M80, 7.5-60x magnification). Four distinct areas corresponding to normal carotid medial wall, the shoulder region of the atherosclerotic plaque as well as the cap region and the necrotic core were identified. Sections of approximately 1 mg

wet weight were dissected from each of these areas and placed into separate wells of a islet capture well culture plate (Seahorse Bioscience) pre-filled with 250 µl warmed DMEM assay medium (37^{o}C). Extracellular flux analysis was performed as described in section (2.3.2.1).

2.3.2.3 Determination of tissue weights for quantification of extracellular flux analysis

After completion of the extracellular flux analysis assay tissue samples were retrieved, padded on absorbing paper to remove excess fluid and weighed on a microbalance (Metler Toledo). Tissue pieces were then transferred to formalin (pH 7.4) for subsequent immunohistochemistry or to a heat block at 80^{o}C for 24 hours to determine dry weights.

2.4 Immunohistochemistry

Mrs Nichola Figg performed immunohistochemistry slide preparation and staining according to established immunohistochemistry techniques as described below.

2.4.1 Tissue preparation

Tissues were fixed in 10% neutral-buffered formalin for at least 12 hours. Tissues were rinsed in PBS, cut into appropriate sized sections, placed in processing cassettes and transferred to a beaker filled with PBS. Tissues were then processed in an automated tissue processor (Leica) and after completion of the processing cycle transferred to the wax bath of the

embedding centre. Tissues were removed from the cassette and placed into a base mould containing liquid paraffin wax. The mould was then placed on the cold plate of the embedding centre to solidify, and then removed from the mould. Paraffin blocks containing human tissues were stored in the block bank store in a designated, monitored and secure area. Blocks were anonymised, catalogued and details entered on the secure laboratory database.

2.4.2 Haematoxylin and eosin stain

Tissues were de-waxed and rehydrated through graded alcohols to Milli-Q H_2O. Slides were placed in haematoxylin solution (Sigma HHS128) for 5 minutes and briefly dipped in de-stain solution (250 ml 50% methanol, 250 ml H_20, 5 ml 2 M HCL) eight times. Slides were then placed into Scott's solution (20 mg magnesium sulphate, 2 mg sodium bicarbonate in 1L H_2O) for 5 minutes followed by eosin solution (Sigma HT110280) for 6 minutes. Slides were quickly rinsed in H_2O and rapidly dehydrated through graded alcohols and two changes of xylene. DPX mountant (Sigma 44581) and coverslips were applied.

2.4.3 CD68 and smooth muscle actin stain of human plaque tissues

Tissues were de-waxed and rehydrated through graded alcohols to Milli-Q H_2O, placed in the antigen un-masking solution (Vector Laboratories, H-3301) and transferred to the pressurised retrieval vessel. After completion of the programme, the sections were retrieved and left to cool to room temperature before washing twice in PBS for 5 minutes each. Sections were

blocked with 1% hydrogen peroxide in PBS for 10 minutes and washed twice in PBS for 5 minutes each. Slides were then incubated with 5% horse serum in PBS for 30 minutes, excess was removed and slides were carefully blotted around the sections. Sections were then incubated in primary antibody (CD68, Dako M0876, diluted 1:100 in 5% horse serum/PBS; Smooth muscle actin, Dako M0851, diluted 1:500 in 1% BSA/PBS) overnight at 4^{o}C. Slides were washed twice in PBS for 5 minutes and secondary antibody (horse anti-mouse, 1:400 in PBS, Vector Laboratories) added for 30 minutes. Slides were washed twice for 5 minutes in PBS and incubated in 3,3-diaminobenzidine (DAB) solution (Vector Laboratories, SK-4100). Reaction was monitored closely under a microscope and slides were then washed twice in H_2O for 5 minutes each. Sections were counterstained as required with haematoxylin as above, dehydrated through graded alcohols to Histo-clear (National Diagnostics, USA, HS-200) and coverslips applied.

2.4.4 Masson's trichrome stain

All reagents for this stain were from Masson's trichrome stain kit (Sigma HT15). Sections were de-waxed to H_2O as above and incubated in preheated Bouin's solution at 56^{o}C for 15 minutes or at room temperature overnight. Slides were cooled in tap water (18-26^{o}C) in a Coplin jar before washing under running tap water until the yellow colour was removed from the sections. Sections were then stained in working Weigert's iron haematoxylin solution for 5 minutes and washed under running tap water for 5 minutes. Sections were rinsed in Milli-Q H_2O and stained with Biebrich Scarlet Acid Fuchsin for 5 minutes before a further rinse in Milli-Q H_2O. Slides were

transferred to working phosphotungstic/phosphomolybdic acid solution for 5 minutes and then aniline blue solution for 5 minutes. Sections were then transferred into 1% acetic acid for 1 minute, rinsed, dehydrated through alcohol, cleared in xylene and mounted as above.

2.4.5 Mac 3 stain

Sections were de-waxed and transferred to water as above and placed into antigen unmasking solution (preheated to 96-98^{o}C) for 30 minutes. Sections were cooled to room temperature for 20 minutes and washed twice in PBS for 5 minutes each. Sections were then incubated in 3% hydrogen peroxide in PBS for 10 minutes, washed twice in PBS for 5 minutes each and blocked with avidin/biotin solution (Vector Laboratories, SP-2001) as per the manufacturers protocol. Slides were then washed twice in PBS for 5 minutes and blocked with 5% rabbit serum in PBS for 1 hour at room temperature. Sections were then incubated with anti-Mac 3 antibody (Pharmingen 01781D, 1:400 in 10% rabbit serum) at 4^{o}C overnight. After two wash steps in PBS for 5 minutes each, sections were incubated in secondary antibody (rabbit anti-rat, Vector Laboratories, 1:400 in PBS) for 30 minutes and washed twice in PBS for 5 minutes. Sections were incubated in avidin/biotin complex (vectastain abc kit, PK-4000, Vector Laboratories), washed twice in PBS for 5 minutes, transferred to 3,3'-diaminobenzidine (DAB) and closely monitored under a microscope. Slides were washed in Milli-Q water, counterstained, dehydrated, cleared and mounted as described above.

2.4.6 Mouse smooth muscle actin stain

A mouse-on-mouse (MOM) immunohistochemistry kit (MOM Elite Peroxidase kit, PK-2200, Vector Laboratories) was used for staining of mouse smooth muscle actin. Sections were transferred to H_2O as described above and placed into a Coplin jar containing antigen unmasking solution preheated in a waterbath to 96-98^{o}C. After 30 minutes incubation the jars were removed from the waterbath and allowed to cool for 20 minutes. Slides were washed twice in PBS for 5 minutes and blocked in 1% hydrogen peroxide in methanol for 15 minutes. After two further wash steps in PBS for 5 minutes the sections were incubated for 1 hour in MOM immunoglobulin blocking reagent as per the manufacturer's protocol. After two washes in PBS for 5 minutes sections were incubated in working solution of MOM diluent, excess diluent was removed and slides were carefully blotted around the sections. Sections were then incubated in primary antibody (Dako anti-smooth muscle actin, clone 1A4, 1:500 in MOM diluent) for 30 minutes. Sections were washed twice in PBS for 5 minutes and then incubated in MOM biotinylated anti-mouse IgG reagent for 10 minutes as per the manufacturer's instructions. After two wash steps in PBS for 5 minutes sections were incubated in ABC reagent for 5 minutes, washed twice and incubated in DAB solution as described above. Sections were counterstained (Haematoxylin) as required, dehydrated and cleared in two changes of histoclear and mounted using histomount (National Diagnostics, HS-103).

2.5 Normalisation of tissue extracellular flux analysis data

Mouse aorta extracellular flux analysis data were normalised to wet weights (see section 2.3.2.3) to allow for variations in the size of tissue samples. Extracellular flux analysis data derived from human atherosclerotic plaque tissue samples were normalised to both wet weights and cell density to take account of different cellularity in the various regions of the atherosclerotic plaque. Cell density was determined in H&E stained slides from tissue pieces after completion of the extracellular flux analysis run and after measurement of wet weights (section 2.3.2.3). A visual field was chosen to contain approximately 20 nuclei in healthy wall samples and was applied to all tissue pieces were immunohistochemistry was available (i.e, N=5 experiments with immunohistochemistry available and 5 tissue pieces per region in each experiment). OCR and ECAR values were then divided by tissue weight and cell count per area for normalisation and comparison across different regions. Cell count per area was derived by counting nuclei per area, irrespective of cell type.

2.6 Incucyte cell-confluency assay

EV RVSMCs were plated in 6-well plates at a density of 50,000 cells per well. Cells were allowed to adhere and then treated with varying doses of OxLDL or vehicle (PBS supplemented with 0.3 mM EDTA) and imaged using an Incucyte HD system (Essenbio) with a 20x objective within a conventional tissue culture incubator (37^{o}C, 5% CO_2). Frames were captured in four-hour intervals across 16 separate regions in each well. The average confluency of

cells in the 16 regions was generated by the software provided. The mean of technical duplicates was then calculated for each treatment group.

2.7 FACS – uptake of 1,1'-dioctadecyl-3,3,3'3'-tetramethyl-indocarbocyanine perchlorate (DiI) labelled OxLDL

To confirm uptake of human OxLDL into RVSMCs, 1,1'-dioctadecyl-3,3,3'3'-tetramethyl-indocarbocyanine perchlorate (DiI)-labelled OxLDL (Intracel, RP-173) was utilised. EV, SIRT- or SIRT+ RVSMCs were plated at a density of 25,000 cells per well in 24-well culture plates and allowed to adhere overnight. Culture medium was changed and cells were treated with 0-100 µg/ml DiI-labelled OxLDL. Cells were washed twice with PBS and trypsinised with 100 µl Trypsin-EDTA for 1 minute at 37^{o}C and 5% CO_2. 1 ml growth medium was added, cells were centrifuged at 2000 rpm for 2 minutes and resuspended in 150 µl stain buffer (BD Biosciences, 554656). Samples were analysed using a C6 Accuri flow cytometer (BD Biosciences). Intact single cells were gated using the forward scatter (FSC) and side scatter (SSC) and 10,000 events were counted using an FL2 optical filter (585/40). Maximum FL2 signal (FL2-H) was used as a measure of DiI-labelled OxLDL uptake.

2.8 Western blotting

2.8.1 Cell lysis

Cells were cultured as described in section 2.2, plated into 6-well plates, treated as indicated in individual experiments, washed, trypsinised and

centrifuged. Cell pellets were then lysed in 50 µl sodium dodecyl sulphate (SDS) lysis buffer (1% w/v SDS, 50 mM Tris-HCL, pH adjusted to 8.0) supplemented with 1:100 protease inhibitor cocktail I (Merck 539131) and 1:100 phosphatase inhibitor cocktail I (Merck 524624). Lysates were sonicated on ice (Sonics and Materials INC, CT, USA, Vibra Cell VCX 130) in two pulses of 10 seconds with pauses of 30 seconds to complete lysis and shear DNA. Samples were centrifuged at 15,000 rpm for 10 minutes at 4^{o}C and the supernatant transferred to new reagent tubes for downstream applications or storage at -80^{o}C.

2.8.2 Bicinchoninic acid protein assay

Protein concentrations of cell lysates were determined by bicinchoninic acid (BCA) protein assay (Pierce BCA Protein Assay Kit, Thermo Scientific, 23227) according to the manufacturer's instructions. A dilution curve was generated using the bovine serum albumin provided in the kit and both standards and samples were prepared in technical duplicates on 96-well plates. After incubation with the BCA reagent at 37^{o}C for 30 minutes absorbance at 562 nm was measured using in a microplate reader (Biotek, Synergy HT, VT, USA).

2.8.3 Sodium dodecyl sulphate gel electrophoresis

10-20 µg of protein was heated (60^{o}C – 95^{o}C for 10 minutes) in appropriate volumes of BOLT^{TM} 4x LDL sample buffer (Novex, B0007) and 10x sample reducing agent (Novex, B0009) and run on pre-cast 4-12% gradient gels or 10% gels (both Invitrogen, Ca, USA) using 3-(*N*-

morpholino)propanesulfonic acid (MOPS) buffer (Invitrogen) at 165 V for 45 minutes. Semi-dry transfer was performed using an iBlot 2 dry blotting system (Invitrogen) at 20 V for 7 minutes and membranes washed for 10 minutes in washing buffer [tris-buffered saline with 0.05% tween-20 (TBST) or phosphate-buffered saline with 0.05% tween-20 (PBST)]. Blocking and antibody incubation was performed as summarised in Table 2-1. Amersham enhanced chemiluminescent (ECL) Western blotting detection reagent or ECL prime Western blotting detection reagent (both GE healthcare) was applied before exposure to X-ray film (Fuji Film) and development. Membranes were washed in washing buffer and antibodies stripped from the membrane using Restore™ Western blot stripping buffer (Thermo Scientific). After a further washing step, membranes were blocked and re-probed as indicated or dried and stored at 4^{o}C for future use. Dr Anna Uryga of Professor Bennett's laboratory advised on antibody optimisation and helped performing Western blots. In particular, one membrane with samples from HVSMCs and plaque VSMCs that was previously run and probed by Dr Uryga was re-probed for ETC complex and ATPase expression in the present study.

2.9 PCR analysis of mitochondrial DNA copy number

The quantification of mtDNA copy number has previously been described and was adapted for this project to measure mtDNA copy number in human and mouse samples (Gammage, Van Haute, & Minczuk, 2016). MtDNA content is quantified through quantitative PCR (qPCR) using the ratio of amplification of short mitochondrial amplicons compared to amplification of a short nuclear control gene.

DNA was isolated from tissues using the GenElute mammalian genomic DNA isolation kit (Sigma, G1N70) as per the manufacturer's instructions. DNA was quantified using a spectrophotometer (NanoDrop, Thermo Fisher).

Primary antibody	Blocking	Conditions of incubation	Wash buffer	Secondary antibody	Conditions of incubation
Monoclonal mouse anti-sirtuin-1 (Cell Signaling Technology, 1F3, 8469)	5% milk in TBST for 1 hr at RT	1:1000 in 5% BSA TBST at 4°C overnight	TBST	Sheep HRP-linked anti-mouse IgG (GE Healthcare, NA931V)	1:5000 in 0.25% milk TBST for 1 hr at RT
Monoclonal rabbit anti-sirtuin-6 (Cell Signaling Technology, D8D12, 12486S)	5% milk in TBST for 1 hr at RT	1:1000 in 5% BSA TBST at 4°C overnight	TBST	Donkey HRP-linked anti-rabbit IgG (GE Healthcare NA934V)	1:5000 in 0.25% milk TBST for 1 hr at RT
Monoclonal mouse anti-actin (Sigma, A 3853)	5% milk in TBST for 1 hr at RT	1:5000 in 5% BSA TBST (Western Blot of RVSMCs) or 1:10000 in 5% BSA PBST (HVSMCs)	TBST (RVSMCs) PBST (HVSMCs)	Sheep HRP-linked anti-mouse IgG (GE Healthcare, NA931V)	1:10000 in 0.25% milk TBST for 1 hr at RT
Mouse monoclonal anti-Keima-Red (Amalgaam MBL, M182-3)	5% BSA in PBST for 1 hr	1:1000 in 5% BSA for 1 hr at RT	PBST	Horse anti-mouse HRP-linked IgG (Cell Signaling Technology, 7076)	1:5000 in 0.25% milk in PBST for 1 hr at RT
Rabbit monoclonal anti- glyceraldehyde 3-phosphate dehydrogenase (GAPDH) (Cell Signaling, 14C10, 2118)	5% milk in PBST for 1 hr at RT	1:1000 in 5% BSA for 1 hr	PBST	Goat anti-rabbit HRP linked IgG (Cell Signaling Technology 7074)	1:3000 in 0.25% mild in PBST for 1 hr at RT
Polyclonal rabbit anti-twinkle (Aviva Systems Biology, ARP36483_P050)	5% milk in PBST for 1 hr at RT	1:1000 in 5% milk in PBST at 4°C overnight	PBST	Goat anti-rabbit HRP linked IgG (Cell Signaling Technology 7074)	1:3000 in 0.25% milk in PBST for 1 hr at RT
Polyclonal rabbit anti PGC-1 (Santa Cruz Biotechnology, sc-13067)	5% milk in PBST for 1 hr at RT	1:2000 in 5% BSA at 4°C overnight	PBST	Goat anti-rabbit HRP linked IgG (Cell Signaling Technology 7074)	1:1000 in 0.25% milk in PBST for 1 hr at RT.

(MS304) CIV subunit I (MS404) and CV alpha subunit (MS507) (Mitosciences, MS604)				7076)	
Polyclonal rabbit anti-citrate synthase (Abcam, ab96600)	5% milk in PBST for 1 hr at RT	1:1000 in 5% BSA at RT for 1 hr	PBST	Goat anti-rabbit HRP linked IgG (Cell Signaling Technology 7074)	1:5000 in 0.25% milk in PBST for 1 hr at RT
Polyclonal rabbit anti-DNA polymerase gamma (Abcam, ab128899)	5% milk in PBST for 1 hr at RT	1:1000 in 5% BSA at 4°C overnight	PBST	Goat anti-rabbit HRP linked IgG (Cell Signaling Technology 7074)	1:3000 in 0.5% milk for 1 hr at RT
Polyclonal rabbit anti-PINK1 (Cell Signaling Technology, 6946)	5% milk in PBST for 1 hr at RT	1:1000 in 5% BSA at 4°C overnight	PBST	Goat anti-rabbit HRP linked IgG (Cell Signaling Technology 7074)	1:3000 in 5% BSA for 1 hr at RT
Polyclonal rabbit anti-TFAM (Cell Signaling Technology, 7495S)	5% milk in PBST for 1 hr at RT	1:1000 in 5% BSA at 4°C overnight	PBST	Goat anti-rabbit HRP linked IgG (Cell Signaling Technology 7074)	1:3000 in 0.5% milk for 1 hr at RT

Table 2-1 Antibodies and blocking agents used in Western blot

TBST: tris-buffered saline supplemented with 0.05% tween; PBST: phosphate-buffered saline supplemented with 0.05% tween; hr: hour; RT: room temperature; BSA: bovine serum albumin; HRP: horse radish peroxidase

Human mtDNA copy number was assessed using primers (900 nmol/L, all from Sigma) that have previously been described (Gammage et al., 2016). Relative mtDNA expression was calculated as the average of two short segments relative to nuclear DNA expression. qPCR was perfomed on a Rotor-Gene 6000 QPCR thermocycler (Corbett Research) using Rotor-gene SYBR green PCR mastermix (Qiagen). Mitochondrial primers were: CACCCAAGAACAGGGTTTGT (forward) and TGGCCATGGGTATGTTGTT-AA (reverse) (short segment "mt3211") and CGTCATTATTGGCTCAAC (forward) and GATGGAGACATACAGAAATAG (reverse) (short segment "mt9827"). Nuclear primers (β_2 microglobulin, B2M) were TGCTGTCTCC-ATGTTTGATGTATCT (forward) and TCTCTGCTCCCCACCTCTAAGT (reverse).

Before measurement of mtDNA copy number, the efficiency of the qPCR reaction was tested through serial dilutions of DNA. The qPCR product was run on a 1% agarose gel and visualised using a UV camera system (Alpha Innotech Corporation, Ca, USA) to confirm amplification of a specific amplification product for each primer pair. For the measurement of mtDNA copy number each qPCR was performed in triplicate using 10 ng of sample DNA in 20 µl reaction volumes. Cycle conditions were 50^{o}C for 2 minutes and 95^{o}C for 10 minutes followed by 40 cycles of 95^{o}C for 15 seconds and 60^{o}C for 60 seconds. Melt-curve analysis was performed following the run to confirm amplification of a single product. Relative amplification of mtDNA was calculated as $2^{\Delta Ct}$ where ΔCt=Ct (nuclear)-Ct (mitochondrial). To correct for the presence of two nuclear copies of B2M mtDNA copy number was calculated as $2 \times 2^{\Delta Ct}$.

Similarly, mouse mtDNA copy number was determined through amplification of one short mitochondrial amplicon relative to a short segment of the beta-globin gene. Primers were used at 5 µmol/L. Mitochondrial primers were GCCAGCCTGACCCATAGCCATAAT (forward) and GCCGGCTG-CGTATTCTACGTTA (reverse, 127 bp product) and nuclear primers (beta-globin, 155 bp product) were TTGAGACTGTG-ATTGGCAATGCCT (forward) and CCAGAAATGCTGGGCGCTCACT (reverse). Cycle conditions were 95ºC for 5 minutes followed by 45 cycles of 95ºC for 5 seconds and 60ºC for 10 seconds.

Rat VSMC copy number was determined as above using primer pairs (500 nmol/L) that have previously been used to determine mtDNA copy number (Gonzalez-Hunt et al., 2016). Mitochondrial primers were CAAACCTTTCCTGCACCTCC (forward) and AGGCGTTCTGATGATGGGAA (reverse, 181 bp fragment) and nuclear primers were GTTCCCGCCTTCTTC-CTCTG (forward) and GTTTGCTTGCCGACTCCTTG (reverse, 144 bp nuclear fragment from 3',5'-cyclic AMP phosphodiesterase). qPCR conditions were 10 minutes at 95^{o}C followed by 40 cycles of 95^{o}C for 15 seconds followed by 60^{o}C for 60 seconds.

2.10 RT-PCR genes involved in mitochondrial turnover

2.10.1 Isolation and reverse transcription of RNA

Isolation of RNA from healthy aortic VSMCs and plaque VSMCs was performed by Dr Aarti Shah in Professor Bennett's laboratory using an

RNeasy kit (Qiagen) as per the manufacturer's instructions. Cells were lysed with 350 µl RLT buffer supplemented with 3.5 µl 2-mercaptoethanol. The sample was passed through a blunt 20-gauge needle 5 times and 350 µl 70% EtOH added. The lysate was transferred to an RNeasy spin column within a 2 ml collection tube and centrifuged for 15 seconds at 8000 x g. The flow through was discarded and 350 µl buffer RW1 added. After centrifugation for 15 seconds at 8000 x g the flow-through was discarded and DNase I, diluted in RNA-free H_20, added to 70 µl buffer RDD and transferred to the spin column. After incubation for 15 minutes 350 µl buffer RW1 was added and the column centrifuged as above and the flow-through was discarded. 500 µl buffer RPE was added and the column centrifuged for 2 minutes at 8000 x g. The column was placed into a new 2 ml collection tube and 50 µl RNase free H_2O was added. After centrifugation for 1 minute at 8000 x g the purity and concentration of the eluted RNA was analysed using a spectrophotometer (NanoDrop, ND-1000).

Reverse transcription of human RNA was done by Dr Aarti Shah using 1 µg total RNA and SuperScript III reverse transcriptase (Invitrogen). Diluted RNA was added to 1 µl oligodT and 1 µl 10 mM dNTP mix (both Invitrogen) to a final volume of 13 µl. The sample was incubated for 5 minutes at 65^{o}C and cooled on ice for at least 1 minute. 4 µl 5x First-Strand Buffer (Invitrogen), 1 µl 0.1M dithiothreitol (DTT), and 1 µl SuperScript III reverse transcriptase were added. After incubation for 60 minutes at 50^{o}C the reaction was inactivated by heating to 70^{o}C for 15 minutes. The cDNA was stored at -20^{o}C until further use.

2.10.2 qPCR of genes involved in mitochondrial shape dynamics

qPCR was done for five target genes involved in mitochondrial fission and fusion and the control gene target 18S using primer pairs (0.5 µM each) and cycling conditions that have previously been described for human samples (Sastre-Serra, Nadal-Serrano, Pons, Roca, & Oliver, 2012) (Table 2-2, Table 2-3). A Rotor-Gene 6000 qPCR thermocycler (Corbett Research) and Rotor-Gene SYBR green PCR mastermix (Qiagen) were used. cDNA was diluted 1:30 and 5 µl of sample was run in triplicate for each target including a 50% cDNA control sample and a no template control in 20 µl reaction volume. Gene expression relative to 18S was calculated as $2^{\Delta Ct}$.

Gene	Forward primer	Reverse primer	Annealing temperature (°C)
18S	GGACACGGACAGGATTGACA	ACCCACGGAATCGAGAAAGA	61
mfn-1	TTGGAGCGGAGACTTAGCAT	TTCGATCAAGTTCCGGATTC	51
mfn-2	AGAGGCATCAGTGAGGTGCT	GCAGAACTTTGTCCCAGAGC	56
opa-1	GGCCAGCAAGATTAGCTACG	ACAATGTCAGGCACAATCCA	51
drp-1	AAGAACCAACCACAGGCAAC	GTTCACGGCATGACCTTTTT	51
fis-1	CTTGCTGTGTCCAAGTCCAA	GCTGAAGGACGAATCTCAGG	53

Table 2-2 Primer pairs used for qPCR of genes involved in mitochondrial shape dynamics

mfn-1: mitofusin 1; mfn-2: mitofusin 2; opa-1: optic atrophy 1; drp-1: dynamin-related protein 1; fis-1: mitochondrial fission 1 protein. Adapted from Sastre-Serra et al. (2012).

Gene	Melting	Annealing	Extension	Cycle number
18S	10 s at 95°C	10 s at 61°C	12 s at 72°C	40
mfn-1	10 s at 95°C	10 s at 51°C	12 s at 72°C	40
mfn-2	10 s at 95°C	10 s at 56°C	12 s at 72°C	40
opa-1	10 s at 95°C	10 s at 51°C	12 s at 72°C	40
drp-1	10 s at 95°C	10 s at 51°C	12 s at 72°C	40
fis-1	10 s at 95°C	10 s at 53°C	12 s at 72°C	40

Table 2-3 Cycling conditions for qPCR of genes involved in mitochondrial shape dynamics

mfn-1: mitofusin 1; mfn-2: mitofusin 2; opa-1: optic atrophy 1; drp-1: dynamin-related protein 1; fis-1: mitochondrial fission 1 protein. Adapted from Sastre-Serra et al. (2012).

2.10.3 qPCR of genes involved in mitophagy

A TaqMan qPCR system was used to determine expression of PINK1 (Hs00260868_m1) and PARK2 (Hs01038322_m1, encoding parkin) genes and the control gene 18S (Hs03003631_g1, Thermo Fisher) on a Rotor-Gene 6000 qPCR thermocycler (Corbett Research) using TaqMan universal PCR mastermix (Thermo Fisher, 4304437). cDNA was diluted 1:30 and 5 µl diluted sample was run in triplicate including 50% cDNA and no template controls in 20 µl reaction volumes. PCR conditions were 95°C for 10 minutes followed by 50 cycles of 95°C for 15 seconds and 60°C for 60 seconds. Gene expression relative to 18S was calculated as $2^{\Delta Ct}$.

2.10.4 qPCR of genes involved in mitochondrial DNA regulation

A TaqMan qPCR system was used to determine expression of TFAM (Hs00273372_s1), C10orf2 (Twinkle, Hs00958168) and PolG (Hs00160298_m1) genes and the control gene 18S (Hs03003631_g1, Thermo Fisher) on a Rotor-Gene 6000 qPCR thermocycler (Corbett Research) using TaqMan universal PCR mastermix (Thermo Fisher, 4304437). cDNA was diluted 1:30 and 5 µl diluted sample was run in triplicate including 50% cDNA and no template controls in 20 µl reaction volumes. PCR conditions were 95^{o}C for 10 minutes followed by 45 cycles of 95^{o}C for 15 seconds and 60^{o}C for 60 seconds. Gene expression relative to 18S was calculated as $2^{\Delta Ct}$.

2.11 Generation of Keima-expressing primary cell cultures

Keima is a coral-derived, acid stable fluorescent protein that demonstrates a pH dependent excitation spectrum (Katayama, Kogure, Mizushima, Yoshimori, & Miyawaki, 2011). Through a mitochondria targeting sequence from COX VIII, this protein allows for quantification of mitophagy through determination of the excitation ratio of the protein (Katayama et al., 2011; Sun et al., 2015). In this project I used a lentiviral strategy to deliver mitochondrially-targeted Keima (Keima in the following) to human aortic or plaque VSMCs. The Keima plasmid (Keima-pLESIP, see also vector map Appendix 8.3) was a gift from Dr Toren Finkel (National Heart, Lung and Blood Institute, Bethesda, USA) and has previously been used to generate lentiviral particles (Sun et al., 2015). The plasmid contains a puromycin

selection cassette. The generation of lentiviral particles and infection of target cells was done with the help of Dr Anna Uryga.

2.11.1 Lentivirus particle production

The plasmids pMD2.G, psPAX (lab stock) and Keima-pLESIP were progagated in One Shot OmniMAX^{TM} 2-T1R chemically-competent *E. coli*. Plasmid DNA was isolated from overnight cultures of *E.coli* in lysogeny broth (LB) supplemented with 100 µg/ml ampicillin using a Qiagen Plasmid Midi Kit (12143) according to the manufacturer's instructions. Plasmid DNA was then precipitated with 2.5 volumes 100% EtOH and 0.1 volumes 3 M sodium acetate (pH 5.2) for 1 hour at room temperature, centrifuged at 14000 rpm for 30 minutes, washed once in 70% EtOH, centrifuged, and re-suspended in tris-EDTA buffer. DNA concentrations were determined using a spectrophotometer (NanoDrop).

7 x 10^5 HEK-293T cells were plated into 60 mm culture dishes using DMEM supplemented with 10% FCS without antibiotics. After 24 hours subconfluent cells were co-transfected with packaging plasmids pMD2.G (250 ng), psPAX (750 ng) and Keima-pLESIP (1 µg) using FuGENE 6 (Roche) and OptiMEM. The transfection medium was replaced with fresh culture medium after 24 hours, pseudo-lentivirus particles were harvested after 48 hours, concentrated using Amicon Ultra-15 centrifugal filter devices and stored at -80^{o}C. A small sample was used for determination of Lentivirus titers using a qPCR lentivirus titration (titer) kit (abm, LV900) according to the manufacturer's instructions.

2.11.2 Infection of HeLa cells and HVSMCs

HeLa cells plated in 6-well plates were infected with a multiplicity of infection (MOI) of 1 in the presence of 8 μg/ml Hexadimethrine bromide (Polybrene, Sigma) using spinoculation at 1500 x g for 30 minutes at room temperature. After an overnight incubation the medium was changed to culture medium or culture medium supplemented with 0.75 μg/ml puromycin. HeLa cells were expanded, frozen for future use or used for Western blotting to confirm expression of Keima and for visualisation using confocal microscopy.

HVSMCs and plaque VSMCs were plated at 100,000 cells per well in 6-well plates and infected using an MOI of 3 as described above. Cells were selected with 1 μg/ml puromycin, expanded, and either re-plated in 35 mm glass bottom culture dishes (gamma-irradiated, poly-d-lysine coated, No 1.5 coverslip, 10 mm glass diameter, P35GC-1.5-10-C, MatTek) for confocal microscopy analysis or frozen and stored in liquid N_2 for future use.

2.12 Confocal microscopy and image analysis

HVSMCs or plaque VSMCs were seeded in glass bottom culture dishes and stained with 1 μg/ml Hoechst 33342 (Thermo Scientific) for 5 minutes and then washed in PBS immediately before analysis on a Leica SP5 confocal microscope using 63X/1.4NA oil objective. Simon McCallum, manager or the flowcytometry core facility, helped with the initial set-up of the SP5 confocal microscope. Fluorescence of Keima was imaged in two channels after sequential excitation with argon laser at 458 nm (coded green) and yellow laser at 561 nm (coded red) using a 580nm to 690nm emission

range. Hoechst 33342 was imaged in a third channel (coded blue) after excitation with UV light. On each experimental day the laser outputs were optimised and then maintained across different groups. At least 20 z-stacks per group were acquired in at least three independent experiments from three different primary cell cultures per group.

Excitation by 561 nm (red) and 458 nm (green) was calculated for each image using ImageJ and a plug-in designed by Dr Richard Butler, Gurdon Institute, Cambridge. This ratio red/green was termed mitophagy index, where higher values infer increased mitophagic flux (Sun et al., 2015). Quantification of mitochondrial shape and was based on a plug-in that has previously been described (Vowinckel, Hartl, Butler, & Ralser, 2015). In short, mitochondria were defined by Otsu thresholding and the surface area (SA) and the volume (V) of the mitochondrial network were calculated. The ratio SA:V allowed for the estimation of mitochondrial shape with lower values signifying a higher degree of mitochondrial fragmentation. The plug-in also calculated a measure of tubularity of the mitochondrial network (compactness), i.e. the variance of radial distance/volume, as described before (Vowinckel et al., 2015).

2.13 Mouse model of atherosclerosis – fat-feeding of ApoE-/- mice

This research has been regulated under the Animals (Scientific Procedures) Act 1986 (amended 2012) following ethical review by the University of Cambridge Animal Welfare and Ethical Review Body (AWERB). ApoE-/- mouse colonies on a C57BL/6 background were kept in the Cardiovascular Division of the University of Cambridge and maintained by animal technicians. All animal experiments were performed with the help of

the animal technician Alison Finigan. After weaning, a proportion of littermate female mice was started on a high-fat 'Western' diet (Special Diets Services 829100, ~21% Fat, ~20% Protein) or kept on standard animal chow (Scientific animal food & engineering, R105-25), as indicated in the individual experiments. When multiple durations of fat-feeding were used in an experiment the start of the high-fat diet was staggered so that at sacrifice aged-matched littermates could also be used.

Mice were sacrificed using rising CO_2 concentrations and subsequent cervical translocation. Blood was collected by cardiac puncture (done by Alison Finigan), centrifuged and serum snap frozen in liquid N_2 and stored at -80^{o}C until use. To increase speed and consistency, Alison Finigan helped with dissection of hearts, livers and aortas for snap freezing in liquid N_2 or downstream applications as described below.

2.13.1 Lipid and cytokine measurement

Serum samples derived from ApoE-/- mice at sacrifice were analysed by the core biochemical assay laboratory (clinical pathology accredited) at Addenbrooke's Hospital, Cambridge. Cholesterol, Triglycerides, HDL and a calculated LDL were determined through standard techniques. A cytokine panel (Mesoscale, Proinflammatory Panel 1, K15048G) was used to measure serum levels of ten analytes: IFN-γ, IL-1β, IL-2, IL-4, IL-5, IL-6, IL-10, IL-12p70, KC/GRO, TNF-α.

2.14 Determination of Mito P/B ratio in mouse aortas

The mitochondria-targeted ratiometric mass spectrometry probe MitoB has been developed to allow the measurement of H_2O_2 *in vivo* (Cocheme et al., 2011) (see Figure 2-1). 25 nmol MitoB in 50 µl 0.9% sterile sodium chloride was injected into the tail vein of the mouse. The injection was done by Alison Finigan. Mice were sacrificed 3 hours after injection using rising CO_2 concentrations and aortas dissected rapidly with further help from Alison Finigan. Aortic samples were snap frozen in liquid N_2 until extraction of MitoB and MitoP.

Tissue was homogenised in 60% acetonitrile and 0.1% formic acid at 4^{o}C in a bullet blender storm (Next Advance, USA), centrifuged at 16,000 x g for 10 minutes and the supernatant transferred to a new reaction tube. The extraction was repeated and the supernatants were pooled, spiked with deuterated d_{15} internal standards of MitoB and MitoP, filtered, dried in a speed vac concentrator and resuspended in 20% acetonitrile and 0.1% formic acid. Standards of MitoB (1- 100 µM) and MitoP (0-25 µM) were prepared in parallel in untreated rat liver tissue homogenate (gift from Tracy Prime).

Detection and quantification of MitoP and MitoB were done by Dr Angela Logan and Dr Sabine Arndt as previously described (Logan et al., 2014). In short, MitoP and MitoB were detected using an I-class Acquity liquid chromatograph attached to a Xevo TQ-S triple quad mass spectrometer (Waters). Data was analysed using MassLynx software, and the amounts of MitoP and MitoB in each sample determined relative to a standard curve allowing for the ratio of MitoP/MitoB to be formed.

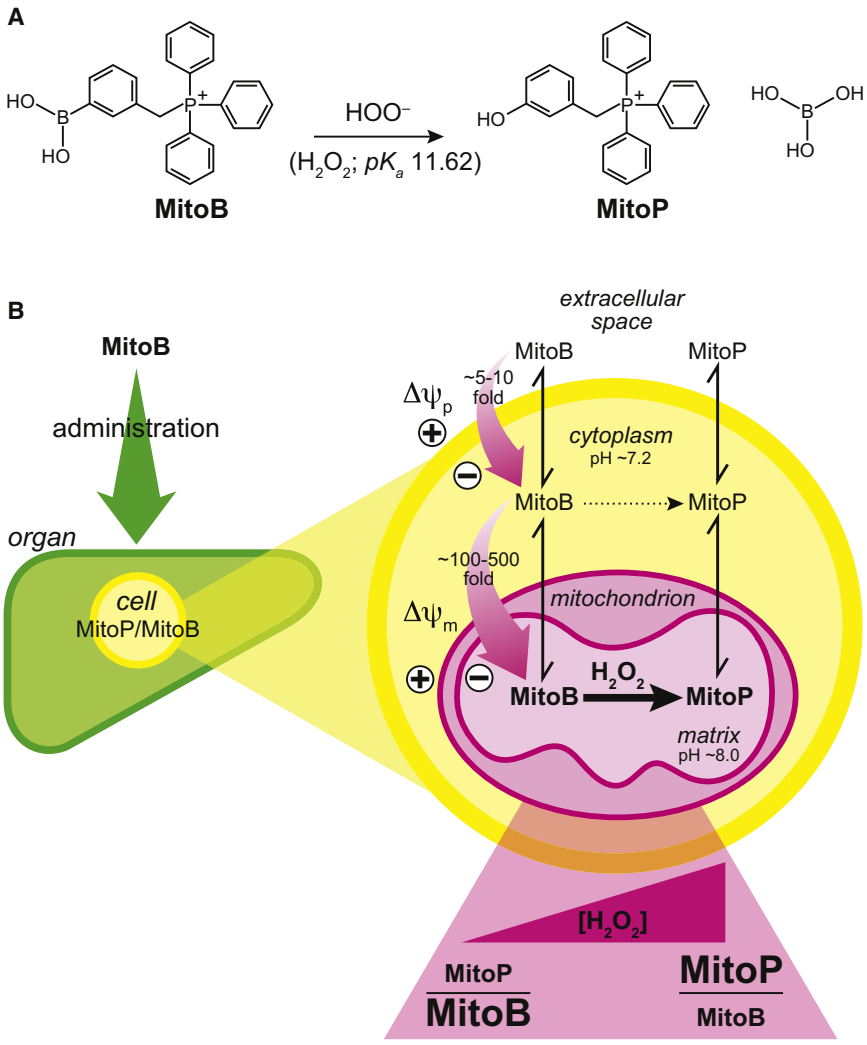

Figure 2-1 Principles of H_2O_2 assessment using MitoB in mice

A) Boronic acid linked to tetraphenolphosphonium (TPP), MitoB, reacts with the conjugate bsae of H_2O_2, HOO-, to form the phenol product MitoP. B) Mice receive a tail vein injection of MitoB. MitoB is then taken up into cells driven by the plasma membrane potential ($\Delta\Psi_p$) and further accumulates in mitochondrial through the mitochondrial membrane potential ($\Delta\Psi_m$). The reaction of A) is facilitated by high mitochondrial concentrations of MitoB and is further enhanced by the alkaline environment such that the reaction primarily occurs within the mitochondrial matrix. The MitoP/MitoB ratio determined through LC-MS/MS is therefore an indicator of mitochondrial H_2O_2 concentrations. Figure adapted from (Cocheme et al., 2011).

2.15 Glutathione recycling assay

The glutathione recycling assay is well established and has been described in detail (Rahman, Kode, & Biswas, 2006). The underlying

reactions are summarised in Figure 2-2. Aortic samples were snap frozen in liquid N_2 after mouse sacrifice. Samples were kept on dry ice, weighed quickly, and lysed in HCL-acidified EtOH (20 µl/mg tissue, pH 1) in CK14 vials (Precellys) using a high speed tissue lyser (Precellys24, Bertin Instruments). 20 µl of sample equivalent to 1 mg of tissue was supplemented with 80 µl 5% sulfosalicylic acid to inhibit γ-glutamyl transferase (γ-GT) and centrifuged at 14,000 rpm for 10 minutes to precipitate proteins and 10 µl of supernatant was then used in the assay. Standards of GSH in 5% 5-sulfosalicylic acid (SSA) were made up at concentrations of 5, 10, 20, 50, and 100 µM. Samples were incubated in a 96-well plate in the presence of 0.5 mM NADPH, 0.5 mM 5,5'-dithio-bis (2-nitrobenzoic acid) (DTNB) and 4 U/ml glutathione reductase. Absorbance of 5'-thio-2-nitrobenzoic acid (TNB) was measured at 412 nm using a Spectramax microplate reader (Molecular devices, CA, USA).

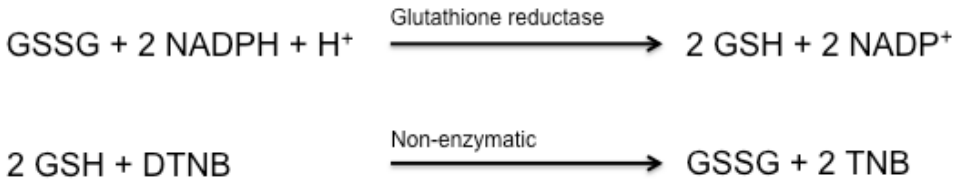

Figure 2-2 Principles of the glutathione recycling assay

Total glutathione concentrations, GSSG and GSH, in mouse aortic samples was determined using the glutathione recycling assay. GSSG/GSH: oxidised/reduced glutathione, $NADP^+$/NADPH: oxidised/reduced nicotinamide adenine dinucleotide phosphate, DTNB: 5,5'-dithio-bis (2-nitrobenzoic acid), also known as Ellman's reagent, TNB: 5'-thio-2-nitrobenzoic acid. TNB is then quantified by absorption at 412 nm.

2.16 Determination of ATP/ADP ratio in mouse aortic tissue

An assay to determine ATP and ADP extracted from tissues based on Strehler (1974) has been established in Dr. Murphy's laboratory and depends on the reactions described in Figure 2-3.

ATP is rapidly degraded in tissues before extraction and snap-frozen tissues (1-5 mg) were therefore ground up without thawing using a pestle and mortar kept on dry ice. ATP and ADP were extracted using 1 ml ice-cold perchloric acid extractant (3% v/v $HClO_4$, 2 mM Na_2EDTA, 0.5% Triton X-100). The pH of 400 µl sample was neutralised (pH 7-7.5) using ice-cold potassium hydroxide buffer (2 M KOH, 2mM Na_2EDTA, 50 mM MOPS), the precipitate was pelleted and the supernatant used in the assay. Standard curves of ATP (0-20 µM) and ADP (0-5 µM) were prepared and neutralised as above. For measurement of ATP, 100 µl of neutralised sample or standard was added to 400 µl Tris-acetate buffer (100 mM Tris, 2 mM Na_2EDTA, 50 mM $MgCl_2$, pH 7.75 with glacial acetic acid). For measurement of ADP, 250 µl neutralised sample was first incubated with 250 µl ATP sulfurylase buffer [5 mM 5'GMP, 20 mM Na_2MoO_4, 0.2 U ATP sulfurylase (New England Biolabs, 0394L), in Tris-HCL buffer (100 mM Tris-HCl, 10 mM $MgCl_2$, pH 8)], shaken at 30^{o}C for 20 minutes and then boiled at 100^{o}C for 5 minutes to deactivate the sulfurylase. 200 µl of this ATP depleted sample was added to 400 µl Tris-acetate buffer. Samples and standards of ATP and ADP were then incubated with 10 µl pyruvate kinase (PK)/phosphoenoylpyruvate (PEP) solution [1.25 µl PK suspension (Sigma P1506), 100 mM PEP] for 30 minutes at 25^{o}C. To test for complete degradation of ATP in the ATP sulfurylase reaction, a sample without addition of PK/PEP solution was incubated in parallel. All standards

and samples were then analysed in an AutoLumat plus (Berthold) luminometer after injection of 100 µl luciferin/luciferase solution [120 µM luciferin (L6882),1.92 µg luciferase protein/ml (Sigma, L9506), 0.4 mg/ml BSA, 7.5 mM DTT made up in Tris-acetate buffer supplemented with 25% glycerol].

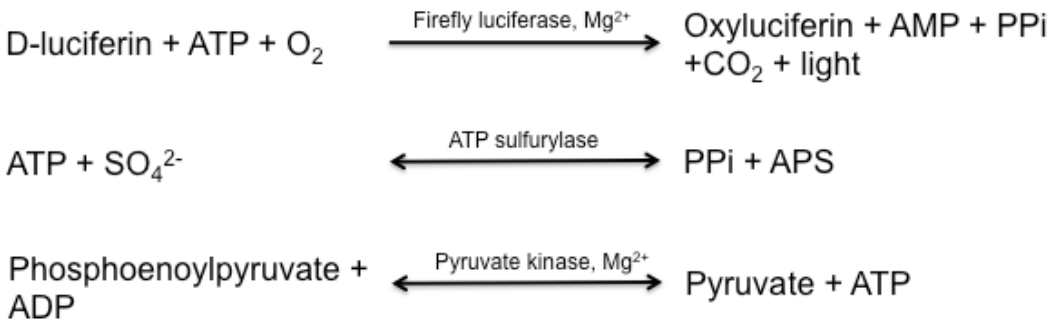

Figure 2-3 Principles of ATP/ADP ratio assay

To measure ATP concentrations D-luciferin reacts, catalysed by luciferase and Mg^{2+}, in the presence of adenosine triphosphate (ATP) and O_2 to Oxyluciferin, adenosine monophosphate, pyrophosphate anion $P_2O_7^{4-}$ (PPi) and CO_2, thereby emitting light. This light emission can be detected using a luminometer. To allow for the measurement of ADP, the ATP in the sample is degraded through the ATP sulfurylase reaction forming PPi and adenosine 5'-phosphosulfate (APS). The remaining ADP is then converted to ATP catalysed by pyruvate kinase and ATP and measured through the D-luciferin/luciferase reaction.

3 Effects of lipids, LPS and sirtuin-1 on cultured rat VSMCs

3.1 Introduction

Different stimuli including exposure to OxLDL or inflammatory mediators as well as the altered expression of proteins such as sirtuins involved in mitochondrial function may all lead to the disruption of mitochondrial performance in atherosclerosis. In this chapter I aim to identify stimuli relevant to atherosclerosis that induce mitochondrial dysfunction in cultured VSMCs using rat VSMCs (RVSMCs) overexpressing sirtuin-1, deacetylase-deficient sirtuin-1, or empty vector that have previously been developed in our laboratory (Gorenne et al., 2013) (section 3.2). In a first set of experiments the uptake of DiI-labelled OxLDL was assessed using flow cytometry (section 3.3). The effects of LDL, OxLDL and LPS on mitochondrial respiration and extracellular acidification of RVSMCs was then examined using a Seahorse extracellular flux analysis assay (section 3.4). The expression of ETC complexes (section 3.5) and mtDNA copy number (section 3.6) were determined after OxLDL treatment.

3.2 Sirtuin-1 expression in rat vascular smooth muscle cell lines

RVSMCs were previously generated by Dr Isabelle Gorenne using retroviruses encoding either the empty vector, human sirtuin-1 or a deacetylase-deficient mutant of human sirtuin-1 in which histidine substitutes tyrosine 365 (sirtuin-1^{H365Y}) (Gorenne et al., 2013). In the following these

RVSMCs are denoted EV, SIRT+ and SIRT-, respectively. To confirm that these cells overexpress sirtuin-1 and that other sirtuins such as sirtuin-6 are not dysregulated, Western blotting was performed. Figure 3-1 demonstrates that expression of human sirtuin-1 is detected in SIRT+ and SIRT- RVSMCs but not in EV RVSMCs. Expression was assessed in whole cell lysates and subcellular localisation of sirtuin-1 was not determined. Endogenous levels of rat sirtuin-1 and sirtuin-6 were not affected by the overexpression of the human isoform. Probing against actin demonstrated equal protein loading.

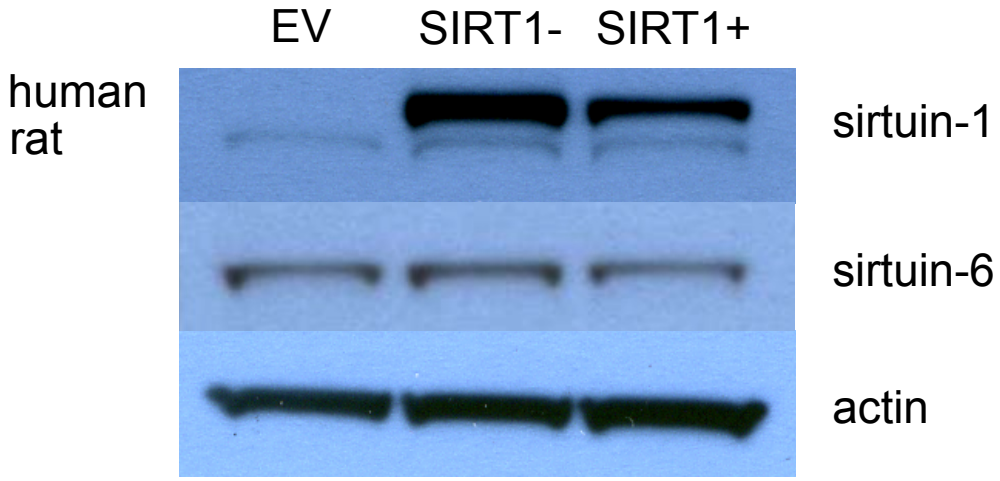

Figure 3-1 Sirtuin-1 and sirtuin-6 expression in RVSMCs

EV, SIRT- and SIRT+ whole cell lysates were subjected to SDS gel electrophoresis using pre-cast 8-12% gradients gels. Membranes were probed for sirtuin-1 and sirtuin-6. Top band of upper panel corresponds to human sirtuin-1 and lower band to rat sirtuin-1. See also Appendix 8.1.

3.3 Uptake of DiI-OxLDL into rat VSMCs

Previous studies in endothelial cells reported that inflammatory cytokines and OxLDL can upregulate the scavenger receptor SR-E1 (LOX-1) (Sawamura et al., 1997) and that such upregulation is diminished in sirtuin-1

siRNA-treated cells (Ma et al., 2013). OxLDL uptake in RVSMCs with or without overexpression of sirtuin-1 was therefore examined. RVSMCs were cultured in 24-well plates prior to treatment with various concentrations of DiI-OxLDL for 24 hours. Cells were trypsinised, fixed and DiI-OxLDL uptake examined by flow cytometry. DiI-OxLDL was taken up in a dose-dependent manner, but was significantly lower in SIRT+, and SIRT- cells compared to EV (Figure 3-2).

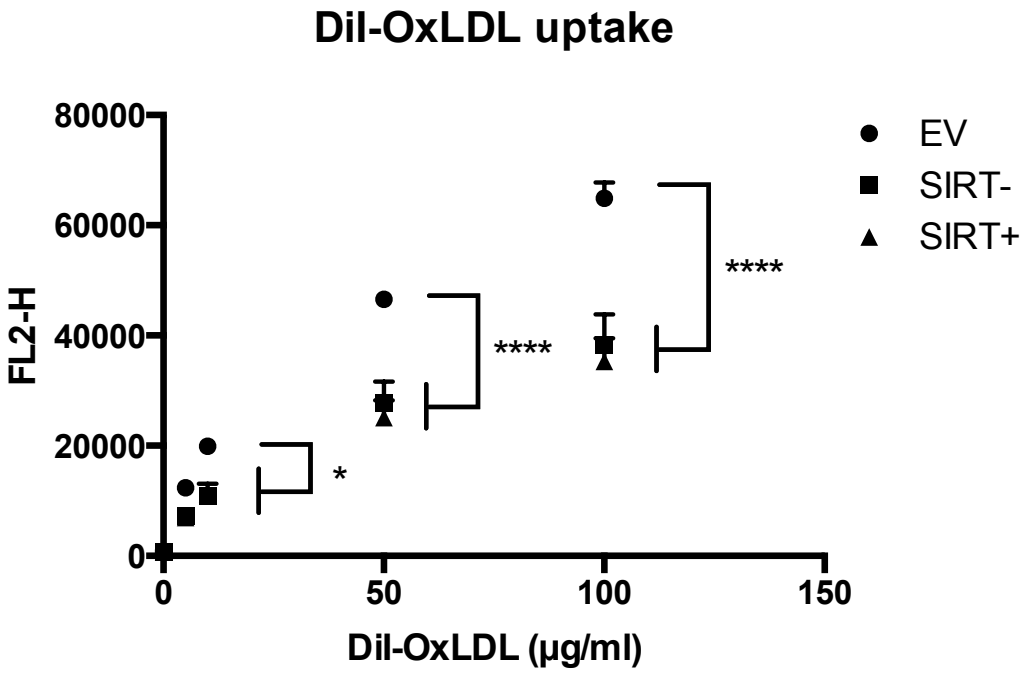

Figure 3-2 DiI-OxLDL uptake in RVSMCs

EV, SIRT- and SIRT+ RVSMCs were treated with varying concentrations of DiI-labelled OxLDL (DiI-OxLDL) for 24 hours, trypsinised and subjected to flow cytometry analysis. The peak fluorescence value (FL2-H) was determined using a BD Accuri flow cytometer. Data are means ± SEM of N=3 independent experiments. * $P<0.05$, **** $P<0.0001$ for EV compared to SIRT- and SIRT+ using two-way ANOVA with Bonferroni's correction for multiple comparisons.

3.4 Extracellular flux analysis

A Seahorse bioscience 96-well extracellular flux analyser (XF96) was used to examine the effects of OxLDL on mitochondrial respiration. The XF96 simultaneously measures the oxygen tension and pH, therefore allowing calculation of the oxygen consumption rate (OCR) and extracellular acidification rate, a measure of glycolysis flux. Through sequential injection of mitochondrial inhibitors (oligomycin, rotenone and antimycin) and the uncoupler FCCP, the OCR for mitochondrial ATP generation can be differentiated from OCR due to proton leak and non-mitochondrial OCR. Uncoupling with FCCP needs to be titrated as uncoupling increases dose-dependently, before plateauing at optimal concentrations and decreasing at supra-optimal concentrations (manufacturer's instructions, www.seahorsebio.com).

As very few studies have been published on mitochondrial function in cultured RVSMCs, the optimal seeding density and FCCP concentrations were determined. RVSMCs were plated at 5000 cells/well in 96-well Seahorse culture plates, incubated for 48 hours, washed once with sterile assay medium, and analysed in the XF96. 2 µg/ml oligomycin and 1 µM each of rotenone/antimycin A were used. The ideal FCCP concentration based on maximal uncoupling for each well was found to be 1 µM and was therefore used in all future experiments (Figure 3-3). At an initial seeding density of 5000 cells/well, baseline OCR prior to injection of any inhibitors was around 200 pmol/min. A baseline OCR of 100 pmol/min aids measurement of oxygen consumption within the dynamic range of the flux analyser (Dr Hannah Bridges, Mitochondrial Biology Unit, Cambridge, personal communication), so

2500 RVSMCs were plated per well in all subsequent experiments. This plating density results in approximately 90-95% confluence after 48 hours.

Subsequently, 2500 EV, SIRT- or SIRT+ RVSMCs were seeded into 96-well plates and incubated for 24 hours prior to treatment with varying doses of LDL, OxLDL and LPS for a further 24 hours. As the mitochondrial inhibitors can be toxic and therefore affect protein concentrations after the assay, a parallel 96-well plate was used to determine protein concentrations after all treatments. All OCR and ECAR values were then normalised to µg protein to allow adjustment for potential differences in cellular density during the run. For assessment of the effects of various treatments, data was expressed as % change from untreated. The resulting data is presented as a comparison of EV, SIRT- and SIRT+ RVSMCs (Figure 3-4) and effects of the treatments on EV (Figure 3-5), SIRT- (Figure 3-6) and SIRT + (Figure 3-7).

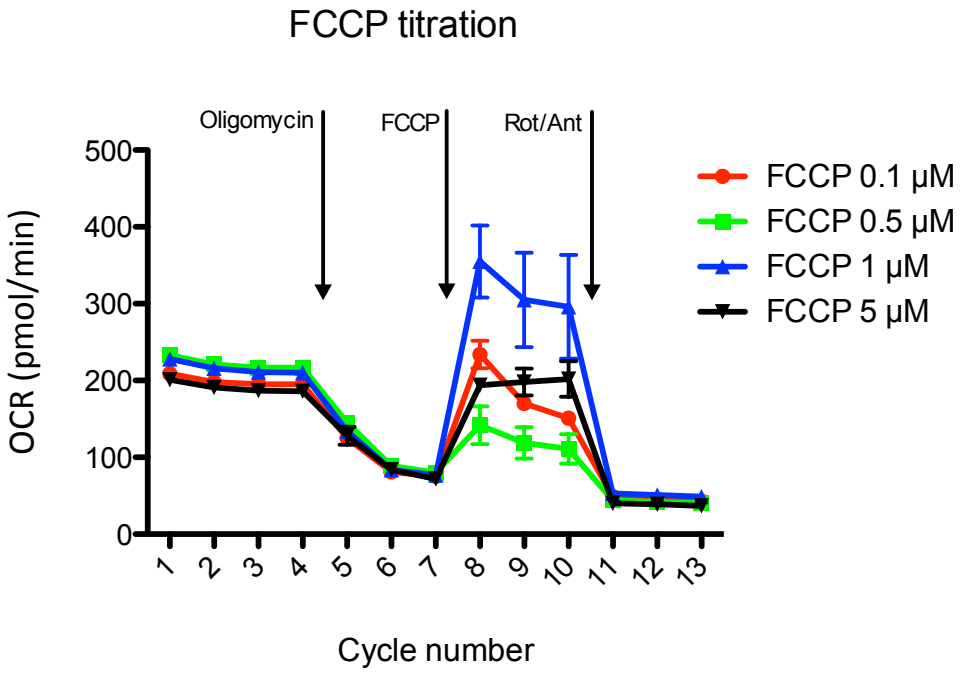

Figure 3-3 Optimisation of FCCP concentration

5000 EV RVSMCs were plated into a 96-well Seahorse culture plate and incubated for 48 hours prior to addition of inhibitors and extracellular flux analysis. Oligomycin (2 µg/ml final concentration), FCCP at various concentrations, and a combination of rotenone (Rot) 1 µM final concentration and antimycin A (Ant) 1 µM final concentration were injected sequentially. Data represent means ± SEM of technical triplicates in one experiment. Each cycle consists of 3 minutes of waiting, 2 minutes of mixing and 3 minutes of O_2 and pH measurement.

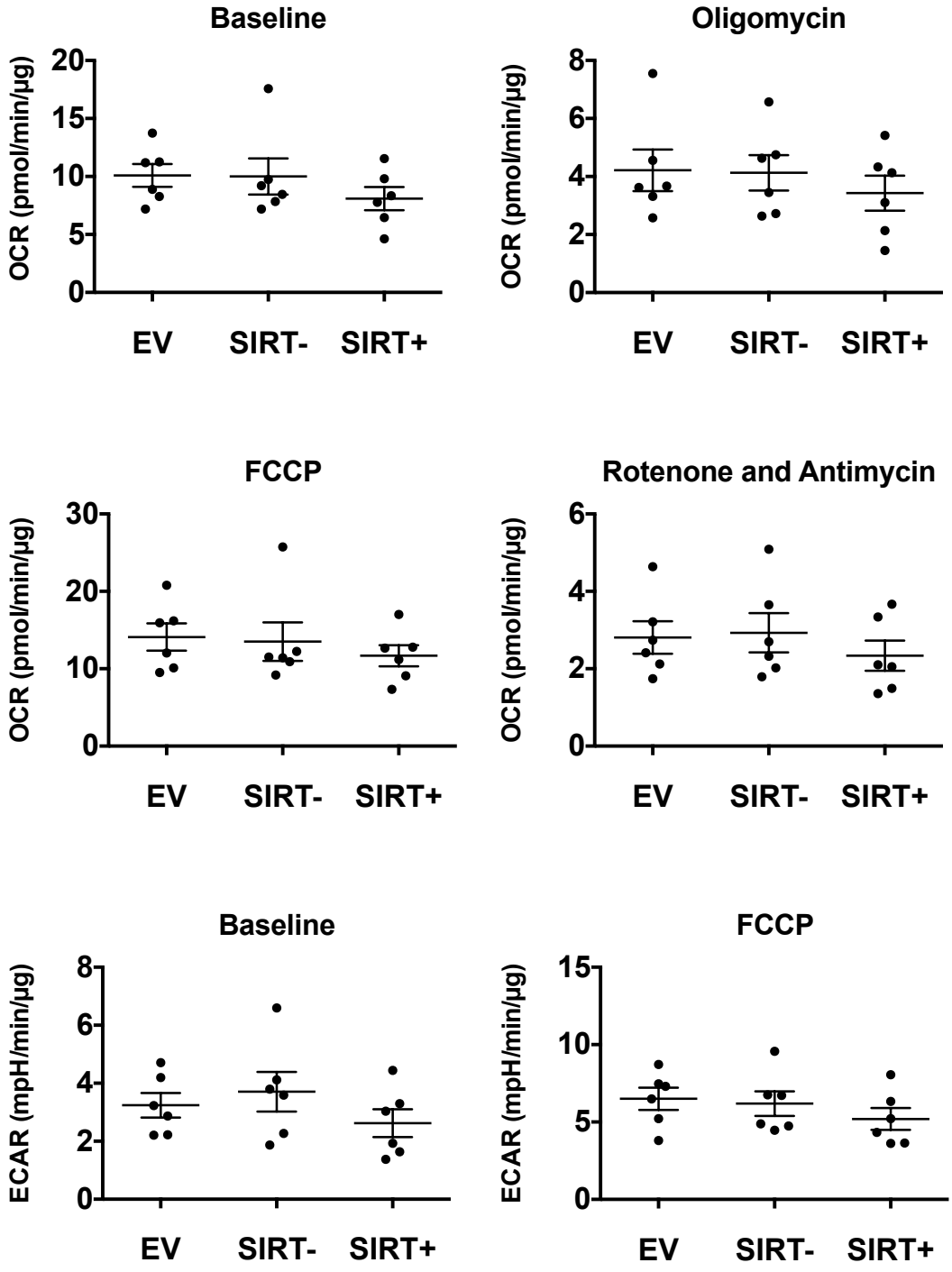

Figure 3-4 OCR and ECAR of EV, SIRT- and SIRT+ RVSMCs

RVSMC lines EV, SIRT- and SIRT+ were analysed using a 96-well plate Seahorse extracellular flux analyser (XF96). Oxygen consumption rate (OCR) and extracellular acidification rate (ECAR) were determined after serial injection of oligomycin (2 µg/ml final concentration), FCCP (1 µM), and a combination of rotenone and antimycin A (1 µM final concentration each) and normalised to amount of protein. Data presented as mean ± SEM of N=6 independent experiments. There were no statistically

significant differences between the cell lines using one-way ANOVA analysis with Bonferroni's correction for multiple comparisons.

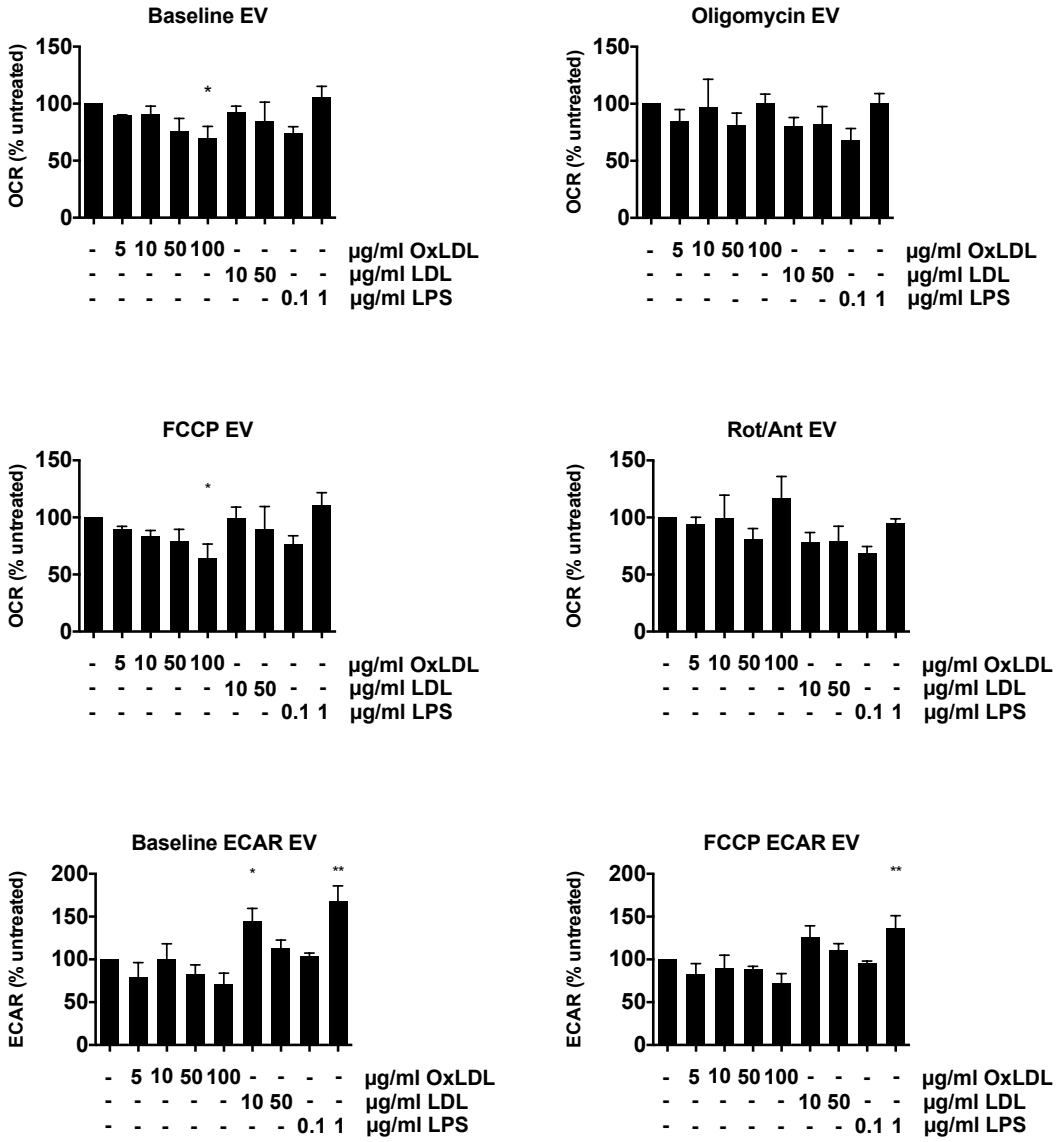

Figure 3-5 OCR and ECAR of EV RVSMCs

EV RVSMCs were analysed using a 96-well plate Seahorse extracellular flux analyser (XF96). Oxygen consumption rate (OCR) and extracellular acidification rate (ECAR) were determined after serial injection of oligomycin (2 µg/ml final concentration), FCCP (1 µM), and a combination of rotenone and antimycin A (1 µM final concentration each) and normalised to amount of protein. Data presented as % baseline (mean ± SEM) from N=3 experiments per treatment group. * $P<0.05$, ** $P<0.01$ using one-way ANOVA with Bonferroni's correction for multiple comparisons.

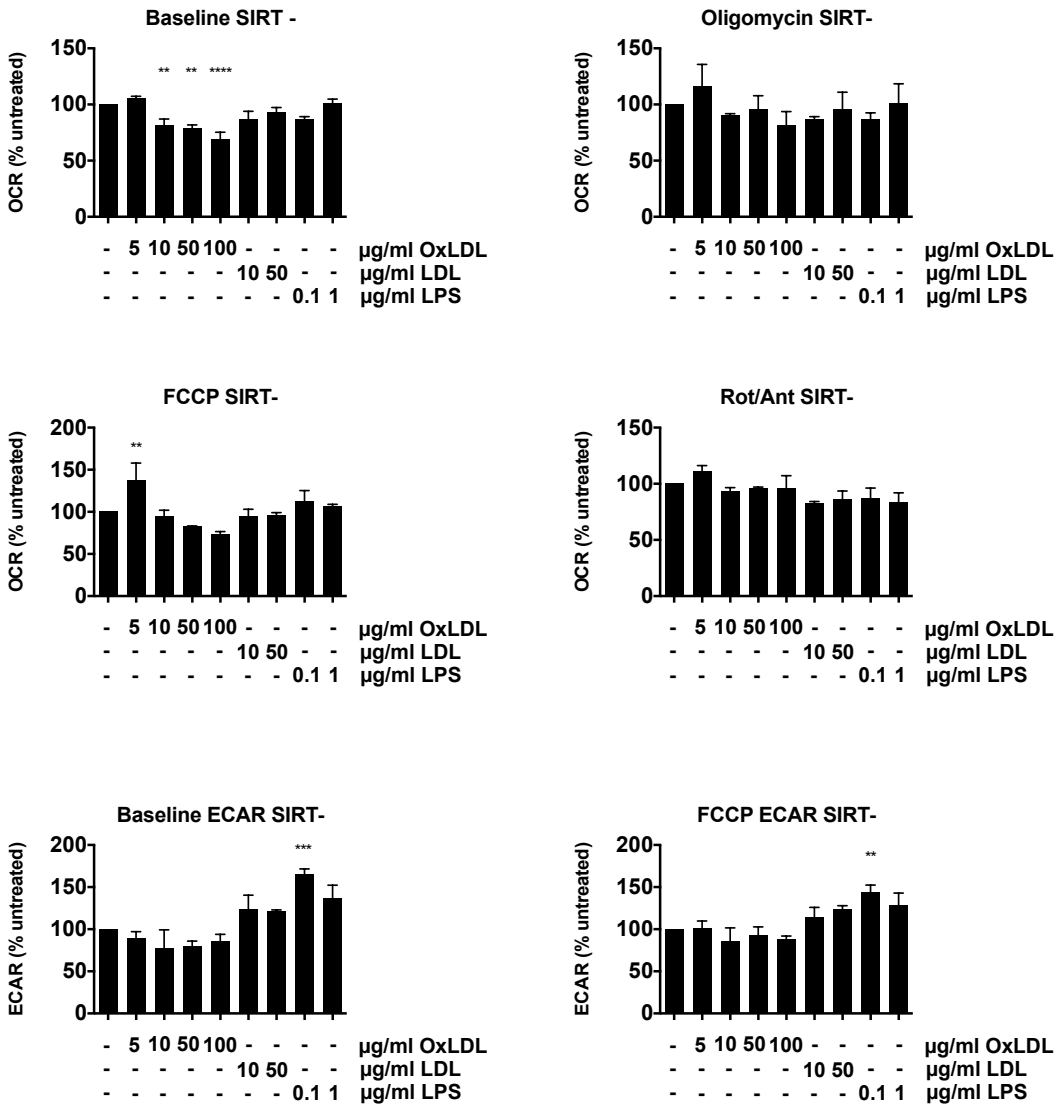

Figure 3-6 OCR and ECAR of SIRT- RVSMCs

SIRT- RVSMCs were analysed using a 96-well plate Seahorse extracellular flux analyser (XF96). Oxygen consumption rate (OCR) and extracellular acidification rate (ECAR) were determined after serial injection of oligomycin (2 µg/ml final concentration), FCCP (1 µM), and a combination of rotenone and antimycin A (1 µM final concentration each) and normalised to amount of protein. Data presented as % baseline (mean ± SEM) from N=3 experiments per treatment group. ** P<0.01, *** P<0.001, **** P<0.0001 using one-way ANOVA with Bonferroni's correction for multiple comparisons.

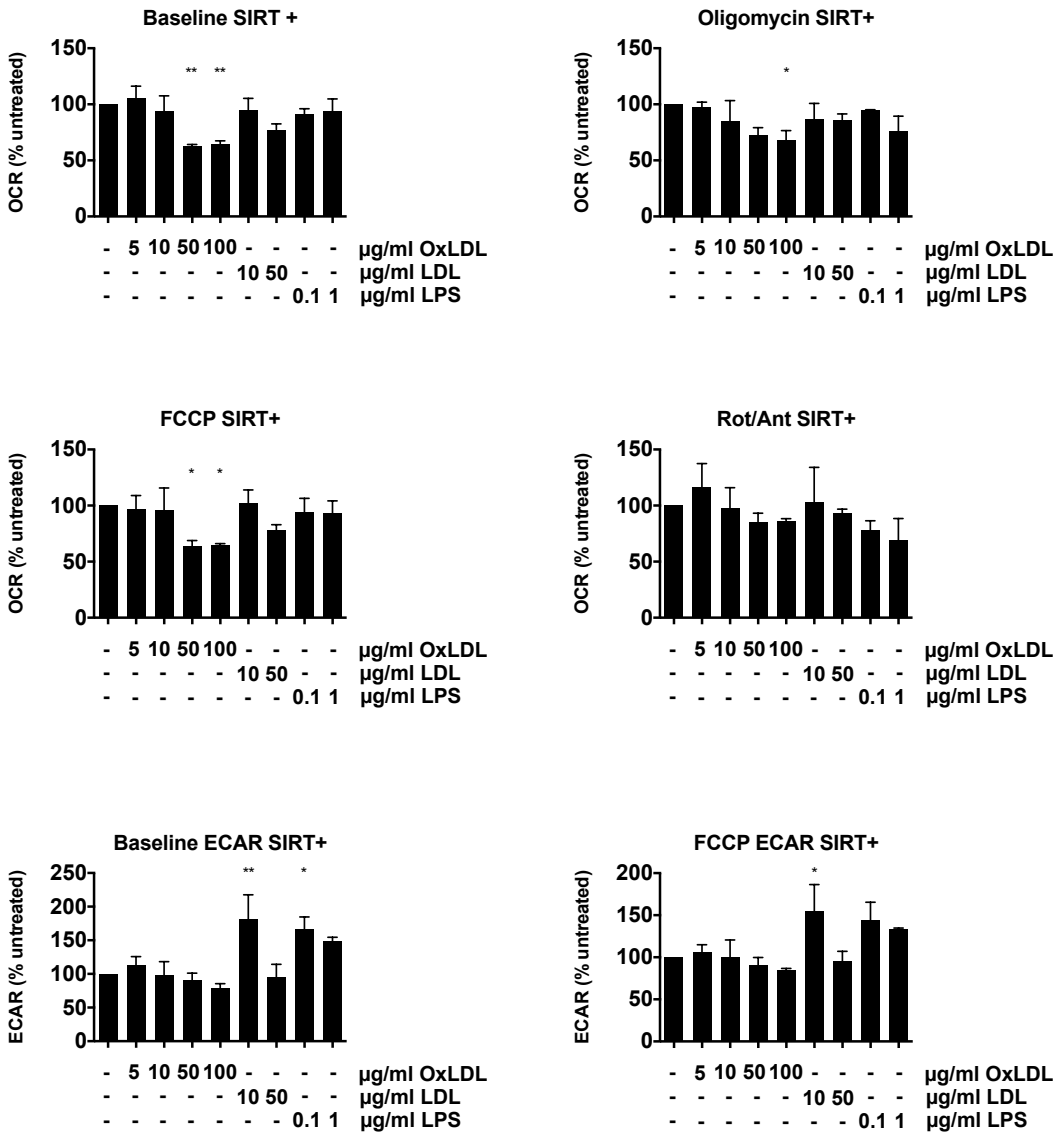

Figure 3-7 OCR and ECAR of SIRT+ RVSMCs

SIRT+ RVSMCs were analysed using a 96-well plate Seahorse extracellular flux analyser (XF96). Oxygen consumption rate (OCR) and extracellular acidification rate (ECAR) were determined after serial injection of oligomycin (2 µg/ml final concentration), FCCP (1 µM), and a combination of rotenone and antimycin A (1 µM final concentration each) and normalised to amount of protein. Data presented as % baseline (mean ± SEM) from N=3 experiments per treatment group. * $P<0.05$, ** $P<0.01$ using one-way ANOVA with Bonferroni's correction for multiple comparisons.

There was no difference in the OCR at baseline and following serial injection of oligomycin, FCCP and the combination of rotenone and antimycin

A between EV, SIRT- and SIRT+ RVSMCs (Figure 3-4). Similarly ECAR did not differ across the cell lines (Figure 3-4). In EV cells, OxLDL, but not LDL, dose-dependently decreased cellular respiration both at baseline and following uncoupling with FCCP (Figure 3-5). LPS (1000 ng/ml) significantly increased ECAR. The pattern of response of SIRT- (Figure 3-6) and SIRT+ (Figure 3-7) was similar. A significant increase in ECAR was also observed with 10 µg/ml LDL. This is surprising and was not observed with 50 µg/ml raising the possibility of an erroneous result, particularly as this effect was not observed across all three cell lines.

3.4.1 RVSMC viability and density after treatment with OxLDL

Although the OCR and ECAR values derived from the extracellular flux analysis were normalised to protein concentrations as a surrogate for cell number, it was important to determine whether the effects of OxLDL were due to effects on overall cell viability or density. The 3-(4,5-dimethylthiazol-2-yl)-2,5-diphenyl tetrazolium bromide (MTT) assay was used to detect cell growth and survival (Mosmann, 1983), where yellow MTT is reduced to a dark blue formazan detected by a 96-well plate reader. The reduction, however, is dependent on NADH/NADPH and a significant proportion of MTT reduction depends on mitochondrial electron transport (Berridge & Tan, 1993). This assay would therefore only be useful if no differences in MTT conversion were observed. As demonstrated in Figure 3-8 OxLDL markedly reduced absorbance in EV, SIRT- and SIRT+ cells. Furthermore, the effects observed after incubation with OxLDL solution may have been due to remnant copper

ions rather than the OxLDL itself, further limiting the use of this assay in the present study. The assay was therefore not used further in this study.

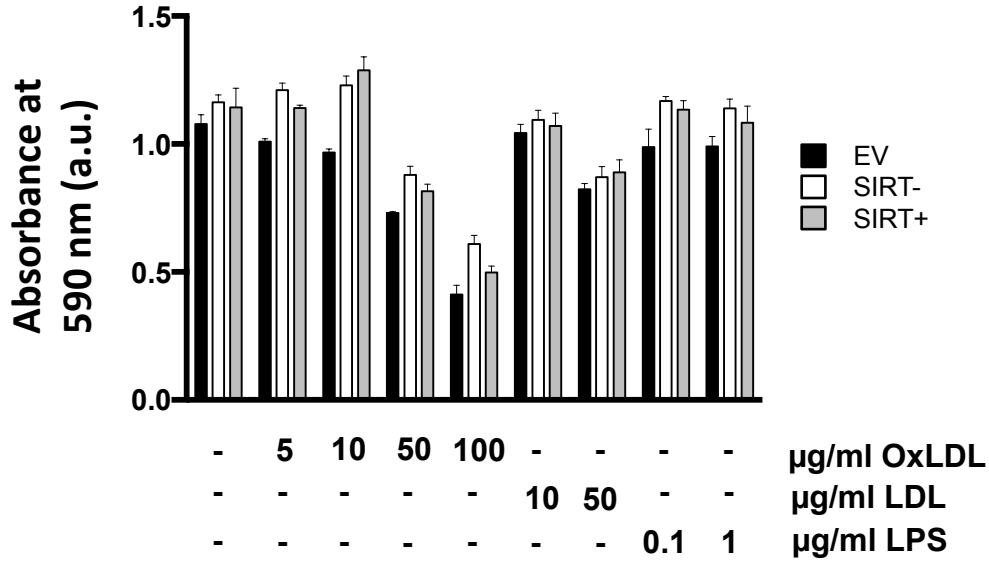

Figure 3-8 MTT assay in RVSMCs treated with atherogenic lipids and LPS

RVSMCs were plated in triplicate wells of 96-well plates, allowed to adhere and treated with varying concentrations of OxLDL, MTT reduction was assessed by absorbance at 590 nm. Data represents mean ± SEM of technical triplicates in one experiment. a.u.: arbitrary unit

Because there were no differences in respiration of SIRT+ and SIRT- compared to EV cells and the responses to OxLDL were similar in both the Seahorse extracellular flux analysis and the MTT assay, SIRT+ and SIRT- RVSMCs were not studied further.

To clarify whether the effects seen during extracellular flux analysis are due to effects on cellularity rather than mitochondrial function, an Incucyte HD live cell imager (Essen Bioscience) was used to directly assess cell density after OxLDL treatment. EV RVSMCs were plated in 6-well culture plates, and

confluence measured every four hours. Although confluence as an outcome measure cannot differentiate between effects on proliferation, cell death and cell shape, it should provide an approximation of total cell number. In preliminary experiments plating densities of 50,000 RVSMCs per well led to near confluence at 72 hours. EV RVSMCs were therefore plated at this density and treated with 5-100 µg/ml OxLDL or vehicle. OxLDL at the concentrations used in the extracellular flux analysis did not decrease cell density (Figure 3-9), suggesting that the reduced respiration observed in previous experiments is due to reduced mitochondrial respiration rather than decreased cell number.

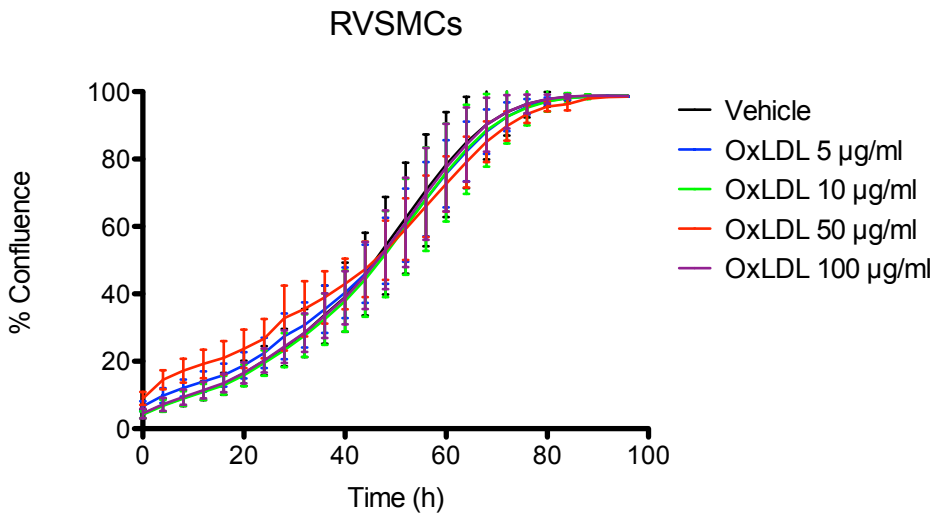

Figure 3-9 Effects of OxLDL on confluence of RVSMCs

EV RVSMCs were seeded into 6-well plates at 50,000 cells per well, and treated with varying doses of OxLDL as indicated of vehicle control (PBS). Confluency was assessed using an Incucyte HD live cell imager placed in a cell culture incubator. Data represents mean % confluence ± SD of N=3 biological replicates with technical duplicates.

3.5 Effects of OxLDL on electron transfer chain complex expression

Section 3.4 has demonstrated that OxLDL decreases OCR in RVSMCs but the mechanism of this effect is not known. One possibility is that OxLDL affects the expression of proteins in the electron transfer chain (ETC), either through damage and subsequent degradation or reduced synthesis. Western blot was therefore used to examine expression of each ETC complex subunit with citrate synthase as a loading control. Administration of the pro-oxidant tert-butyl hydroperoxide (t-BHP), an oxidative damage-causing agent, was used as a positive control. OxLDL did not affect the expression of any of the subunits tested, whereas t-BHP significantly decreased complex I expression (Figure 3-10).

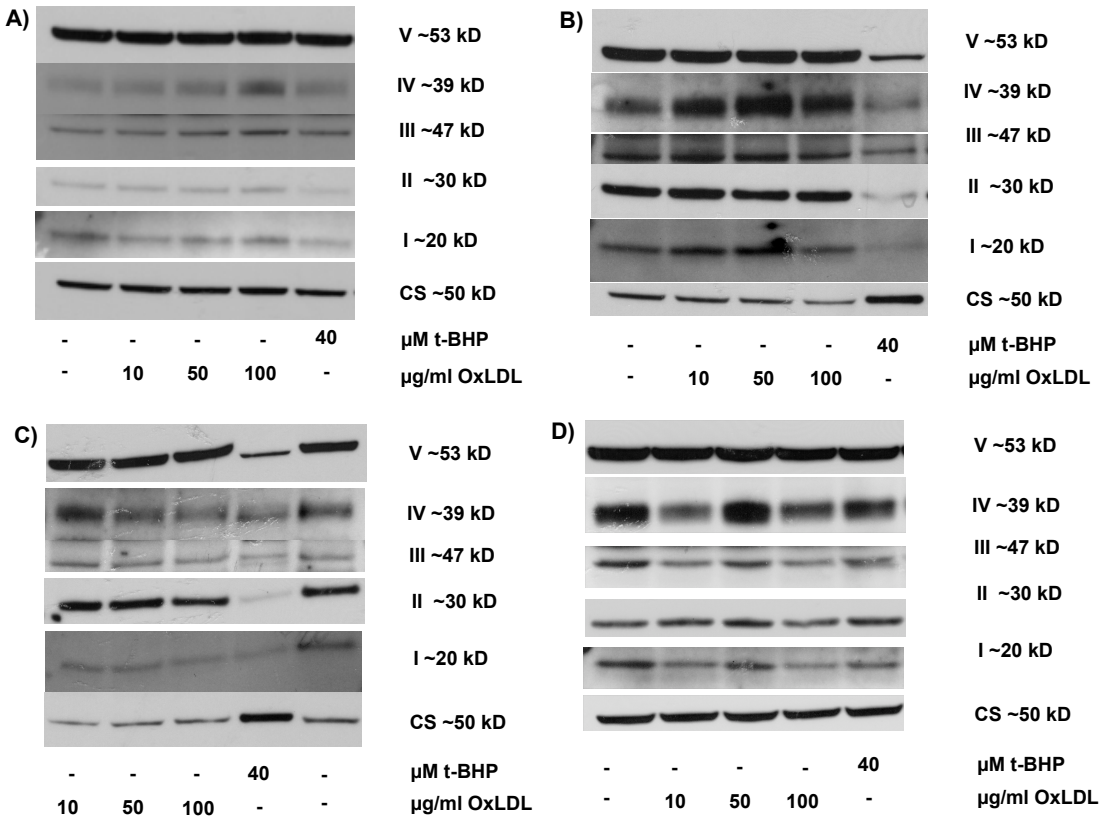

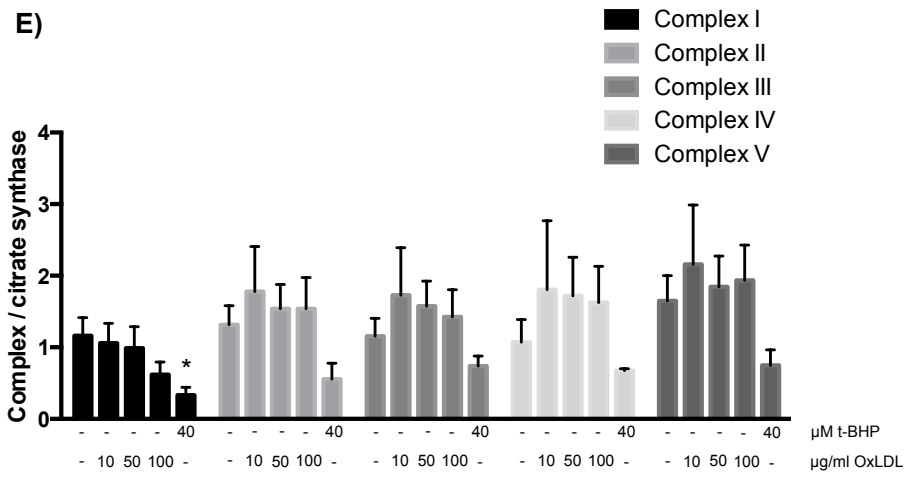

Figure 3-10 Western blots of electron transfer chain complexes in RVSMCs

A) – D) Western blot of whole cell lysates after treatment with OxLDL or t-BHP. I-V corresponds to subunits of electron transport chain complexes and ATP synthase. CS: citrate synthase. Intensity of bands in Western blots varied across different complexes and different exposure times were therefore used. Note different loading order in Western blot C. E) Densitometry analysis of N=4 Western blots normalised to citrate synthase. Results expressed as mean ± SEM. * $P<0.05$ using one-way ANOVA. See also Appendix 8.1.

3.6 Effects of OxLDL on mitochondrial DNA copy number

mtDNA copy number is highly correlated to mitochondrial gene expression levels and mitochondrial mass across different tissues (D'Erchia et al., 2015), such that reduced mtDNA copy number may be an alternative explanation for the reduced respiration rate after OxLDL treatment. mtDNA copy number was determined by amplification of a short segment of mtDNA normalised to a short segment of nuclear DNA. The qPCR was first validated demonstrating comparable reaction efficiencies for the nuclear and mitochondrial amplicon and satisfactory melt curve analysis (Figure 3-11). No statistically significant differences of mtDNA copy number were observed after OxLDL or t-BHP treatment (Figure 3-12).

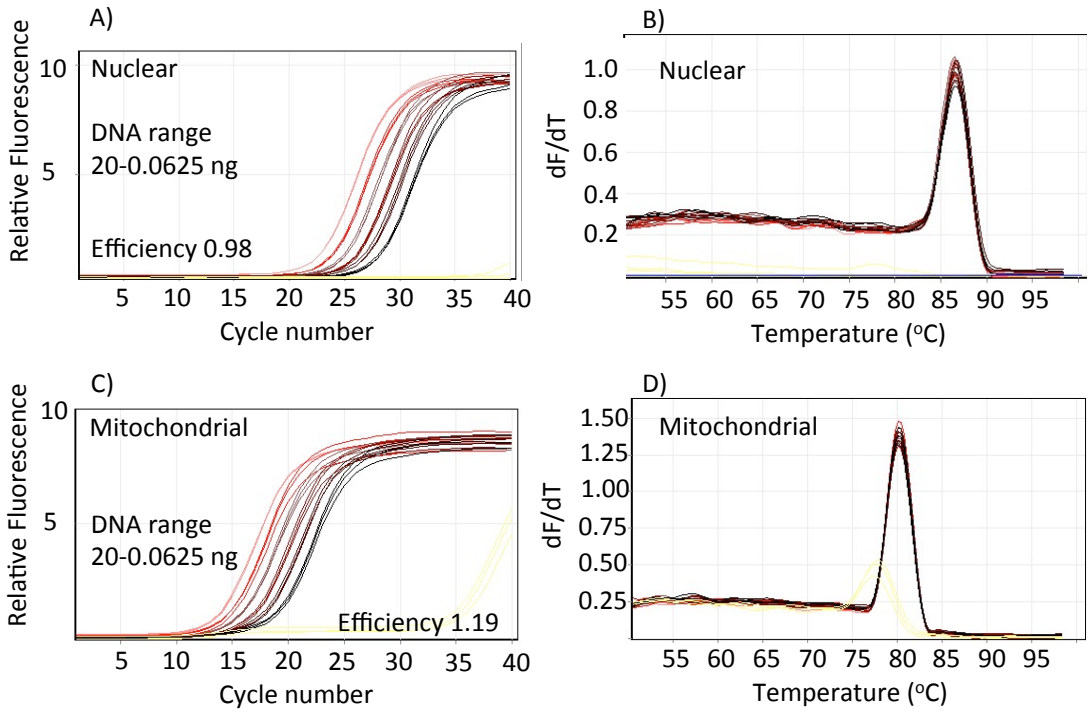

Figure 3-11 Validation of qPCR for rat mitochondrial DNA copy number

Rat DNA was serially diluted (1:2) ranging from 20-0.625 ng and qPCR reactions were run in triplicate on a Corbett Rotor-Gene™ 6000 QPCR thermocycler. A) There is linearity of the nuclear amplification over a wide DNA input range. The efficiency of the reaction was 0.98. B) Melt curve analysis suggests amplification of a single product. C) Linearity of the mitochondrial reaction is demonstrated over a wide DNA input range and the amplification had a comparable efficiency (1.19). D) Melt curve analysis of the mitochondrial reaction suggests amplification of a single product. dF/dT: the derivative of fluorescence (F) with respect to temperature (T).

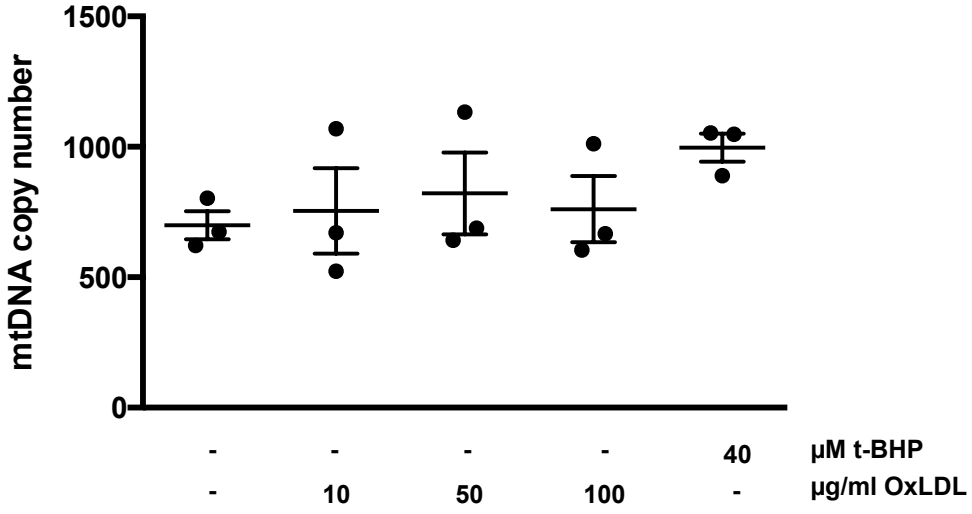

Figure 3-12 Mitochondrial DNA copy number in RVSMCs

EV RVSMCs were treated with varying doses of OxLDL or t-BHP for 24 hours as indicated and DNA was isolated using the GenElute mammalian genomic DNA isolation kit (Sigma). MtDNA copy number relative to nuclear DNA was determined by qPCR in N=3 independent experiments. No statistically significant differences were observed using one-way ANOVA.

3.7 Discussion

MtDNA damage has been described in human atherosclerosis, and previous studies have shown that mtDNA damage in both vessel wall and haematopoietic cells can promote atherosclerosis and/or changes in plaque composition (E. Yu et al., 2013). However, it is currently unclear which of the mediators of atherosclerosis lead to mitochondrial damage during atherogenesis, and whether any of them reduce mitochondrial function. The effects of several known atherogenic factors on RVSMCs were therefore studied including sirtuin-1, which regulates PGC-1α, inflammatory mediators (represented by LPS), and lipids or oxidised lipids.

Treatment of EV, SIRT- and SIRT+ RVSMCs with OxLDL dose-dependently decreased OCR whereas LDL and LPS did not have similar effects. The effects of OxLDL on OCR and MTT reduction in EV RVSMCs were not due to changes in cell density, further suggesting that they may be due to direct effects on mitochondrial function. However, OxLDL did not reduce ETC complex expression or mtDNA copy number. Although mtDNA copy number correlates to mitochondrial mass (D'Erchia et al., 2015) other techniques such as electron microscopy or citrate synthase activity assays could have been used to help determine mitochondrial density in VSMCs

upon OxLDL treatment. This would have helped to clarify whether changes in OCR after OxLDL treatment were due to altered mitochondrial function or due to overall reduced mitochondrial density.

A previous study has shown that OxLDL reduces respiration of VSMCs both at baseline and following uncoupling (Ahn et al., 2010). In this study, reduced respiration was also associated with reduced intracellular ATP content, although ADP levels were not reported making interpretation of the bioenergetics consequences of this decrease difficult. The study also does not investigate whether LDL itself exerts effects on respiration (Ahn et al., 2010), although LDL did not cause significant reduction in respiration in the current study, suggesting that it is the oxidation of the lipid rather than the lipid itself that exerts an effect.

OxLDL induces ROS production (Guo et al., 2014), which in turn could lead to mitochondrial dysfunction through damage of mitochondrial proteins or mtDNA. However, OxLDL did not affect ETC proteins as determined by Western blot, whereas the positive control t-BHP caused a significant reduction in complex I expression. Similarly, mtDNA copy number was not altered after OxLDL treatment. Another possibility is that ROS cause posttranslational modifications of mitochondrial proteins thereby affecting their function. For example, the ND3 subunit of complex I contains a redox-sensitive cysteine (Cys39) which can alter the activity of complex I (Chouchani et al., 2013). An alternative explanation for reduced mitochondrial respiration could be the induction of mitochondrial damage and subsequent mitophagy. This hypothesis is evaluated in chapter 6.

A limitation of the present study is that the oxidation state of the OxLDL solution has not been assessed. The solution used was copper oxidised and therefore a highly oxidised LDL form rather than a minimally oxidised LDL. However, because OxLDL is not a pure chemical additional batch control- and quality control experiments could have been considered.

In the present study overexpression of either sirtuin-1 or the deacetylase deficient isoform of sirtuin-1 did not significantly affect respiration in RVSMCs. However, the present study is limited in that the activity of sirtuin-1 in overexpressing cell lines has not been assessed. Furthermore, the subcellular localisation of the overexpressed sirtuin-1 has not been assessed and it is unclear whether the overexpressed sirtuin-1 fulfils its physiological role. Without such assessment it remains to be determined whether sirtuin-1 overexpression affects cellular or mitochondrial metabolism and the data from the Seahorse extracellular flux analysis therefore needs to be interpreted with caution. A previous study suggested that overexpression of sirtuin-1 reduces oxygen consumption rate in PC12 cells by approximately 25% (Nemoto et al., 2005). Sirtuin-1 binds to p53, Foxo3a and importantly PGC-1α and deacetylates these proteins. Sirtuin-1 may therefore lead to decreased PGC-1α activity and reduced respiratory complex expression (Nemoto et al., 2005). However, the mechanisms by which sirtuin-1 could affect metabolism may not only depend on the deacetylation of PGC-1α. For example, a mutation in sirtuin-1, sirtuin-1^{G261A}, which abrogates its ADP-ribosyltransferase activity but leaves its deacetylation activity intact, does not affect the oxygen consumption rate (Nemoto et al., 2005). This suggests that sirtuin-1 may not act through deacetylation of PGC-1α alone (Nemoto et al., 2005).

Sirtuin-1 may also alter mitochondrial physiology through effects on mitophagy, as overexpression of sirtuin-1 increases whereas knockout of sirtuin-1 decreases autophagy (I. H. Lee et al., 2008). Mechanistically, sirtuin-1 deacetylates autophagy components ATG5, ATG7 and ATG8 and sirtuin-1 -/- mice have similar phenotypes as ATG5-/- mice (I. H. Lee et al., 2008).

Another interesting observation from the current study is that SIRT- and SIRT+ have significantly diminished OxLDL uptake. Again, this data needs to be interpreted with caution, as sirtuin-1 activity has not been assessed. From previous studies we know that inhibition of sirtuin-1 using siRNA can increase SR-E1 (LOX-1) expression (Ma et al., 2013). The differences in uptake in this study may be consistent with sirtuin-1-induced downregulation of SR-E1 leading to decreased uptake of OxLDL. As the effect on OxLDL uptake is also present in the SIRT- cells this process appears to be independent of the deacetylation activity of sirtuin-1. Despite the decreased OxLDL uptake observed in SIRT+ and SIRT- cells, the functional consequences of OxLDL treatment in the extracellular flux analysis and the MTT assay are comparable to EV cells. Endogenous rat sirtuin-1 expression has not been altered in our SIRT+ and SIRT- cell lines. Thus the endogenous sirtuin-1 present in EV RVSMCs may be entirely sufficient for cellular function and additional expression of human SIRT+ or SIRT- may not exert large effects. Ideally endogenous sirtuin-1 should be knocked-out, for example through use of a CRISPR-cas 9 system or temporarily downregulated by the use of siRNA to draw conclusions on the effects of sirtuin-1 in RVSMCs.

Only LPS consistently increased the ECAR as a measure of glycolysis in all three cell lines tested. LPS as a pro-inflammatory mediator has

previously been shown to upregulate glycolytic pathways in monocytes, and at least partly acts through succinate-mediated stabilisation of HIF-1α (Tannahill et al., 2013).

In summary, the findings in this chapter indicate that OxLDL and LPS can affect mitochondrial function and VSMC metabolism through effects on respiration and glycolysis, respectively. However, the results obtained in rat VSMCs may not necessarily apply to atherosclerosis, a complex disease involving potentially multiple DAMPs acting simultaneously on various cell types within the plaque. It is therefore important to determine whether mitochondrial dysfunction occurs in atherosclerosis and VSMCs derived from atherosclerotic plaques as described in the following chapters.

4 Effects of fat-feeding on ApoE-/- mice

4.1 Introduction

The previous chapter described experiments using OxLDL to reduce mitochondrial oxygen consumption rate in cultured RVSMCs. To investigate whether hyperlipidaemia can also induce mitochondrial dysfunction in the development of atherosclerosis I next tested the effects of fat-feeding on mitochondrial function in aortas of ApoE-/- mice. These mice are frequently used as a model of atherosclerosis, as discussed in section 1.1.6. When ApoE-/- mice were fat a high-fat diet for up to 8 weeks, their cholesterol and triglyceride levels increased, but the serum cytokine levels remained largely unaffected (section 4.2). Previous work in our laboratory has demonstrated that fat-feeding of ApoE-/- mice leads to mtDNA damage in aortas that occurs prior to the development of atherosclerosis (E. Yu et al., 2013). However, this study did not investigate whether the mtDNA damage observed had any functional consequences on mitochondria. I hypothesised that mitochondrial damage and dysfunction may be early events in atherogenesis prior to the development of advanced atherosclerotic lesions. To investigate the functional effects of fat-feeding on mouse aortas I therefore adapted the Seahorse extracellular flux assay for use of aortic tissue samples (section 4.3). Fat-feeding did not significantly affect mitochondrial respiration in ApoE-/- mouse aortas at up to 8 weeks of fat-feeding (section 4.4). Immunohistochemistry of aortic tissue in these mice confirmed the absence of atherosclerosis at these early time points (section 4.5). However, in accordance with previous findings of increased mtDNA damage (E. Yu et al.,

2013), mtDNA copy number relative to nuclear DNA was reduced (section 4.6). The ATP/ADP ratio did not change in ApoE-/- mouse aortas after fat-feeding (section 4.7). Similarly, mitochondrial ROS and glutathione levels were not affected (section 4.8). To test whether I missed effects of fat-feeding on mitochondrial function developing at later time points I then repeated the Seahorse extracellular flux analysis assay in aortas from ApoE-/- mice on high-fat diet for 14 weeks (section 4.9) but there was no difference between the groups.

4.2 Serum lipid and cytokine levels of ApoE-/- mice after fat-feeding

Female ApoE-/- mice were fat a high-fat diet for up to 8 weeks. Serum samples were obtained from ApoE-/- mice, fat-fed ad libitum, i.e. not fasted, in the morning by cardiac puncture and analysed for serum cholesterol, HDL and triglyceride levels by the central biochemistry service at Addenbrooke's Hospital. Fat-feeding primarily increased cholesterol concentrations (Figure 4-1) rather than triglyceride concentrations consistent with published findings in our laboratory (E. Yu et al., 2013). However, previously reported cholesterol concentrations after fat-feeding were considerably higher (Nakashima et al., 1994; Plump et al., 1992). Plump et al. (1992) originally reported total cholesterol concentrations after fat-feeding of 1821 ± 395 mg/dl (~ 47 ± 10 mmol/l) when sampled in the afternoon, whilst Nakashima et al. (1994) reported values ranging from 1085 mg/dl to 4402 mg/dl (~ 28 mmol/l to 114 mmol/l). Whilst minor differences in cholesterol concentrations could be due to diurnal variation (Ferrell & Chiang, 2015) and slightly different diets used, the

concentrations observed in this study and in previous studies from our laboratory (E. Yu et al., 2013) are considerably lower than previously reported.

In parallel, serum cytokine levels were assayed by the central biochemistry service (Figure 4-2). Only TNF-α was significantly increased after fat-feeding, whereas other cytokines were not altered or large variations existed between mice precluding meaningful interpretation given the relatively small sample sizes. The variability in IL-6 and CXCL1 cytokine concentrations was largely due to one mouse in the 2-week fat-feeding group and one mouse in the 8-week fat-feeding group. In the case of IL-6 for example the concentration of cytokine in the 8-week fat feeding group were 2564.7 pg/ml, 26.0 pg/ml, 29.2 pg/ml and 23.6 pg/ml. The mouse with very high cytokine levels may have carried another pathology affecting cytokine levels such as an infection or cancer, which was not investigated in the present study. Due to the small sample size formal outlier analysis was not conducted.

In the present study fat-feeding increased TNF-α to between 15-36 pg/ml compared to baseline levels of 7-13 pg/ml. Together the increased cholesterol and cytokine concentrations observed after fat-feeding suggest that the diet exerts the desired proatherogenic effects in ApoE-/- mice.

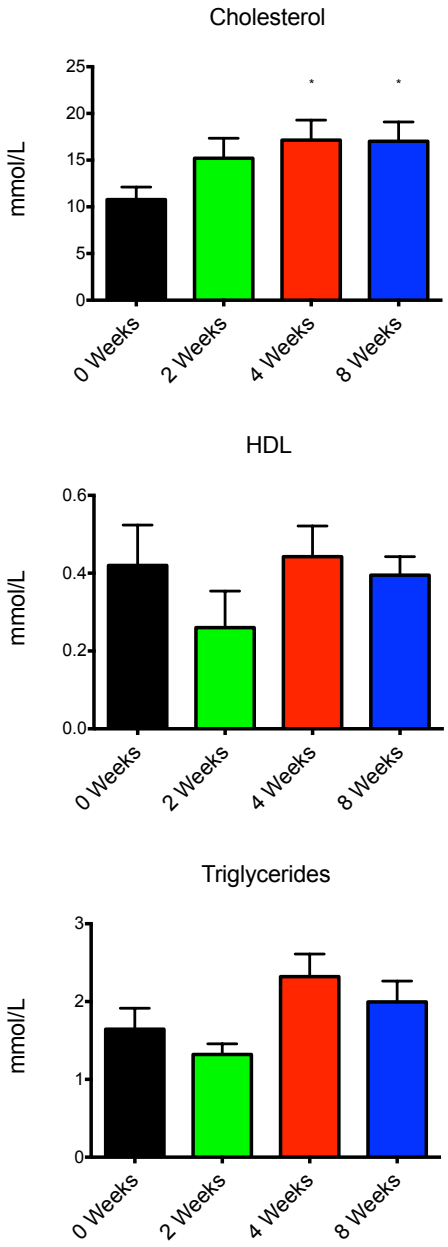

Figure 4-1 Serum cholesterol and triglyceride concentrations in ApoE-/- mice with or without fat-feeding

Blood of littermate ApoE-/- mice fed a 'western' high-fat diet for 0, 2, 4, or 8 weeks was obtained through cardiac puncture directly after sacrifice. Serum of N=4 animals per group was analysed. Data are mean ±SEM. *P<0.05 using one-way ANOVA with Bonferroni's correction for multiple comparisons.

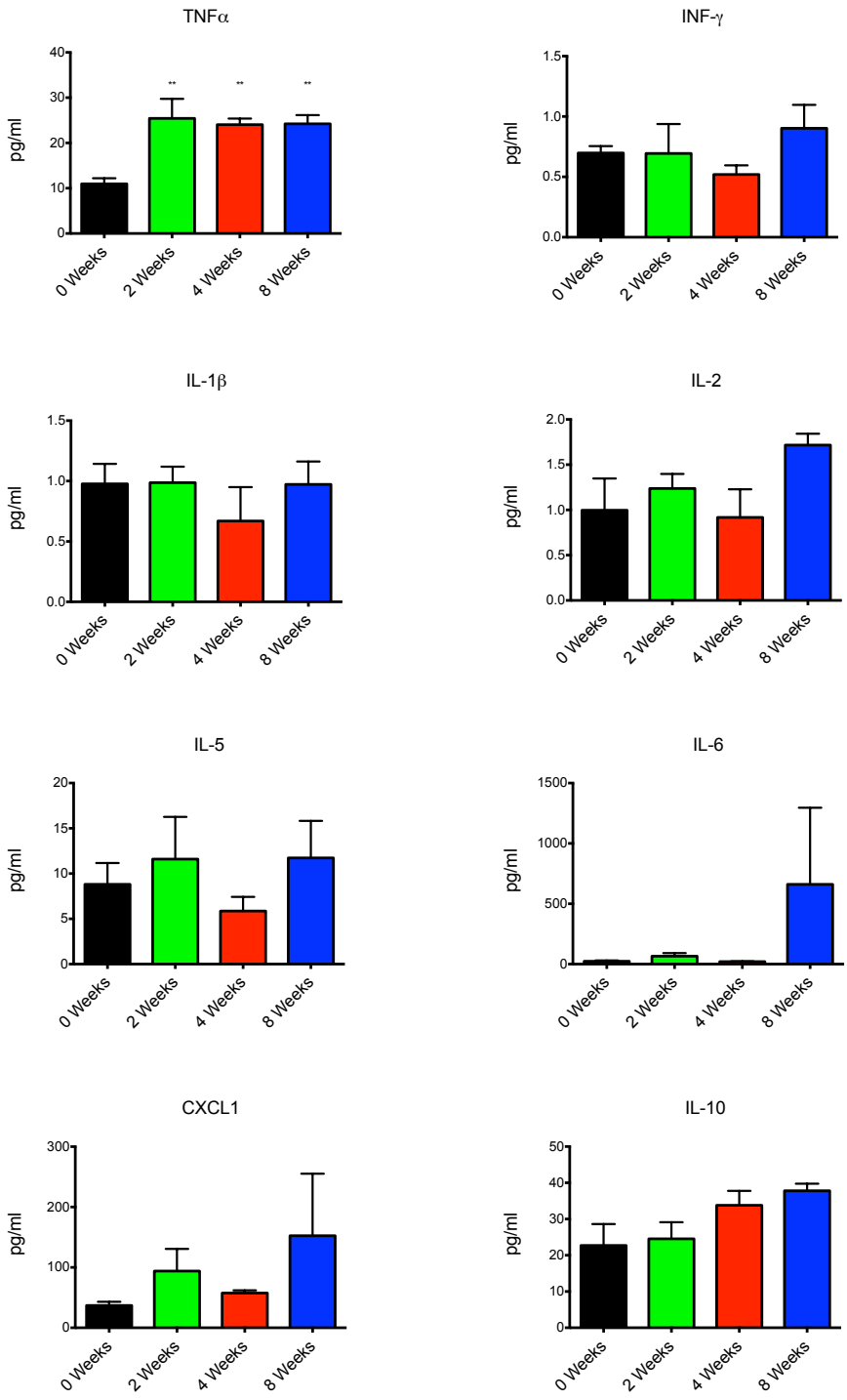

Figure 4-2 Serum cytokine concentrations in ApoE-/- mice with or without fat-feeding

Blood of littermate ApoE-/- mice fed a 'western' high-fat diet for 0, 2, 4, or 8 weeks was obtained through cardiac puncture directly after sacrifice. Serum concentrations of tumour necrosis factor 1α (TNF-α), interleukin (IL) 1β (IL1β), IL2, IL5, IL6, IL10, interferon γ (IFNγ), The chemokine (CXC motif) ligand 1 (CXCL1, also known as KC/GRO) were assessed by the core biochemical assay laboratory using a Meso Scale multiplex kit. Serum of N=4 animals per group was analysed. Data are

mean ±SEM. **P<0.01 using one-way ANOVA with Bonferroni's correction for multiple comparisons.

4.3 Optimisation of extracellular flux analysis of mouse aortic tissues

Although mtDNA damage has been demonstrated in atherosclerosis, to my knowledge, the functional consequences of such damage have not yet been assessed in whole tissue. My aim was therefore to establish an assay that provides information on mitochondrial function in aortic tissues. Indeed, the extracellular flux assay described in section (3.4) has recently been adapted to study tissues aiming to get a better understanding of mitochondrial function than could be achieved through study of cells in culture (Dunham-Snary et al., 2014; Feeley et al., 2014; Fried, Moffat, Seifert, & Oshinsky, 2014).

Pancreatic islet capture plates have been developed which contain a 0.25 mm deep and 3.17 mm wide depression in each well which can subsequently be covered by a custom mesh mounted on a plastic ring. Although developed to measure mitochondrial bioenergetics of pancreatic islets, these custom culture plates have been adapted to study the mitochondrial bioenergetics of whole fat tissue (Dunham-Snary et al., 2014) and subsequently also brain tissue (Fried et al., 2014). During this project a method describing extracellular flux analysis in mouse aortic tissue (Feeley et al., 2014) has also become available. The inhibitor concentrations of oligomycin (10 µg/ml), antimycin A (10 µM) and FCCP (1 µM) were adapted from the latter study (Feeley et al., 2014). Similarly, rotenone was used at 10 µM in combination with antimycin.

Initial experiments were conducted to determine how best to prepare the aortic tissue for the assay. In a first experiment I compared sample preparation in warm (37°C) DMEM compared to cold (4°C) PBS. Less variation between tissue samples and a higher respiratory reserve capacity (RRC) were observed when the aorta was prepared in warm DMEM compared to cold PBS (Figure 4-3). In the following, tissue samples were therefore prepared in warm DMEM. In a further optimisation step, dissected aortas were either left as aortic rings or opened longitudinally to form aortic sheets. Aortic rings resulted in less intra-experimental variation (Figure 4-4) and in subsequent experiments aortic rings were therefore left intact.

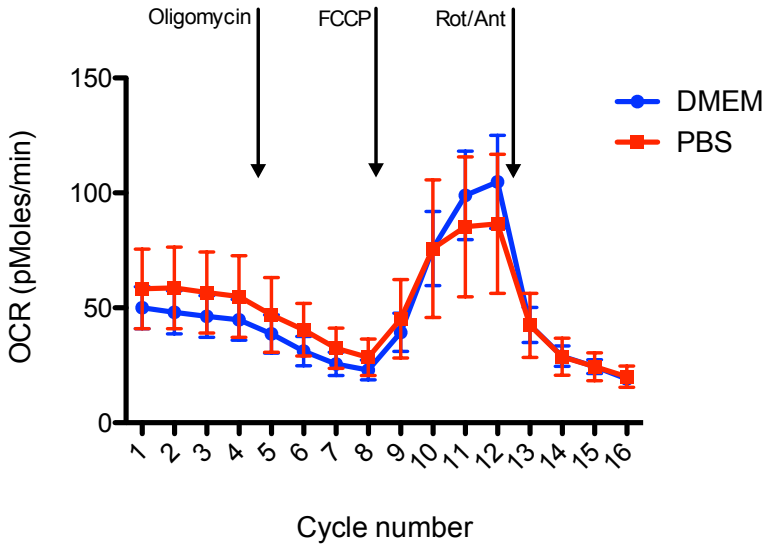

Figure 4-3 Aortic preparation for extracellular flux analysis

Mouse aortas were dissected in either DMEM at 37°C or PBS at 4°C and cut open longitudinally to form aortic sheets. Tissue pieces were then analysed using an islet capture plate and capture rings in a Seahorse XF24e extracellular flux analyser. Oligomycin (10 µg/ml final assay concentration), FCCP (1 µM) and a combination of rotenone (Rot, 10 µM) and antimycin A (ant, 10 µM) were injected using ports A-C of the assay plate as indicated. Four measurement cycles were completed before and after each of the inhibitors. Data represents mean ± SEM of technical replicates of one experiment.

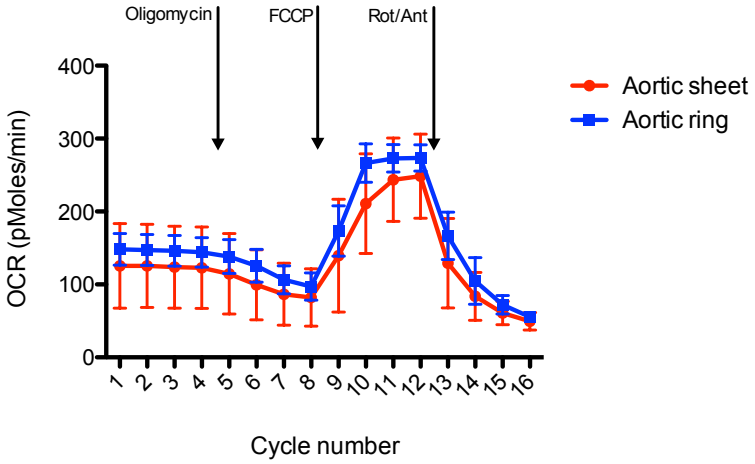

Figure 4-4 Aortic sheets and aortic rings in extracellular flux analysis

Mouse aortas were dissected in DMEM at 37°C and either left as intact rings, or cut open longitudinally to form aortic sheets. Tissue pieces were then analysed using an islet capture plate and capture rings in a Seahorse XF24e extracellular flux analyser. Oligomycin (10 µg/ml final assay concentration), FCCP (1 µM) and a combination of rotenone (Rot, 10 µM) and antimycin A (ant, 10 µM) were injected using ports A-C of the assay plate as indicated. Four measurement cycles were completed before and after each of the inhibitors. Data represents mean ± SEM of technical replicates of one experiment.

4.4 Extracellular flux analysis of ApoE-/- mouse aortas

Next, extracellular flux analysis of aortic tissues derived from ApoE-/- mice was performed. Mice were fed a 'western' high-fat diet for 2, 4, or 8 weeks or alternatively left on normal chow (0 weeks of high-fat diet). The starting point of fat-feeding was staggered so that littermates were all sacrificed on the same day of an experiment aged 15 weeks. Rising CO_2 concentrations with subsequent cervical dislocation and cardiac puncture were used to kill the animals. After snap freezing liver and heart samples the aortas were quickly dissected in pre-warmed DMEM (37°C) and run in the extracellular flux assay. There was no significant difference in the OCR in these mice at any time point (Figure 4-5). Similarly, there was no significant

difference in the ECAR at baseline and after injection of oligomycin and FCCP (Figure 4-5). However, following injection of rotenone and antimycin ECAR was significantly lower in mice without fat-feeding (0 weeks) compared to fat-fed mice (Figure 4-5). This result needs to be interpreted with caution as the assay was designed to mainly detect differences in OCR and injection of rotenone and antimycin is not normally used in assays designed to evaluate ECAR (manufacturer's instructions).

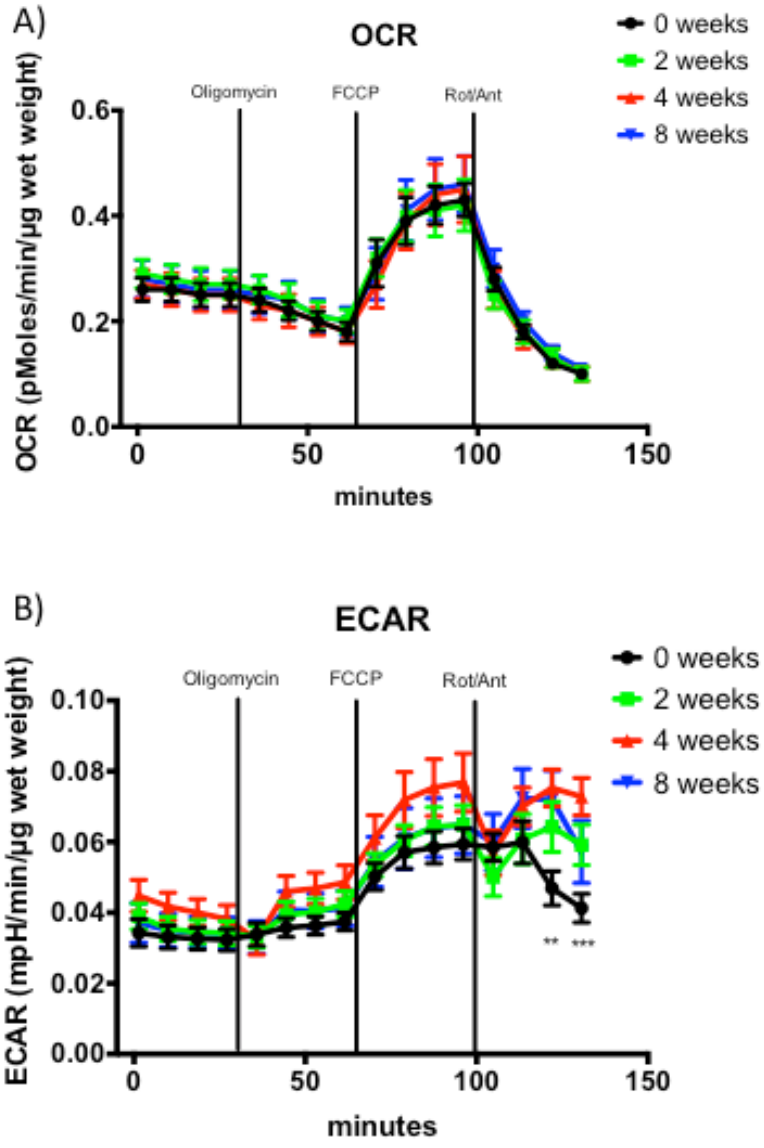

Figure 4-5 Extracellular flux analysis of ApoE-/- mouse aortas after fat-feeding

Aortas were dissected in pre-warmed DMEM after sacrifice of ApoE-/- mice with or without fat-feeding. Aortic tissue samples from aortic arch to proximal abdominal aorta were secured in 24-well islet capture wells using the mesh provided with the kit. Oligomycin (10 µg/ml final assay concentration), FCCP (1 µM) and a combination of rotenone and antimycin A(Rot/Ant, 10 µM each) were injected through ports A-C of a 24-well extracellular flux analyser (Seahorse 24XFe) and the oxygen consumption rate (OCR) and the extracellular acidification rate (ECAR) were determined. After completion of the run the tissue pieces were retrieved and weighed to allow normalisation of the data. A) OCR normalised to tissue wet weight (mmol/min/µg wet weight). B) ECAR normalised to tissue wet weight (mpH/min/µg wet weight), **P<0.01 0 weeks vs 4 weeks and 8 weeks, ***P<0.001 0 weeks v 4 weeks, two-way ANOVA with Tukey correction for multiple comparisons.

4.5 Immunohistochemistry of mouse aortas after fat-feeding

To confirm that ApoE-/- mice have not developed significant atherosclerosis after fat-feeding for up to 8 weeks tissue pieces were retrieved from the Seahorse extracellular flux analysis plates after completion of the run, weighed, fixed in formalin and immunohistochemistry was performed. From the aortic tissue pieces that were used in extracellular flux analysis (aortic arch to proximal abdominal aorta) the aortic arch is the area most prone to develop atherosclerosis (Nakashima et al., 1994) and was therefore analysed. As demonstrated in representative images in Figure 4-6 no significant atherosclerosis was present in the aortic arch with or without fat-feeding.

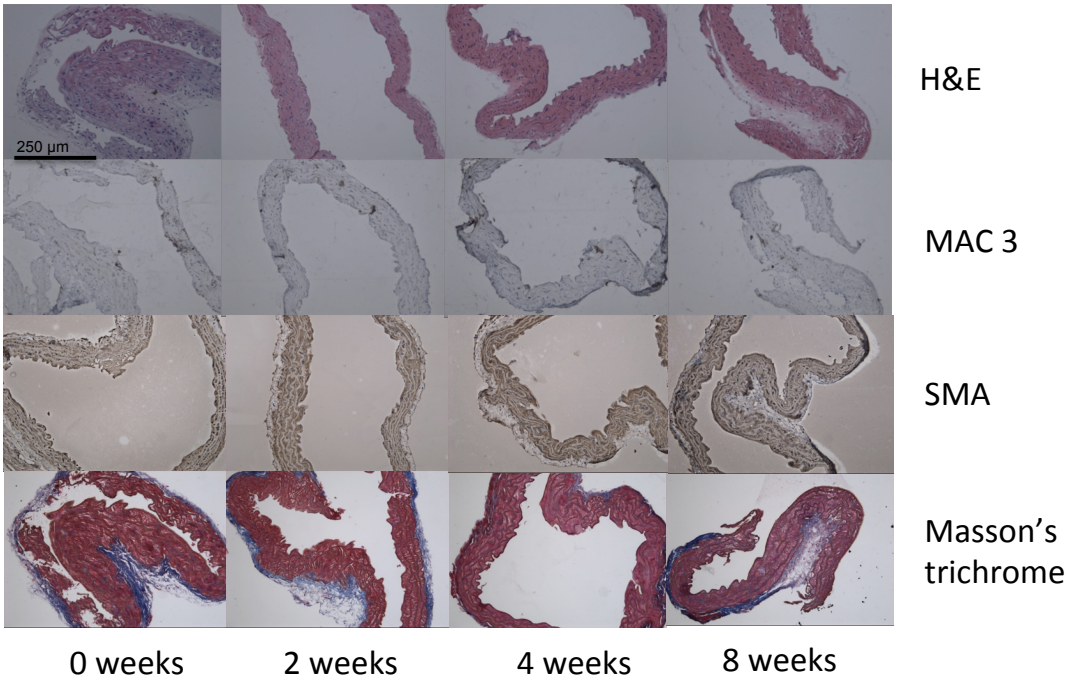

Figure 4-6 Immunohistochemistry of ApoE-/- mouse aortas after high-fat diet

After completion of the Seahorse extracellular flux analysis run, aortic arch tissue pieces were fixed in formalin and immunohistochemistry was performed. Haematoxylin and eosin stain (H&E): nuclei (blue) and eosinophilic structures such as cytoplasm (red). MAC3: immunohistochemistry against surface macrophage marker. SMA: immunohistochemistry against smooth muscle cell actin. Masson's trichrome stain: smooth muscle cells/cytoplasm (red), collagen (blue) and nuclei (brown). Representative images are shown. No atherosclerotic plaques were visualised in aortic arches of N=4 animals per group.

4.6 mtDNA copy number

In section 3.6 I described that mtDNA copy number correlates well with mitochondrial mass across different tissues (D'Erchia et al., 2015). I therefore tested whether prolonged fat-feeding, known to induce mtDNA damage (E. Yu et al., 2013), also affects mtDNA copy number. qPCR was used to determine the amplification of a short mitochondrial segment relative to a nuclear DNA segment. First, serial dilutions of DNA were run to determine the reaction efficiency of the mitochondrial and nuclear PCR reactions (Figure 4-7). To confirm amplification of a single product of the right size, the PCR product

was run on a 1% Agarose gel, and DNA visualised using UV light after staining with GelRed (Figure 4-8). After validation of the qPCR assay for mtDNA copy number, DNA samples from aortas after fat-feeding were analysed. Fat-feeding for 4 or 8 weeks significantly reduced mtDNA copy number in mouse aortas compared to no fat-feeding (Figure 4-9).

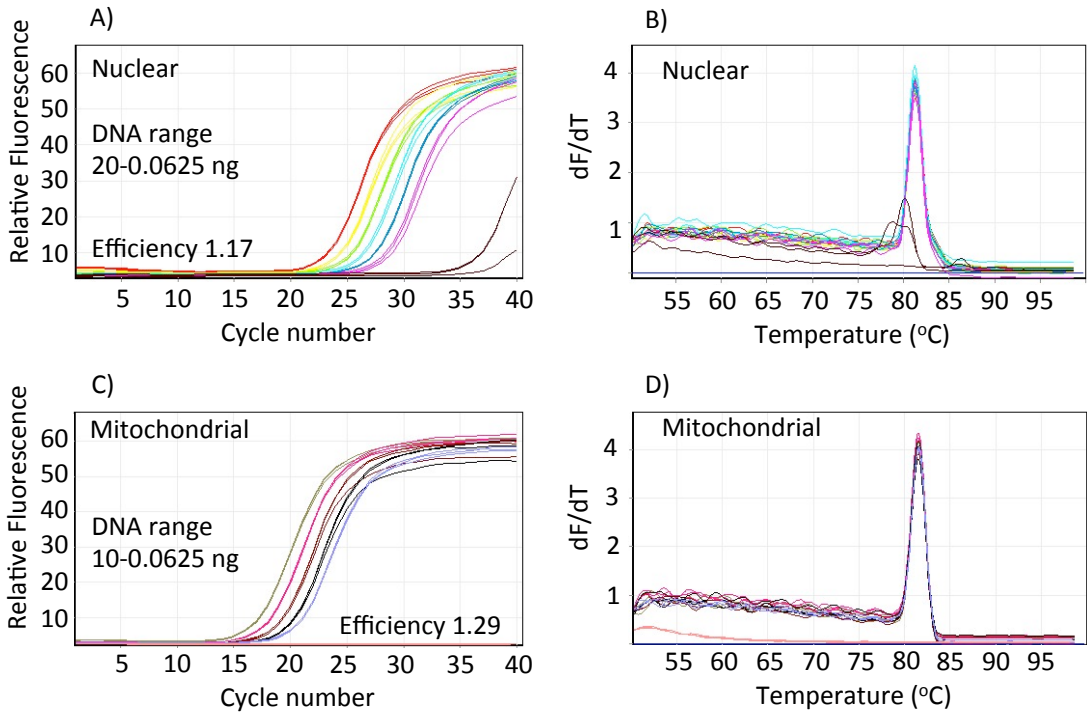

Figure 4-7 Validation of qPCR efficiency for mouse nuclear and mitochondrial DNA reactions

Mouse DNA was serially diluted (1:2) and qPCR reactions were run in triplicate on a Corbett Rotor-Gene™ 6000 QPCR thermocycler. A) The nuclear reaction was linear with an efficiency of 1.17 in the DNA range 20-0.625 ng. B) Melt curve analysis suggests amplification of a single product. The mitochondrial reaction (C) was linear and had a comparable efficiency (1.29) in the DNA loading range 10-0.0625 ng. D) Melt curve analysis of the mitochondrial reaction suggests amplification of a single product. dF/dT: the derivative of fluorescence (F) with respect to temperature (T).

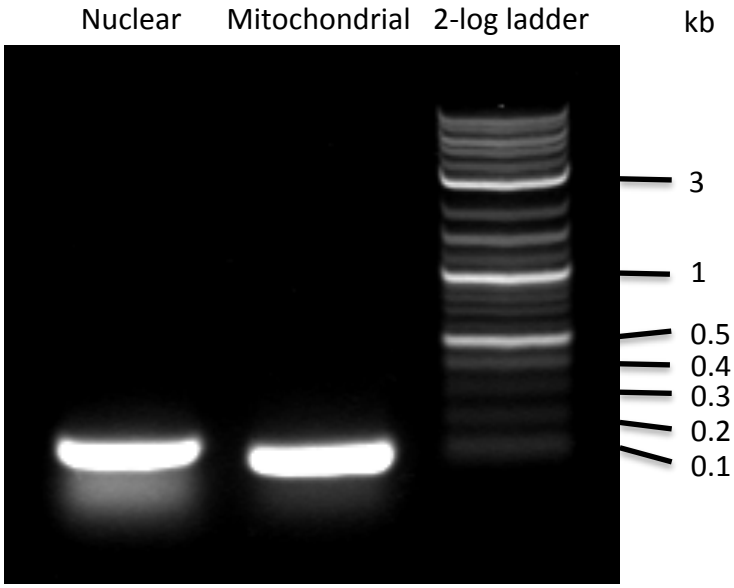

Figure 4-8 Confirmation of single PCR product from mouse nuclear and mitochondrial reactions

10 µl of PCR product from nuclear DNA reaction and mitochondrial DNA reaction were run on a 1% agarose gel, stained with GelRed and visualised by UV light. Nuclear amplicon is expected to be 155 bp, mitochondrial amplicon is expected to be 127 bp. Expected molecular weight of 2-log ladder ranging from 0.1-10 kb is shown in the right lane.

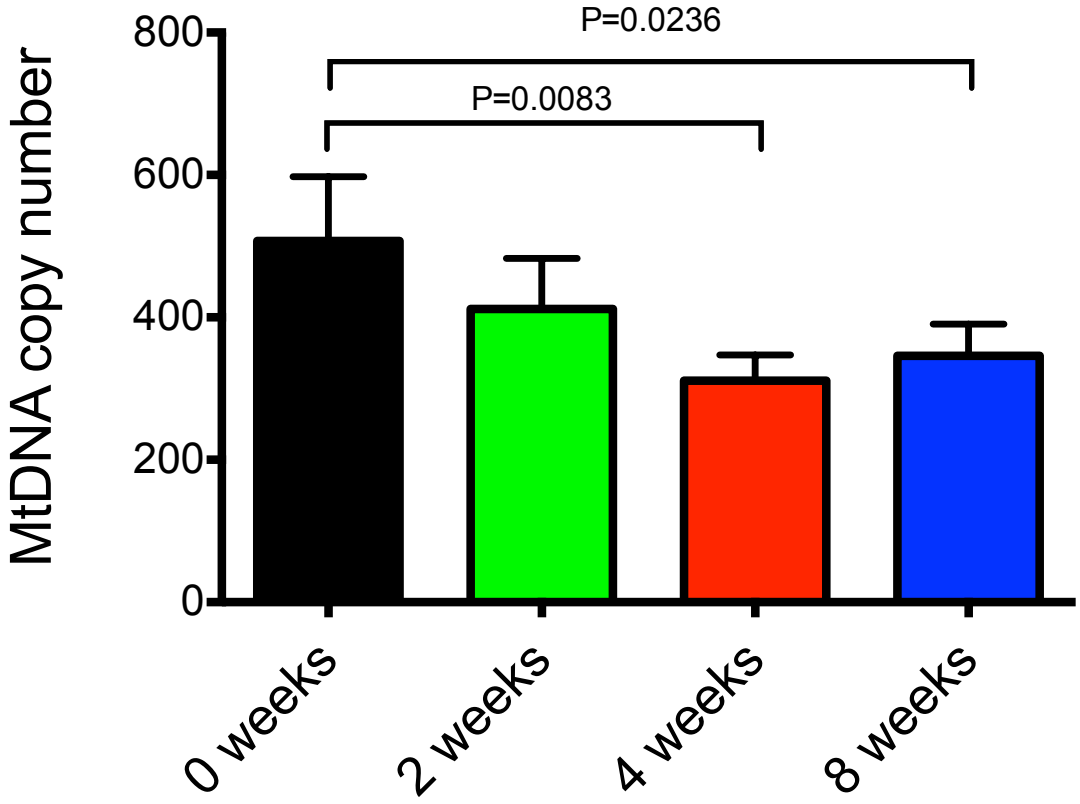

Figure 4-9 Effects of fat-feeding on mtDNA copy number in ApoE-/- mouse aortas

DNA was isolated from aortas of ApoE-/- mice after fat-feeding or from littermate control ApoE-/- mice kept on standard chow. qPCR is used to amplify a short mtDNA segment (127 bp) and a short nuclear DNA segment (β-globin, 155 bp product). MtDNA copy number is calculated as $2x2^{\Delta ct}$, where ΔCt=Ct(mtDNA)-Ct(nuclearDNA). This formula contains a correction by the factor 2 to account for 2 copies of the β-globin gene in the genome. N=5 mice per group, one-way ANOVA (Fisher's test) was used for statistical analysis.

4.7 ATP/ADP ratio

To get an alternative readout of mitochondrial function the ATP/ADP ratio was measured in aortas from ApoE-/- with and without fat-feeding. I used an assay where ATP is required for a luciferase/luciferin reaction creating light emission, which is quantified by a luminometer. ADP is quantified after degradation of ATP in the sample, conversion of ADP to ATP, and quantification of ATP. Standard curves for ATP and ADP were used for normalisation and the ratio ATP/ADP was formed. ATP and ADP were isolated from snap frozen aortic samples. Variability was great between samples but the data was not suggestive of large changes in the ATP/ADP ratio after fat-feeding (Figure 4-10).

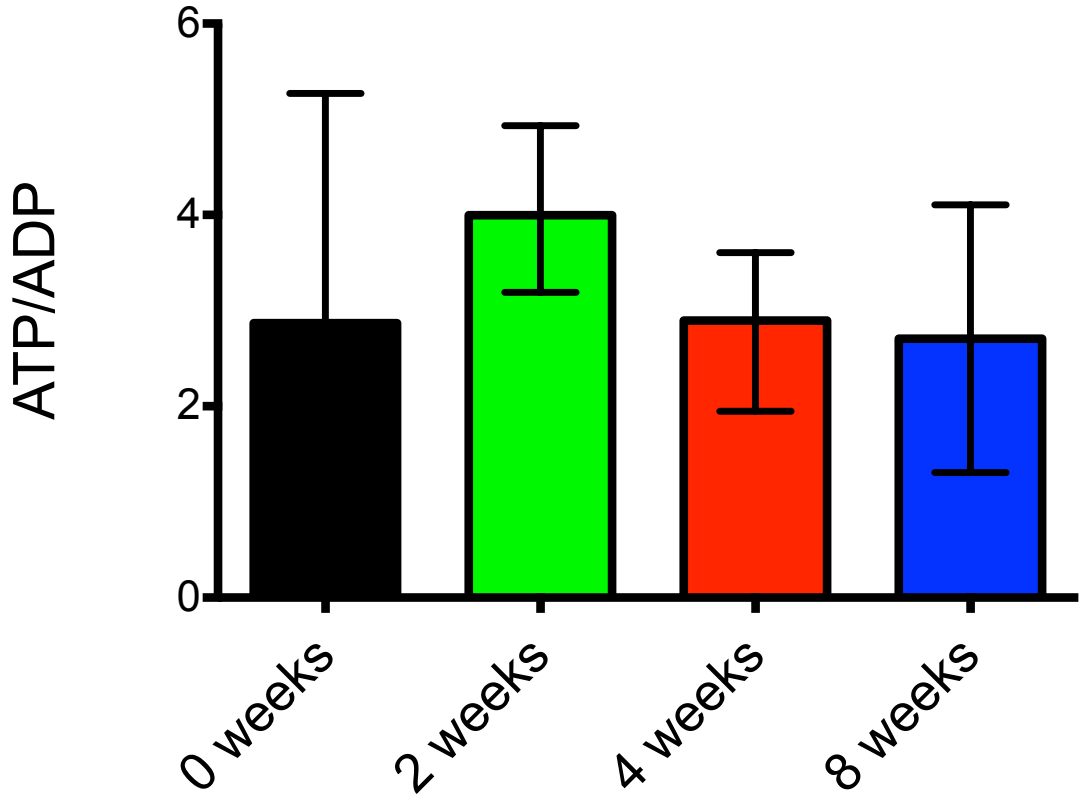

Figure 4-10 ATP/ADP ratio in aortas from ApoE-/- mice after fat-feeding

Aortic tissues were snap frozen and ATP and ADP were extracted in perchloric acid to avoid degradation. ATP concentrations were determined using a luciferase/luciferin assay. ADP concentrations were determined following ATP degradation and conversion of ADP to ATP and subsequent ATP measurement by luciferase/luciferin assay. N=3 per group (N=2 for 8 weeks of fat-feeding due to sample loss). Data are mean ± range. There were no statistical differences between 0, 2 and 4 weeks of fat-feeding using one-way ANOVA (Fisher's test). 8 weeks was excluded from statistical analysis due to sample loss.

4.8 MitoP/B ratio and glutathione levels in tissues from ApoE-/- mice after fat-feeding

Previous studies have demonstrated that increased concentrations of ROS can be detected during atherosclerosis in mouse aortas (M. Ekstrand et al., 2015). However, the source of ROS remains unclear. To measure mitochondrial ROS production the mitochondrially targeted probe, MitoB, has been developed which accumulates in mitochondria and is converted by H_2O_2

to from MitoP. Our laboratory has recently demonstrated that fat-feeding of ApoE-/- mice for 14 weeks induces mitochondrial ROS production as determined by quantification of the MitoP/B ratio using mass spectroscopy (E. P. K. Yu et al., 2017). However, it remained unclear whether ROS increase prior to the development of atherosclerotic lesion, i.e. after short-term fat-feeding of ApoE-/- mice. I therefore determined the MitoP/B ratio of ApoE-/- mice fat-fed for 8 weeks in comparison to littermate control mice kept on normal chow. Figure 4-11 demonstrates that ROS production in aortas is not affected in ApoE-/- mice after 8 weeks of fat-feeding (see also Appendix 8.4). Unexpectedly, mitochondrial ROS production was significantly reduced in livers of fat-fed mice. Previous studies have shown that MitoP/B ratios can vary across tissues (Logan et al., 2014; E. Yu et al., 2013), a potential explanation for the higher ratios observed in aortas is the longer exposure to atmospheric oxygen concentrations due to longer dissection times. Although not formally assessed, mouse hearts and liver were snap-frozen faster than mouse aortas for which dissection took several minutes. Such differences cast doubt about the validity of this approach to determine ROS in mouse aortas.

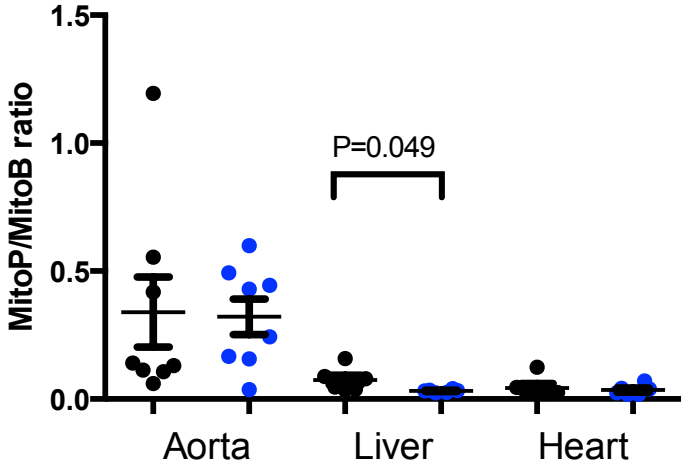

Figure 4-11 MitoB/P ratio in aorta, liver and heart of ApoE-/- mice

After weaning ApoE-/- mice were fat-fed for 8 weeks or kept on normal chow. 25 nmol MitoB was injected into the tail-vein and mice were sacrificed 3 hours later. Aortic, liver and heart tissue was snap frozen until extraction of MitoB and MitoP in acetonitrile and formic acid. Concentrations of MitoB and MitoP were determined using mass spectroscopy with deuterated d_{15} internal standards. Black circles: normal chow, blue circles: fat-feeding for 8 weeks. N=6-8 mice for each group. Unpaired two-tailed t-test assuming equal variation was used for statistical analysis for each tissue type.

To get further evidence of effects of fat-feeding on ROS production in mouse aortas I also determined total glutathione levels. 8 weeks of fat-feeding did not affect total glutathione levels in ApoE-/- mouse aortas (Figure 4-12) supporting the observation of unaffected mitochondrial ROS concentrations. This data needs to be interpreted with caution as the dissection of mouse aortas took several minutes after mouse sacrifice which may have affected glutathione concentrations in the tissues.

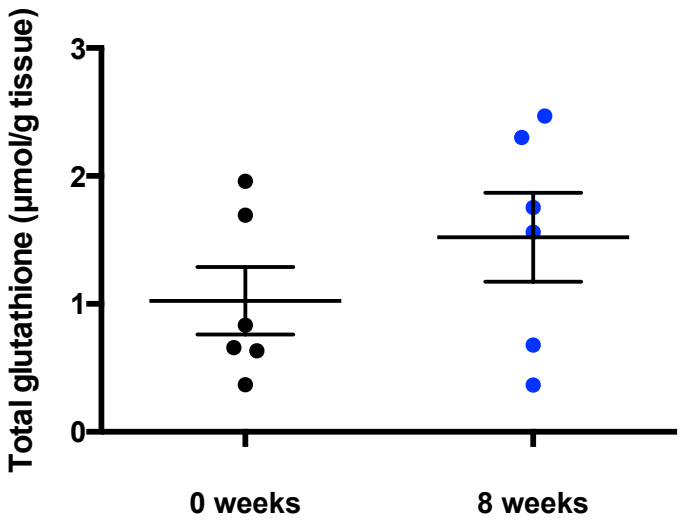

Figure 4-12 Total glutathione levels in ApoE-/- mice after fat-feeding

Total glutathione was extracted from snap frozen aorta samples of ApoE-/- mice fed a high-fat diet for 8 weeks or kept on normal chow. Total glutathione levels were determined using a recycling assay, thus measuring both GSH and GSSG. Standards of GSH were used to determine quantities of total glutathione in the tissue. N=6 aortas in each group. No statistical significant differences were observed using unpaired two-tailed t-test with equal variation.

4.9 Extracellular flux analysis of ApoE-/- mouse aortas after 14 weeks of fat-feeding

Because fat-feeding of ApoE-/- mice for up to 8 weeks induced very few changes I repeated the Seahorse extracellular flux analysis in ApoE-/- mice after 14 weeks of fat-feeding. This duration of fat-feeding is expected to induce atherosclerosis in ApoE-/- mouse aortas (E. Yu et al., 2013). Because of the longer period of fat-feeding, mice studied in this set of experiments were 21 weeks old, whereas mice in the experiments described in section 4.4 were 15 weeks old. Again, there was no significant change in the OCR or ECAR of aortas from ApoE-/- mice after 14 weeks of fat-feeding compared to littermate control mice on standard chow.

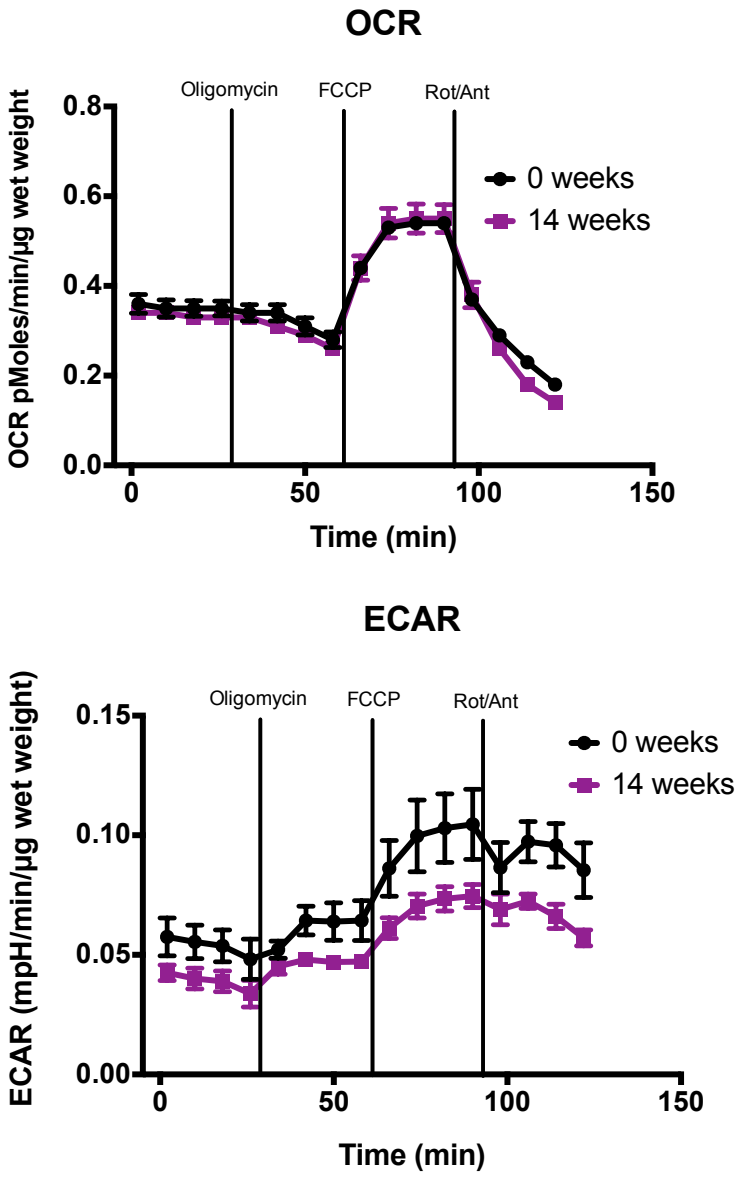

Figure 4-13 Extracellular flux analysis of aortic tissues from ApoE-/- mice after fat-feeding for 14 weeks

Aortas were dissected in pre-warmed DMEM after sacrifice of ApoE-/- mice with or without fat-feeding for 14 weeks. Aortic tissue samples from aortic arch to proximal abdominal aorta were secured in 24-well islet capture wells using the mesh provided with the kit. Oligomycin (10 µg/ml final assay concentration), FCCP (1 µM) and a combination of rotenone and antimycin A(Rot/Ant, 10 µM each) were injected through ports A-C of a 24-well extracellular flux analyser (Seahorse 24XFe) and the oxygen consumption rate (OCR) and the extracellular acidification rate (ECAR) were determined. After completion of the run the tissue pieces were retrieved and weighed to allow normalisation of the data. A) OCR normalised to tissue wet weight (mmol/min/µg wet weight). B) ECAR normalised to tissue wet weight (mpH/min/µg wet weight). N=4 animals per group, no statistical significant

differences between groups were observed using serial unpaired two-tailed t-tests with Holm-Sidak correction for multiple comparisons.

4.10 Discussion

Previous work in our laboratory has shown that fat-feeding of ApoE-/- mice induces mtDNA damage prior to the development of atherosclerotic lesions (E. Yu et al., 2013). However, the functional consequences of such damage were not known. In this part of the project I adapted the Seahorse extracellular flux analysis assay to assess the OCR and ECAR in aortic tissue from ApoE-/- after fat-feeding.

First I confirmed that fat-feeding of ApoE-/- mice had the desired pro-atherogenic effects. Serum concentrations of cholesterol significantly increased with fat-feeding as expected from previous studies in our laboratory (E. Yu et al., 2013), although the effect size of fat-feeding was smaller than previously reported (Plump et al., 1992). The discrepancies may in part be explained by different sampling times of blood with effects of the circadian rhythm and fasting state of mice as well as slight variations in the diet provided. However, the 'western' diet chosen for the present study (Special Diets Services 829100, ~21% Fat, ~20% Protein) should resemble the diet used by Plump et al. (1992) relatively closely. Future studies in our laboratory should aim to investigate the reasons for these differences in cholesterol levels in greater detail to allow better comparability of our studies using ApoE-/- mice on high-fat diet to studies by other research groups.

There was also an increase in serum TNF-α cytokine levels after fat-feeding, but other inflammatory cytokines such as IL1β were not changed. In the present study fat-feeding increased TNF-α to between 15-36 pg/ml

compared to baseline levels of 7-13 pg/ml. For comparison, LPS treatment of mice increases serum TNF-α to above 10^3 pg/ml (Mills et al., 2016), however, fat-feeding of ApoE-/- mice, even for prolonged periods of over one year, only increases TNF-α concentrations to approximately three times baseline levels (Dinh et al., 2017). Thus the effects of fat-feeding on serum cytokine levels are expected to be relatively small, consistent with the findings in the present study.

To assess the respiration of aortic tissue of fat-fed ApoE-/- mice I adapted the Seahorse extracellular flux assay for the measurement of tissue samples. This assay has previously been used for the measurement of fat (Dunham-Snary et al., 2014), brain (Fried et al., 2014) and aortic (Feeley et al., 2014) tissues. The final assay inhibitory concentrations were adapted from Feeley et al. (2014) as their technique analysed the same tissue as the present study. In a first set of experiments I further optimised the handling of aortic tissue after sacrifice of the mice. Preparation in warm DMEM led to less intra-experimental variation compared to preparation in ice-cold PBS and was therefore used in subsequent experiments. Similarly, keeping mouse aortic rings intact rather than cutting them longitudinally to form aortic sheets led to more consistent measurements. This may be due to additional tissue damage introduced by the scissors in the aortic sheet group. Consequently, aortic rings were left intact in the following experiments.

After optimisation, Seahorse extracellular flux analysis was performed on aortas derived from ApoE-/- mice with or without fat-feeding. No differences in OCR or ECAR were observed between groups. There is limited data available to compare the results of the present study against. In a

description of the Seahorse method on mouse aortic tissues, the authors reported on a single experiment comparing fat-fed ApoE-/- mice with ApoE-/- mice on a normal chow (Feeley et al., 2014). There were numerical differences in the OCR between the groups, with the OCR being higher in the fat-fed group, but the analysis was based on two mice per group and therefore no statistical analysis was provided. In isolated rat hearts, increased availability of fatty acids as metabolites leads to increased OCR, probably in part due to increased uncoupling of mitochondria (Cole et al., 2011). However, oxidation of lipid species and formation of OxLDL may also decrease OCR of VSMCs as demonstrated in a previous study (Ahn et al., 2010) and the present study (see chapter 3). There are at least two explanations for not observing any differences in OCR in aortas after fat-feeding in the present study. The stimulatory effects of lipids on respiration in mouse aortas may be less pronounced than in cardiac tissues, as the energy requirements are considerably lower. Furthermore, the assay was performed in the presence of glucose such that changes in β-oxidation of fatty acids would not be adequately captured. Mouse aortas were also assessed at a time point where no significant atherosclerotic lesions have developed. A detailed analysis of lesion development, their timing and location has previously been performed by Nakashima et al. (1994). This study suggests that foam cell lesions and at least intermediate lesions should have been visible after 8 weeks of fat-feeding. Similarly, a previous study from our lab suggests that although lesion development at this stage is small (E. Yu et al., 2013) it can be detected with H&E staining as early as 7 weeks after fat-feeding. A possible explanation for the relatively small lesion sizes in our

laboratory could be the weaker effects of our western diet on total cholesterol concentrations compared to previous studies (Nakashima et al., 1994; Plump et al., 1992) and in the present study also the area of aorta that was sampled, i.e. excluding the aortic root which develops atherosclerotic lesions first.

In a further experiment mice were therefore fat-fed for 14 weeks at which point atherosclerotic lesions are expected to be well established. However, no changes in OCR and ECAR were observed in these experiments either. The method may not be sensitive enough to detect subtle changes in metabolism or oxygen consumption. Even after 14 weeks of fat-feeding the proportion of aorta affected by atherosclerosis is less than 10% once the aortic root is excluded (E. Yu et al., 2013); thus the OCR in this assay will mainly be determined by healthy tissue.

Another limitation of the present technique is the sacrifice of animals through the use of rising CO2 concentrations. It is well established that hypoxia can decrease metabolic rates of mammals but the effects of CO2 have generally been less studied (Saiki & Mortola, 1996). Although CO2 concentrations up to 5% do not affect metabolism of rats (Saiki & Mortola, 1996), it is currently unclear whether higher concentrations used in the present study to sacrifice the animals could affect metabolism. Tissues were dissected in atmospheric CO2 concentrations but I cannot exclude an effect of prior high CO2 exposure on metabolism or viability of mitochondria. Future experiments should use alternative means of sacrifice such as cervical dislocation to study metabolism of tissues.

In line with the results of the Seahorse extracellular flux analysis there were no obvious effects of fat-feeding on the ATP/ADP ratio, with the caveat

that the dataset was small. Similarly, fat-feeding did not affect the production of mitochondrial ROS as determined by the MitoP/B ratio, nor did it affect total glutathione levels. The redox state or the presence of redox stress could additionally have been investigated by other techniques, for example using 2',7' –dichlorofluorescin diacetate (DCFDA) dye (E. Yu et al., 2013), however this would not have been able to differentiate between mitochondrial generated ROS or ROS generated from other cellular sites. The only significant difference induced by fat-feeding was a reduction in mtDNA copy number. This is consistent with previous work in our laboratory demonstrating increased aortic mtDNA damage after fat-feeding of ApoE-/- mice. Thus, mtDNA damage and a reduction in mtDNA copy number may occur prior to the development of functional consequences.

5 Mitochondrial dysfunction in human atherosclerosis

5.1 Introduction

In this chapter I investigate whether the mtDNA damage that is present in advanced human atherosclerosis (E. Yu et al., 2013) has functional consequences. For this, the Seahorse extracellular flux assay was used to measure the OCR and ECAR of tissues derived from carotid endarterectomies (section 5.2). The respiratory reserve capacity of the diseased cap and core regions were significantly lower compared to relatively unaffected media. Similar to mouse tissue exposed to high lipids (section 4.6) a reduced mtDNA copy number was found in tissue derived from carotid endarterectomies (section 5.3). Consistent with these findings the expression of complexes I and II of the ETC were reduced in VSMCs cultured from carotid endarterectomies (section 5.4). However, Seahorse extracellular flux analysis of VSMCs derived from plaque or aorta did not recapitulate the findings from whole tissues (section 5.5).

5.2 Human atherosclerotic plaque tissue extracellular flux analysis

Tissues derived from carotid endarterectomies were obtained from surgical theatres at Addenbrooke's Hospital, Cambridge. All specimens were from male patients. The average age of the donors was 69.4 years ± 8.47 years (standard deviation). Four distinct areas corresponding to normal

carotid medial wall, the shoulder region of the atherosclerotic plaque as well as the cap region and the necrotic core were identified (for an illustration of the definitions of medial wall, shoulder region, cap region and necrotic core region see Figure 5-1).

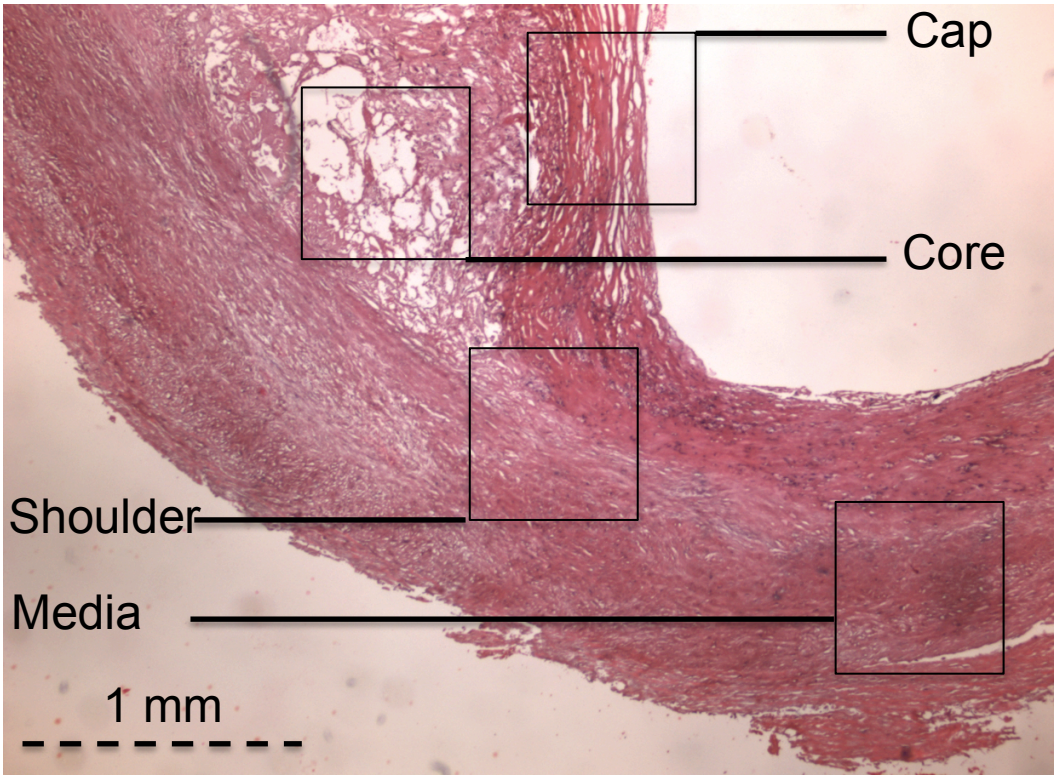

Figure 5-1 Illustration of sample areas for Seahorse extracellular flux experiments of carotid endarterectomies.

Hematoxylin and eosin stain of human carotid endarterectomy sample. Top right: lumen. Sample areas used for Seahorse experiments and scale bar are depicted for illustration.

Five sections of approximately 1 mg each were dissected from each of these areas and analysed in a Seahorse extracellular flux analyser. To confirm that the appropriate regions were sampled and to allow for normalisation against cellular density in addition to wet weight, the tissue pieces were retrieved and subjected to standard immunohistochemistry. Representative images are presented in Figure 5-2. Whilst the media and

shoulder regions are relatively similar, there are clear differences in the staining pattern of the cap and core regions compared to the media. Whilst the media and the shoulder region stain for smooth muscle actin, less staining is observed in the cap and the core areas. Masson's trichrome stain reveals collagen staining, particularly in the cap and the core regions. CD68 as a marker of macrophages is found in the core region, but also in the cap and shoulder region. The mean cellular density across different plaque regions is depicted in Figure 5-3. For normalisation of Seahorse data, each OCR and ECAR value was therefore normalised to the wet weight and nuclei count of the corresponding tissue sample.

The results of the Seahorse extracellular flux analysis of tissues from carotid endarterectomies are shown in Figure 5-4. Only the healthy wall and the shoulder region of the plaque responded significantly to FCCP uncoupling by increasing oxygen consumption. Accordingly, the RRC of the media was significantly higher than in the cap region.

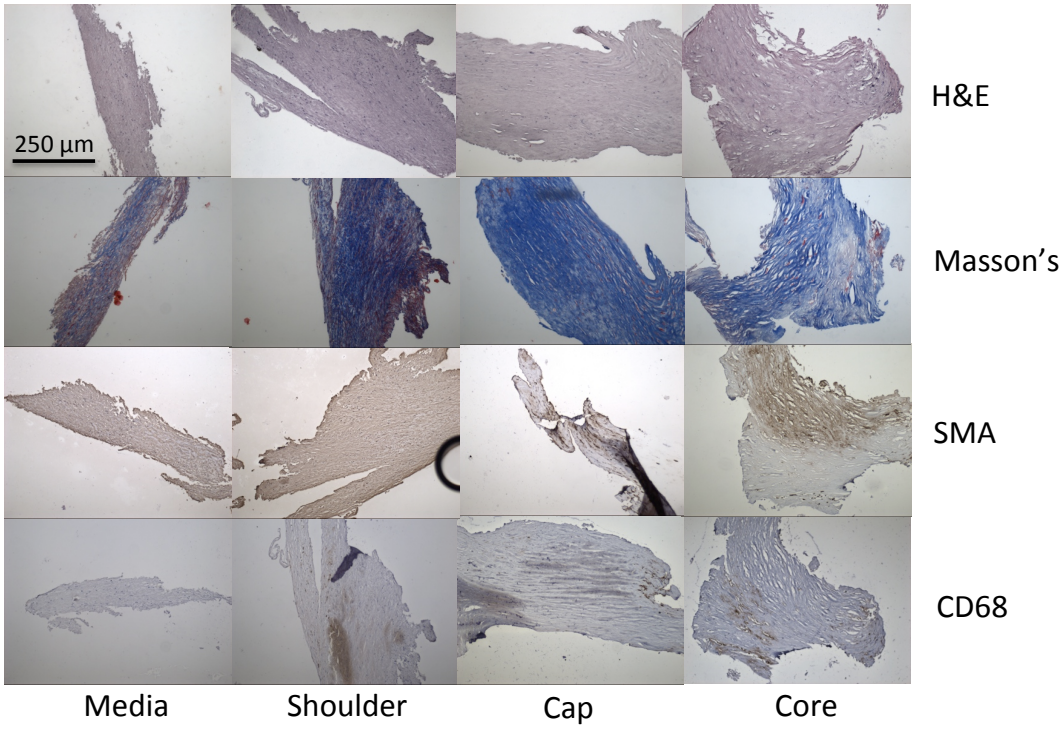

Figure 5-2 Immunohistochemistry of human tissue from carotid endarterectomies

After completion of the Seahorse extracellular flux analysis run, tissue pieces were fixed in formalin and immunohistochemistry was performed. Haematoxylin and eosin stain (H&E): nuclei (blue) and eosinophilic structures such as cytoplasm (red). Masson's trichrome stain: smooth muscle cells/cytoplasm (red), collagen (blue) and nuclei (brown). SMA: immunohistochemistry against smooth muscle cell actin. CD68: immunohistochemistry against surface macrophage marker. Representative images of N=5 experiments are shown using 100x magnification. A scale bar is depicted in the top left image.

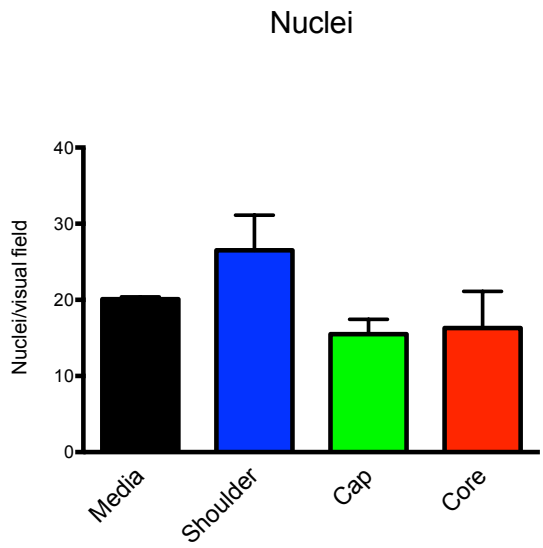

Figure 5-3 Cellular density in carotid atherosclerotic plaque regions

Cellular density was determined by counting nuclei in representative visual fields in 5 independent experiments. Five tissue pieces per region were counted in each experiment. There were no statistically significant differences in cellularity between the groups using one-way ANOVA with Bonferroni's correction for multiple comparisons.

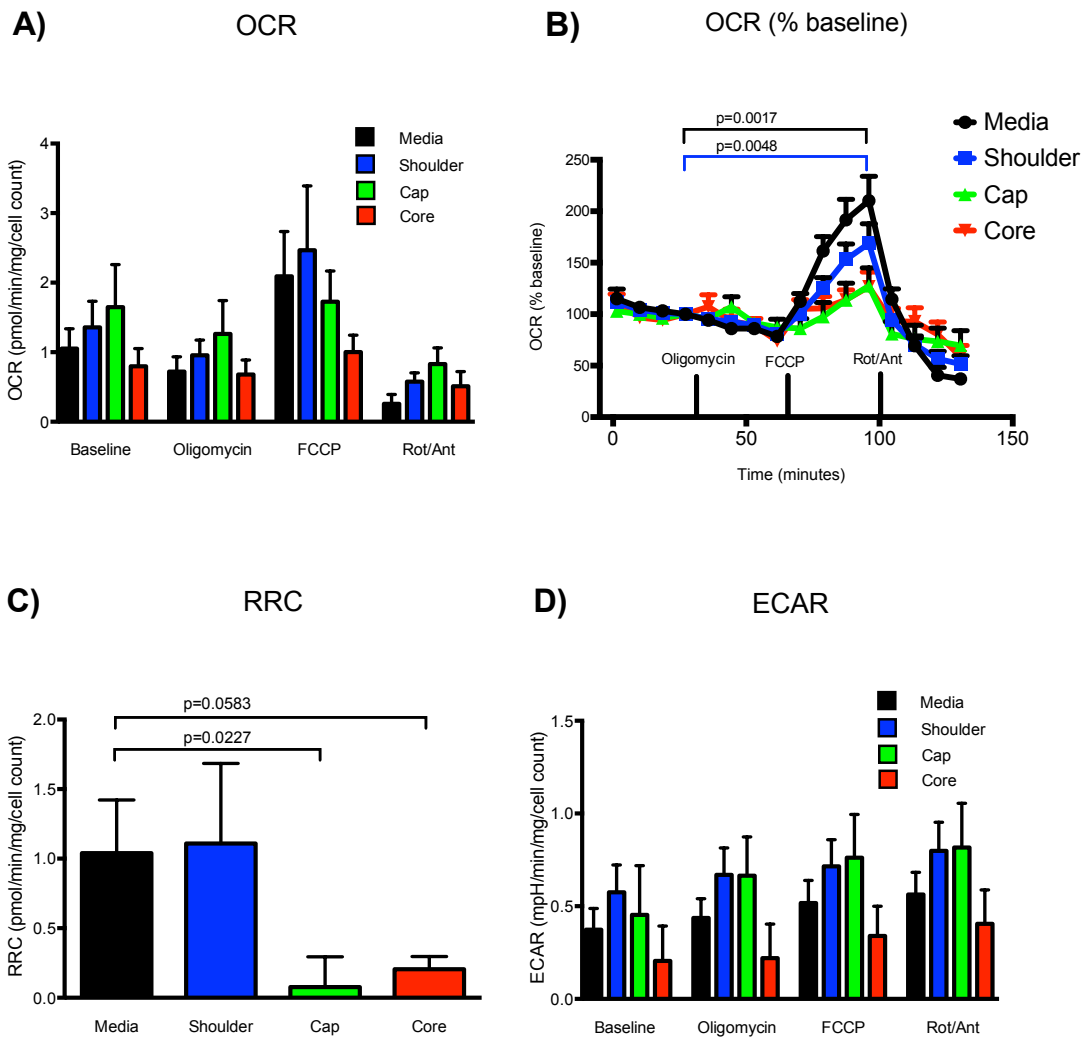

Figure 5-4 Seahorse extracellular flux analysis of tissues derived from carotid endarterectomies

Seahorse extracellular flux analysis was performed on tissue samples derived from human carotid endarterectomy specimens. The media, shoulder, cap and core regions were identified and samples weighing approximately 1 mg were dissected and analysed in Seahorse islet capture plates on a XF24e platform. Data was normalised to individual tissue wet weights and nuclear density. A) Oxygen consumption rate (OCR) at baseline and after serial injection of oligomycin (10 µg/ml final assay concentration), FCCP (1 µM) and a combination of rotenone and antimycin A (Rot/Ant, 10 µM each). N=5 carotid endarterectomy samples B) OCR expressed as % baseline (i.e. last measurement before oligomycin injection). N=6 carotid endarterectomy samples. Unpaired two-tailed t-tests with Holm-Sidak method for correction of multiple comparisons. C) Respiratory reserve capacity (RRC) of different regions of the plaque. N=5 carotid endarterectomy samples, ANOVA with Bonferroni's correction for multiple comparisons. D) Extracellular acidification rate (ECAR) at baseline and after serial injection of oligomycin, FCCP and a combination of rotenone and antimycin.

5.3 Mitochondrial DNA copy number in plaque and healthy tissues

mtDNA copy number is highly correlated to mitochondrial gene expression levels and mitochondrial mass across different tissues (D'Erchia et al., 2015), such that a reduction in mtDNA copy number may be a possible explanation for the reduced respiratory reserve capacity in cap and core regions. mtDNA copy number was therefore determined using the qPCR method comparing the amplification of two short mitochondrial DNA segments (mt3211 and mt9827) to the amplification of a short nuclear segment (β_2 microglobulin). The reaction efficiency of the nuclear amplification was similar to the mitochondrial segments using DNA in the range of 50-0.2 ng (Figure 5-5). Amplification of a single product in each reaction was confirmed by electrophoresis on a 1% agarose gel (Figure 5-6).

Age- and sex- matched samples of carotid endarterectomies and healthy aortas were derived from our internal tissue bank. The average age of donors for aortic tissue was 71.7 years ± 8.3 years (SD) and that of carotid tissue was 70.6 years ± 11.1 years (SD). 66% of both aortic tissue donors and carotid tissue donors were male. mtDNA copy number was significantly reduced in tissues derived from plaques compared to healthy aortas (Figure 5-7).

5.4 Expression of electron transfer complexes in plaque and aortic VSMCs

A reduced RRC of plaque tissue may be explained by changes in the expression of complexes of the ETC. To test this hypothesis, Western blot

was performed on cell lysates from plaque and aortic VSMCs. The average age of donors for aortic VSMCs was 48.6 years ± 26.0 years (SD), the average age of plaque VSMC donors was 65.2 years ± 3.9 years (SD). All donors of aortic VSMCs were male, but only 40% of plaque VSMC donors were male. Figure 5-8 demonstrates that the expression of complexes I and II was significantly reduced in plaque VSCMs compared to aortic VSMCs.

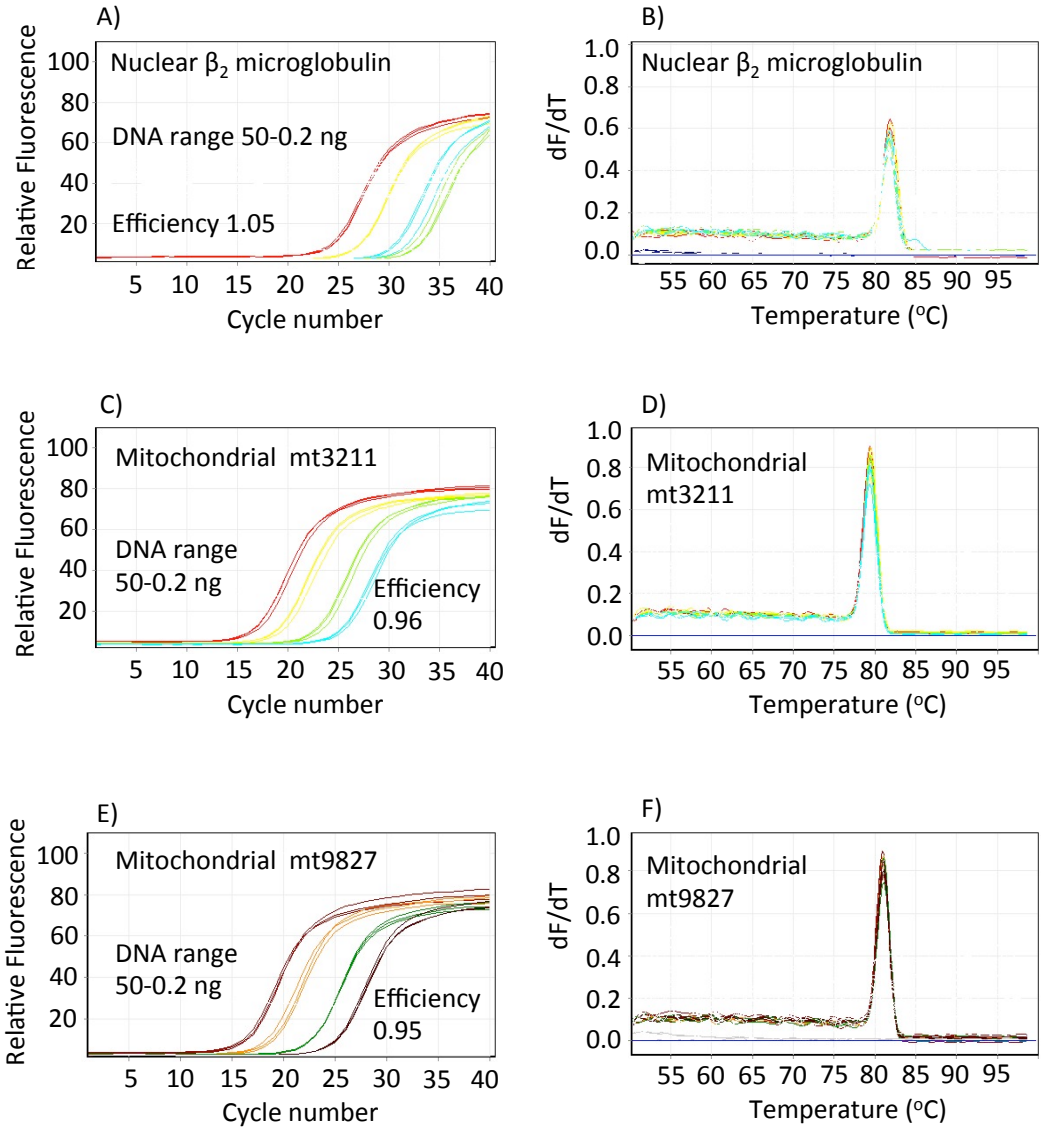

Figure 5-5 Validation of qPCR for human mtDNA copy number

Human DNA was serially diluted (50 ng, 10 ng, 1 ng and 0.2 ng) and qPCR reactions were run in triplicate on a Corbett Rotor-Gene™ 6000 QPCR thermocycler. Linearity of nuclear reaction (A) and mitochondrial reactions mt3211 (C) and mt9827 (E) with appropriate reaction efficiencies and corresponding melt curve analyses (B, D, F) are shown. dF/dT: the derivative of fluorescence (F) with respect to temperature (T).

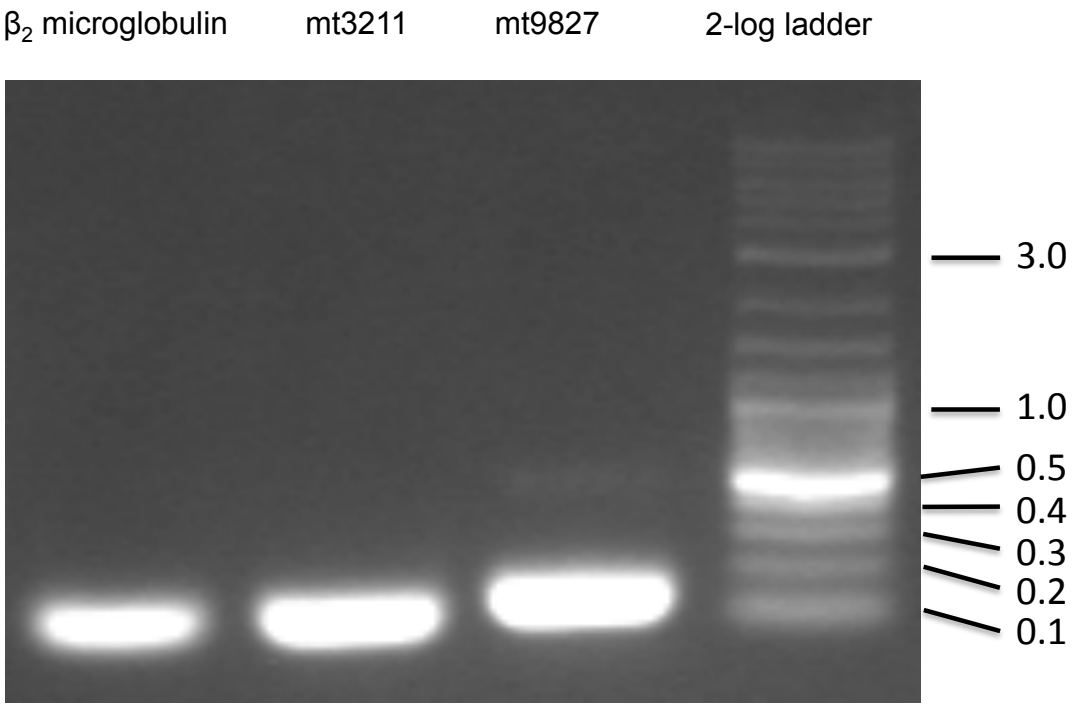

Figure 5-6 Confirmation of single PCR product from human nuclear and mitochondrial reactions

10 µl of PCR product from nuclear DNA reaction (β_2 microglobulin) and mitochondrial DNA reactions (mt3211 and mt9827) were run on a 1% agarose gel, stained with GelRed and visualised by UV light. 2-log ladder ranging from 0.1-10 kb is shown in the right lane. Expected amplicon sizes are: β_2 microglobulin – 86 bp, mt3211 – 87 bp, mt9827 – 147 bp.

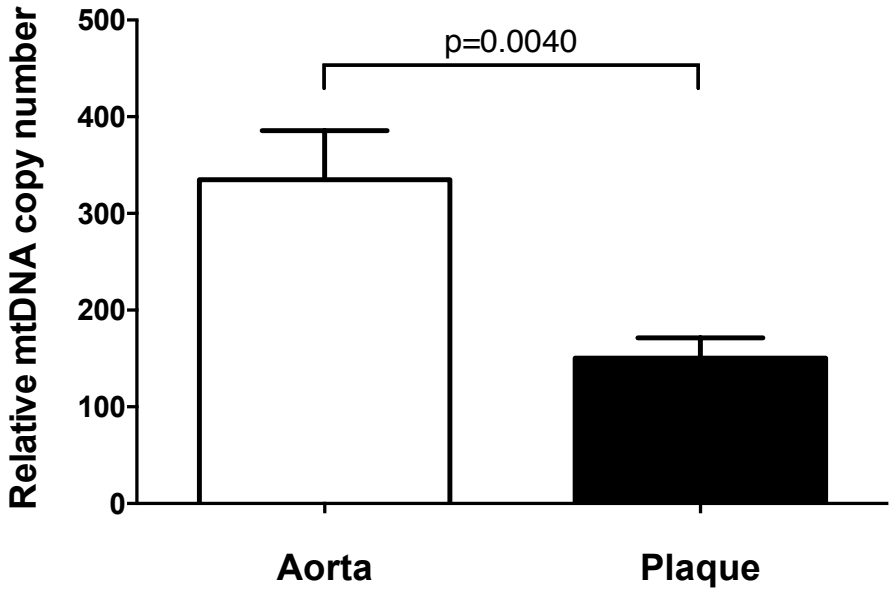

Figure 5-7 Mitochondrial DNA copy number in carotid atherosclerotic plaques and healthy aortas

DNA was isolated from snap frozen tissues derived from carotid endarterectomies (plaque) and healthy aortas. qPCR was performed to amplify two short mtDNA segments and a short nuclear DNA segment (β_2 microglobulin). The average Ct value for the two short mtDNA segments, Ct(mtDNA), was formed. MtDNA copy number was calculated as $2x2^{\Delta ct}$, where ΔCt=Ct(mtDNA)-Ct(nuclearDNA). This formula contains a correction by the factor 2 to account for 2 copies of the β_2 microglobulin gene in the genome. Data represents mean ± SEM of N=9 per group. Unpaired two-tailed t-test was used to determine statistical significance.

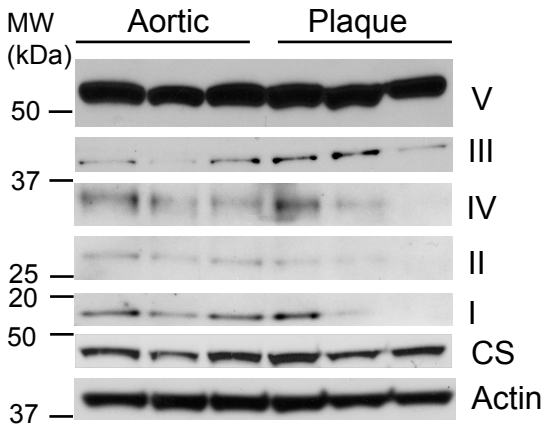
MW
(kDa)
Aortic
Plaque
50
37
25
20
50
37
V
III
IV
II
I
CS
Actin

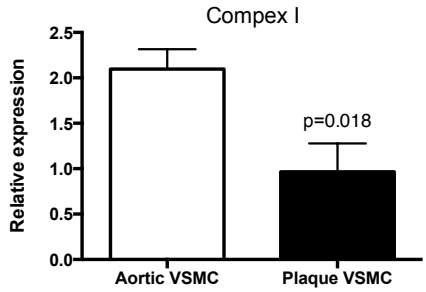
Compex I
Relative expression
2.5
2.0
1.5
1.0
0.5
0.0
p=0.018
Aortic VSMC
Plaque VSMC

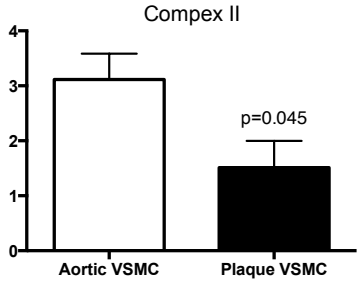
Compex II
4
3
2
1
0
p=0.045
Aortic VSMC
Plaque VSMC

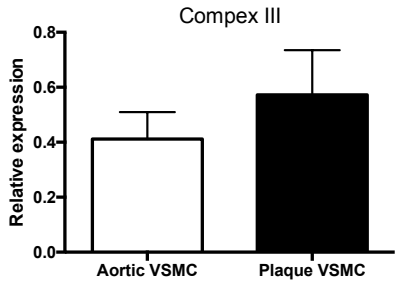
Compex III
Relative expression
0.8
0.6
0.4
0.2
0.0
Aortic VSMC
Plaque VSMC

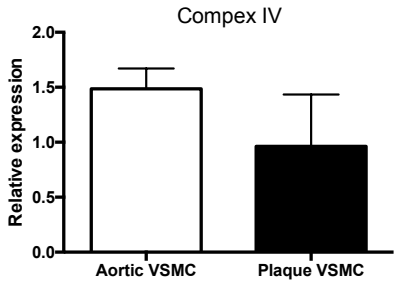
Compex IV
Relative expression
2.0
1.5
1.0
0.5
0.0
Aortic VSMC
Plaque VSMC

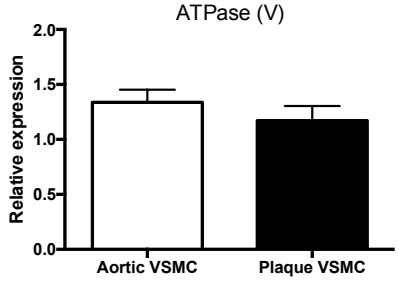
ATPase (V)
Relative expression
2.0
1.5
1.0
0.5
0.0
Aortic VSMC
Plaque VSMC

Figure 5-8 Expression of electron transfer chain complexes in plaque and aortic VSMCs

Whole cell lysates of aortic and plaque VSMCs were run on 8-12% gradient SDS gels. Western blot (top) and quantification (bottom) of protein expression of mitochondrial protein complexes within the electron transport chain [Complexes I-IV and ATPase (V)] is depicted. Data are mean ± SEM of N=3 (III-V) or N=5 (I-II) primary cell lines per group relative to citrate synthase (CS). See also Appendix 8.1.

5.5 Oxygen consumption rate of cultured VSMCs derived from atherosclerotic plaques or healthy aortas

VSMCs are the main cellular component of the media and the fibrous cap. To help clarify whether the reduced RRC observed in diseased tissue is permanent (and therefore present in cells cultured from the plaque) or potentially reversible, I cultured VSMCs derived from carotid endarterectomies and aortas under standard conditions and subjected them to Seahorse extracellular flux analysis. To do this, FCCP concentrations in the assay were optimised for use in human VSMCs (Figure 5-9) and 1 µM FCCP were used in the following. Aortic VSMC donors were 62.4 years ± 6.7 years old and all male, plaque VSMC donors were 71.8 years ± 10.8 years old and all male. As demonstrated in Figure 5-10 there were no significant differences in the OCR or ECAR of HVSMCs and plaque VSMCs.

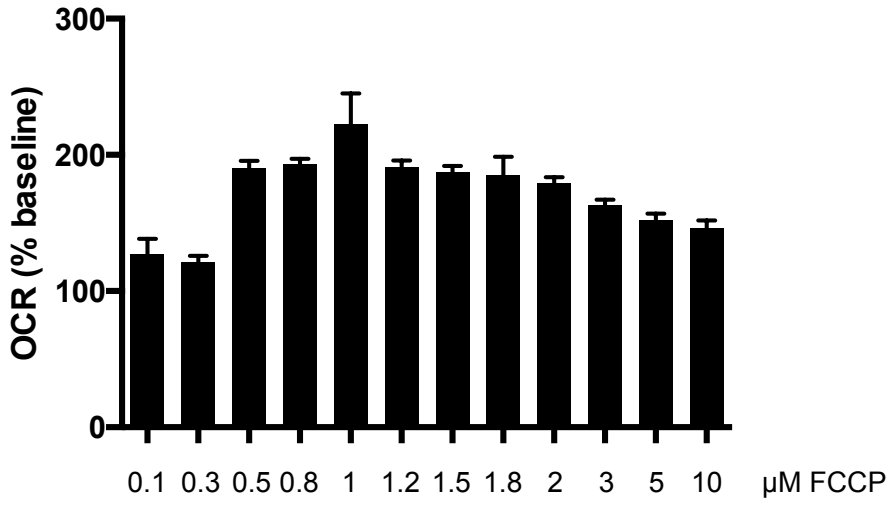

Figure 5-9 FCCP titration for Seahorse extracellular flux analysis in HVSMCs

HVSMCs were plated into a 96-well Seahorse culture plate and allowed to adhere overnight prior to extracellular flux analysis. OCR expressed as % baseline is shown for various concentrations of FCCP. Data represent means ± SEM of technical replicates in one experiment. 1 µM FCCP induced the highest OCR of the doses tested.

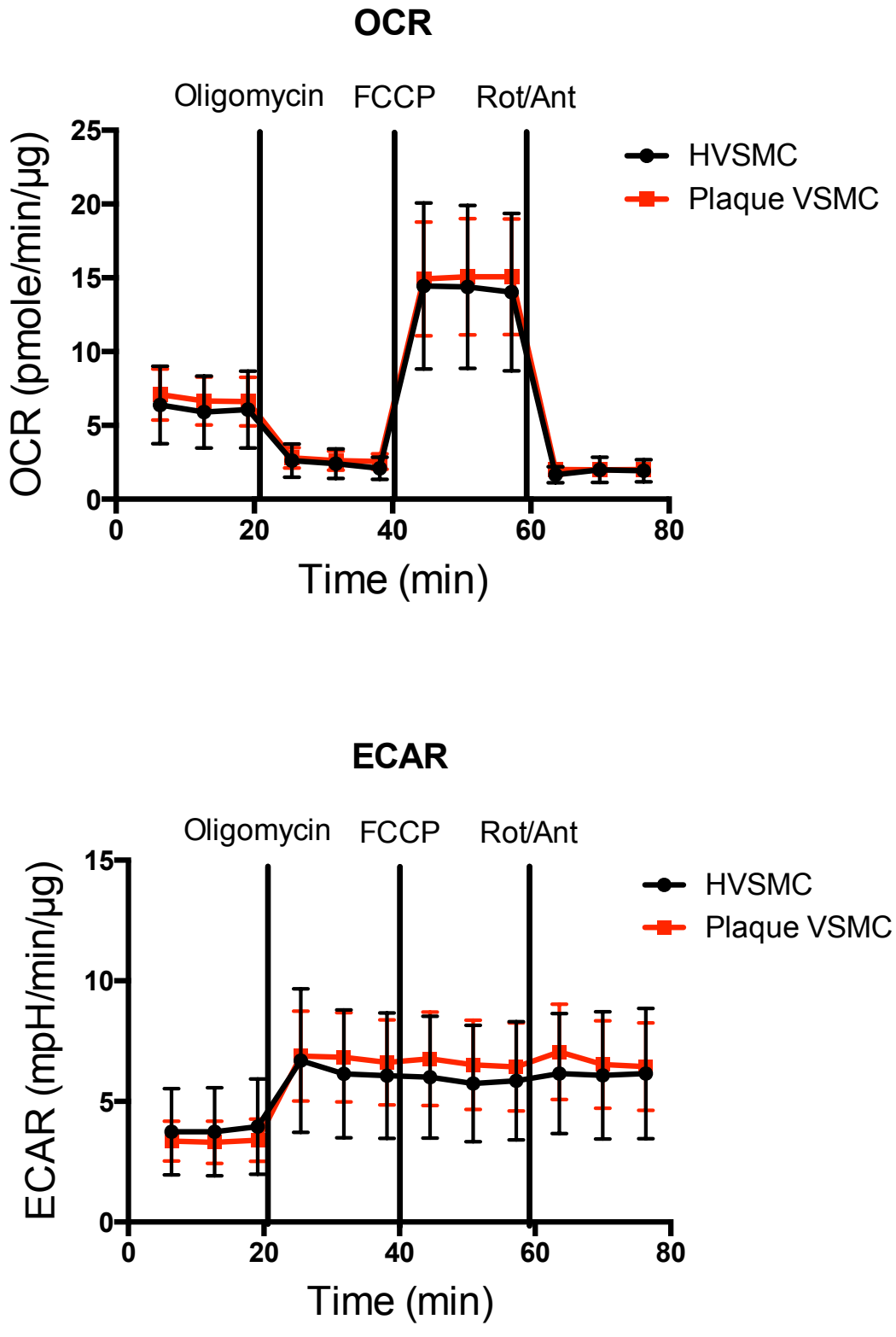

Figure 5-10 Seahorse extracellular flux analysis of HVSMCs and plaque VSMCs

HVSMCs and plaque VSMCs were plated into Seahorse 96 well culture plates and were allowed to adhere for at least 16 hours. The oxygen consumption rate (OCR) and extracellular acidification rate (ECAR) were determined before and after serial injection of oligomycin (2 µg/ml final assay

concentration), FCCP (1 μM) and a combination of rotenone (Rot, 1 μM) and antimycin A (Ant, 1 μM) as shown. Data represents mean ± SEM of N=6 experiments. There were no significant differences between groups using multiple two-tailed t-tests adjusted for multiple comparisons using Holm-Sidak method.

5.6 Discussion

To my knowledge this is the first report demonstrating altered mitochondrial respiration in diseased human tissue using the Seahorse extracellular flux analysis technique. Despite the data variability, a significant reduction in the response to FCCP was observed in the diseased cap and core regions of the plaque. This finding was supported by evidence of reduced mtDNA copy number in plaque tissue compared to healthy aortic tissue. Reduced mitochondrial respiration after uncoupling may relate to reduced protein expression of the ETC complexes I and II in plaque VSMCs demonstrated in this chapter. Reduced mitochondrial respiration, however, was not observed in plaque VSMCs compared to healthy VSMCs.

Microdissecting atherosclerotic plaques for Seahorse extracellular flux analysis is technically challenging. Therefore, the n-numbers of the present study are relatively small. It is possible that the areas identified and analysed may not completely represent the healthy media, shoulder region or the cap and core regions. For example, samples thought to derive from the shoulder region, may, to a degree, have included tissue from the neighbouring core region. For this reason, immunohistochemistry was performed on tissue pieces after completion of the assay, demonstrating different areas of the atherosclerotic plaque can be sampled. Furthermore, contamination of samples with adjacent areas should lead to a reduced effect size such that

this study may have underestimated the true differences present *in vivo* rather than overestimating them. Data was normalised to both the tissue weight and cellularity suggesting that the differences observed were not due to tissue mass or cellular density. Furthermore, the ECAR increased in all regions after serial injections of mitochondrial inhibitors suggesting that all plaque areas remained metabolically active. However I cannot rule out that some of the differences observed between the regions are driven by differences in cellular composition of the sampled areas. For example, the core region may have contained more inflammatory cells than the media explaining the different Seahorse extracellular flux analysis profile. Since the completion of the experimental work for this study Dr Mercer's group has published a similar study examining different areas of human atherosclerotic plaque derived from carotid endarterectomies for respiration (Docherty, Carswell, Friel, & Mercer, 2018). Not only did that study confirm the findings of reduced respiration in the cap and core region of human atherosclerosis presented here, but also attempted to quantify the cellular composition of the different regions of the plaque in more detail. Their work suggests that although the shoulder region and the core region have higher proportions of inflammatory cells, the composition of the cap region and the healthy media is very similar. The present study did not determine viability of cells in the regions sampled and it is therefore possible that the differences observed reflect a general decline in cellular viability rather than a defect that is specific to mitochondria.

One of the advantages of the Seahorse assay is that it allows for the simultaneous assessment of mitochondrial respiration in up to 20 tissue samples. However, the laborious post assay sample validation using

immunohistochemistry and determination of cellular density may limit its widespread use in the assessment of mitochondrial function in diseased tissues.

In the present work, mtDNA copy number was reduced in plaque tissue compared to healthy aortic tissue. This observation fits with a previous report from our laboratory demonstrating increased mtDNA damage in plaques compared to aortas (E. Yu et al., 2013) and with reduced mitochondrial respiration in the present study. Similarly, the reduced expression of ETC complexes I and II in plaque VSMCs could offer an explanation of the reduced mitochondrial respiration observed in diseased plaque tissue. Complex I is particularly prone to oxidative damage due to its size and composition from multiple subunits as well as its exposure to high concentrations of ROS (Murphy, 2009; J. Zhu, Vinothkumar, & Hirst, 2016). There is evidence that reduced activity of ETC complexes I and II are relevant to other human diseases. For example, mutations of vacuolar sorting protein 35 (VPS35), known to cause Parkinson's disease, also lead to reduced complex I and II assembly and activity and increased mitochondrial fragmentation (W. Wang et al., 2016; L. Zhou, Wang, Hoppel, Liu, & Zhu, 2017).

Using cultured VSMCs from plaques or aortas, however, I did not demonstrate any difference in the OCR or ECAR using the Seahorse extracellular flux assay. This result was surprising, given the reduced expression of complexes I and II in these cells. The disconnection between protein expression of ETC complexes and results from the extracellular flux analysis is concerning. There was, however, a great variability in the extracellular flux analysis of cultured human cells leading to large standard

errors. It may therefore be possible that any potential effect of reduced expression of complexes I and II was not captured in this assay. The result of the present study is also contradicting previous experiments in our laboratory, which demonstrated a clear difference in OCR and RRC in plaque VSMCs compared to aortic VSMCs (E. P. K. Yu et al., 2017). Of note, the experiments that were previously conducted had much lower standard errors. It may be that the differences in the results are due to a slightly different population of VSMCs investigated. VSMCs were cultured from plaques containing very diseased core areas as well as shoulder, cap and media regions. During cell culture a subset of more viable cells originating from the media may become selected thus diminishing any differences seen between aortic and plaque VSMCs. Discrepancies in experiments using cultured VSMCs underline the importance of validating findings in whole tissues as presented in the present study, whenever possible.

Taken together, the results from this chapter add to the growing evidence of mitochondrial dysfunction in aging and age-related diseases. For example, because approximately 95% of ATP in healthy hearts is formed through mitochondrial oxidative phosphorylation (De Jong & Lopaschuk, 2017) and mtDNA defects can lead to primary cardiomyopathies (Casademont & Miro, 2002), mitochondrial dysfunction has also been implicated in heart failure. We know that deficiencies in electron transfer chain complex I can lead to severe cardiomyopathy (Chouchani, Methner, et al., 2014) and that impaired cardiac energy reserves, measured as the phosphocreatine/ATP ratio, correlate with heart failure symptoms and predict mortality in dilated cardiomyopathy in humans (Neubauer et al., 1997;

Neubauer et al., 1992). It is frequently assumed that in heart failure there is a switch from oxidative phosphorylation of fatty acids and other substrates towards increased glycolysis (Lopaschuk, 2017). It has been proposed that this metabolic switch is a consequence of reduced mitochondrial oxidative capacity and reduced expression of genes required for fatty acid oxidation (De Jong & Lopaschuk, 2017). A switch to glycolysis could be an adaptive response to preserve ATP stores, however, a mismatch between glycolysis and oxidative phosphorylation could lead to lactate production, intracellular acidification and functional impairment (Lopaschuk, 2017).

Mitochondrial dysfunction has also been implicated in a variety of neurodegenerative diseases including Alzheimer's, Parkinson's and Huntington's diseases. Deprivation of nerve growth factor (NGF) is a well-characterised model of programmed cell death in neurons offering similarities to vulnerable neurons in the ageing brain (McManus et al., 2014). Removal of NGF increases mitochondrial ROS production in neurons that can lead to caspase-dependent and independent cell death. Two cell lines, 7WD4 and 7PA2, widely used as models for Alzheimer's disease, demonstrate reduced respiration and increased glycolysis, decreased mitochondrial membrane potential and ATP content as well as dysfunctional ETC complexes I and IV (Krako et al., 2013). Similarly, ETC complex I impairment and ROS production are thought to be key modulators in experimental models of Parkinson's disease (Mounsey & Teismann, 2010). Another mechanism in the disease pathology of Parkinson's may be defective mitophagy. Mutations in the genes of PINK1 or parkin, important actors in mitophagy, cause dopaminergic neuron degeneration in *Drosophila melanogaster* (Clark et al., 2006; Park et

al., 2006) and cause early-onset Parkinson's disease (Kitada et al., 1998; Valente et al., 2004). The role of mitophagy in VSMCs is further assessed in chapter 6.

In summary, I have demonstrated that mitochondrial respiration is reduced in the cap and the core region of human atherosclerotic plaques. This reduction may partly be explained by reduced expression of ETC complexes I and II in VSMCs derived from such plaques. mtDNA copy number is also reduced in human atherosclerotic plaques supporting previous findings of increased mtDNA damage.

6 Assessment of mitochondrial turnover in human VSMCs derived from atherosclerotic plaques and healthy aortas

6.1 Introduction

The previous chapter has determined that there is mitochondrial dysfunction in human atherosclerosis manifest as reduced respiration and reduced mtDNA copy number as well as reduced expression of complexes I and II of the ETC in plaque VSMCs. To maintain mitochondrial homeostasis, various mechanisms have been identified, that allow cells to address mitochondrial damage. One of the key mechanisms for the degradation of dysfunctional mitochondria is mitophagy (section 1.2.3.1). After discussing and validating the use of the mitochondrially targeted mitophagy probe Keima (sections 6.2-6.3) I demonstrate that OxLDL but not LDL or LPS induce mitophagy in healthy human VSMCs (section 6.4) without effects on mitochondrial shape. I further demonstrate increased mitophagy and altered mitochondrial shape in plaque VSMCs compared to healthy aortic VSMCs (section 6.5). Expression of genes involved in mitochondrial fission and fusion (section 6.6) and biogenesis and repair (section 6.7), was assessed in plaque VSMCs and healthy aortic VSMCs but no significant differences were observed.

6.2 Approaches to mitophagy

Mitophagy in mammalian cell can be assessed through a variety of techniques, each with their own advantages and limitations. Up to now no consensus has emerged as to which method is superior (Klionsky et al., 2012). A direct way to detect mitophagy is through use of electron microscopy with identification of mitochondria within autophagosomes (Chu, 2010). However, electron microscopy is time-consuming and expensive and can potentially be subjective. Another method that is frequently used relies on the demonstration of colocalisation of mitochondria or mitochondrial proteins with lysosomes. For example, labelling of mitochondria can be achieved with MitoTracker Green FM and lysosomes can be labelled with LysoTracker Red. A positive colocalisation then leads to a yellow signal in the merged channels (Klionsky et al., 2012). Alternatively, colocalisation of autophagy markers such as LC3 with mitochondrial proteins such as LAMP1 or FUNDC1 has been used in the detection of mitophagy (L. Liu et al., 2012). However, this approach may cause artefacts as LC3 can also be incorporated into protein aggregates independently of autophagy (Kuma, Matsui, & Mizushima, 2007). Another way to quantify mitophagy is through the assessment of loss of mitochondrial mass using flow cytometry, immunocytochemistry and Western blot of mitochondrial proteins (Klionsky et al., 2012). Electron microscopy can further help identify loss of mitochondria, or qPCR as described in this thesis can be used to quantify mtDNA which is closely related to mitochondrial mass (see section 2.9). Further evidence of mitophagy has also been sought by confirming involvement of the PINK1/Parkin pathway. As PINK1 degradation is inhibited after inner mitochondrial membrane depolarisation (see section

1.2.3.1) increased PINK1 protein levels are supportive of mitophagy. Alternatively, Parkin translocation to the mitochondria can indicate mitophagy (Swiader et al., 2016), although both of these approaches on their own are not sufficient to prove mitophagy.

A novel method to quantify mitophagy uses a fluorescent variant of the coral-derived protein Keima (Kogure et al., 2006). When targeted to mitochondria, Keima allows for the detection of mitophagy based on a pH-dependent shift in the excitation spectrum once mitochondria are delivered to the lysosome (Katayama et al., 2011). Keima can be excited at 440 nm at the physiological mitochondrial matrix pH ~8, but the excitation spectrum shifts to allow excitation at 586 nm once mitochondria are targeted to the lysosome with an acidic pH (Figure 6-1).

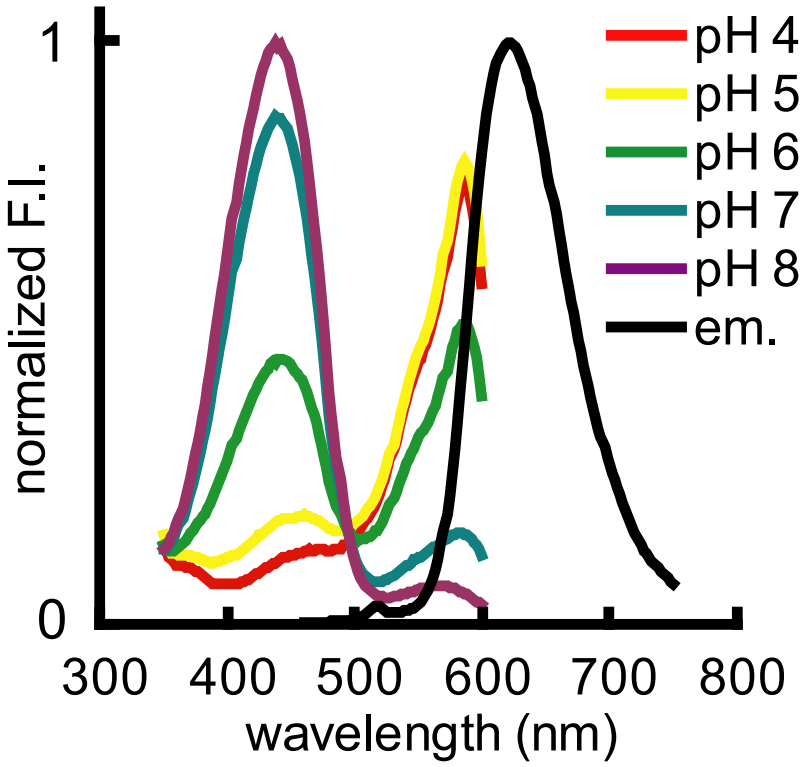

Figure 6-1 pH-dependent excitation spectrum of keima

Excitation spectra of keima at pH 4-8 and fixed emission spectrum is illustrated. F.I. fluorescence intensity. Reproduced from Katayama et al. (2011).

Since Keima is resistant to lysosomal degradation, the Keima signal can be used to infer cumulative mitophagy (Sun et al., 2015). Keima-based assessment of mitophagy has been validated against parkin translocation as well as colocalisation with lysosomes (Katayama et al., 2011; Sun et al., 2015). The method has already been used to demonstrate increased mitophagy in PolG mice, which have high levels of mtDNA damage, during hypoxia, and in a mouse model of B16 melanoma cell injection (Sun et al., 2015). Decreased mitophagy was observed with ageing in WT mice and in mice expressing the transgene for human Huntingtin's protein, which has deleterious effects on mitochondrial function (Sun et al., 2015).

6.3 Use of Keima-expressing lentiviral particles

Because of the limited availability of plaque VSMCs I considered the approach using Keima to assess mitophagy to be most promising. A lentiviral strategy was chosen as this would lead to stable expression of Keima and infection can also occur in non-dividing cells (Naldini et al., 1996). Lentiviral particles were generated in HEK-293T cells, harvested, and concentrated. qPCR was performed to determine lentiviral copy number. Lentiviral particles were then used to infect target HeLa cells to validate the method. As demonstrated in Figure 6-2 lentiviral infection of HeLa cells resulted in protein expression of Keima. The expression of Keima was then assessed using a SP5 confocal microscope (Leica) after plating HeLa cells into glass-bottom culture dishes for live cell imaging. Structures resembling mitochondrial

networks could be visualised but there was variability in the Keima signal across cells (Figure 6-3). Areas of Keima signal corresponding to normal pH (green Keima in the following) and acidic pH (red Keima in the following) were visible in cells.

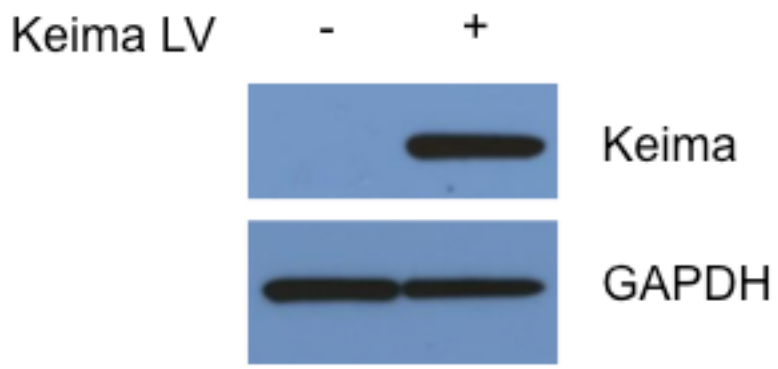

Figure 6-2 Keima expression in HeLa cells after lentiviral infection

Western blot confirmed expression of Keima protein in HeLa cells infected with Keima lentiviral particles (Keima LV). Glyceraldehyde 3-phosphate dehydrogenase (GAPDH) was used as loading control. See also Appendix 8.1.

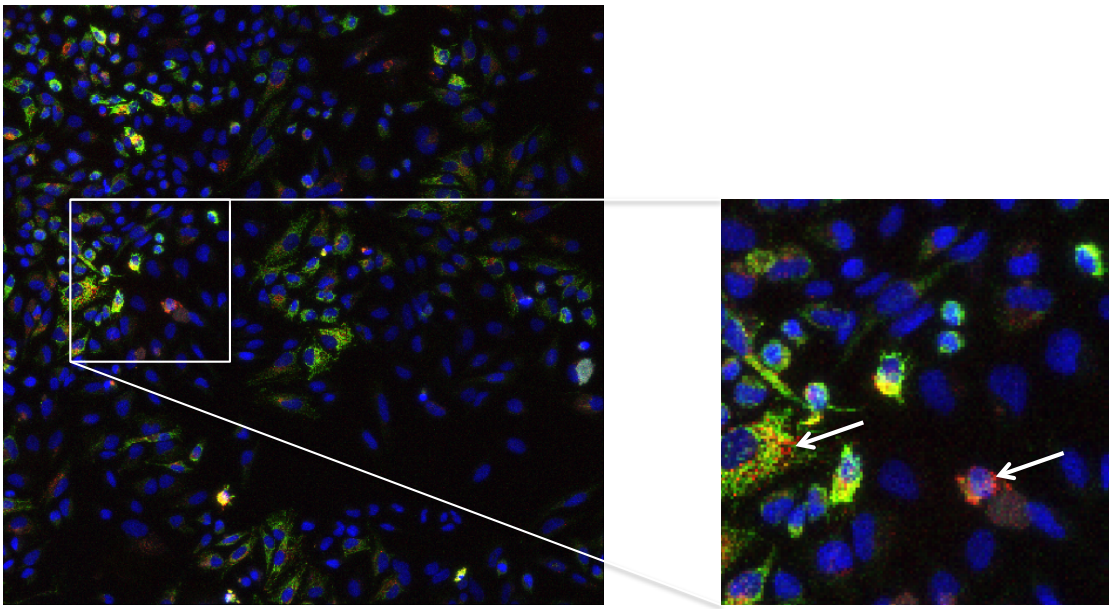

Figure 6-3 Keima expression in HeLa cells assessed by confocal microscopy

HeLa cells were infected with Keima -expressing lentiviral particles and selected with puromycin. Cells were then plated in MatTek glass bottom culture dishes and allowed to adhere. Nuclei were stained with Hoechst 33342 and cells were imaged using a SP5 confocal microscope (Leica). A 10x/0.3 PL Fluotar lens was used and three channels were acquired after serial excitation with UV (nuclei, coded blue), an argon laser at 458 nm (Keima at normal pH, coded green) and a yellow laser at 561 nm (acidic mitochondria, coded red). A composite image of the maximum projection of an imaging z-stack is shown on the left. The magnified area on the right demonstrates areas of red Keima signal (arrows). The magnified area appears pixelated due to the limit of resolution at this magnification

Next, human VSMCs were infected with Keima lentiviral particles and selected with puromycin before plating on glass bottom culture dishes for Hoechst 33342 staining and live cell imaging. The three donors for aortic VSMCs were 69.7 years ± 18.1 years (SD) and all male, the three donors of plaque VSMCs were 66.0 years ± 5.3 years (SD) and 66.7% were male. Although proliferation and viability of human VSMCs was not assessed in the present study there is evidence that plaque VSMCs have reduced proliferation, increased cell death and earlier cell senescence compared to healthy VSMCs (Bennett, Macdonald, Chan, Boyle, & Weissberg, 1998). Infection with Keima lentiviral particles was therefore conducted as early as possible, between passage 3 and 9 for all VSMC lines. Cells were imaged on a SP5 confocal microscope using a 63x/1.4-0.6 Oil lens and serial excitation to visualise nuclei as well as green and red Keima. Figure 6-4 illustrates mitochondrial networks in untreated cells (A) and rounded mitochondrial fragments with red Keima signal indicating mitophagy after FCCP treatment (B).

A)

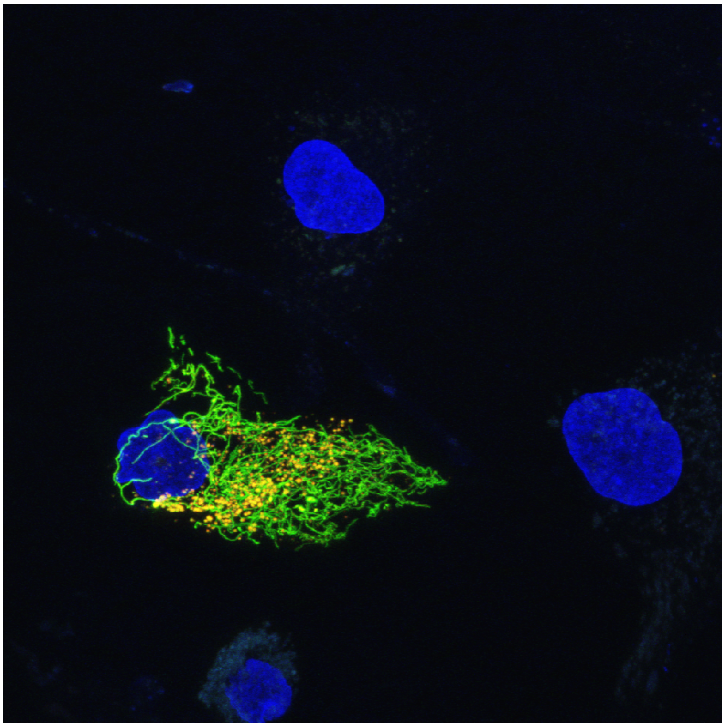

B)

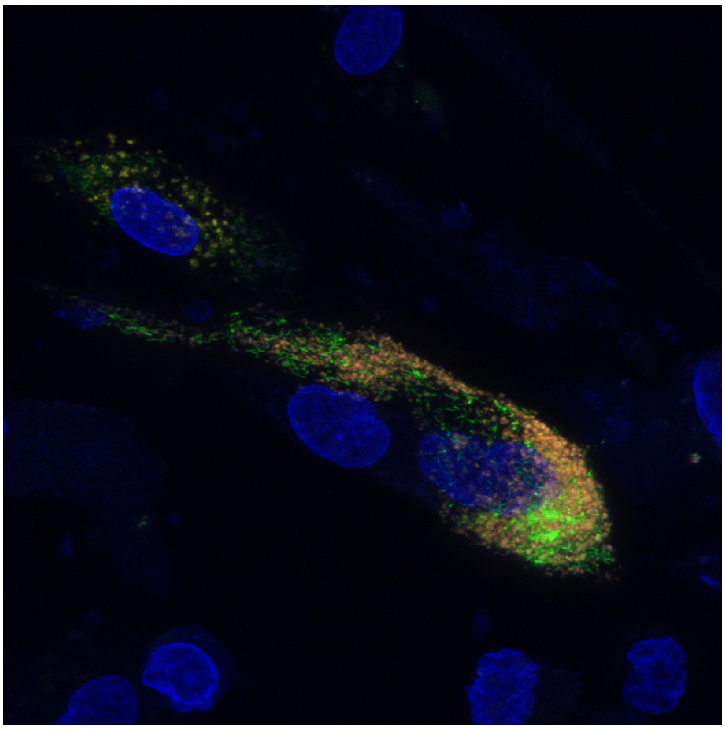

Figure 6-4 Keima confocal imaging in human VSMCs

Human VSMCs were infected with Keima-expressing lentiviral particles and selected with puromycin. Cells were then plated in MatTek glass bottom culture dishes and allowed to adhere. Nuclei were

stained with Hoechst 33342 and cells were imaged using a SP5 confocal microscope (Leica). A 63x/1.4-0.6 PL Apo oil lens was used and three channels were acquired after serial excitation with UV (nuclei, coded blue), an argon laser at 458 nm (Keima at normal pH, coded green) and a yellow laser at 561 nm (acidic mitochondria, coded red). Representative composite images of the maximum projection of z-stacks are shown in A) untreated HVSMCs and B) following treatment with 5 μM FCCP for 24 hours. FCCP appeared to induce fragmentation of mitochondria and induce mitophagy with a shift towards red Keima signal.

To investigate the effects of atherogenic lipids on mitophagy and to determine whether plaque VSMCs have altered mitophagy, cells were subjected to confocal microscopy assessment of Keima as described above. The consistency of labelling of either human VSMCs or plaque VSMCs was not formally assessed; instead confocal microscopy focused on cells with intense keima signal to generate images with sufficient resolution. At least 20 z-stacks were acquired in at least three independent experiments from three different primary cell cultures per group. These experiments were conducted in parallel but for clarity of data presentation the results are divided into the effects of atherogenic lipids, LPS and bafilomycin on healthy VSMCs (section 6.4) and the comparison of plaque VSMCs with and without treatment with OxLDL and FCCP compared to aortic VSMCs (section 6.5).

6.4 Effects of OxLDL and FCCP on mitophagy and mitochondrial shape of human VSMCs

Figure 6-5 depicts representative images of aortic VSMCs with and without treatment with OxLDL, LDL, LPS, Bafilomycin and FCCP. To objectively assess changes in mitochondrial shape and Keima signal an image J plug-in was designed by Richard Butler (the Gurdon Institute,

University of Cambridge). This plug-in is based on the published MitoLoc plug-in (Vowinckel et al., 2015) but allows for the assessment of green, red or the combined Keima signal. Using the combined red and green Keima signal and an Otsu thresholding method, the programme uses the resulting 3D mask to calculate the outputs surface area/volume (SA:V) and compactness as previously derscribed for MitoLoc. The ratio SA:V is expected to be higher in rounded fragmented mitochondria compared to mitochondrial networks and has therefore been used as measure of mitochondrial fragmentation. Compactness describes the variance of the radial distance/volume and offers an estimate of the tubularity of the mitochondrial network. The means of signal intensity derived from the voxels of red and green Keima were used to calculate the mitophagy index (red/green).

OxLDL significantly increased mitophagy in HVSMCs after 24 hours, as did the positive control FCCP (Figure 6-6). The results from 4 hours and 16 hours of treatment with OxLDL are inconclusive at the sample size. LDL did not exert an effect on mitophagy, nor did LPS. Bafilomycin, an inhibitor of the vacuolar type H^+-ATPase responsible for lysosomal acidification, also increased the red/green ratio probably reflecting slower Keima degradation in the lysosomes rather than increased mitophagy. The data from mitochondrial shape assessment was more variable (Figure 6-6). FCCP treatment decreased the SA:V ratio suggesting increased mitochondrial fragmentation; however there were no significant differences after OxLDL, LDL, LPS or bafilomycin treatment. The measure of compactness showed even higher variation and did not demonstrate any differences between groups.

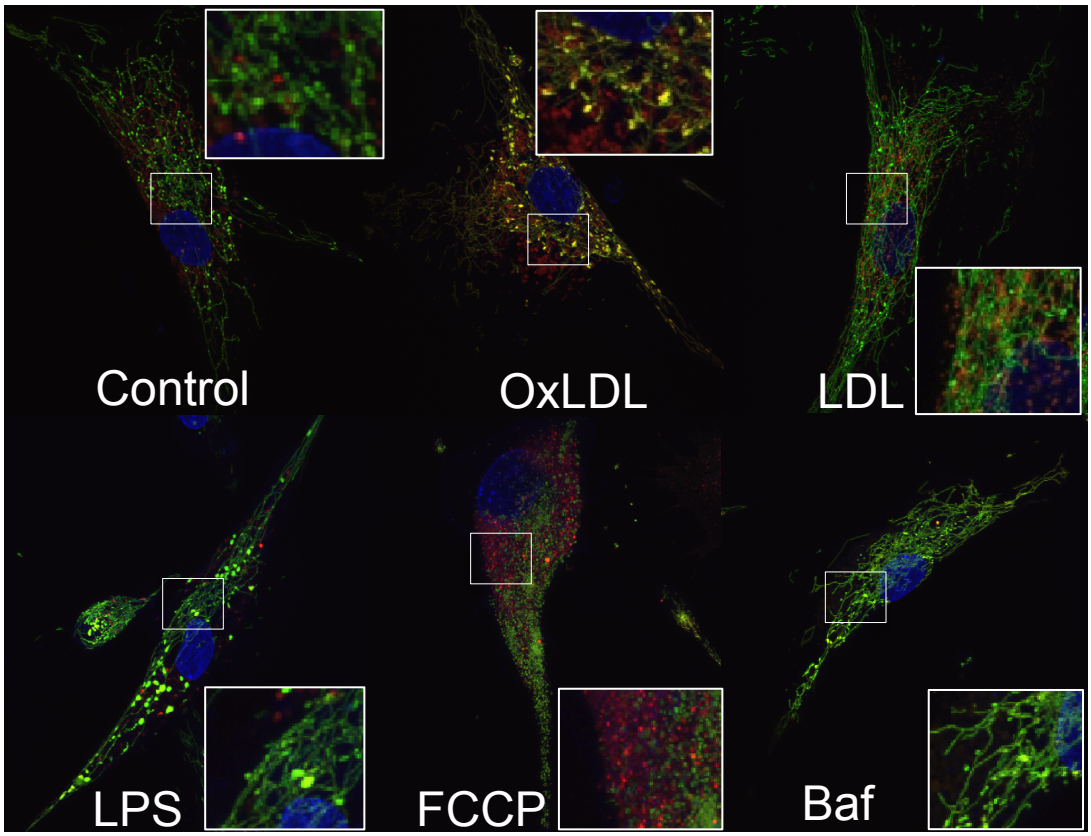

Figure 6-5 Representative confocal microscopy images of mitophagy in HVSMCs

Human VSMCs were infected with Keima-expressing lentiviral particles and selected with puromycin. Cells were then plated in MatTek glass bottom culture dishes and allowed to adhere before treatment. Nuclei were stained with Hoechst 33342 and cells were imaged using a SP5 confocal microscope (Leica). A 63x/1.4-0.6 PL Apo oil lens was used and three channels were acquired after serial excitation with UV (nuclei, coded blue), an argon laser at 458 nm (Keima at normal pH, coded green) and a yellow laser at 561 nm (acidic mitochondria, coded red). Control: Vehicle (PBS) treatment for 24 hours, OxLDL: 100 µg/ml for 24 hours, LDL: 100 µg/ml for 24 hours, LPS: 1000 ng/ml, FCCP (5 µM for 24 hours), Baf: bafilomycin (30 nM for 6 hours). Representative composite images of the maximum projection of z-stacks are shown. High magnification field (box) demonstrates red Keima signal in OxLDL (100 µg/ml for 24 hours) and FCCP (5 µM for 24 hours) treated cells.

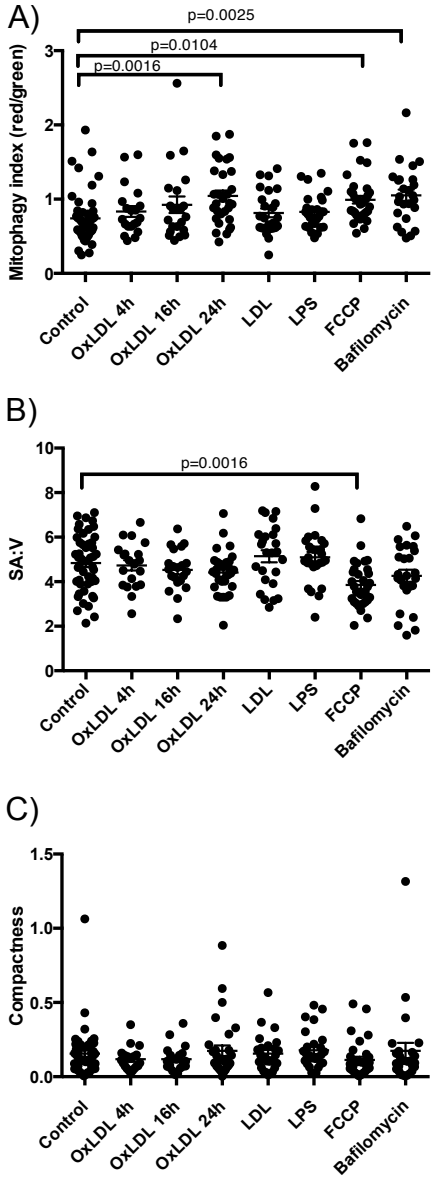

Figure 6-6 Mitophagy and mitochondrial shape in human VSMCs

Human VSMCs were infected with Keima expressing lentiviral particles and selected with puromycin. Cells were then plated in MatTek glass bottom culture dishes and allowed to adhere before treatment. Nuclear were stained with Hoechst 33342 and cells were imaged using a SP5 confocal microscope (Leica). A 63x/1.4-0.6 PL Apo oil lens was used and three channels were acquired after serial excitation with UV (nuclei, coded blue), an argon laser at 458 nm (Keima at normal pH, coded green) and a yellow laser at 561 nm (acidic mitochondria, coded red). Control: Vehicle (PBS) treatment for 24 hours, OxLDL: 100 µg/ml for 24 hours, LDL: 100 µg/ml for 24 hours, LPS: 1000 ng/ml, FCCP (5 µM for 24 hours), bafilomycin (30nM for 6 hours). Quantification of the mitophagy index (A), SA:V (B) and compactness (C) from at least 20 z-stacks from at least three independent experiments from three different primary cell cultures per group were analysed using ImageJ and the mitochondrial morphology plug-in. For B) ROUT analysis was performed to identify outliers using a maximum false

discovery rate of 0.1% (the most stringent setting in Prism 6). 2 outliers from a total of 229 data points were identified and removed prior to analysis. One-way ANOVA with Bonferroni's correction for multiple comparison was performed.

6.5 Mitophagy and mitochondrial shape in plaque VSMCs compared to healthy VSMCs

Previous chapters have shown that mtDNA copy number is reduced in plaques compared to healthy aortas, RRC is impaired in the diseased cap region of human plaques, and VSMCs derived from carotid endarterectomies have decreased expression of complexes I and II of the ETC. Such mitochondrial dysfunction may have effects on mitochondrial shape and mitophagy and was therefore assessed in plaque VSMCs with and without treatment with OxLDL and FCCP in comparison to healthy VSMCs. Representative images are shown in Figure 6-7. Plaque VSMCs had increased mitophagy and increased mitochondrial fragmentation whilst the interpretation of data on the tubularity (compactness) was hindered by large variations (Figure 6-8). Mitophagy in plaque VSMCs could not be further induced by either OxLDL or FCCP.

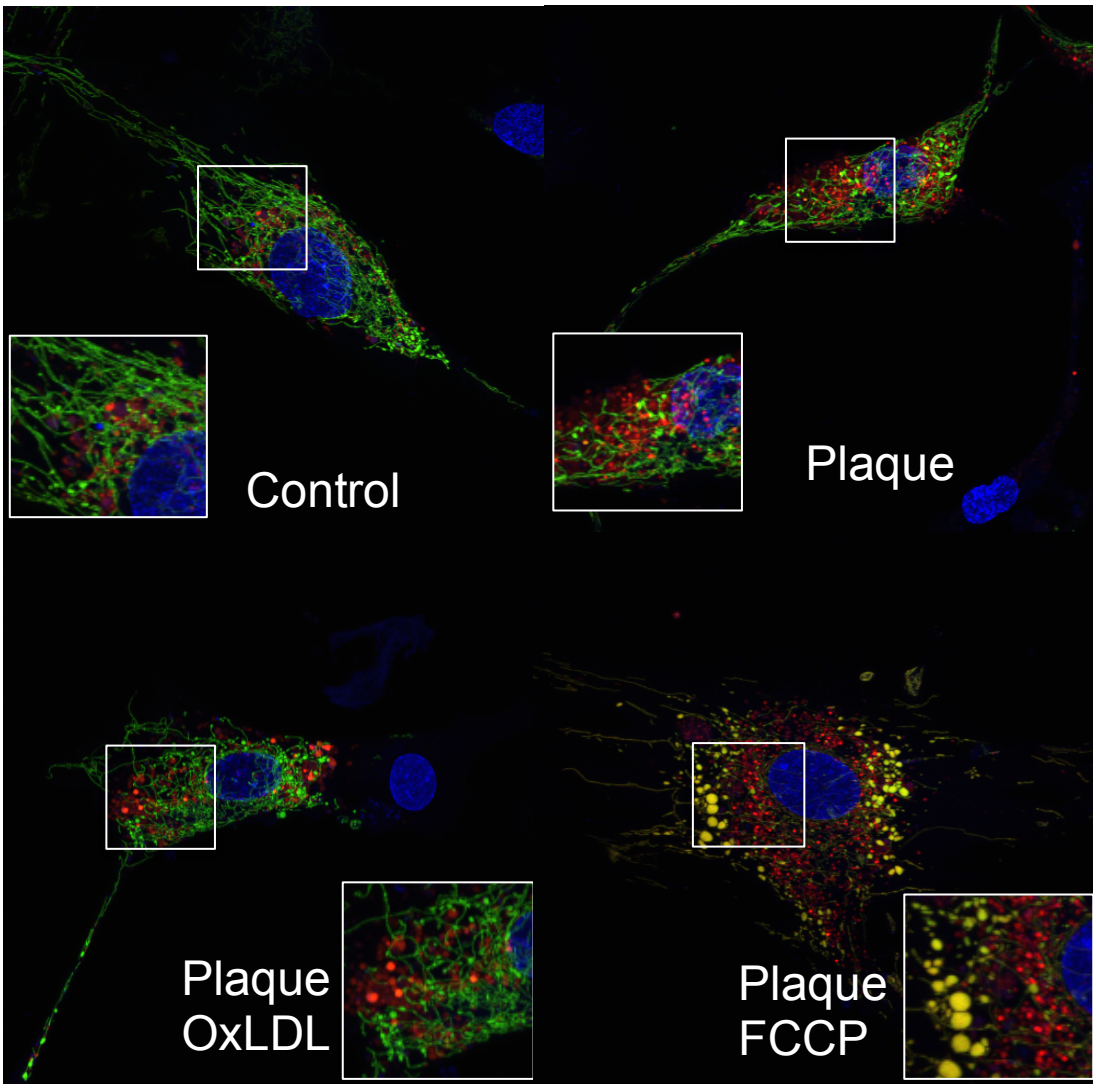

Figure 6-7 Representative confocal microscopy images of mitophagy in plaque and healthy HVSMCs

Human VSMCs were infected with Keima expressing lentiviral particles and selected with puromycin. Cells were then plated in MatTek glass bottom culture dishes and allowed to adhere before treatment. Nuclei were stained with Hoechst 33342 and cells were imaged using a SP5 confocal microscope (Leica). A 63x/1.4-0.6 PL Apo oil lens was used and three channels were acquired after serial excitation with UV (nuclei, coded blue), an argon laser at 458 nm (Keima at normal pH, coded green) and a yellow laser at 561 nm (acidic mitochondria, coded red). Control: Vehicle (PBS) treatment of aortic VSMCs, plaque: vehicle (PBS) treated HVSMCs derived from carotid endarterectomies ± OxLDL (100 µg/ml for 24 hours) or FCCP (5 µM for 24 hours) treatment. Representative composite images of the maximum projection of z-stacks are shown. High magnification field (box) for each image is shown.

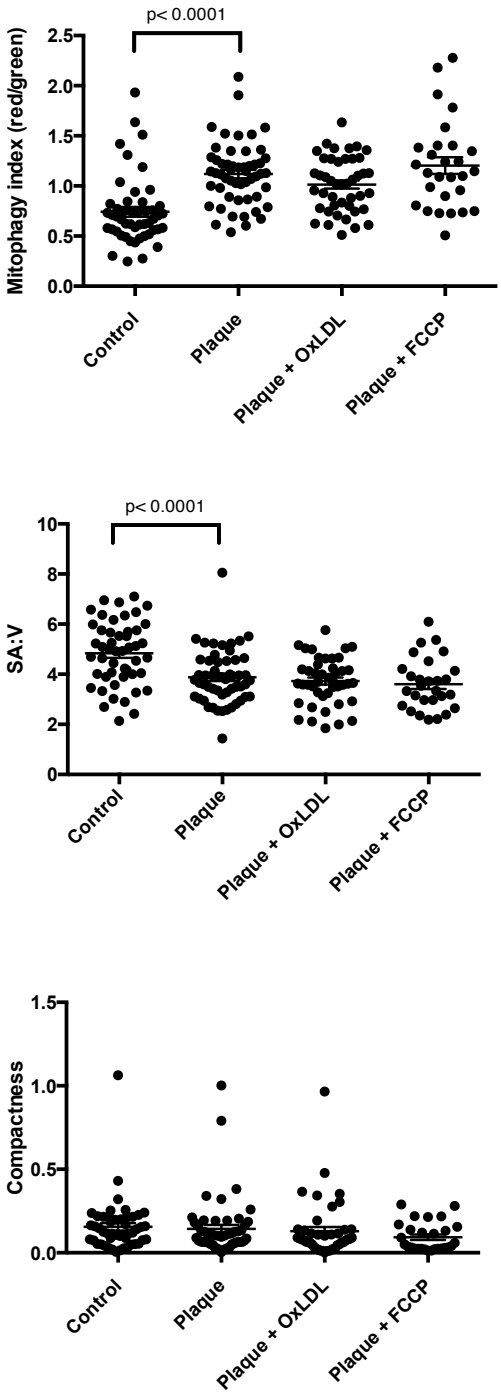

Figure 6-8 Mitophagy and mitochondrial shape in plaque VSMCs compared to healthy VSMCs

Human VSMCs and plaque VSMCs were infected with Keima expressing lentiviral particles and selected with puromycin. Cells were then plated in MatTek glass bottom culture dishes and allowed to adhere before treatment. Nuclei were stained with Hoechst 33342 and cells were imaged using a SP5 confocal microscope (Leica). A 63x/1.4-0.6 PL Apo oil lens was used and three channels were acquired after serial excitation with UV (nuclei, coded blue), an argon laser at 458 nm (Keima at

normal pH, coded green) and a yellow laser at 561 nm (acidic mitochondria, coded red). Control: Vehicle (PBS) treatment, plaque: vehicle (PBS) treated HVSMCs derived from carotid endarterectomies ± OxLDL (100 μg/ml for 24 hours) and FCCP (5 μM for 24 hours) treatment. Quantification of the mitophagy index (A), SA:V (B) and compactness (C) from at least 28 z-stacks from at least three independent experiments from three different primary cell cultures per group were analysed using ImageJ and the mitochondrial morphology plug-in. One-way ANOVA with Bonferroni's correction for multiple comparison was performed.

To get supporting evidence of increased mitophagy in plaque VSMCs compared to healthy aortic VSMCs, expression of PINK1, a key mediator of mitophagy, was performed. Mitochondrial inner membrane depolarisation inhibits uqiquitination and degradation of PINK1 thereby facilitating the recruitment of parkin to mitochondria inducing the targeting of dysfunctional mitochondria to the autophagolysosome (see section 1.2.3.1). Western blotting of PINK1 has previously been used as evidence of mitophagy in VSMCs exposed to OxLDL (Swiader et al., 2016).

Although mRNA levels of PINK1, determined by reverse transcription PCR (RT-PCR), did not differ between plaque VSMCs [donor age 67.3 years ± 5 years (SD)] and healthy aortic VSMCs [donor age 70.7 years ± 11.9 years (SD)], plaque VSMCs [donor age 66 years ± 5.3 years (SD), 66.7% male] had higher protein expression of PINK1 compared to aortic VSMCs [donor age 62 years ± 23.8 years (SD), 100% male] supporting the finding of increased mitophagy in these cells (Figure 6-9).

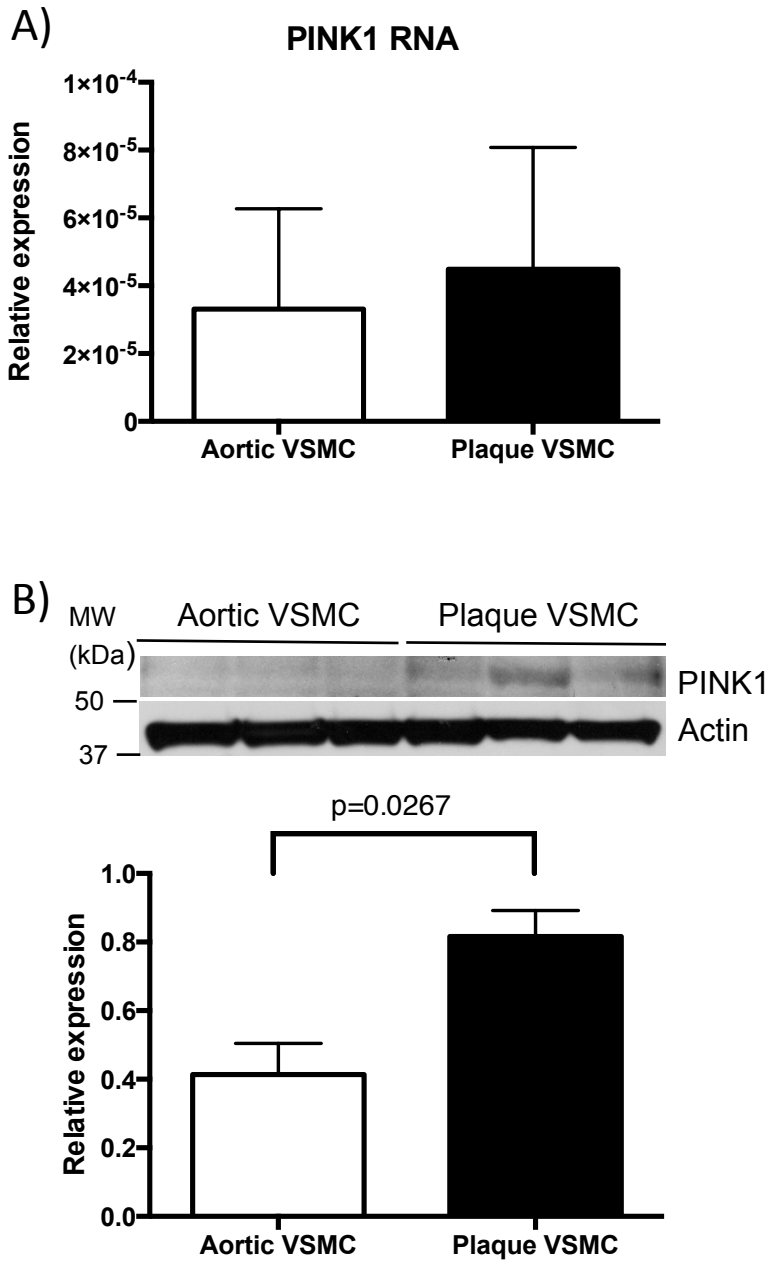

Figure 6-9 PINK1 expression in Plaque and healthy aortic VSMCs

A) RT PCR of PINK1 normalised to 18S. RNA was extracted from plaque and healthy aortic VSMCs and converted to cDNA. qPCR of cDNA was performed for PINK1 and 18S as an internal control. Relative expression was calculated according to the ΔCt method. N=6 healthy aortic VSMC lines, N=4 plaque VSMC lines. No significant differences were observed using unpaired two-tailed t-test assuming equal variation. B) Western blot of PINK1 expression in plaque and healthy aortic VSMCs. Whole cell lysates of aortic VSMC and plaque VSMC-lines were run on 8-12% gradient gels and membranes were probed with anti-PINK1 and anti-actin antibodies. Densitometry was performed using ImageJ. Relative expression of PINK1 compared to actin expressed as mean ± SEM of N=3 is illustrated. Unpaired two-tailed t-test with equal variation was used for statistical analysis. See also Appendix 8.1.

6.6 Mitochondrial fission genes in atherosclerotic plaques vs healthy aortas.

Because plaque VSMCs demonstrated an altered shape of the mitochondrial network with increased fragmentation compared to healthy aortic VSMCs, I next investigated whether the genes involved in mitochondrial shape dynamics were also differentially expressed. RT-PCR of RNA extracted from four plaque VSMC lines [donor age 67.3 years ± 5 years (SD), 75% male] and six aortic VSMC lines [donor age 70.7 years ± 11.9 years (SD), 100% male] did not demonstrate differences in gene expression of mitofusin-1 (mfn-1), mitofusin-2 (mfn-2), mitochondrial fusion protein opa-1, mitochondrial fission-1 protein (fis-1) and dynamin-related protein-1 (drp-1) (Figure 6-10).

Western blot was performed to determine protein expression of these genes, however, this was not successful due to non-specific binding of the antibodies used and the low expression of the protein (see Appendix 8.1). As there were no changes in expression levels of genes involved in mitochondrial shape dynamics at least at mRNA level, and as protein levels could not be determined by Western blot I did not investigate changes in mitochondrial shape further at this point.

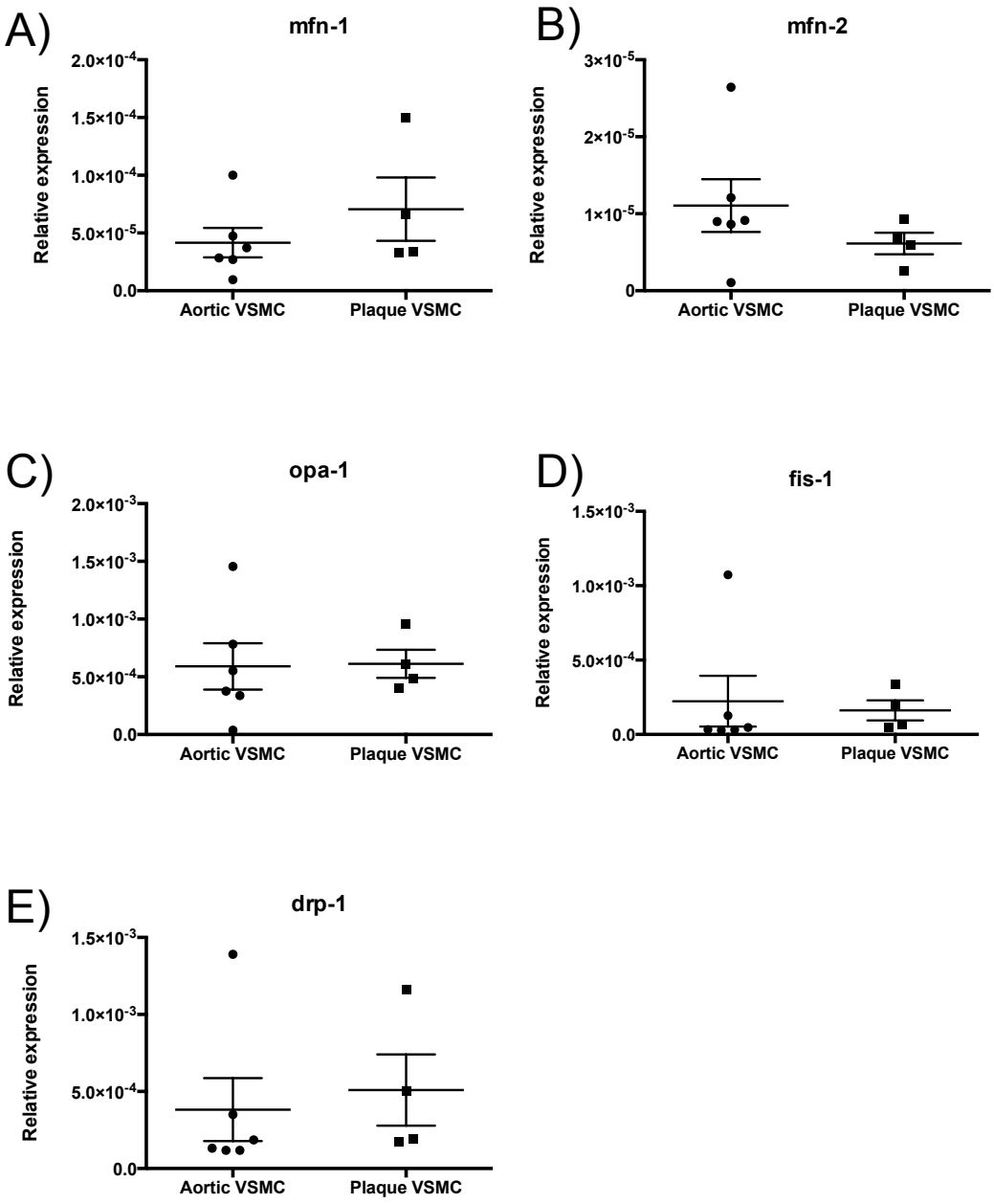

Figure 6-10 mRNA expression of genes involved in mitochondrial shape dynamics

RNA was extracted from plaque and healthy aortic VSMCs and converted to cDNA. RT PCR of A) mitofusin-1 (mfn-1), B) mitofusin-2 (mfn-2), C) mitochondrial fusion protein opa-1, D) mitochondrial fission-1 protein (fis-1), E) dynamin-related protein-1 (drp-1) normalised to 18S. Relative expression was calculated according to the ΔCt method. N=6 healthy aortic VSMC lines, N=4 plaque VSMC lines. Data are means ± SEM. No significant differences were observed using unpaired two-tailed t-test with equal variation.

6.7 Expression of genes involved in mitochondrial biogenesis

Mitophagy and mitochondrial biogenesis are processes that are highly regulated and linked (see 1.2.3.1 and 1.2.3.2). Mitophagy, not balanced by mitochondrial biogenesis, may therefore lead to reduced mitochondrial mass or mtDNA content. To test whether genes involved in mtDNA replication and repair are upregulated in plaque VSMCs I first used RT-PCR. As demonstrated in Figure 6-11 the expression of Twinkle, TFAM and PolG were not altered in plaque VSMCs [donor age 67.3 years ± 5 years (SD), 75% male] compared to healthy aortic VSMCs [donor age 70.7 years ± 11.9 years (SD), 100% male]. However, in the case of PolG there is the possibility of a type II error as the statistical analysis presented uses the assumption of normal distribution (unpaired two-tailed t-test). However, a test of normality could not be performed due to sample size.

Next, Western blot was used to test for differential protein expression of PGC-1α, Twinkle, TFAM and PolG in plaque [donor age 66 years ± 5.3 years (SD), 66.7% male] and healthy aortic VSMCs [donor age 62 years ± 23.8 years (SD), 100% male] (Figure 6-12). The expression pattern was variable within groups and no significant differences were observed. Interestingly, whilst the analysis of mRNA suggested that PolG is either unchanged or possibly upregulated in plaque VSMCs there was no such trend of increased PolG expression at protein level in plaque VSMCs.

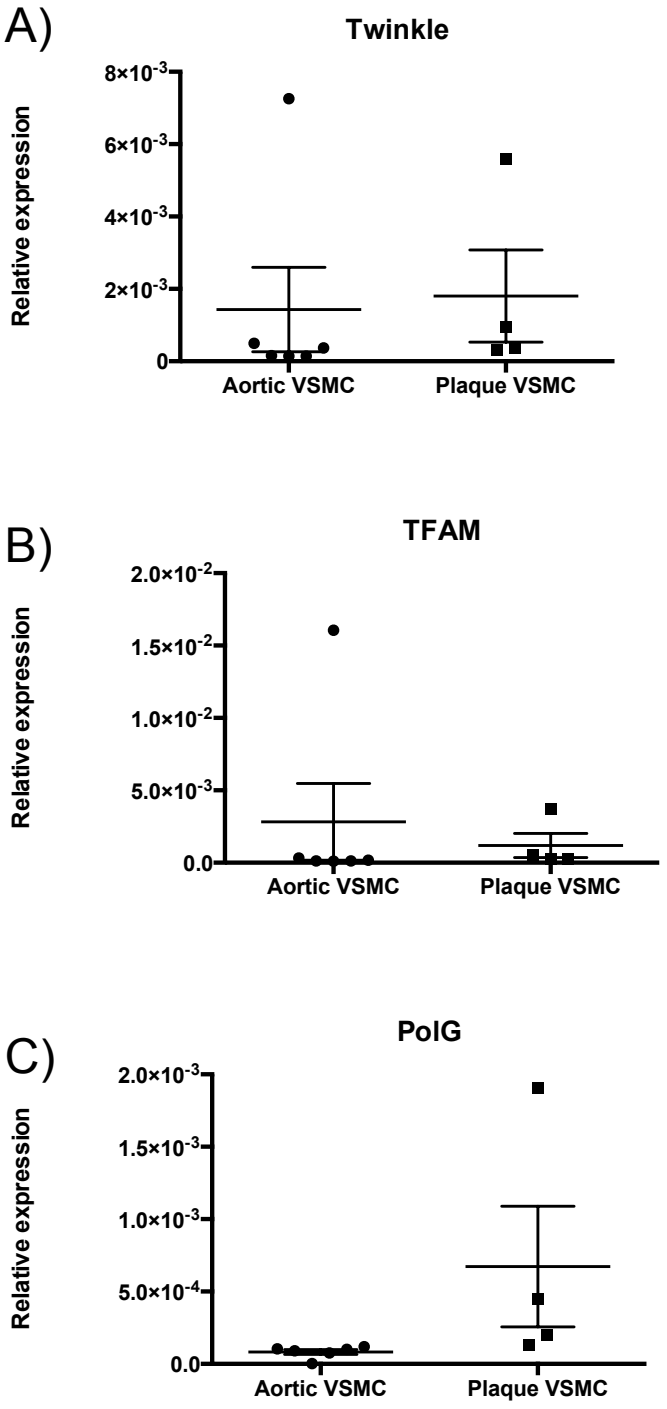

Figure 6-11 mRNA expression of Twinkle, TFAM and PolG in plaque and healthy aortic VSMCs

RT PCR of A) Twinkle, B) TFAM and C) PolG normalised to 18S. RNA was extracted from plaque and healthy aortic VSMCs and converted to cDNA. Relative expression was calculated according to the ΔCt method. N=6 healthy aortic VSMC lines, N=4 plaque VSMC lines. Data are means ± SEM. No significant differences were observed using unpaired two-tailed t-test with equal variation.

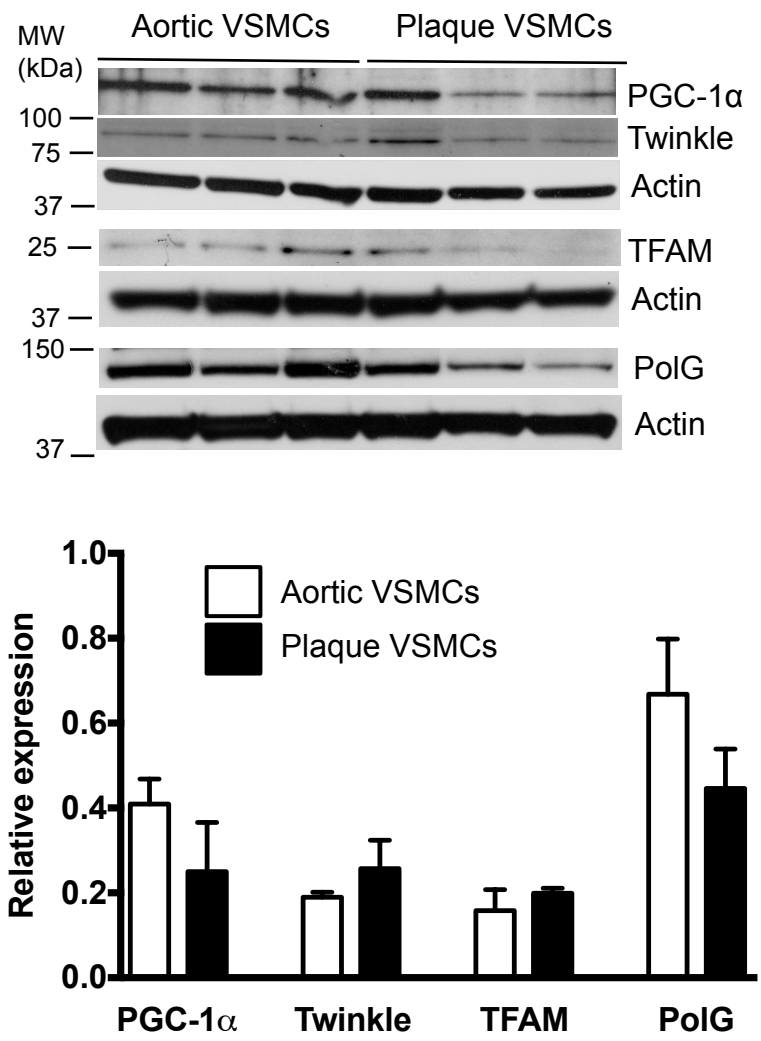

Figure 6-12 Protein expression of Twinkle, TFAM and PolG in plaque and healthy aortic VSMCs

Whole cell lysates of aortic VSMC and plaque VSMC-lines were run on 8-12% gradient gels and membranes were probed with anti-PGC-1α, anti-Twinkle, anti-TFAM, anti-PolG or anti-actin antibodies as indicated. Densitometry was performed using ImageJ. Relative expression of proteins of interest compared to actin is expressed as mean ± SEM of N=3 cell lines each. No statistically significant differences were observed using unpaired two-tailed t-test with equal variation. See also Appendix 8.1.

6.8 Discussion

In this chapter I have demonstrated the feasibility of lentiviral-mediated Keima transfection of human cells to analyse mitophagy. Both HeLa and

subsequently HVSMCs were infected resulting in stable expression of Keima, and changes in Keima fluorescence could be used to detect changes in mitophagy in human VSMCs. For example, FCCP, a mitochondrial uncoupler known to induce mitophagy caused changes in mitochondrial organisation resulting in a more fragmented appearance of mitochondria. In accordance with previous findings, FCCP induced mitophagy in this study.

OxLDL but not LDL or LPS induced mitophagy in HVSMCs but interestingly mitochondrial fragmentation was not significantly affected. There are a number of possible explanations for this. First, the resolution achieved using the technique presented here may not be sufficient to conclusively map the mitochondrial network and fragmented mitochondria within the cell, such that more subtle changes in mitochondrial fragmentation may have been missed. Second, mitochondria that have been damaged by OxLDL exposure and subsequently fragmented may have been diverted to autophagolysosomes, such that the overall number of fragmented mitochondria remains unchanged. Increased fragmentation induced by OxLDL could also be balanced by areas of mitochondrial hyperfusion allowing for the exchange of proteins and RNAs between polarised and depolarised mitochondria. In contrast, the effects of FCCP may be more severe, causing depolarisation and fragmentation of large areas of the mitochondrial network. During this project Dr Vindis' group (Toulouse University, France) investigated the effects of OxLDL on mitophagy in immortalised human VSMC-lines in greater detail. They demonstrated that OxLDL induces DRP-1 dependent mitochondrial fragmentation in human VSMCs (Swiader et al., 2016), which was accompanied by increased ROS production assessed by MitoSOX red

dye and a decrease in the inner mitochondrial membrane potential measured with the JC-1 dye. Following OxLDL treatment PINK1 was stabilised and Parkin translocated to mitochondria.

However, the finding that mitophagy is increased and that mitochondria are more fragmented in plaque VSMCs has not been described before. PINK1 protein stabilisation in plaque VSMCs further supports the finding of increased mitophagy in plaque VSMCs, with no changes in RNA levels or expression of proteins mediating mitochondrial fission and fusion. Mitophagy in VSMCs has been proposed to be a protective mechanism against apoptosis induced by atherogenic lipids (Swiader et al., 2016). This theory was supported by data demonstrating that inhibition of mitophagy using siRNA targeting PINK1 or Parkin increased OxLDL induced apoptosis of VSMCs.

Because Keima is, to a degree, resistant to lysosomal degradation, the red Keima signal has been interpreted as mitophagy occurring over time, and therefore representing mitophagy flux (Sun et al., 2015). However, an alternative explanation for the increased red Keima signal in plaque VSMCs in this study could be dysfunctional and therefore delayed lysosomal degradation of the Keima protein. Methods to determine autophagic flux include the quantification of the degradation of proteins involved in the formation of autophagosomes such as LC3 (Bauvy, Meijer, & Codogno, 2009). Indeed, Western blot analysis of LC3-I and LC3-II in samples from human carotid endarterectomies and from healthy mammary arteries suggest that autophagy is increased in human atherosclerosis (Martinet & De Meyer, 2009). A previous study has reported reduced autophagic flux in mouse atherosclerosis (Razani et al., 2012). P62, a chaperone shuttling proteins for

lysosomal degradation that is inversely related to autophagic flux, was increased in atherosclerotic arteries of mice. However, p62 was mainly detected in plaque macrophages rather than VSMCs (Razani et al., 2012). Assessment of human atherosclerotic lesions using electron microscopy suggests that autophagy occurs in both the fibrous cap and the atherosclerotic core and indeed in all main cell types involved in atherosclerosis (Perrotta, 2013). Although the possibility of decreased lysosomal activity in plaque VSMCs has not been excluded in this study, increased PINK1 stabilisation and changes in mitochondrial shape point towards increased mitophagy as an explanation for the increased red Keima signal in the present study.

Mitophagy and mitochondrial biogenesis are closely regulated. One of the key regulators of mitochondrial biogenesis in humans is PGC-1α, a member of the PCG-1 family of co-activators, which acts as a sensor of the energy status of cells such as NAD+/NADH and AMP/ATP ratios (Friedman & Nunnari, 2014). PGC-1α activation leads to the expression of mitochondrial proteins including TFAM (Picca & Lezza, 2015), an important regulator of mtDNA copy number (M. I. Ekstrand et al., 2004). The expression of PGC-1α was not altered in plaque VSMCs compared to healthy VSMCs. Modulation of PGC-1α activity through acetylation or phosphorylation, however, were not assessed in this study. Nevertheless, the expression of the downstream target TFAM, was not affected either. Furthermore, other factors involved in the regulation of mtDNA copy number and repair such as Twinkle and PolG were also not dysregulated in plaque VSMCs. The results of increased mitophagy without compensatory upregulation of mitochondrial biogenesis and repair

further support the finding of decreased mtDNA copy number in carotid atherosclerotic plaques compared to healthy aortas described in chapter 5.3.

The results of this chapter add to the growing evidence that modulation of mitophagy could be a target in the treatment of atherosclerosis. Rapamycin, also known as sirolimus, is a strong inhibitor of mTOR complex 1 (mTORC1) and inducer of autophagy and has been successfully used in drug-eluting vascular stents to inhibit re-occlusion (De Meyer et al., 2015). Its effects were long thought to be mediated through inhibition of VSMCs proliferation, although other inhibitors of VSMCs proliferation, such as paclitaxel, have been less successful and the effects of rapamycin and its derivatives may in part be mediated through effects on autophagy (De Meyer et al., 2015). Although systemic administration of rapamycin has been shown to exert protective effects on atherosclerosis in animal models (Chen et al., 2009; Waksman et al., 2003), systemic administration has also proatherogenic side effects such as dyslipidaemia and hyperglycaemia (De Meyer et al., 2015). Nevertheless, there are several other drugs that have the potential to induce autophagy including acid sphingomyelinase, calcium channel blockers, metformin, resveratrol, spermidine, trehalose and valproic acid [reviewed in (De Meyer et al., 2015)]. Through better understanding of mitophagy the development of specific modulators of this process may become possible. For example, the activity of PINK1 can be enhanced through the ATP analogue kinetin triphosphate (KTP), thereby increasing parkin recruitment to depolarised mitochondria (Hertz et al., 2013). Interestingly, kinetin, the precursor to KTP, has already been used in human

clinical trials of an unrelated disorder (familial dysautonomia) (Hertz et al., 2013).

Targeting mitochondrial biogenesis could also be a therapeutic target in atherosclerosis. For example, resveratrol an activator of the sirtuin-1-PGC-1α pathway, has received attention due to its promising preclinical effects on ageing and age-related diseases (de Oliveira et al., 2016). The mechanism of action, however, is not limited to induction of mitochondrial biogenesis and its effects in humans have not been rigorously tested (de Oliveira et al., 2016; Tome-Carneiro et al., 2013; Zordoky et al., 2015). The development of specific inducers of mitochondrial biogenesis is therefore a promising area (Cameron, Beeson, & Schnellmann, 2016).

7 Conclusion

Mitochondria regulate various processes within cells that determine cell fate, proliferation and senescence as well as inflammation. Because of the importance of these processes in a variety of diseases and ageing, several research groups have focused on the role of mitochondria and metabolism in neurodegenerative disease, cancer and cardiovascular disease. However, despite the increasing interest in the role of mitochondria in atherosclerosis, much of the data available to date is correlative and a causative role of mitochondrial dysfunction in atherogenesis has not been firmly established. The present study adds to the growing evidence of the importance of mitochondrial biology in atherosclerosis.

To my knowledge, mitochondrial respiration has not been assessed in human atherosclerotic tissues, yet. Because mitochondrial respiration can currently not be assessed in atherosclerotic tissue *in vivo*, I have adapted the Seahorse extracellular flux analysis assay to study human tissues immediately after carotid endarterectomy. This *ex vivo* approach should reflect *in vivo* conditions as closely as technically possible at present. Indeed, due to limitations in studying cultured cells as a proxy for disease processes several other groups have recently adapted this assay to study freshly prepared tissue samples. Thus far the Seahorse extracellular flux assay has been used to study brain tissue as well as fat tissue and more recently aortic tissue (Dunham-Snary et al., 2014; Feeley et al., 2014; Fried et al., 2014). However, the current study is the first to investigate different areas of human atherosclerotic arterial tissue. The data presented in this study is normalised to both tissue mass and cellular density allowing for comparison of respiration

across different areas of the human atherosclerotic plaque. Using this novel method, I have demonstrated that the cap and the core regions of the human atherosclerotic plaque have reduced mitochondrial respiration.

I investigated the reasons for such reduced respiration in the atherosclerotic plaques first through determination of the protein expression of complexes of the ETC. The expression of complexes I and II was reduced in VSMCs cultured from human atherosclerotic plaques compared to healthy arteries and this may in part explain the reduced respiration observed in atherosclerotic plaques.

From the present study it remains unclear whether energy stores such as the ATP/ADP ratio are affected in human atherosclerotic plaques or whether ATP generation through alternative pathways can compensate for the reduced mitochondrial respiration. For example, high-energy phosphate store depletion, i.e. phosphocreatine, has been implicated in reduced contractility of cardiomyocytes in heart failure [reviewed in Doenst, Nguyen, and Abel (2013)]. Reduced energy availability in VSMCs of the atherosclerotic cap could potentially affect plaque stability, however this is an area that has not been investigated, yet.

It has long been known that in atherosclerosis there is increased mtDNA damage, however until now it was unclear whether such damage has functional consequences on mitochondrial biology. Respiration and the generation of ATP are key roles of mitochondria. Further studies should investigate whether the decreased respiration observed in this study leads to a metabolic shift with higher reliance on other sources of energy generation such as glycolysis. A metabolic switch with reliance on aerobic glycolysis

rather than oxidative phosphorylation (Warburg metabolism) is well described in cancer cells, but is also observed in immune cells, such as dendritic cells, upon activation (Mills et al., 2016; Tannahill et al., 2013). Further studies should seek to determine whether such a metabolic switch also occurs in atherosclerosis and whether modulation of cellular and mitochondrial metabolism could be a target in atherosclerosis.

The current study did not investigate other aspects of mitochondrial biology and signalling in human atherosclerotic plaques. Altered mitochondrial biology may affect cellular signalling through effects on cell proliferation, cell survival or cell death and future studies should aim to establish whether altered mitochondrial biology in human atherosclerosis affects these processes.

Importantly, I have not demonstrated causality of mitochondrial dysfunction in atherosclerosis. However, we know from previous studies that mtDNA damage can accelerate atherogenesis. ApoE-/- mice with defective polymerase γ proofreading capacity (ApoE-/- PolG-/-) have markedly increased mtDNA damage and show signs of accelerated ageing including premature greying of the fur, kyphosis and weight loss (E. Yu et al., 2013). When fat a high-fat diet, these mice develop increased atherosclerotic plaques compared to ApoE-/- prior to the development of other age related degenerative diseases. ApoE-/- PolG-/- mice also have decreased complex I expression and reduced mitochondrial respiration of aortic tissue, similarly to the observation of reduced expression of the electron transfer chain complex I and II in human atherosclerotic plaques in the present study. Thus, causing artificial mtDNA damage as in the ApoE-/- PolG-/- model can perpetuate

atherogenesis but it remains to be established whether the relatively mild mtDNA damage and mitochondrial dysfunction observed in human atherosclerosis are sufficient to affect disease progression.

Recently, several attempts have been made to modulate mitochondrial function with the aim of changing disease progression. For example, MitoQ, an anti-oxidant targeted to mitochondria, reverses some of the ageing related loss of endothelium-dependent vasodilation in mice (Gioscia-Ryan et al., 2014). Chronic administration of MitoQ in ApoE-/-ATM-/- mice did not significantly reduce atherosclerotic plaque development but decreased macrophage content in the plaque suggesting effects at least on plaque composition and stability (J. R. Mercer et al., 2012). Similarly, in animal models of neurodegenerative diseases such as spinocerebellar ataxia type 1 (Stucki et al., 2016) and Parkinson's disease (Ghosh et al., 2010) MitoQ elicited protective effects. However, a randomised, placebo-controlled clinical trial of MitoQ failed to elicit protective effects in humans with Parkinson's disease (Snow et al., 2010). Such discrepancies underline the importance of studying human disease rather than relying on inference from animal models alone. Understanding the role of mitochondrial dysfunction in human disease may help identify further targets for manipulation of mitochondrial function. It may not be the amount of ROS generated by mitochondria and the resulting oxidative damage per se that is responsible for disease progression but rather other aspects of mitochondrial signalling that affects cellular function.

Mitochondrial fission and fusion and mitophagy have emerged as key processes of mitochondrial homeostasis. Through fission and mitophagy dysfunctional mitochondria can be degraded to preserve a pool of functioning

mitochondria. Fusion of mitochondria is thought to facilitate communication between mitochondria and thereby access to proteins only encoded in the mitochondrion, and to buffer transient mitochondrial defects [reviewed in Friedman and Nunnari (2014)]. To study mitophagy in VSMCs from healthy aortas and human atherosclerotic plaques I have used a novel fluorescent reporter, Keima. This acid-stable protein is targeted to mitochondria and its excitation spectrum is pH dependent such that mitochondria that have been delivered to autophagolysosomes can be differentiated from healthy mitochondria. Using a lentiviral infection strategy allowed for this probe to be expressed in human VSMCs derived from aortas and atherosclerotic plaques. To my knowledge, this is the first study using lentivirus-mediated Keima infection of diseased primary human cell lines to study mitophagy. I have shown that mitophagy is stimulated by OxLDL in human primary VSMCs and that increased basal levels of mitophagy are a feature of VSMCs derived from atherosclerotic plaques. Mitophagy has been found to be protective in cultured VSMCs cell lines exposed to OxLDL at least partly by decreasing apoptosis (Swiader et al., 2016). Targeting this pathway therefore holds promise in the treatment of human atherosclerosis. At least in animal models of atherosclerosis, the induction of mitophagy through rapamycin administration has been encouraging (Chen et al., 2009; Waksman et al., 2003). However, to be clinical useful in human disease, induction of mitophagy would have to be targeted more specifically to the vascular tissue to avert the systemic side effects observed with systemic rapamycin administration.

Changes in mitochondrial shape, mitophagy and mitochondrial biogenesis are closely linked processes. In the present study, mitochondrial shape and mitophagy were found to be altered in human VSMCs derived from atherosclerotic plaques and in aortic VSMCs treated with the uncoupler FCCP as a control. Furthermore, PINK1 expression as a marker of mitophagy was also elevated in plaque VSMCs further supporting the observation of increased mitophagy in plaque VSMCs

Despite increased mitophagy in plaque VSMCs compared to healthy aortic VSMCs there was no compensatory upregulation of mitochondrial biogenesis or mitochondrial DNA repair both at RNA and protein level. This is an interesting observation that warrants further studies and is another plausible explanation for the decreased mitochondrial respiration observed in diseased human atherosclerotic plaques. Indeed, in the present study mtDNA copy number was significantly reduced in plaque tissues compared to healthy aortic tissues. Further studies in our laboratory have demonstrated that increasing mitochondrial DNA copy number in ApoE-/- mice through transgenic overexpression of twinkle helicase leads to plaques with increased cap/core ratios suggestive of higher stability after fat-feeding (E. P. K. Yu et al., 2017). Twinkle overexpression preserved electron transfer chain complex I expression and was associated with increased mitochondrial respiration. Although targeting of twinkle in human atherosclerosis itself is unlikely to be a useful clinical target, increasing mitochondrial biogenesis may be more promising. Inducers of mitochondrial biogenesis including resveratrol and their effects on atherosclerosis need to be rigorously studied at molecular level and

in diseases associated with mitochondrial dysfunction such as atherosclerosis.

The present study also confirms findings of previous studies demonstrating reduced mitochondrial respiration of VSMC after OxLDL stimulation (Ahn et al., 2010). LDL, that has not been altered through oxidation, however, does not elicit similar effects. Similarly, a high-fat diet alone, in the absence of established atherosclerosis, does not alter aortic respiration in ApoE-/- mice. However, the latter findings need to be interpreted with caution as the assay was conducted *ex vivo* in the presence of glucose and any effects on beta-oxidation of fatty acids would not have been captured adequately. Future studies should therefore study aortic tissue metabolism using various metabolites including fatty acids.

Together the data from the current study support a model where OxLDL induces acute damage to mitochondria in VSMCs thereby causing reduced mitochondrial respiration and activation of mitophagy to help preserve mitochondrial homeostasis. Plaque VSMCs, chronically exposed to oxidised lipid species, show increased mitophagy without compensatory up-regulation of genes involved in mitochondrial biogenesis. Consequently, mtDNA copy number is reduced in atherosclerotic plaques compared to healthy arteries. Mitochondrial dysfunction in atherosclerotic plaques could then perpetuate disease progression through effects on cell viability, senescence and pro-inflammatory signalling. Mitochondrial function in the cap region of the atherosclerotic plaque could be an important determinant of cap thickness and therefore atherosclerotic plaque stability.

8 Appendices

8.1 Full scans of Western blots

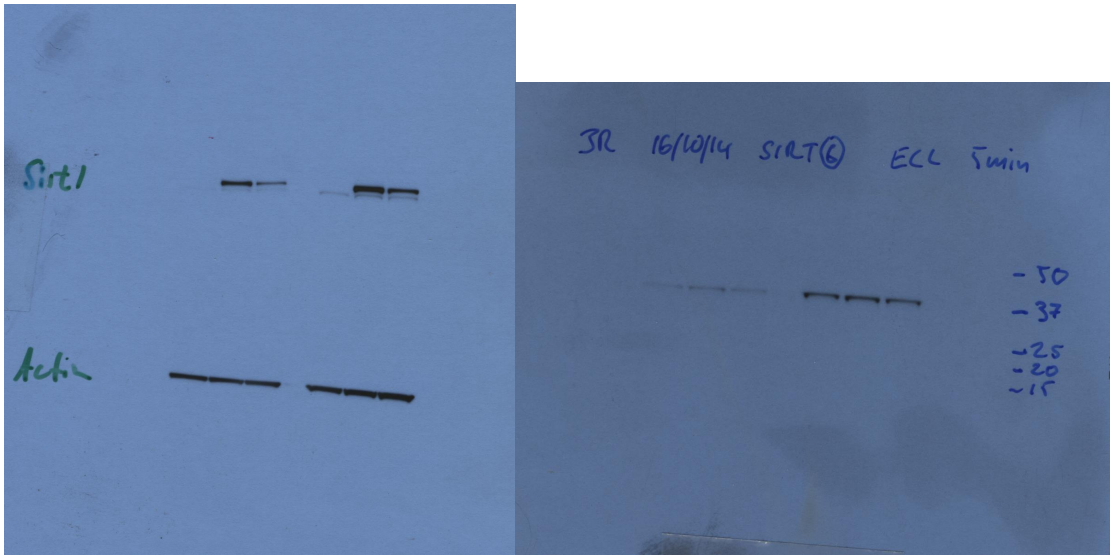

Figure 8-1 Western blots corresponding to Figure 3-1

Left: sirtuin-1 in upper panel, actin in lower panel. Right: sirtuin-6

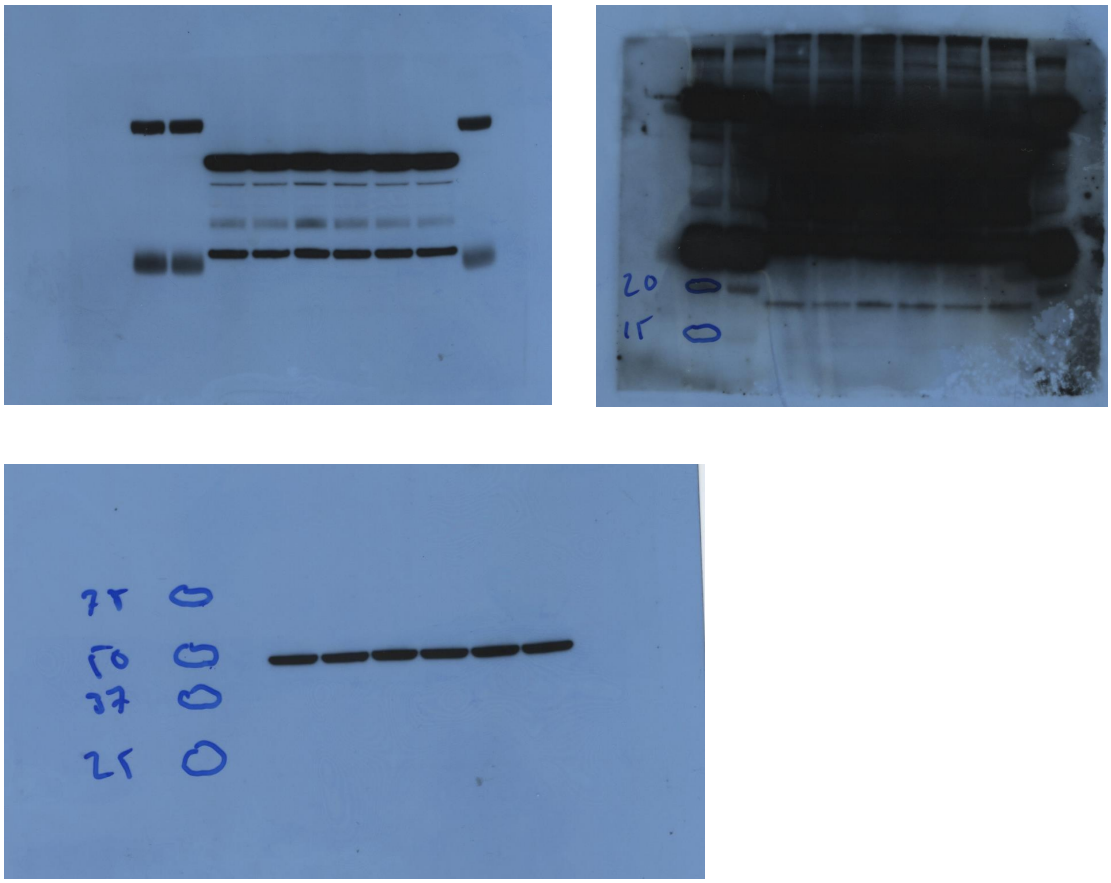

Figure 8-2 Western blots corresponding to Figure 3-10

All Western blots correspond to Figure 3-10 A. Top panel: example of short exposure (left) and long exposure (right) of ETC complexes in RVSMCs. Various exposure lengths were required to capture individual complexes. Bottom: longer exposure of Western blot for citrate synthase. Note reversed order, i.e. lane 6 above corresponds to lane 1 in Figure 3-10.

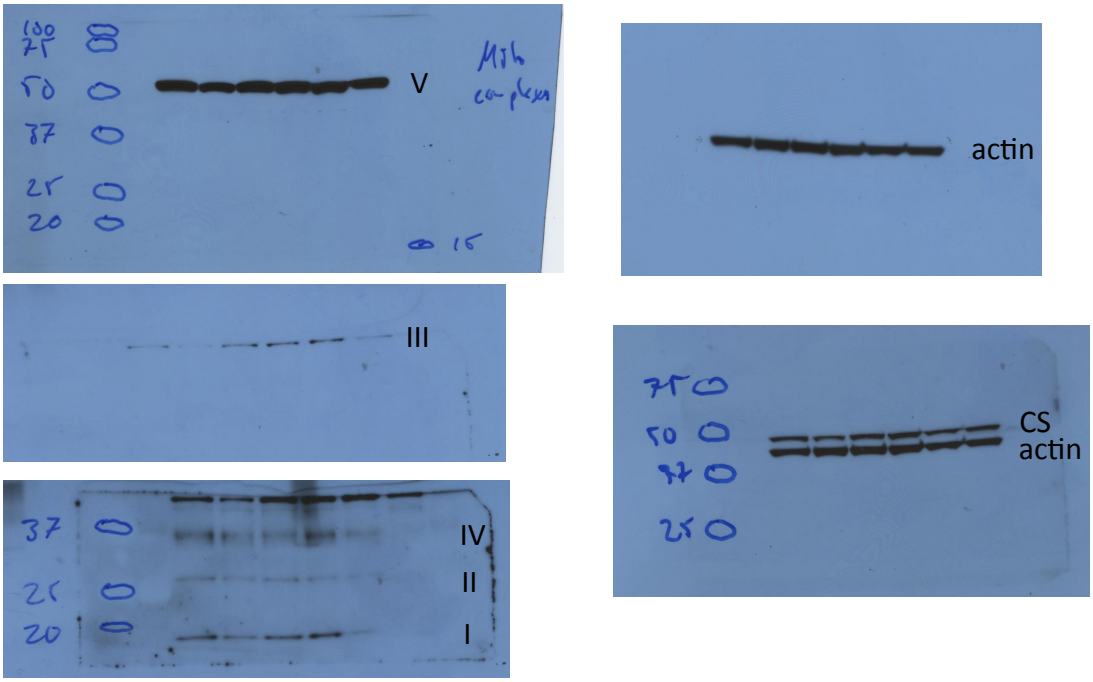

Figure 8-3 Western blots corresponding to Figure 5-8

ETC complexes in HVSMCs. Left: complex V (top), complex III (middle) and complexes IV, II and I (bottom). Right: actin (top) and citrate synthase (CS bottom).

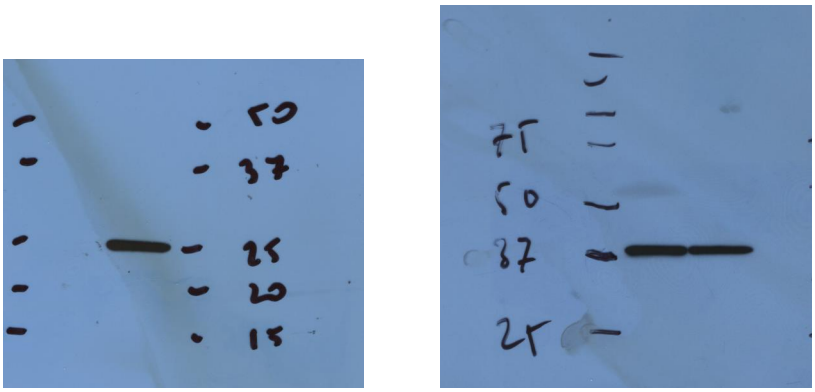

Figure 8-4 Western blots corresponding to Figure 6-2

Left: Keima expression, right: GAPDH expression in HeLa cells with (right lane) and without (left lane) keima lentiviral infection.

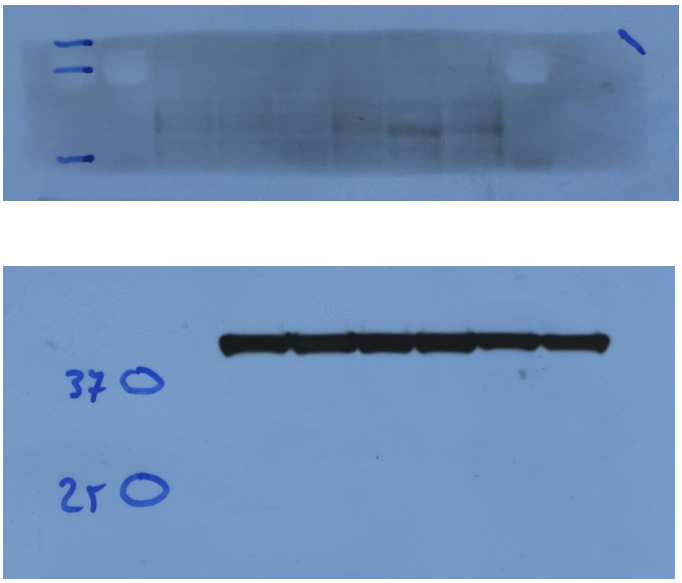

Figure 8-5 Western blots corresponding to Figure 6-9 B

Western blot for PINK1 (top) and actin (bottom). First three lanes derived from aortic HVSMCs and last three lanes derived from plaque HVSMCs

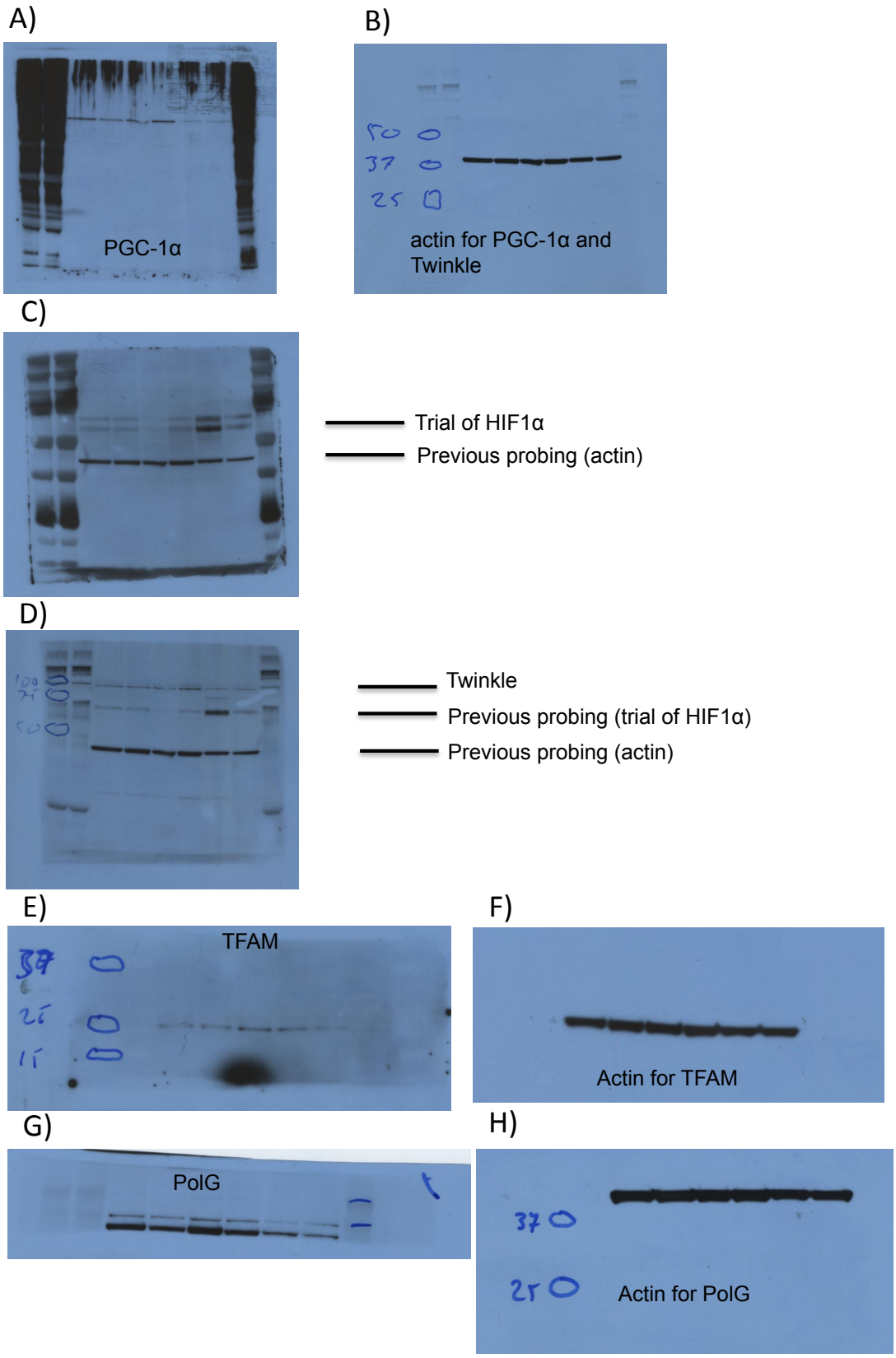

Figure 8-6 Western blots corresponding to Figure 6-12

A) Western blot probing for PGC-1α, B) reprobing of membrane for actin, C) trial of Western blot for HIF1α (using antibody NB100-105, Novus Biologicals, 1:500 in 5% BSA PBST, secondary 1:1000 anti-mouse, Cell Signaling Technology, 7076, in 0.25% milk PBST). Bands do not match expected molecular weight, however these bands were still visible when re-probing the membrane for Twinkle (D). Western blot for TFAM (E) and corresponding actin (F). Western blot for PolG and corresponding actin (H).

8.2 Unsuccessful Western blots of proteins involved in mitochondrial shape dynamics

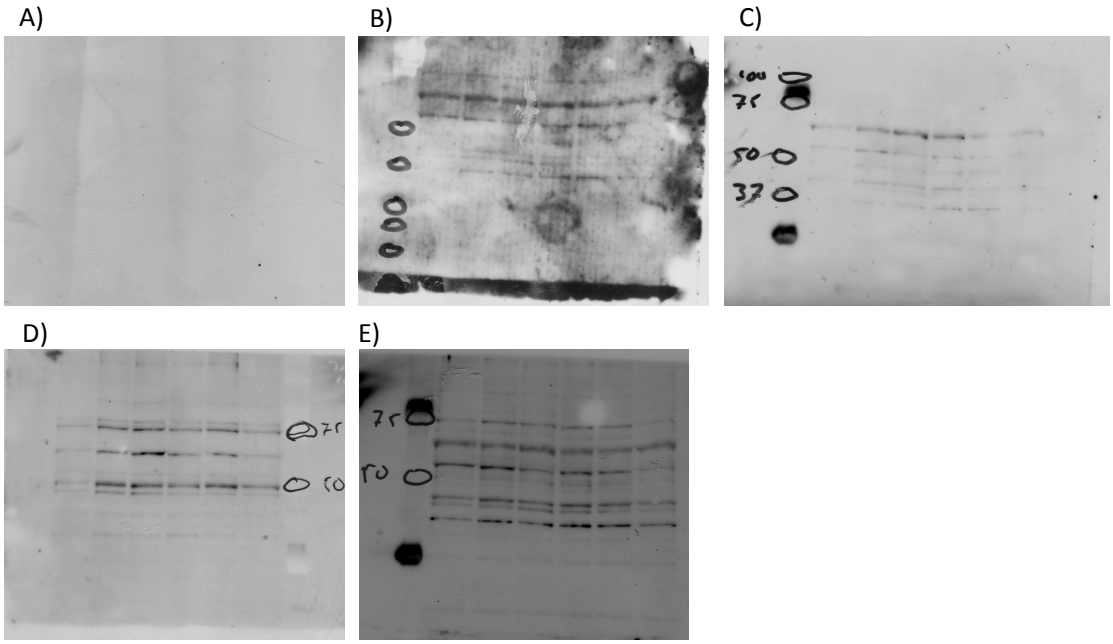

Figure 8-7 Unsuccessful Western blots of proteins involved in mitochondrial shape dynamics

Representative unsuccessful Western blots of proteins involved in mitochondrial shape dynamics are shown. The antibodies were tested under various conditions but no clear bands representing the protein of interest alone were detected. A) OPA1: Santa Cruz sc-393296 mouse monoclonal antibody; B) Fis1: Santa Cruz sc-376337 mouse monoclonal antibody; C) MFN2 : Santa Cruz sc-515647 mouse monoclonal antibody; D) DRP1: Santa Cruz sc-32898 rabbit polyclonal antibody; E) MFN1: Santa Cruz SC-166644 mouse monoclonal antibody.

8.3 Vector map of pLESIP vector

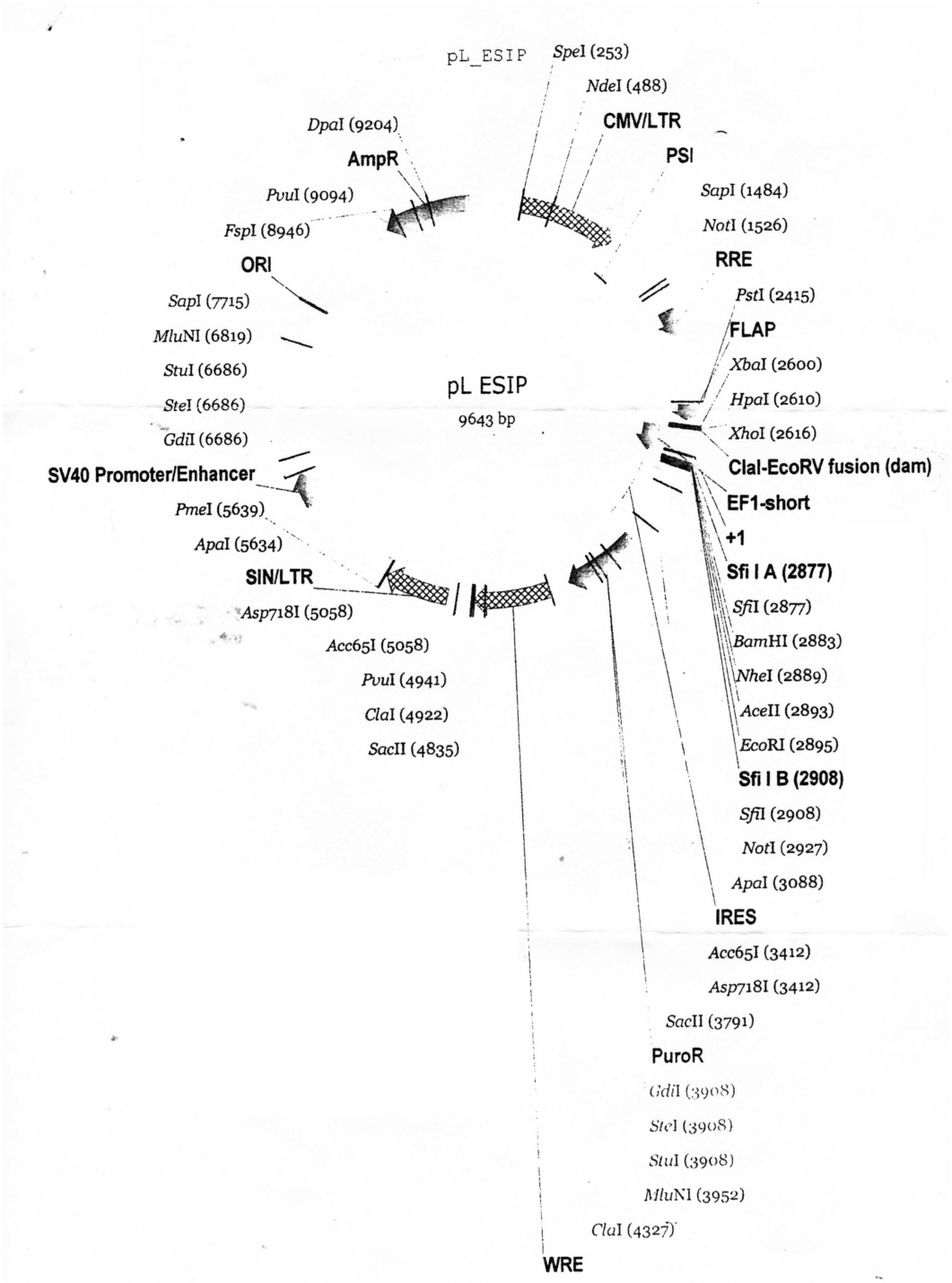

Figure 8-8 Vector map of pLESIP vector

Vector map of pLESIP vector. Keima has been inserted between Sfi I A (2877) and Sfi I B (2908) sites. The vector contains an ampicillin resistance cassette and a puromycin resistance cassette.

8.4 LC-MS/MS of MitoB and MitoP

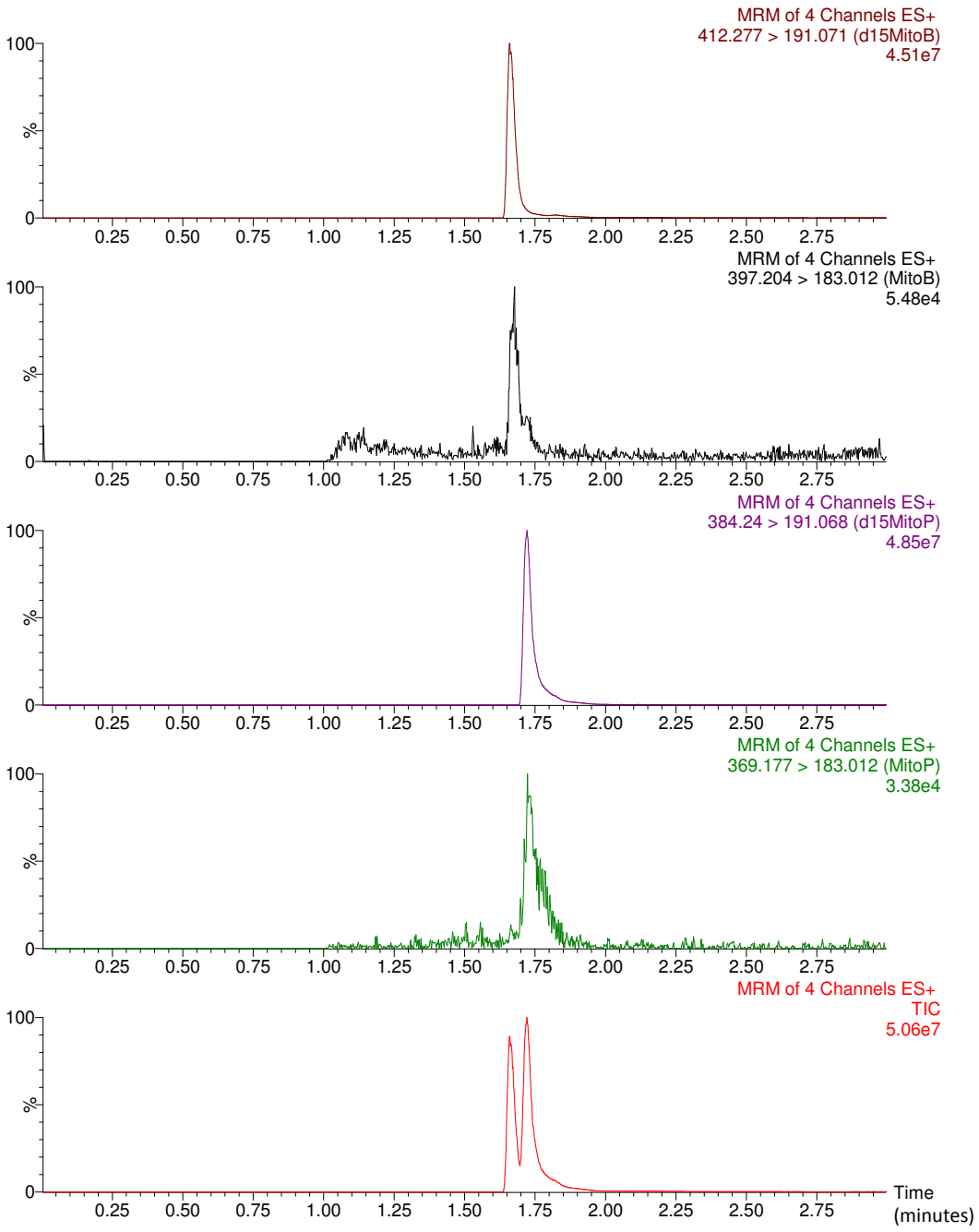

Figure 8-9 Examples of LC-MS/MS chromatograms used for quantification of MitoB and MitoP

Multiple reaction monitoring (MRM) for the analysis of d15MitoB, MitoB, d15MitoP and MitoP and total ion chromatogram (TIC). ES+ electrospray positive. Area under the curve was formed for peaks and concentrations of MitoB and MitoP were calculated using standard curves.

9 References

Ahn, S. Y., Choi, Y. S., Koo, H. J., Jeong, J. H., Park, W. H., Kim, M., . . . Pak, Y. K. (2010). Mitochondrial dysfunction enhances the migration of vascular smooth muscles cells via suppression of Akt phosphorylation. *Biochim Biophys Acta, 1800*(3), 275-281. doi:10.1016/j.bbagen.2009.09.005

Andrienko, T. N., Pasdois, P., Pereira, G. C., Ovens, M. J., & Halestrap, A. P. (2017). The role of succinate and ROS in reperfusion injury - A critical appraisal. *J Mol Cell Cardiol, 110*, 1-14. doi:10.1016/j.yjmcc.2017.06.016

Balaban, R. S., Nemoto, S., & Finkel, T. (2005). Mitochondria, oxidants, and aging. *Cell, 120*(4), 483-495. doi:10.1016/j.cell.2005.02.001

Ballinger, S. W., Patterson, C., Knight-Lozano, C. A., Burow, D. L., Conklin, C. A., Hu, Z., . . . Runge, M. S. (2002). Mitochondrial integrity and function in atherogenesis. *Circulation, 106*(5), 544-549.

Ballinger, S. W., Patterson, C., Yan, C. N., Doan, R., Burow, D. L., Young, C. G., . . . Runge, M. S. (2000). Hydrogen peroxide- and peroxynitrite-induced mitochondrial DNA damage and dysfunction in vascular endothelial and smooth muscle cells. *Circ Res, 86*(9), 960-966.

Bauvy, C., Meijer, A. J., & Codogno, P. (2009). Assaying of autophagic protein degradation. *Methods Enzymol, 452*, 47-61. doi:10.1016/S0076-6879(08)03604-5

Ben Trivedi, A., Kitabatake, N., & Doi, E. (1990). Toxicity of dimethyl sulfoxide as a solvent in bioassay system with HeLa cells evaluated colorimetrically with 3-(4,5-dimethylthiazol-2-yl)-2,5-diphenyl-tetrazolium bromide. *Agric Biol Chem, 54*(11), 2961-2966.

Bennett, M. R., Macdonald, K., Chan, S. W., Boyle, J. J., & Weissberg, P. L. (1998). Cooperative interactions between RB and p53 regulate cell proliferation, cell senescence, and apoptosis in human vascular smooth muscle cells from atherosclerotic plaques. *Circ Res, 82*(6), 704-712.

Berliner, J. A., Territo, M. C., Sevanian, A., Ramin, S., Kim, J. A., Bamshad, B., . . . Fogelman, A. M. (1990). Minimally modified low density lipoprotein stimulates monocyte endothelial interactions. *J Clin Invest, 85*(4), 1260-1266. doi:10.1172/JCI114562

Berridge, M. V., & Tan, A. S. (1993). Characterization of the cellular reduction of 3-(4,5-dimethylthiazol-2-yl)-2,5-diphenyltetrazolium bromide (MTT): subcellular localization, substrate dependence, and involvement of

mitochondrial electron transport in MTT reduction. *Arch Biochem Biophys, 303*(2), 474-482. doi:10.1006/abbi.1993.1311

Bobryshev, Y. V., & Lord, R. S. (1995). S-100 positive cells in human arterial intima and in atherosclerotic lesions. *Cardiovasc Res, 29*(5), 689-696.

Bogenhagen, D. F. (1999). Repair of mtDNA in vertebrates. *Am J Hum Genet, 64*(5), 1276-1281. doi:10.1086/302392

Boring, L., Gosling, J., Cleary, M., & Charo, I. F. (1998). Decreased lesion formation in CCR2-/- mice reveals a role for chemokines in the initiation of atherosclerosis. *Nature, 394*(6696), 894-897. doi:10.1038/29788

Botto, N., Rizza, A., Colombo, M. G., Mazzone, A. M., Manfredi, S., Masetti, S., . . . Andreassi, M. G. (2001). Evidence for DNA damage in patients with coronary artery disease. *Mutat Res, 493*(1-2), 23-30.

Bridges, H. R., Jones, A. J., Pollak, M. N., & Hirst, J. (2014). Effects of metformin and other biguanides on oxidative phosphorylation in mitochondria. *Biochem J, 462*(3), 475-487. doi:10.1042/BJ20140620

Bruick, R. K., & McKnight, S. L. (2001). A conserved family of prolyl-4-hydroxylases that modify HIF. *Science, 294*(5545), 1337-1340. doi:10.1126/science.1066373

Brunet, A., Sweeney, L. B., Sturgill, J. F., Chua, K. F., Greer, P. L., Lin, Y., . . . Greenberg, M. E. (2004). Stress-dependent regulation of FOXO transcription factors by the SIRT1 deacetylase. *Science, 303*(5666), 2011-2015. doi:10.1126/science.1094637

Bulua, A. C., Simon, A., Maddipati, R., Pelletier, M., Park, H., Kim, K. Y., . . . Siegel, R. M. (2011). Mitochondrial reactive oxygen species promote production of proinflammatory cytokines and are elevated in TNFR1-associated periodic syndrome (TRAPS). *J Exp Med, 208*(3), 519-533. doi:10.1084/jem.20102049

Burke, A. P., Farb, A., Malcom, G. T., Liang, Y. H., Smialek, J., & Virmani, R. (1997). Coronary risk factors and plaque morphology in men with coronary disease who died suddenly. *N Engl J Med, 336*(18), 1276-1282. doi:10.1056/NEJM199705013361802

Burr, S. P., Costa, A. S., Grice, G. L., Timms, R. T., Lobb, I. T., Freisinger, P., . . . Nathan, J. A. (2016). Mitochondrial Protein Lipoylation and the 2-Oxoglutarate Dehydrogenase Complex Controls HIF1alpha Stability in Aerobic Conditions. *Cell Metab, 24*(5), 740-752. doi:10.1016/j.cmet.2016.09.015

Calvert, P. A., Obaid, D. R., O'Sullivan, M., Shapiro, L. M., McNab, D., Densem, C. G., . . . Bennett, M. R. (2011). Association between IVUS findings and adverse outcomes in patients with coronary artery disease: the VIVA (VH-IVUS in Vulnerable Atherosclerosis) Study.

JACC Cardiovasc Imaging, 4(8), 894-901. doi:10.1016/j.jcmg.2011.05.005

Cameron, R. B., Beeson, C. C., & Schnellmann, R. G. (2016). Development of Therapeutics That Induce Mitochondrial Biogenesis for the Treatment of Acute and Chronic Degenerative Diseases. *J Med Chem, 59*(23), 10411-10434. doi:10.1021/acs.jmedchem.6b00669

Canto, C., Gerhart-Hines, Z., Feige, J. N., Lagouge, M., Noriega, L., Milne, J. C., . . . Auwerx, J. (2009). AMPK regulates energy expenditure by modulating NAD+ metabolism and SIRT1 activity. *Nature, 458*(7241), 1056-1060. doi:10.1038/nature07813

Canugovi, C., Maynard, S., Bayne, A. C., Sykora, P., Tian, J., de Souza-Pinto, N. C., . . . Bohr, V. A. (2010). The mitochondrial transcription factor A functions in mitochondrial base excision repair. *DNA Repair (Amst), 9*(10), 1080-1089. doi:10.1016/j.dnarep.2010.07.009

Carrodeguas, J. A., Theis, K., Bogenhagen, D. F., & Kisker, C. (2001). Crystal structure and deletion analysis show that the accessory subunit of mammalian DNA polymerase gamma, Pol gamma B, functions as a homodimer. *Mol Cell, 7*(1), 43-54.

Casademont, J., & Miro, O. (2002). Electron transport chain defects in heart failure. *Heart Fail Rev, 7*(2), 131-139.

Casalone, R., Granata, P., Minelli, E., Portentoso, P., Giudici, A., Righi, R., . . . Frigerio, B. (1991). Cytogenetic analysis reveals clonal proliferation of smooth muscle cells in atherosclerotic plaques. *Hum Genet, 87*(2), 139-143.

Chandel, N. S., McClintock, D. S., Feliciano, C. E., Wood, T. M., Melendez, J. A., Rodriguez, A. M., & Schumacker, P. T. (2000). Reactive oxygen species generated at mitochondrial complex III stabilize hypoxia-inducible factor-1alpha during hypoxia: a mechanism of O2 sensing. *J Biol Chem, 275*(33), 25130-25138. doi:10.1074/jbc.M001914200

Chappell, J., Harman, J. L., Narasimhan, V. M., Yu, H., Foote, K., Simons, B. D., . . . Jorgensen, H. F. (2016). Extensive Proliferation of a Subset of Differentiated, yet Plastic, Medial Vascular Smooth Muscle Cells Contributes to Neointimal Formation in Mouse Injury and Atherosclerosis Models. *Circ Res, 119*(12), 1313-1323. doi:10.1161/CIRCRESAHA.116.309799

Chen, Zhong, L., Zhang, L., Ji, X. P., Zhang, M., Zhao, Y. X., . . . Zhang, Y. (2009). Oral rapamycin attenuates inflammation and enhances stability of atherosclerotic plaques in rabbits independent of serum lipid levels. *Br J Pharmacol, 156*(6), 941-951. doi:10.1111/j.1476-5381.2008.00102.x

Chen, H., Chomyn, A., & Chan, D. C. (2005). Disruption of fusion results in mitochondrial heterogeneity and dysfunction. *J Biol Chem, 280*(28), 26185-26192. doi:10.1074/jbc.M503062200

Chistiakov, D. A., Orekhov, A. N., & Bobryshev, Y. V. (2016). Immune-inflammatory responses in atherosclerosis: Role of an adaptive immunity mainly driven by T and B cells. *Immunobiology, 221*(9), 1014-1033. doi:10.1016/j.imbio.2016.05.010

Choi, S. H., Harkewicz, R., Lee, J. H., Boullier, A., Almazan, F., Li, A. C., . . . Miller, Y. I. (2009). Lipoprotein accumulation in macrophages via toll-like receptor-4-dependent fluid phase uptake. *Circ Res, 104*(12), 1355-1363. doi:10.1161/CIRCRESAHA.108.192880

Chouchani, E. T., James, A. M., Fearnley, I. M., Lilley, K. S., & Murphy, M. P. (2011). Proteomic approaches to the characterization of protein thiol modification. *Curr Opin Chem Biol, 15*(1), 120-128. doi:10.1016/j.cbpa.2010.11.003

Chouchani, E. T., Methner, C., Buonincontri, G., Hu, C. H., Logan, A., Sawiak, S. J., . . . Krieg, T. (2014). Complex I deficiency due to selective loss of Ndufs4 in the mouse heart results in severe hypertrophic cardiomyopathy. *PLoS One, 9*(4), e94157. doi:10.1371/journal.pone.0094157

Chouchani, E. T., Methner, C., Nadtochiy, S. M., Logan, A., Pell, V. R., Ding, S., . . . Murphy, M. P. (2013). Cardioprotection by S-nitrosation of a cysteine switch on mitochondrial complex I. *Nat Med, 19*(6), 753-759. doi:10.1038/nm.3212

Chouchani, E. T., Pell, V. R., Gaude, E., Aksentijevic, D., Sundier, S. Y., Robb, E. L., . . . Murphy, M. P. (2014). Ischaemic accumulation of succinate controls reperfusion injury through mitochondrial ROS. *Nature, 515*(7527), 431-435. doi:10.1038/nature13909

Chu, C. T. (2010). A pivotal role for PINK1 and autophagy in mitochondrial quality control: implications for Parkinson disease. *Hum Mol Genet, 19*(R1), R28-37. doi:10.1093/hmg/ddq143

Clark, I. E., Dodson, M. W., Jiang, C., Cao, J. H., Huh, J. R., Seol, J. H., . . . Guo, M. (2006). Drosophila pink1 is required for mitochondrial function and interacts genetically with parkin. *Nature, 441*(7097), 1162-1166. doi:10.1038/nature04779

Clarke, M. C., Figg, N., Maguire, J. J., Davenport, A. P., Goddard, M., Littlewood, T. D., & Bennett, M. R. (2006). Apoptosis of vascular smooth muscle cells induces features of plaque vulnerability in atherosclerosis. *Nat Med, 12*(9), 1075-1080. doi:10.1038/nm1459

Clayton, D. A., Doda, J. N., & Friedberg, E. C. (1974). The absence of a pyrimidine dimer repair mechanism in mammalian mitochondria. *Proc Natl Acad Sci U S A, 71*(7), 2777-2781.

Cocheme, H. M., Quin, C., McQuaker, S. J., Cabreiro, F., Logan, A., Prime, T. A., . . . Murphy, M. P. (2011). Measurement of H2O2 within living Drosophila during aging using a ratiometric mass spectrometry probe targeted to the mitochondrial matrix. *Cell Metab, 13*(3), 340-350. doi:10.1016/j.cmet.2011.02.003

Cole, M. A., Murray, A. J., Cochlin, L. E., Heather, L. C., McAleese, S., Knight, N. S., . . . Clarke, K. (2011). A high fat diet increases mitochondrial fatty acid oxidation and uncoupling to decrease efficiency in rat heart. *Basic Res Cardiol, 106*(3), 447-457. doi:10.1007/s00395-011-0156-1

Collins, Y., Chouchani, E. T., James, A. M., Menger, K. E., Cocheme, H. M., & Murphy, M. P. (2012). Mitochondrial redox signalling at a glance. *J Cell Sci, 125*(Pt 4), 801-806. doi:10.1242/jcs.098475

Cominacini, L., Pasini, A. F., Garbin, U., Davoli, A., Tosetti, M. L., Campagnola, M., . . . Sawamura, T. (2000). Oxidized low density lipoprotein (ox-LDL) binding to ox-LDL receptor-1 in endothelial cells induces the activation of NF-kappaB through an increased production of intracellular reactive oxygen species. *J Biol Chem, 275*(17), 12633-12638.

Corral-Debrinski, M., Horton, T., Lott, M. T., Shoffner, J. M., Beal, M. F., & Wallace, D. C. (1992). Mitochondrial DNA deletions in human brain: regional variability and increase with advanced age. *Nat Genet, 2*(4), 324-329. doi:10.1038/ng1292-324

Corral-Debrinski, M., Shoffner, J. M., Lott, M. T., & Wallace, D. C. (1992). Association of mitochondrial DNA damage with aging and coronary atherosclerotic heart disease. *Mutat Res, 275*(3-6), 169-180.

Cortopassi, G. A., & Arnheim, N. (1990). Detection of a specific mitochondrial DNA deletion in tissues of older humans. *Nucleic Acids Res, 18*(23), 6927-6933.

Cox, A. G., Winterbourn, C. C., & Hampton, M. B. (2010). Mitochondrial peroxiredoxin involvement in antioxidant defence and redox signalling. *Biochem J, 425*(2), 313-325. doi:10.1042/BJ20091541

D'Erchia, A. M., Atlante, A., Gadaleta, G., Pavesi, G., Chiara, M., De Virgilio, C., . . . Pesole, G. (2015). Tissue-specific mtDNA abundance from exome data and its correlation with mitochondrial transcription, mass and respiratory activity. *Mitochondrion, 20*, 13-21. doi:10.1016/j.mito.2014.10.005

Dare, A. J., Bolton, E. A., Pettigrew, G. J., Bradley, J. A., Saeb-Parsy, K., & Murphy, M. P. (2015). Protection against renal ischemia-reperfusion

injury in vivo by the mitochondria targeted antioxidant MitoQ. *Redox Biol, 5*, 163-168. doi:10.1016/j.redox.2015.04.008

Dawber, T. R., Moore, F. E., & Mann, G. V. (1957). Coronary heart disease in the Framingham study. *Am J Public Health Nations Health, 47*(4 Pt 2), 4-24.

De Jong, K. A., & Lopaschuk, G. D. (2017). Complex Energy Metabolic Changes in Heart Failure With Preserved Ejection Fraction and Heart Failure With Reduced Ejection Fraction. *Can J Cardiol, 33*(7), 860-871. doi:10.1016/j.cjca.2017.03.009

De Meyer, G. R., Grootaert, M. O., Michiels, C. F., Kurdi, A., Schrijvers, D. M., & Martinet, W. (2015). Autophagy in vascular disease. *Circ Res, 116*(3), 468-479. doi:10.1161/CIRCRESAHA.116.303804

de Oliveira, M. R., Nabavi, S. F., Manayi, A., Daglia, M., Hajheydari, Z., & Nabavi, S. M. (2016). Resveratrol and the mitochondria: From triggering the intrinsic apoptotic pathway to inducing mitochondrial biogenesis, a mechanistic view. *Biochim Biophys Acta, 1860*(4), 727-745. doi:10.1016/j.bbagen.2016.01.017

Dinh, Q. N., Chrissobolis, S., Diep, H., Chan, C. T., Ferens, D., Drummond, G. R., & Sobey, C. G. (2017). Advanced atherosclerosis is associated with inflammation, vascular dysfunction and oxidative stress, but not hypertension. *Pharmacol Res, 116*, 70-76. doi:10.1016/j.phrs.2016.12.032

Docherty, C. K., Carswell, A., Friel, E., & Mercer, J. R. (2018). Impaired mitochondrial respiration in human carotid plaque atherosclerosis: A potential role for Pink1 in vascular smooth muscle cell energetics. *Atherosclerosis, 268*, 1-11. doi:10.1016/j.atherosclerosis.2017.11.009

Doenst, T., Nguyen, T. D., & Abel, E. D. (2013). Cardiac metabolism in heart failure: implications beyond ATP production. *Circ Res, 113*(6), 709-724. doi:10.1161/CIRCRESAHA.113.300376

Dromparis, P., & Michelakis, E. D. (2013). Mitochondria in vascular health and disease. *Annu Rev Physiol, 75*, 95-126. doi:10.1146/annurev-physiol-030212-183804

Du, X., Edelstein, D., Obici, S., Higham, N., Zou, M. H., & Brownlee, M. (2006). Insulin resistance reduces arterial prostacyclin synthase and eNOS activities by increasing endothelial fatty acid oxidation. *J Clin Invest, 116*(4), 1071-1080. doi:10.1172/JCI23354

Duewell, P., Kono, H., Rayner, K. J., Sirois, C. M., Vladimer, G., Bauernfeind, F. G., . . . Latz, E. (2010). NLRP3 inflammasomes are required for atherogenesis and activated by cholesterol crystals. *Nature, 464*(7293), 1357-1361. doi:10.1038/nature08938

Dunham-Snary, K. J., Sandel, M. W., Westbrook, D. G., & Ballinger, S. W. (2014). A method for assessing mitochondrial bioenergetics in whole white adipose tissues. *Redox Biol, 2*, 656-660. doi:10.1016/j.redox.2014.04.005

Ekstrand, M., Gustafsson Trajkovska, M., Perman-Sundelin, J., Fogelstrand, P., Adiels, M., Johansson, M., . . . Levin, M. (2015). Imaging of Intracellular and Extracellular ROS Levels in Atherosclerotic Mouse Aortas Ex Vivo: Effects of Lipid Lowering by Diet or Atorvastatin. *PLoS One, 10*(6), e0130898. doi:10.1371/journal.pone.0130898

Ekstrand, M. I., Falkenberg, M., Rantanen, A., Park, C. B., Gaspari, M., Hultenby, K., . . . Larsson, N. G. (2004). Mitochondrial transcription factor A regulates mtDNA copy number in mammals. *Hum Mol Genet, 13*(9), 935-944. doi:10.1093/hmg/ddh109

Epstein, A. C., Gleadle, J. M., McNeill, L. A., Hewitson, K. S., O'Rourke, J., Mole, D. R., . . . Ratcliffe, P. J. (2001). C. elegans EGL-9 and mammalian homologs define a family of dioxygenases that regulate HIF by prolyl hydroxylation. *Cell, 107*(1), 43-54.

Falkenberg, M., Larsson, N. G., & Gustafsson, C. M. (2007). DNA replication and transcription in mammalian mitochondria. *Annu Rev Biochem, 76*, 679-699. doi:10.1146/annurev.biochem.76.060305.152028

Fedorowicz, M. A., de Vries-Schneider, R. L., Rub, C., Becker, D., Huang, Y., Zhou, C., . . . Przedborski, S. (2014). Cytosolic cleaved PINK1 represses Parkin translocation to mitochondria and mitophagy. *EMBO Rep, 15*(1), 86-93. doi:10.1002/embr.201337294

Feeley, K. P., Westbrook, D. G., Bray, A. W., & Ballinger, S. W. (2014). An ex-vivo model for evaluating bioenergetics in aortic rings. *Redox Biol, 2C*, 1003-1007. doi:10.1016/j.redox.2014.08.008

Ferrell, J. M., & Chiang, J. Y. (2015). Short-term circadian disruption impairs bile acid and lipid homeostasis in mice. *Cell Mol Gastroenterol Hepatol, 1*(6), 664-677. doi:10.1016/j.jcmgh.2015.08.003

Finichiu, P. G., Larsen, D. S., Evans, C., Larsen, L., Bright, T. P., Robb, E. L., . . . Murphy, M. P. (2015). A mitochondria-targeted derivative of ascorbate: MitoC. *Free Radic Biol Med, 89*, 668-678. doi:10.1016/j.freeradbiomed.2015.07.160

Finkel, T., Deng, C. X., & Mostoslavsky, R. (2009). Recent progress in the biology and physiology of sirtuins. *Nature, 460*(7255), 587-591. doi:10.1038/nature08197

Fried, N. T., Moffat, C., Seifert, E. L., & Oshinsky, M. L. (2014). Functional mitochondrial analysis in acute brain sections from adult rats reveals mitochondrial dysfunction in a rat model of migraine. *Am J Physiol Cell Physiol, 307*(11), C1017-1030. doi:10.1152/ajpcell.00332.2013

Friedman, J. R., & Nunnari, J. (2014). Mitochondrial form and function. *Nature, 505*(7483), 335-343. doi:10.1038/nature12985

Gammage, P. A., Van Haute, L., & Minczuk, M. (2016). Engineered mtZFNs for Manipulation of Human Mitochondrial DNA Heteroplasmy. *Methods Mol Biol, 1351*, 145-162. doi:10.1007/978-1-4939-3040-1_11

Getz, G. S., & Reardon, C. A. (2012). Animal models of atherosclerosis. *Arterioscler Thromb Vasc Biol, 32*(5), 1104-1115. doi:10.1161/ATVBAHA.111.237693

Ghosh, A., Chandran, K., Kalivendi, S. V., Joseph, J., Antholine, W. E., Hillard, C. J., . . . Kalyanaraman, B. (2010). Neuroprotection by a mitochondria-targeted drug in a Parkinson's disease model. *Free Radic Biol Med, 49*(11), 1674-1684. doi:10.1016/j.freeradbiomed.2010.08.028

Gioscia-Ryan, R. A., LaRocca, T. J., Sindler, A. L., Zigler, M. C., Murphy, M. P., & Seals, D. R. (2014). Mitochondria-targeted antioxidant (MitoQ) ameliorates age-related arterial endothelial dysfunction in mice. *J Physiol, 592*(12), 2549-2561. doi:10.1113/jphysiol.2013.268680

Gonzalez-Hunt, C. P., Rooney, J. P., Ryde, I. T., Anbalagan, C., Joglekar, R., & Meyer, J. N. (2016). PCR-Based Analysis of Mitochondrial DNA Copy Number, Mitochondrial DNA Damage, and Nuclear DNA Damage. *Curr Protoc Toxicol, 67*, 20 11 21-20 11 25. doi:10.1002/0471140856.tx2011s67

Gorenne, I., Kumar, S., Gray, K., Figg, N., Yu, H., Mercer, J., & Bennett, M. (2013). Vascular smooth muscle cell sirtuin 1 protects against DNA damage and inhibits atherosclerosis. *Circulation, 127*(3), 386-396. doi:10.1161/CIRCULATIONAHA.112.124404

Graziewicz, M. A., Longley, M. J., & Copeland, W. C. (2006). DNA polymerase gamma in mitochondrial DNA replication and repair. *Chem Rev, 106*(2), 383-405. doi:10.1021/cr040463d

Greene, A. W., Grenier, K., Aguileta, M. A., Muise, S., Farazifard, R., Haque, M. E., . . . Fon, E. A. (2012). Mitochondrial processing peptidase regulates PINK1 processing, import and Parkin recruitment. *EMBO Rep, 13*(4), 378-385. doi:10.1038/embor.2012.14

Group, M. A.-A. S. (1994). Effect of simvastatin on coronary atheroma: the Multicentre Anti-Atheroma Study (MAAS). *Lancet, 344*(8923), 633-638.

Group, S. S. S. S. (1994). Randomised trial of cholesterol lowering in 4444 patients with coronary heart disease: the Scandinavian Simvastatin Survival Study (4S). *Lancet, 344*(8934), 1383-1389.

Gu, L., Okada, Y., Clinton, S. K., Gerard, C., Sukhova, G. K., Libby, P., & Rollins, B. J. (1998). Absence of monocyte chemoattractant protein-1 reduces atherosclerosis in low density lipoprotein receptor-deficient mice. *Mol Cell, 2*(2), 275-281.

Guo, R., Su, Y., Liu, B., Li, S., Zhou, S., & Xu, Y. (2014). Resveratrol suppresses oxidised low-density lipoprotein-induced macrophage apoptosis through inhibition of intracellular reactive oxygen species generation, LOX-1, and the p38 MAPK pathway. *Cell Physiol Biochem, 34*(2), 603-616. doi:10.1159/000363026

Handschin, C., & Spiegelman, B. M. (2006). Peroxisome proliferator-activated receptor gamma coactivator 1 coactivators, energy homeostasis, and metabolism. *Endocr Rev, 27*(7), 728-735. doi:10.1210/er.2006-0037

Hansson, G. K., & Libby, P. (2006). The immune response in atherosclerosis: a double-edged sword. *Nat Rev Immunol, 6*(7), 508-519. doi:10.1038/nri1882

Hatzistamou, J., Kiaris, H., Ergazaki, M., & Spandidos, D. A. (1996). Loss of heterozygosity and microsatellite instability in human atherosclerotic plaques. *Biochem Biophys Res Commun, 225*(1), 186-190. doi:10.1006/bbrc.1996.1151

Hayakawa, M., Torii, K., Sugiyama, S., Tanaka, M., & Ozawa, T. (1991). Age-associated accumulation of 8-hydroxydeoxyguanosine in mitochondrial DNA of human diaphragm. *Biochem Biophys Res Commun, 179*(2), 1023-1029.

Hayashi, J., Ohta, S., Kikuchi, A., Takemitsu, M., Goto, Y., & Nonaka, I. (1991). Introduction of disease-related mitochondrial DNA deletions into HeLa cells lacking mitochondrial DNA results in mitochondrial dysfunction. *Proc Natl Acad Sci U S A, 88*(23), 10614-10618.

Head, B., Griparic, L., Amiri, M., Gandre-Babbe, S., & van der Bliek, A. M. (2009). Inducible proteolytic inactivation of OPA1 mediated by the OMA1 protease in mammalian cells. *J Cell Biol, 187*(7), 959-966. doi:10.1083/jcb.200906083

Hertz, N. T., Berthet, A., Sos, M. L., Thorn, K. S., Burlingame, A. L., Nakamura, K., & Shokat, K. M. (2013). A neo-substrate that amplifies catalytic activity of parkinson's-disease-related kinase PINK1. *Cell, 154*(4), 737-747. doi:10.1016/j.cell.2013.07.030

Herzig, S., Long, F., Jhala, U. S., Hedrick, S., Quinn, R., Bauer, A., . . . Montminy, M. (2001). CREB regulates hepatic gluconeogenesis through the coactivator PGC-1. *Nature, 413*(6852), 179-183. doi:10.1038/35093131

Holt, I. J., Harding, A. E., & Morgan-Hughes, J. A. (1988). Deletions of muscle mitochondrial DNA in patients with mitochondrial myopathies. *Nature, 331*(6158), 717-719. doi:10.1038/331717a0

Howitz, K. T., Bitterman, K. J., Cohen, H. Y., Lamming, D. W., Lavu, S., Wood, J. G., . . . Sinclair, D. A. (2003). Small molecule activators of

sirtuins extend Saccharomyces cerevisiae lifespan. *Nature, 425*(6954), 191-196. doi:10.1038/nature01960

Hurd, T. R., James, A. M., Lilley, K. S., & Murphy, M. P. (2009). Chapter 19 Measuring redox changes to mitochondrial protein thiols with redox difference gel electrophoresis (redox-DIGE). *Methods Enzymol, 456*, 343-361. doi:10.1016/S0076-6879(08)04419-4

Ikeda, M., Ide, T., Fujino, T., Arai, S., Saku, K., Kakino, T., . . . Sunagawa, K. (2015). Overexpression of TFAM or twinkle increases mtDNA copy number and facilitates cardioprotection associated with limited mitochondrial oxidative stress. *PLoS One, 10*(3), e0119687. doi:10.1371/journal.pone.0119687

Ishibashi, S., Brown, M. S., Goldstein, J. L., Gerard, R. D., Hammer, R. E., & Herz, J. (1993). Hypercholesterolemia in low density lipoprotein receptor knockout mice and its reversal by adenovirus-mediated gene delivery. *J Clin Invest, 92*(2), 883-893. doi:10.1172/JCI116663

Janabi, M., Yamashita, S., Hirano, K., Sakai, N., Hiraoka, H., Matsumoto, K., . . . Matsuzawa, Y. (2000). Oxidized LDL-induced NF-kappa B activation and subsequent expression of proinflammatory genes are defective in monocyte-derived macrophages from CD36-deficient patients. *Arterioscler Thromb Vasc Biol, 20*(8), 1953-1960.

Janero, D. R. (1990). Malondialdehyde and thiobarbituric acid-reactivity as diagnostic indices of lipid peroxidation and peroxidative tissue injury. *Free Radic Biol Med, 9*(6), 515-540.

Jin, S. M., Lazarou, M., Wang, C., Kane, L. A., Narendra, D. P., & Youle, R. J. (2010). Mitochondrial membrane potential regulates PINK1 import and proteolytic destabilization by PARL. *J Cell Biol, 191*(5), 933-942. doi:10.1083/jcb.201008084

Jonasson, L., Holm, J., Skalli, O., Bondjers, G., & Hansson, G. K. (1986). Regional accumulations of T cells, macrophages, and smooth muscle cells in the human atherosclerotic plaque. *Arteriosclerosis, 6*(2), 131-138.

Kabeya, Y., Mizushima, N., Ueno, T., Yamamoto, A., Kirisako, T., Noda, T., . . . Yoshimori, T. (2000). LC3, a mammalian homologue of yeast Apg8p, is localized in autophagosome membranes after processing. *EMBO J, 19*(21), 5720-5728. doi:10.1093/emboj/19.21.5720

Katayama, H., Kogure, T., Mizushima, N., Yoshimori, T., & Miyawaki, A. (2011). A sensitive and quantitative technique for detecting autophagic events based on lysosomal delivery. *Chem Biol, 18*(8), 1042-1052. doi:10.1016/j.chembiol.2011.05.013

Kelso, G. F., Porteous, C. M., Coulter, C. V., Hughes, G., Porteous, W. K., Ledgerwood, E. C., . . . Murphy, M. P. (2001). Selective targeting of a

redox-active ubiquinone to mitochondria within cells: antioxidant and antiapoptotic properties. *J Biol Chem, 276*(7), 4588-4596. doi:10.1074/jbc.M009093200

Kitada, T., Asakawa, S., Hattori, N., Matsumine, H., Yamamura, Y., Minoshima, S., . . . Shimizu, N. (1998). Mutations in the parkin gene cause autosomal recessive juvenile parkinsonism. *Nature, 392*(6676), 605-608. doi:10.1038/33416

Klionsky, D. J., Abdalla, F. C., Abeliovich, H., Abraham, R. T., Acevedo-Arozena, A., Adeli, K., . . . Zuckerbraun, B. (2012). Guidelines for the use and interpretation of assays for monitoring autophagy. *Autophagy, 8*(4), 445-544.

Kogure, T., Karasawa, S., Araki, T., Saito, K., Kinjo, M., & Miyawaki, A. (2006). A fluorescent variant of a protein from the stony coral Montipora facilitates dual-color single-laser fluorescence cross-correlation spectroscopy. *Nat Biotechnol, 24*(5), 577-581. doi:10.1038/nbt1207

Kondapalli, C., Kazlauskaite, A., Zhang, N., Woodroof, H. I., Campbell, D. G., Gourlay, R., . . . Muqit, M. M. (2012). PINK1 is activated by mitochondrial membrane potential depolarization and stimulates Parkin E3 ligase activity by phosphorylating Serine 65. *Open Biol, 2*(5), 120080. doi:10.1098/rsob.120080

Korhonen, J. A., Pham, X. H., Pellegrini, M., & Falkenberg, M. (2004). Reconstitution of a minimal mtDNA replisome in vitro. *EMBO J, 23*(12), 2423-2429. doi:10.1038/sj.emboj.7600257

Kovanen, P. T., Kaartinen, M., & Paavonen, T. (1995). Infiltrates of activated mast cells at the site of coronary atheromatous erosion or rupture in myocardial infarction. *Circulation, 92*(5), 1084-1088.

Koyano, F., Okatsu, K., Kosako, H., Tamura, Y., Go, E., Kimura, M., . . . Matsuda, N. (2014). Ubiquitin is phosphorylated by PINK1 to activate parkin. *Nature, 510*(7503), 162-166. doi:10.1038/nature13392

Krako, N., Magnifico, M. C., Arese, M., Meli, G., Forte, E., Lecci, A., . . . Cattaneo, A. (2013). Characterization of mitochondrial dysfunction in the 7PA2 cell model of Alzheimer's disease. *J Alzheimers Dis, 37*(4), 747-758. doi:10.3233/JAD-130728

Kris-Etherton, P. M., Lichtenstein, A. H., Howard, B. V., Steinberg, D., Witztum, J. L., Nutrition Committee of the American Heart Association Council on Nutrition, P. A., & Metabolism. (2004). Antioxidant vitamin supplements and cardiovascular disease. *Circulation, 110*(5), 637-641. doi:10.1161/01.CIR.0000137822.39831.F1

Krishnamurthi, R. V., Feigin, V. L., Forouzanfar, M. H., Mensah, G. A., Connor, M., Bennett, D. A., . . . Group, G. B. D. S. E. (2013). Global

and regional burden of first-ever ischaemic and haemorrhagic stroke during 1990-2010: findings from the Global Burden of Disease Study 2010. *Lancet Glob Health, 1*(5), e259-281. doi:10.1016/S2214-109X(13)70089-5

Kroemer, G., Galluzzi, L., & Brenner, C. (2007). Mitochondrial membrane permeabilization in cell death. *Physiol Rev, 87*(1), 99-163. doi:10.1152/physrev.00013.2006

Kuhn, H., Belkner, J., Wiesner, R., Schewe, T., Lankin, V. Z., & Tikhaze, A. K. (1992). Structure elucidation of oxygenated lipids in human atherosclerotic lesions. *Eicosanoids, 5*(1), 17-22.

Kuma, A., Matsui, M., & Mizushima, N. (2007). LC3, an autophagosome marker, can be incorporated into protein aggregates independent of autophagy: caution in the interpretation of LC3 localization. *Autophagy, 3*(4), 323-328.

Landar, A., Zmijewski, J. W., Dickinson, D. A., Le Goffe, C., Johnson, M. S., Milne, G. L., . . . Darley-Usmar, V. M. (2006). Interaction of electrophilic lipid oxidation products with mitochondria in endothelial cells and formation of reactive oxygen species. *Am J Physiol Heart Circ Physiol, 290*(5), H1777-1787. doi:10.1152/ajpheart.01087.2005

Larsson, N. G. (2010). Somatic mitochondrial DNA mutations in mammalian aging. *Annu Rev Biochem, 79*, 683-706. doi:10.1146/annurev-biochem-060408-093701

Lee, I. H., Cao, L., Mostoslavsky, R., Lombard, D. B., Liu, J., Bruns, N. E., . . . Finkel, T. (2008). A role for the NAD-dependent deacetylase Sirt1 in the regulation of autophagy. *Proc Natl Acad Sci U S A, 105*(9), 3374-3379. doi:10.1073/pnas.0712145105

Lee, J. Y., Jung, G. Y., Heo, H. J., Yun, M. R., Park, J. Y., Bae, S. S., . . . Kim, C. D. (2006). 4-Hydroxynonenal induces vascular smooth muscle cell apoptosis through mitochondrial generation of reactive oxygen species. *Toxicol Lett, 166*(3), 212-221. doi:10.1016/j.toxlet.2006.07.305

Levitan, I., Volkov, S., & Subbaiah, P. V. (2010). Oxidized LDL: diversity, patterns of recognition, and pathophysiology. *Antioxid Redox Signal, 13*(1), 39-75. doi:10.1089/ars.2009.2733

Lewinska, A., Wnuk, M., Slota, E., & Bartosz, G. (2007). Total anti-oxidant capacity of cell culture media. *Clin Exp Pharmacol Physiol, 34*(8), 781-786. doi:10.1111/j.1440-1681.2007.04637.x

Libby, P. (2012). Inflammation in atherosclerosis. *Arterioscler Thromb Vasc Biol, 32*(9), 2045-2051. doi:10.1161/ATVBAHA.108.179705

Liu, B., Du, Q., Chen, L., Fu, G., Li, S., Fu, L., . . . Bin, C. (2016). CpG methylation patterns of human mitochondrial DNA. *Sci Rep, 6*, 23421. doi:10.1038/srep23421

Liu, J., Cao, L., Chen, J., Song, S., Lee, I. H., Quijano, C., . . . Finkel, T. (2009). Bmi1 regulates mitochondrial function and the DNA damage response pathway. *Nature, 459*(7245), 387-392. doi:10.1038/nature08040

Liu, L., Feng, D., Chen, G., Chen, M., Zheng, Q., Song, P., . . . Chen, Q. (2012). Mitochondrial outer-membrane protein FUNDC1 mediates hypoxia-induced mitophagy in mammalian cells. *Nat Cell Biol, 14*(2), 177-185. doi:10.1038/ncb2422

Logan, A., Shabalina, I. G., Prime, T. A., Rogatti, S., Kalinovich, A. V., Hartley, R. C., . . . Murphy, M. P. (2014). In vivo levels of mitochondrial hydrogen peroxide increase with age in mtDNA mutator mice. *Aging Cell, 13*(4), 765-768. doi:10.1111/acel.12212

Lopaschuk, G. D. (2017). Metabolic Modulators in Heart Disease: Past, Present, and Future. *Can J Cardiol, 33*(7), 838-849. doi:10.1016/j.cjca.2016.12.013

Ma, L., Liu, X., Zhao, Y., Chen, B., Li, X., & Qi, R. (2013). Ginkgolide B reduces LOX-1 expression by inhibiting Akt phosphorylation and increasing Sirt1 expression in oxidized LDL-stimulated human umbilical vein endothelial cells. *PLoS One, 8*(9), e74769. doi:10.1371/journal.pone.0074769

Mabile, L., Meilhac, O., Escargueil-Blanc, I., Troly, M., Pieraggi, M. T., Salvayre, R., & Negre-Salvayre, A. (1997). Mitochondrial function is involved in LDL oxidation mediated by human cultured endothelial cells. *Arterioscler Thromb Vasc Biol, 17*(8), 1575-1582.

Mach, F., Sauty, A., Iarossi, A. S., Sukhova, G. K., Neote, K., Libby, P., & Luster, A. D. (1999). Differential expression of three T lymphocyte-activating CXC chemokines by human atheroma-associated cells. *J Clin Invest, 104*(8), 1041-1050. doi:10.1172/JCI6993

Mahmoudi, M., Gorenne, I., Mercer, J., Figg, N., Littlewood, T., & Bennett, M. (2008). Statins use a novel Nijmegen breakage syndrome-1-dependent pathway to accelerate DNA repair in vascular smooth muscle cells. *Circ Res, 103*(7), 717-725. doi:10.1161/CIRCRESAHA.108.182899

Martinet, W., & De Meyer, G. R. (2009). Autophagy in atherosclerosis: a cell survival and death phenomenon with therapeutic potential. *Circ Res, 104*(3), 304-317. doi:10.1161/CIRCRESAHA.108.188318

Mayr, M., Chung, Y. L., Mayr, U., Yin, X., Ly, L., Troy, H., . . . Xu, Q. (2005). Proteomic and metabolomic analyses of atherosclerotic vessels from apolipoprotein E-deficient mice reveal alterations in inflammation, oxidative stress, and energy metabolism. *Arterioscler Thromb Vasc Biol, 25*(10), 2135-2142. doi:10.1161/01.ATV.0000183928.25844.f6

McBride, H. M., Neuspiel, M., & Wasiak, S. (2006). Mitochondria: more than just a powerhouse. *Curr Biol, 16*(14), R551-560. doi:10.1016/j.cub.2006.06.054

McBride, W., Lange, R. A., & Hillis, L. D. (1988). Restenosis after successful coronary angioplasty. Pathophysiology and prevention. *N Engl J Med, 318*(26), 1734-1737. doi:10.1056/NEJM198806303182606

McManus, M. J., Murphy, M. P., & Franklin, J. L. (2014). Mitochondria-derived reactive oxygen species mediate caspase-dependent and -independent neuronal deaths. *Mol Cell Neurosci, 63*, 13-23. doi:10.1016/j.mcn.2014.09.002

Medzhitov, R., & Janeway, C. A., Jr. (1997). Innate immunity: the virtues of a nonclonal system of recognition. *Cell, 91*(3), 295-298.

Mehta, J. L., Sanada, N., Hu, C. P., Chen, J., Dandapat, A., Sugawara, F., . . . Sawamura, T. (2007). Deletion of LOX-1 reduces atherogenesis in LDLR knockout mice fed high cholesterol diet. *Circ Res, 100*(11), 1634-1642. doi:10.1161/CIRCRESAHA.107.149724

Menu, P., Pellegrin, M., Aubert, J. F., Bouzourene, K., Tardivel, A., Mazzolai, L., & Tschopp, J. (2011). Atherosclerosis in ApoE-deficient mice progresses independently of the NLRP3 inflammasome. *Cell Death Dis, 2*, e137. doi:10.1038/cddis.2011.18

Mercer, J., Mahmoudi, M., & Bennett, M. (2007). DNA damage, p53, apoptosis and vascular disease. *Mutat Res, 621*(1-2), 75-86. doi:10.1016/j.mrfmmm.2007.02.011

Mercer, J. R., Cheng, K. K., Figg, N., Gorenne, I., Mahmoudi, M., Griffin, J., . . . Bennett, M. (2010). DNA damage links mitochondrial dysfunction to atherosclerosis and the metabolic syndrome. *Circ Res, 107*(8), 1021-1031. doi:10.1161/CIRCRESAHA.110.218966

Mercer, J. R., Yu, E., Figg, N., Cheng, K. K., Prime, T. A., Griffin, J. L., . . . Bennett, M. R. (2012). The mitochondria-targeted antioxidant MitoQ decreases features of the metabolic syndrome in ATM+/-/ApoE-/- mice. *Free Radic Biol Med, 52*(5), 841-849. doi:10.1016/j.freeradbiomed.2011.11.026

Messner, M. C., Albert, C. J., McHowat, J., & Ford, D. A. (2008). Identification of lysophosphatidylcholine-chlorohydrin in human atherosclerotic lesions. *Lipids, 43*(3), 243-249. doi:10.1007/s11745-008-3151-z

Milenkovic, D., Matic, S., Kuhl, I., Ruzzenente, B., Freyer, C., Jemt, E., . . . Larsson, N. G. (2013). TWINKLE is an essential mitochondrial helicase required for synthesis of nascent D-loop strands and complete mtDNA replication. *Hum Mol Genet, 22*(10), 1983-1993. doi:10.1093/hmg/ddt051

Mills, E. L., Kelly, B., Logan, A., Costa, A. S., Varma, M., Bryant, C. E., . . . O'Neill, L. A. (2016). Succinate Dehydrogenase Supports Metabolic Repurposing of Mitochondria to Drive Inflammatory Macrophages. *Cell, 167*(2), 457-470 e413. doi:10.1016/j.cell.2016.08.064

Mondy, J. S., Lindner, V., Miyashiro, J. K., Berk, B. C., Dean, R. H., & Geary, R. L. (1997). Platelet-derived growth factor ligand and receptor expression in response to altered blood flow in vivo. *Circ Res, 81*(3), 320-327.

Mosmann, T. (1983). Rapid colorimetric assay for cellular growth and survival: application to proliferation and cytotoxicity assays. *J Immunol Methods, 65*(1-2), 55-63.

Mounsey, R. B., & Teismann, P. (2010). Mitochondrial dysfunction in Parkinson's disease: pathogenesis and neuroprotection. *Parkinsons Dis, 2011*, 617472. doi:10.4061/2011/617472

Murphy, M. P. (2009). How mitochondria produce reactive oxygen species. *Biochem J, 417*(1), 1-13. doi:10.1042/BJ20081386

Murphy, M. P. (2012). Mitochondrial thiols in antioxidant protection and redox signaling: distinct roles for glutathionylation and other thiol modifications. *Antioxid Redox Signal, 16*(6), 476-495. doi:10.1089/ars.2011.4289

Murray, C. J., Vos, T., Lozano, R., Naghavi, M., Flaxman, A. D., Michaud, C., . . . Memish, Z. A. (2012). Disability-adjusted life years (DALYs) for 291 diseases and injuries in 21 regions, 1990-2010: a systematic analysis for the Global Burden of Disease Study 2010. *Lancet, 380*(9859), 2197-2223. doi:10.1016/S0140-6736(12)61689-4

Nakai, A., Yamaguchi, O., Takeda, T., Higuchi, Y., Hikoso, S., Taniike, M., . . . Otsu, K. (2007). The role of autophagy in cardiomyocytes in the basal state and in response to hemodynamic stress. *Nat Med, 13*(5), 619-624. doi:10.1038/nm1574

Nakashima, Y., Plump, A. S., Raines, E. W., Breslow, J. L., & Ross, R. (1994). ApoE-deficient mice develop lesions of all phases of atherosclerosis throughout the arterial tree. *Arterioscler Thromb, 14*(1), 133-140.

Nakashima, Y., Raines, E. W., Plump, A. S., Breslow, J. L., & Ross, R. (1998). Upregulation of VCAM-1 and ICAM-1 at atherosclerosis-prone sites on the endothelium in the ApoE-deficient mouse. *Arterioscler Thromb Vasc Biol, 18*(5), 842-851.

Naldini, L., Blomer, U., Gallay, P., Ory, D., Mulligan, R., Gage, F. H., . . . Trono, D. (1996). In vivo gene delivery and stable transduction of nondividing cells by a lentiviral vector. *Science, 272*(5259), 263-267.

Nemoto, S., Fergusson, M. M., & Finkel, T. (2005). SIRT1 functionally interacts with the metabolic regulator and transcriptional coactivator PGC-1{alpha}. *J Biol Chem, 280*(16), 16456-16460. doi:10.1074/jbc.M501485200

Neubauer, S., Horn, M., Cramer, M., Harre, K., Newell, J. B., Peters, W., . . . Kochsiek, K. (1997). Myocardial phosphocreatine-to-ATP ratio is a predictor of mortality in patients with dilated cardiomyopathy. *Circulation, 96*(7), 2190-2196.

Neubauer, S., Krahe, T., Schindler, R., Horn, M., Hillenbrand, H., Entzeroth, C., . . . et al. (1992). 31P magnetic resonance spectroscopy in dilated cardiomyopathy and coronary artery disease. Altered cardiac high-energy phosphate metabolism in heart failure. *Circulation, 86*(6), 1810-1818.

Niessner, A., Sato, K., Chaikof, E. L., Colmegna, I., Goronzy, J. J., & Weyand, C. M. (2006). Pathogen-sensing plasmacytoid dendritic cells stimulate cytotoxic T-cell function in the atherosclerotic plaque through interferon-alpha. *Circulation, 114*(23), 2482-2489. doi:10.1161/CIRCULATIONAHA.106.642801

Niki, E. (2018). Oxidant-specific biomarkers of oxidative stress. Association with atherosclerosis and implication for antioxidant effects. *Free Radic Biol Med, 120*, 425-440. doi:10.1016/j.freeradbiomed.2018.04.001

Nishikawa, T., Edelstein, D., Du, X. L., Yamagishi, S., Matsumura, T., Kaneda, Y., . . . Brownlee, M. (2000). Normalizing mitochondrial superoxide production blocks three pathways of hyperglycaemic damage. *Nature, 404*(6779), 787-790. doi:10.1038/35008121

Oka, T., Hikoso, S., Yamaguchi, O., Taneike, M., Takeda, T., Tamai, T., . . . Otsu, K. (2012). Mitochondrial DNA that escapes from autophagy causes inflammation and heart failure. *Nature, 485*(7397), 251-255. doi:10.1038/nature10992

Okamoto, K., Kondo-Okamoto, N., & Ohsumi, Y. (2009). Mitochondria-anchored receptor Atg32 mediates degradation of mitochondria via selective autophagy. *Dev Cell, 17*(1), 87-97. doi:10.1016/j.devcel.2009.06.013

Okatsu, K., Oka, T., Iguchi, M., Imamura, K., Kosako, H., Tani, N., . . . Matsuda, N. (2012). PINK1 autophosphorylation upon membrane potential dissipation is essential for Parkin recruitment to damaged mitochondria. *Nat Commun, 3*, 1016. doi:10.1038/ncomms2016

Palazon, A., Goldrath, A. W., Nizet, V., & Johnson, R. S. (2014). HIF transcription factors, inflammation, and immunity. *Immunity, 41*(4), 518-528. doi:10.1016/j.immuni.2014.09.008

Papa, L., Gomes, E., & Rockwell, P. (2007). Reactive oxygen species induced by proteasome inhibition in neuronal cells mediate mitochondrial dysfunction and a caspase-independent cell death. *Apoptosis, 12*(8), 1389-1405. doi:10.1007/s10495-007-0069-5

Papadopoulou, C., Corrigall, V., Taylor, P. R., & Poston, R. N. (2008). The role of the chemokines MCP-1, GRO-alpha, IL-8 and their receptors in the adhesion of monocytic cells to human atherosclerotic plaques. *Cytokine, 43*(2), 181-186. doi:10.1016/j.cyto.2008.05.009

Paramel Varghese, G., Folkersen, L., Strawbridge, R. J., Halvorsen, B., Yndestad, A., Ranheim, T., . . . Sirsjo, A. (2016). NLRP3 Inflammasome Expression and Activation in Human Atherosclerosis. *J Am Heart Assoc, 5*(5). doi:10.1161/JAHA.115.003031

Park, J., Lee, S. B., Lee, S., Kim, Y., Song, S., Kim, S., . . . Chung, J. (2006). Mitochondrial dysfunction in Drosophila PINK1 mutants is complemented by parkin. *Nature, 441*(7097), 1157-1161. doi:10.1038/nature04788

Pelletier, M., Lepow, T. S., Billingham, L. K., Murphy, M. P., & Siegel, R. M. (2012). New tricks from an old dog: mitochondrial redox signaling in cellular inflammation. *Semin Immunol, 24*(6), 384-392. doi:10.1016/j.smim.2013.01.002

Perrotta, I. (2013). The use of electron microscopy for the detection of autophagy in human atherosclerosis. *Micron, 50*, 7-13. doi:10.1016/j.micron.2013.03.007

Picca, A., & Lezza, A. M. (2015). Regulation of mitochondrial biogenesis through TFAM-mitochondrial DNA interactions: Useful insights from aging and calorie restriction studies. *Mitochondrion, 25*, 67-75. doi:10.1016/j.mito.2015.10.001

Ploumi, C., Daskalaki, I., & Tavernarakis, N. (2017). Mitochondrial biogenesis and clearance: a balancing act. *FEBS J, 284*(2), 183-195. doi:10.1111/febs.13820

Plump, A. S., Smith, J. D., Hayek, T., Aalto-Setala, K., Walsh, A., Verstuyft, J. G., . . . Breslow, J. L. (1992). Severe hypercholesterolemia and atherosclerosis in apolipoprotein E-deficient mice created by homologous recombination in ES cells. *Cell, 71*(2), 343-353.

Pohjoismaki, J. L., Williams, S. L., Boettger, T., Goffart, S., Kim, J., Suomalainen, A., . . . Braun, T. (2013). Overexpression of Twinkle-helicase protects cardiomyocytes from genotoxic stress caused by reactive oxygen species. *Proc Natl Acad Sci U S A, 110*(48), 19408-19413. doi:10.1073/pnas.1303046110

Poole, A. C., Thomas, R. E., Andrews, L. A., McBride, H. M., Whitworth, A. J., & Pallanck, L. J. (2008). The PINK1/Parkin pathway regulates

mitochondrial morphology. *Proc Natl Acad Sci U S A, 105*(5), 1638-1643. doi:10.1073/pnas.0709336105

Prabhudas, M., Bowdish, D., Drickamer, K., Febbraio, M., Herz, J., Kobzik, L., . . . El Khoury, J. (2014). Standardizing scavenger receptor nomenclature. *J Immunol, 192*(5), 1997-2006. doi:10.4049/jimmunol.1490003

Rahman, I., Kode, A., & Biswas, S. K. (2006). Assay for quantitative determination of glutathione and glutathione disulfide levels using enzymatic recycling method. *Nat Protoc, 1*(6), 3159-3165. doi:10.1038/nprot.2006.378

Razani, B., Feng, C., Coleman, T., Emanuel, R., Wen, H., Hwang, S., . . . Semenkovich, C. F. (2012). Autophagy links inflammasomes to atherosclerotic progression. *Cell Metab, 15*(4), 534-544. doi:10.1016/j.cmet.2012.02.011

Ricci, R., Sumara, G., Sumara, I., Rozenberg, I., Kurrer, M., Akhmedov, A., . . . Luscher, T. F. (2004). Requirement of JNK2 for scavenger receptor A-mediated foam cell formation in atherogenesis. *Science, 306*(5701), 1558-1561. doi:10.1126/science.1101909

Roshan, M. H., Tambo, A., & Pace, N. P. (2016). The Role of TLR2, TLR4, and TLR9 in the Pathogenesis of Atherosclerosis. *Int J Inflam, 2016*, 1532832. doi:10.1155/2016/1532832

Ross, R. (1999). Atherosclerosis--an inflammatory disease. *N Engl J Med, 340*(2), 115-126. doi:10.1056/NEJM199901143400207

Roth, G. A., Nguyen, G., Forouzanfar, M. H., Mokdad, A. H., Naghavi, M., & Murray, C. J. (2015). Estimates of global and regional premature cardiovascular mortality in 2025. *Circulation, 132*(13), 1270-1282. doi:10.1161/CIRCULATIONAHA.115.016021

Rubic, T., Lametschwandtner, G., Jost, S., Hinteregger, S., Kund, J., Carballido-Perrig, N., . . . Carballido, J. M. (2008). Triggering the succinate receptor GPR91 on dendritic cells enhances immunity. *Nat Immunol, 9*(11), 1261-1269. doi:10.1038/ni.1657

Sagan, L. (1967). On the origin of mitosing cells. *J Theor Biol, 14*(3), 255-274.

Saiki, C., & Mortola, J. P. (1996). Effect of CO2 on the metabolic and ventilatory responses to ambient temperature in conscious adult and newborn rats. *J Physiol, 491 (Pt 1)*, 261-269.

Sastre-Serra, J., Nadal-Serrano, M., Pons, D. G., Roca, P., & Oliver, J. (2012). Mitochondrial dynamics is affected by 17beta-estradiol in the MCF-7 breast cancer cell line. Effects on fusion and fission related genes. *Int J Biochem Cell Biol, 44*(11), 1901-1905. doi:10.1016/j.biocel.2012.07.012

Sawamura, T., Kume, N., Aoyama, T., Moriwaki, H., Hoshikawa, H., Aiba, Y., . . . Masaki, T. (1997). An endothelial receptor for oxidized low-density lipoprotein. *Nature, 386*(6620), 73-77. doi:10.1038/386073a0

Scheibye-Knudsen, M., Fang, E. F., Croteau, D. L., Wilson, D. M., 3rd, & Bohr, V. A. (2015). Protecting the mitochondrial powerhouse. *Trends Cell Biol, 25*(3), 158-170. doi:10.1016/j.tcb.2014.11.002

Schwartz, D., Andalibi, A., Chaverri-Almada, L., Berliner, J. A., Kirchgessner, T., Fang, Z. T., . . . et al. (1994). Role of the GRO family of chemokines in monocyte adhesion to MM-LDL-stimulated endothelium. *J Clin Invest, 94*(5), 1968-1973. doi:10.1172/JCI117548

Shimada, K., Crother, T. R., Karlin, J., Dagvadorj, J., Chiba, N., Chen, S., . . . Arditi, M. (2012). Oxidized mitochondrial DNA activates the NLRP3 inflammasome during apoptosis. *Immunity, 36*(3), 401-414. doi:10.1016/j.immuni.2012.01.009

Smirnova, E., Shurland, D. L., Ryazantsev, S. N., & van der Bliek, A. M. (1998). A human dynamin-related protein controls the distribution of mitochondria. *J Cell Biol, 143*(2), 351-358.

Snow, B. J., Rolfe, F. L., Lockhart, M. M., Frampton, C. M., O'Sullivan, J. D., Fung, V., . . . Protect Study, G. (2010). A double-blind, placebo-controlled study to assess the mitochondria-targeted antioxidant MitoQ as a disease-modifying therapy in Parkinson's disease. *Mov Disord, 25*(11), 1670-1674. doi:10.1002/mds.23148

Steele, P. M., Chesebro, J. H., Stanson, A. W., Holmes, D. R., Jr., Dewanjee, M. K., Badimon, L., & Fuster, V. (1985). Balloon angioplasty. Natural history of the pathophysiological response to injury in a pig model. *Circ Res, 57*(1), 105-112.

Stewart, C. R., Stuart, L. M., Wilkinson, K., van Gils, J. M., Deng, J., Halle, A., . . . Moore, K. J. (2010). CD36 ligands promote sterile inflammation through assembly of a Toll-like receptor 4 and 6 heterodimer. *Nat Immunol, 11*(2), 155-161. doi:10.1038/ni.1836

Strehler, B. L. (1974). Adenosine-5'-triphosphate and creatine phosphate determination with luciferase. . In Bergmeyer (Ed.), *Methods of enzymatic analysis* (Vol. 4, pp. 2112-2126). New York: Academic Press.

Strowig, T., Henao-Mejia, J., Elinav, E., & Flavell, R. (2012). Inflammasomes in health and disease. *Nature, 481*(7381), 278-286. doi:10.1038/nature10759

Stucki, D. M., Ruegsegger, C., Steiner, S., Radecke, J., Murphy, M. P., Zuber, B., & Saxena, S. (2016). Mitochondrial impairments contribute to Spinocerebellar ataxia type 1 progression and can be ameliorated by

the mitochondria-targeted antioxidant MitoQ. *Free Radic Biol Med, 97*, 427-440. doi:10.1016/j.freeradbiomed.2016.07.005

Sucu, N., Unlu, A., Tamer, L., Aytacoglu, B., Ercan, B., Dikmengil, M., & Atik, U. (2003). 3-Nitrotyrosine in atherosclerotic blood vessels. *Clin Chem Lab Med, 41*(1), 23-25. doi:10.1515/CCLM.2003.005

Sun, N., Yun, J., Liu, J., Malide, D., Liu, C., Rovira, II, . . . Finkel, T. (2015). Measuring In Vivo Mitophagy. *Mol Cell, 60*(4), 685-696. doi:10.1016/j.molcel.2015.10.009

Suzuki, H., Kurihara, Y., Takeya, M., Kamada, N., Kataoka, M., Jishage, K., . . . et al. (1997). A role for macrophage scavenger receptors in atherosclerosis and susceptibility to infection. *Nature, 386*(6622), 292-296. doi:10.1038/386292a0

Swiader, A., Nahapetyan, H., Faccini, J., D'Angelo, R., Mucher, E., Elbaz, M., . . . Vindis, C. (2016). Mitophagy acts as a safeguard mechanism against human vascular smooth muscle cell apoptosis induced by atherogenic lipids. *Oncotarget, 7*(20), 28821-28835. doi:10.18632/oncotarget.8936

Tanaka, A., Ide, T., Fujino, T., Onitsuka, K., Ikeda, M., Takehara, T., . . . Sunagawa, K. (2013). The overexpression of Twinkle helicase ameliorates the progression of cardiac fibrosis and heart failure in pressure overload model in mice. *PLoS One, 8*(6), e67642. doi:10.1371/journal.pone.0067642

Tanaka, H., Mendonca, M. S., Bradshaw, P. S., Hoelz, D. J., Malkas, L. H., Meyn, M. S., & Gilley, D. (2005). DNA damage-induced phosphorylation of the human telomere-associated protein TRF2. *Proc Natl Acad Sci U S A, 102*(43), 15539-15544. doi:10.1073/pnas.0507915102

Tannahill, G. M., Curtis, A. M., Adamik, J., Palsson-McDermott, E. M., McGettrick, A. F., Goel, G., . . . O'Neill, L. A. (2013). Succinate is an inflammatory signal that induces IL-1beta through HIF-1alpha. *Nature, 496*(7444), 238-242. doi:10.1038/nature11986

Tome-Carneiro, J., Larrosa, M., Gonzalez-Sarrias, A., Tomas-Barberan, F. A., Garcia-Conesa, M. T., & Espin, J. C. (2013). Resveratrol and clinical trials: the crossroad from in vitro studies to human evidence. *Curr Pharm Des, 19*(34), 6064-6093.

Trifunovic, A., Wredenberg, A., Falkenberg, M., Spelbrink, J. N., Rovio, A. T., Bruder, C. E., . . . Larsson, N. G. (2004). Premature ageing in mice expressing defective mitochondrial DNA polymerase. *Nature, 429*(6990), 417-423. doi:10.1038/nature02517

Triolo, T., & Sternglanz, R. (1996). Role of interactions between the origin recognition complex and SIR1 in transcriptional silencing. *Nature, 381*(6579), 251-253. doi:10.1038/381251a0

Twig, G., Elorza, A., Molina, A. J., Mohamed, H., Wikstrom, J. D., Walzer, G., . . . Shirihai, O. S. (2008). Fission and selective fusion govern mitochondrial segregation and elimination by autophagy. *EMBO J, 27*(2), 433-446. doi:10.1038/sj.emboj.7601963

Tyynismaa, H., Sembongi, H., Bokori-Brown, M., Granycome, C., Ashley, N., Poulton, J., . . . Suomalainen, A. (2004). Twinkle helicase is essential for mtDNA maintenance and regulates mtDNA copy number. *Hum Mol Genet, 13*(24), 3219-3227. doi:10.1093/hmg/ddh342

Valente, E. M., Abou-Sleiman, P. M., Caputo, V., Muqit, M. M., Harvey, K., Gispert, S., . . . Wood, N. W. (2004). Hereditary early-onset Parkinson's disease caused by mutations in PINK1. *Science, 304*(5674), 1158-1160. doi:10.1126/science.1096284

Vayssier-Taussat, M., Camilli, T., Aron, Y., Meplan, C., Hainaut, P., Polla, B. S., & Weksler, B. (2001). Effects of tobacco smoke and benzo[a]pyrene on human endothelial cell and monocyte stress responses. *Am J Physiol Heart Circ Physiol, 280*(3), H1293-1300.

Vaziri, H., Dessain, S. K., Ng Eaton, E., Imai, S. I., Frye, R. A., Pandita, T. K., . . . Weinberg, R. A. (2001). hSIR2(SIRT1) functions as an NAD-dependent p53 deacetylase. *Cell, 107*(2), 149-159.

Vowinckel, J., Hartl, J., Butler, R., & Ralser, M. (2015). MitoLoc: A method for the simultaneous quantification of mitochondrial network morphology and membrane potential in single cells. *Mitochondrion, 24*, 77-86. doi:10.1016/j.mito.2015.07.001

Waksman, R., Pakala, R., Burnett, M. S., Gulick, C. P., Leborgne, L., Fournadjiev, J., . . . Hellinga, D. (2003). Oral rapamycin inhibits growth of atherosclerotic plaque in apoE knock-out mice. *Cardiovasc Radiat Med, 4*(1), 34-38.

Wallace, D. C., Singh, G., Lott, M. T., Hodge, J. A., Schurr, T. G., Lezza, A. M., . . . Nikoskelainen, E. K. (1988). Mitochondrial DNA mutation associated with Leber's hereditary optic neuropathy. *Science, 242*(4884), 1427-1430.

Wang, C., Chen, L., Hou, X., Li, Z., Kabra, N., Ma, Y., . . . Chen, J. (2006). Interactions between E2F1 and SirT1 regulate apoptotic response to DNA damage. *Nat Cell Biol, 8*(9), 1025-1031. doi:10.1038/ncb1468

Wang, J., Uryga, A. K., Reinhold, J., Figg, N., Baker, L., Finigan, A., . . . Bennett, M. (2015). Vascular Smooth Muscle Cell Senescence Promotes Atherosclerosis and Features of Plaque Vulnerability.

Circulation, 132(20), 1909-1919. doi:10.1161/CIRCULATIONAHA.115.016457

Wang, W., Wang, X., Fujioka, H., Hoppel, C., Whone, A. L., Caldwell, M. A., . . . Zhu, X. (2016). Parkinson's disease-associated mutant VPS35 causes mitochondrial dysfunction by recycling DLP1 complexes. *Nat Med, 22*(1), 54-63. doi:10.1038/nm.3983

Weissberg, P. L., Clesham, G. J., & Bennett, M. R. (1996). Is vascular smooth muscle cell proliferation beneficial? *Lancet, 347*(8997), 305-307.

Wen, H., Ting, J. P., & O'Neill, L. A. (2012). A role for the NLRP3 inflammasome in metabolic diseases--did Warburg miss inflammation? *Nat Immunol, 13*(4), 352-357. doi:10.1038/ni.2228

Witztum, J. L., & Lichtman, A. H. (2014). The influence of innate and adaptive immune responses on atherosclerosis. *Annu Rev Pathol, 9*, 73-102. doi:10.1146/annurev-pathol-020712-163936

Wright, S. D., Burton, C., Hernandez, M., Hassing, H., Montenegro, J., Mundt, S., . . . Chao, Y. S. (2000). Infectious agents are not necessary for murine atherogenesis. *J Exp Med, 191*(8), 1437-1442.

Wu, Z., Puigserver, P., Andersson, U., Zhang, C., Adelmant, G., Mootha, V., . . . Spiegelman, B. M. (1999). Mechanisms controlling mitochondrial biogenesis and respiration through the thermogenic coactivator PGC-1. *Cell, 98*(1), 115-124. doi:10.1016/S0092-8674(00)80611-X

Xu, Q., Dietrich, H., Steiner, H. J., Gown, A. M., Schoel, B., Mikuz, G., . . . Wick, G. (1992). Induction of arteriosclerosis in normocholesterolemic rabbits by immunization with heat shock protein 65. *Arterioscler Thromb, 12*(7), 789-799.

Yamada, K., Sugiyama, S., Kosaka, K., Hayakawa, M., & Ozawa, T. (1995). Early appearance of age-associated deterioration in mitochondrial function of diaphragm and heart in rats treated with doxorubicin. *Exp Gerontol, 30*(6), 581-593.

Youle, R. J., & Narendra, D. P. (2011). Mechanisms of mitophagy. *Nat Rev Mol Cell Biol, 12*(1), 9-14. doi:10.1038/nrm3028

Yu, E., Calvert, P. A., Mercer, J. R., Harrison, J., Baker, L., Figg, N. L., . . . Bennett, M. R. (2013). Mitochondrial DNA damage can promote atherosclerosis independently of reactive oxygen species through effects on smooth muscle cells and monocytes and correlates with higher-risk plaques in humans. *Circulation, 128*(7), 702-712. doi:10.1161/CIRCULATIONAHA.113.002271

Yu, E. P. K., Reinhold, J., Yu, H., Starks, L., Uryga, A. K., Foote, K., . . . Bennett, M. (2017). Mitochondrial Respiration Is Reduced in Atherosclerosis, Promoting Necrotic Core Formation and Reducing

Relative Fibrous Cap Thickness. *Arterioscler Thromb Vasc Biol*. doi:10.1161/ATVBAHA.117.310042

Yu, T., Robotham, J. L., & Yoon, Y. (2006). Increased production of reactive oxygen species in hyperglycemic conditions requires dynamic change of mitochondrial morphology. *Proc Natl Acad Sci U S A, 103*(8), 2653-2658. doi:10.1073/pnas.0511154103

Zani, I. A., Stephen, S. L., Mughal, N. A., Russell, D., Homer-Vanniasinkam, S., Wheatcroft, S. B., & Ponnambalam, S. (2015). Scavenger receptor structure and function in health and disease. *Cells, 4*(2), 178-201. doi:10.3390/cells4020178

Zhang, Q., Raoof, M., Chen, Y., Sumi, Y., Sursal, T., Junger, W., . . . Hauser, C. J. (2010). Circulating mitochondrial DAMPs cause inflammatory responses to injury. *Nature, 464*(7285), 104-107. doi:10.1038/nature08780

Zhang, S. H., Reddick, R. L., Piedrahita, J. A., & Maeda, N. (1992). Spontaneous hypercholesterolemia and arterial lesions in mice lacking apolipoprotein E. *Science, 258*(5081), 468-471.

Zheng, F., Xing, S., Gong, Z., Mu, W., & Xing, Q. (2014). Silence of NLRP3 suppresses atherosclerosis and stabilizes plaques in apolipoprotein E-deficient mice. *Mediators Inflamm, 2014*, 507208. doi:10.1155/2014/507208

Zhou, L., Wang, W., Hoppel, C., Liu, J., & Zhu, X. (2017). Parkinson's Disease-Associated Pathogenic VPS35 Mutation Causes Complex I Deficits. *Biochim Biophys Acta*. doi:10.1016/j.bbadis.2017.07.032

Zhou, R., Yazdi, A. S., Menu, P., & Tschopp, J. (2011). A role for mitochondria in NLRP3 inflammasome activation. *Nature, 469*(7329), 221-225. doi:10.1038/nature09663

Zhu, J., Vinothkumar, K. R., & Hirst, J. (2016). Structure of mammalian respiratory complex I. *Nature, 536*(7616), 354-358. doi:10.1038/nature19095

Zhu, L., Wang, Q., Zhang, L., Fang, Z., Zhao, F., Lv, Z., . . . Zhang, C. Y. (2010). Hypoxia induces PGC-1alpha expression and mitochondrial biogenesis in the myocardium of TOF patients. *Cell Res, 20*(6), 676-687. doi:10.1038/cr.2010.46

Zhu, X. D., Zhuang, Y., Ben, J. J., Qian, L. L., Huang, H. P., Bai, H., . . . Chen, Q. (2011). Caveolae-dependent endocytosis is required for class A macrophage scavenger receptor-mediated apoptosis in macrophages. *J Biol Chem, 286*(10), 8231-8239. doi:10.1074/jbc.M110.145888

Ziviani, E., Tao, R. N., & Whitworth, A. J. (2010). Drosophila parkin requires PINK1 for mitochondrial translocation and ubiquitinates mitofusin. *Proc*

Natl Acad Sci U S A, 107(11), 5018-5023. doi:10.1073/pnas.0913485107

Zordoky, B. N., Robertson, I. M., & Dyck, J. R. (2015). Preclinical and clinical evidence for the role of resveratrol in the treatment of cardiovascular diseases. *Biochim Biophys Acta, 1852*(6), 1155-1177. doi:10.1016/j.bbadis.2014.10.016